Lawrence Berkeley National Laboratory
Recent Work

Title
THE DEVELOPMENT OF LARGE HIGH CURRENT DENSITY SUPERCONDUCTING SOLENOID MAGNETS FOR USE IN HIGH ENERGY PHYSICS EXPERIMENTS

Permalink
https://escholarship.org/uc/item/14v982dv

Author
Green, Michael A.
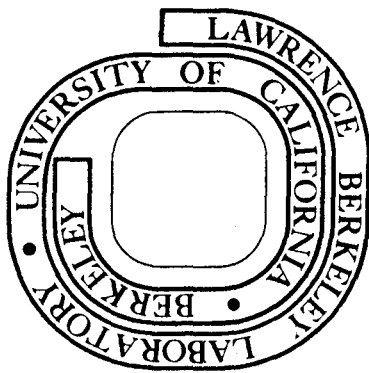
Publication Date
1977-05-01

THE DEVELOPMENT OF LARGE HIGH CURRENT DENSITY SUPERCONDUCTING SOLENOID MAGNETS FOR USE IN HIGH ENERGY PHYSICS EXPERIMENTS

Michael A. Green
Ph. D. thesis

May 1977

DISCLAIMER

THE DEVELOPMENT OF LARGE HIGH CURRENT DENSITY SUPERCONDUCTING
SOLENOID MAGNETS FOR USE IN HIGH ENERGY PHYSICS EXPERIMENTS

Michael A. Green

(Ph.D. Thesis)

May 1977

THE DEVELOPMENT OF LARGE HIGH CURRENT DENSITY SUPERCONDUCTING MAGNETS
FOR USE IN HIGH ENERGY PHYSICS EXPERIMENTS

Contents

NOMENCLATURE

The symbols used in this report are listed and defined below. In most cases, their definitions are given again as they occur in the text. The units corresponding to the symbol definitions are the standard SI electrical and mechanical units and, occasionally, a non standard or English system unit which, when used, is pointed out in the text. The electrical system utilized is a rationalized MKS system with the permeability of vacuum set equal to $\mu_o = 4\pi \times 10^{-7}$.

LIST OF SYMBOLS

Symbol	Definition	Units
A	surface area exposed to liquid helium per m^3 of superconductor volume	m^2
a_1	radius of the coil	m
a_2	radius of the bore tube	m
B	magnetic induction	T
B_o	magnetic induction	T
ΔB	total magnetic induction change	T
$\dot{B}$	rate of magnetic induction change dB/dt	Ts^{-1}
$\dot{B}_c$	critical rate of magnetic induction change	Ts^{-1}
C	specific heat per unit volume	$Jm^{-3}K^{-1}$
C_{cu}	specific heat per unit volume of copper	$Jm^{-3}K^{-1}$
C_m	specific heat per unit volume of low resistance normal metal	$Jm^{-3}K^{-1}$
D	inside diameter of the cooling tube	m
d	superconductor matrix diameter	m
d_f	superconductor filament diameter	m

E	electromagnetic energy in the magnet	J
E_H	energy dissipated as heat in the magnet	J
E_{Hc}	energy dissipated as heat in the coil	J
E_{HAL}	energy dissipated as heat in the bore tube	J
$F(T)$ or $F(t)$	integral of $J^2 dt$	$A^2 m^{-4} S$
$F^*(T)$ or $F^*(t)$	modified integral of $J^2 dt$	$A^2 m^{-4} S$
f	fanning friction factor	
f	fraction of magnetic energy ending up in the bore tube	
G	superconductor a.c. loss per unit volume for a given flux change	Jm^{-3}
G_o	superconductor hysteritic a.c. loss per unit volume for a given flux change	Jm^{-3}
H_{CRIT}	enthalpy per unit volume at the super-conductor critical temperature	Jm^{-3}
Ho	enthalpy per unit volume at the normal operating temperature for the superconductor	Jm^{-3}
$H_{AL}(T)$	enthalpy per unit volume of aluminum at a temperature T	Jm^{-3}
i	current	A
i_1	current in the coil	A
i_0	starting current in the coil	A
i_2	current in the bore tube	A
I	measured current in the coil	A
I_A	measured current in the A coil	A
I_B	measured current in the B coil	A

I_{A+B}	measured current in the A + B coils	A
I_o	measured starting current in coil	A
$J(t)$	current density in the superconductor	Am^{-2}
J_{min}	minimum current density in the super-conductor matrix	Am^{-2}
J_{max}	maximum current density in the super-conductor matrix	Am^{-2}
J_{cs}	operating current density in the matrix of a cryogenically stable superconductor	Am^{-2}
J_c	superconducting filament critical current density	Am^{-2}
L	self inductance	H
L_1	self inductance of the coil	H
L_2	self inductance of the bore tube	H
L_A	self inductance of the A coil	H
L_B	self inductance of the B coil	H
L_{A+B}	self inductance of the A + B coils	H
ℓ_1	length of the coil	m
ℓ_2	length of the bore tube	m
ℓ_c	superconductor twist length	m
M	mutual inductance	H
M_{12}	mutual inductance between the coil and the bore tube	
$M_{A,B}$	mutual inductance between the A and B coils	H
$M_{A+B,A}$	mutual inductance between the A + B coils and the A coil	

$M_{A+B,B}$	mutual inductance between the A + B coils and the B coil	H
$M_{A,PA}$	mutual inductance between the A coil and the A pickup coil	
$M_{A,PB}$	mutual inductance between the A coil and the B pickup coil	H
$M_{B,PA}$	mutual inductance between the B coil and the A pickup coil	H
$M_{B,PB}$	mutual inductance between the B coil and the B pickup coil	H
$M_{A+B,PA}$	mutual inductance between the H + B coils and the A pickup coil	H
$M_{A+B,PB}$	mutual inductance between the A + B coils and the B pickup coil	H
$\dot{m}$	helium mass flow through the cooling circuit	Kgs^{-1}
N_1	number of turns in the coil	
N_P	number of turns in the pickup coil	
n	exponent number	
ΔP	pressure drop along cooling circuit	Pa or Nm^{-2}
$P(t)$	pickup coil signal as a function of time t	V
P_A	signal from A pickup coil	V
P_B	signal from B pickup coil	V
Q	heat flux transmitted to boil helium	Wm^{-2}
R	resistance	ohm
R_1	resistance of the coil circuit	ohm
R_2	resistance of the bore tube circuit	ohm

$R_c(t)$	resistance of the coil as a function of time	ohm
$R_b(t)$	resistance of the bore tube as a function of time	ohm
R_e	external resistor resistance	ohm
R_s	current shunt resistance	ohm
R_{con}	resistance constant for the coil	ohm m^{-2}
R_I	current ratio $I(t)/I(o)$	
R_ϕ	magnetic flux or total current ratio $\Phi(t)/\Phi(o)$	
Re	reynolds number	
r	copper to superconductor ratio	
r^*	ratio of low resistance normal metal to superconductor plus high resistance normal metal	
$S(t)$	signal from the current shunt	V
S	thickness of the superconductor on a thin solenoid	m
T	temperature	K
T_{hot}	hot spot temperature	K
t	time	
V	measured voltage	V
V_A	voltage across the A coil	V
V_B	voltage across the B coil	V
V_{COM}	voltage between the A and B coils	V
V_{AL}	volume of the aluminum bore tube	m^3

V_Q	quench propagation velocity	ms^{-1}
w	distance between filaments	m
z	length of the cooling tube	m
α	coupling coefficient between the coil and the bore tube	
α	ratio of quench velocity from turn to turn to the quench velocity along the wire	
α_{cu}	thermal diffusivity of copper	m^2s^{-1}
Γ	number of particles to pass through a wall without interaction	
Γ_o	original number of particles to hit the wall	
ε	$1 - \alpha$ one minus the coupling coefficient	
λ	radiation thickness of the wall	radiation lengths
λ	$1/(r + 1)$ ratio of superconductor to the metal	
μ	viscosity	$kgs^{-1}m^{-1}$
μ_o	magnetic permeability of vacuum $\mu_o = 4\pi \times 10^{-7}$	Hm^{-1}
ρ	mass density	kgm^{-3}
ρ	electrical resistivity	ohm m
$\rho_{cu}(T)$	electrical resistivity of copper as a function of temperature	ohm m
$\rho_m(T)$	electrical resistivity of low resistance normal metal	ohm m
ρ^*	average resistivity of the matrix material near the filaments	ohm m

σ	signal from the shunt signal integrator	V
$\tau(t)$	time constant as a function of time	s
τ_1	coil time constant	s
τ_2	bore tube time constant	s
τ_s	short time constant for the coupled coil system	s
τ_L	long time constant for the coupled coil system	s
$\tau_c(t)$	measured time constant for the coil as a function of time	s
$\tau_{AL}(t)$	measured time constant for the bore tube as a function of time	s
τ_{I1}	shunt signal integrator time constant	s
τ_{I2}	coil signal integrator time constant	s
$\Xi(t)$	ratio of superconductor matrix current density as a function of time with the initial matrix current density	
$\Phi(t)$	total magnetic flux as a function of time	weber
$\Phi_c(t)$	magnetic flux due to current in the coil as a function of time	weber
$\Phi_{AL}(t)$	magnetic flux due to current in the bore tube as a function of time	weber
Ψ	signal from the P signal integrator	V

THE DEVELOPMENT OF LARGE HIGH CURRENT DENSITY SUPERCONDUCTING MAGNETS
FOR USE IN HIGH ENERGY PHYSICS EXPERIMENTS

Michael A. Green

Mechanical Engineering Department
Lawrence Berkeley Laboratory
University of California
Berkeley, California 94720

ABSTRACT

This report describes the development of a unique type of large
superconducting solenoid magnet, characterized by very high current
density windings and a two-phase helium tubular cooling system. The
development of the magnet's conceptual design and the construction
of two test solenoids are described. The successful test of the super-
conducting coil and its tubular cooling refrigeration system is presented.
The safety, environmental and economic impacts of the test program
on future developments in high energy physics are shown.

Large solid angle particle detectors for colliding beam physics
will analyze both charged and neutral particles. In many cases, these
detectors will require neutral particles, such as gamma rays, to pass
through the magnet coil with minimum interaction. The magnet coils
must be as thin as possible. The use of superconducting windings
allows one to minimize radiation thickness, while at the same time
maximizing charged particle momentum resolution and saving substantial
quantities of electrical energy.

One must operate the superconductor in the coil at current densities
approaching 10^9 Am^{-2} in order to minimize radiation thickness. The
detector magnets will have stored magnetic energies approaching 10 MJ.
Magnets of this stored energy normally operate at current densities

below 10^8 Am^{-2}. The key to operating a large solenoid magnet at current densities of 10^9 Am^{-2} is the use of a closely coupled, low resistance bore tube. This bore tube permits one to remove most of the current in the superconducting coil without developing high transient voltages. As a result, damage to the magnet is prevented in the event it should turn normal while operating at high current densities.

Two one-meter diameter test solenoids were built using two different superconductors. The construction and instrumentation of these two magnets are described. Each of the two magnets has a low resistance aluminum bore tube, a high current density winding, and a layer of aluminum tubes which carry two-phase helium. The whole assembly is cast in filled epoxy to form a single integrated unit which has minimum radiation thickness.

The tubular cooling system eliminates most of the problems which are found in the cryogenic systems of large superconducting magnets. This two-phase cooling system was successfully tested using a helium refrigerator. The magnets were stable at temperatures around 4.8 K. The cool down and operating characteristics of the two-phase cooling system are presented in this report.

The magnetic tests of the solenoid were entirely successful even when the solenoid coil current density was over 10^9 Am^{-2}. The low resistance bore tube behaved entirely as the theory predicted. The magnets were driven normal artificially by using small quench coils, and accurate measurements of normal region propagation were made. The current shift from the coil to the bore tube was measured as the magnet turned normal. This current shift resulted in a new phenomenon

0 0 0 0 4 6 0 1 1 0 2

-xvii-

called "quench back". Strain measurements in the magnet bore tube show how the epoxy in the two magnets behaved.

The results of the experimental measurements show that large high current density solenoid magnets can be made to operate at high stored energies. The superconducting magnet development described in this report has a positive safety and environmental impact. The use of large high current density thin superconducting solenoids has been proposed in two high energy physics experiments to be conducted at the Stanford Linear Accelerator Center and Cornell University as a result of the successful experiments described in this report.

I. HIGH ENERGY PHYSICS AND THIN SUPERCONDUCTING SOLENOIDS

Some of the most exciting high energy physics today is being done at the Stanford Linear Accelerator Center (SLAC) in the United States and at the Deutsche Electron Synchrotron (DESY) in Hamburg, West Germany. At both laboratories there exist electron-positron colliding beam storage rings where collisions take place at center of mass energies as high as 8 GeV.

At SPEAR, the electron-positron storage ring facility at SLAC, three new particles called ψ particles have been discovered.[1] One of these particles (the lowest mass particle) was discovered simultaneously by a group at the Brookhaven National Laboratory,[2] who call the new particle a J particle. A group at Frascati[3] in Italy and a group at DESY[4] in Germany have confirmed the existence of some of the new particles. In addition, a Lawrence Berkeley Laboratory (LBL) SLAC group has apparently confirmed the existence of charm[5], one of the basic properties of quarks, which, according to modern particle physics theory, are the building blocks from which other particles are fabricated.

Much of the interesting physics done at SPEAR has been done in a magnetic detector, called MARK I,[6] which uses conventional water-cooled coils. The MARK I magnet generates a magnetic induction of 0.4 tesla inside a solenoid which is 3 meters in diameter and 3 meters long. The purpose of the large magnetic field volume is to detect and analyze the momentum of the charged particles.

The next generation of electron-positron storage rings, now under construction at SLAC[7] and DESY,[8] will require even larger and more complicated magnetic detectors. The scheduled turn-on date for PETRA,

the 19 GeV electron-positron storage rings at DESY, is early 1979. The turn-on date for PEP, the SLAC-LBL 18 GeV machine under construction at SLAC, will be early 1980. A number of the proposals for magnetic detectors for PEP and PETRA use thin superconducting solenoid magnets[9-11]; this paper aims to conceptualize such a magnet for use in the PEP system.

Before proceeding with conceptual design of a thin superconducting solenoid for a magnetic detector, it is useful to ask three questions: (1) What is the geometry of the experiment? (2) Why use a superconducting solenoid? (3) And, why use a thin superconducting solenoid? The answer to these questions is the motivation behind the LBL large thin superconducting solenoid development program.

1.1. What is the Geometry of the Experiment?

Both the PEP and the PETRA machines will be circular machines with circumferences of about 2 kilometers. The PEP machine will be divided into six superperiods, each with a long experimental straight section about 40 meters long. At the center of these straight sections bunches of electrons and positrons will collide, creating fragments to be analyzed by the high energy physicist. Figure 1 is an aerial view, and Figure 2 is a schematic view of the PEP machine. Since the collisions of the electrons and positrons will occur only at or near the center of these long straight sections, the experiment with its magnetic and non-magnetic detectors must be built around the center of the straight section. The beam pipe forms a natural axis for the experiment. For this reason most of the experiments proposed for PEP and PETRA have cylindrical symmetry with the axis of the cylinder being the electron-positron beam itself.
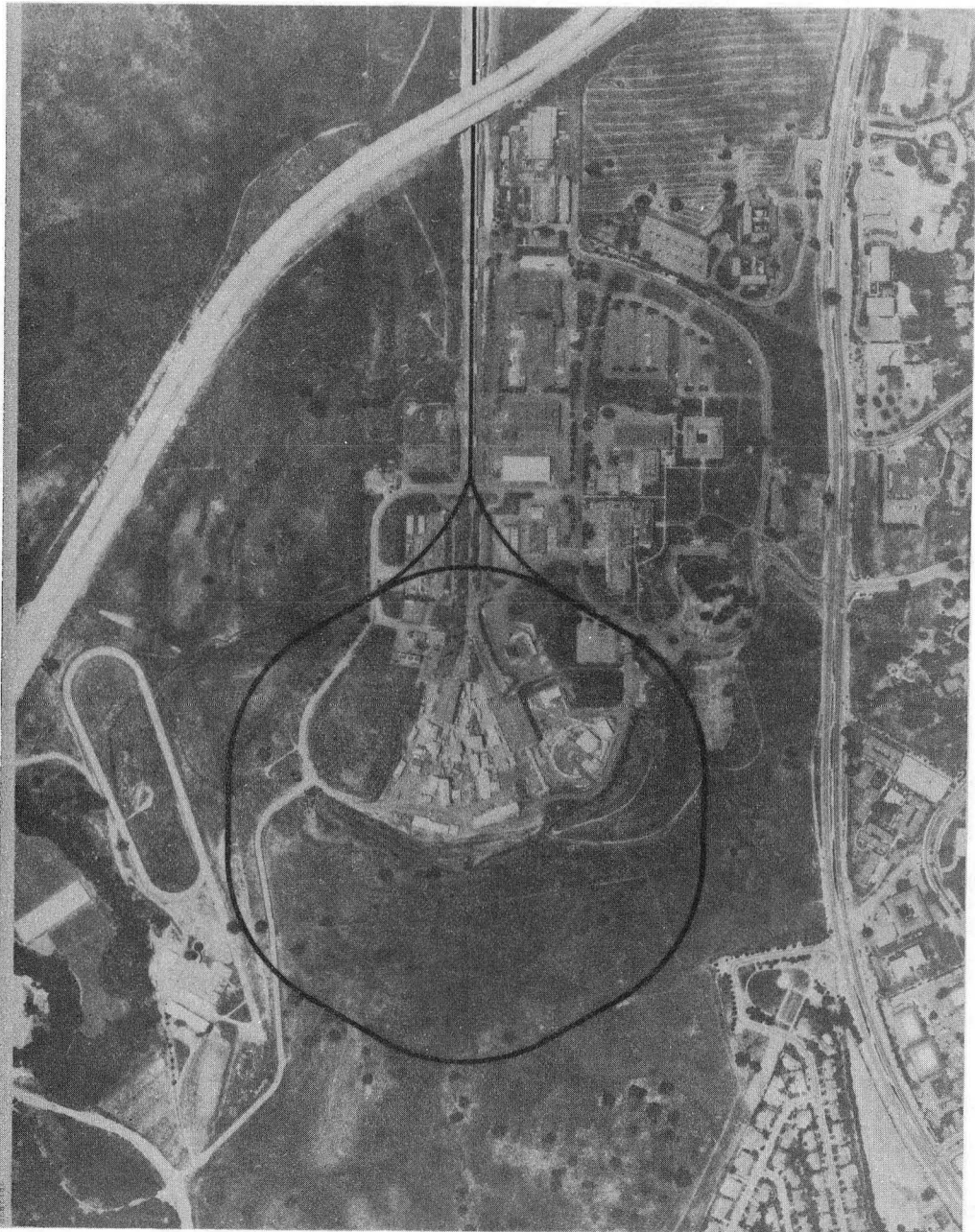
XBB 776-5800

Fig. 1. An aerial view of the Stanford Linear Accelerator.
The location of the PEP Colliding Beam Machine is shown
in black. (Note Interstate 280 between San Francisco
and San Jose cuts across the upper left-hand corner, and
Sand Hill Road runs down the right side of the picture.)

-4-

PEP Ring Parameters

Ring Circumference	2000 m
Number of Interaction Regions	6
Maximum Energy	18 GeV
Length of the Interaction Region	20 m
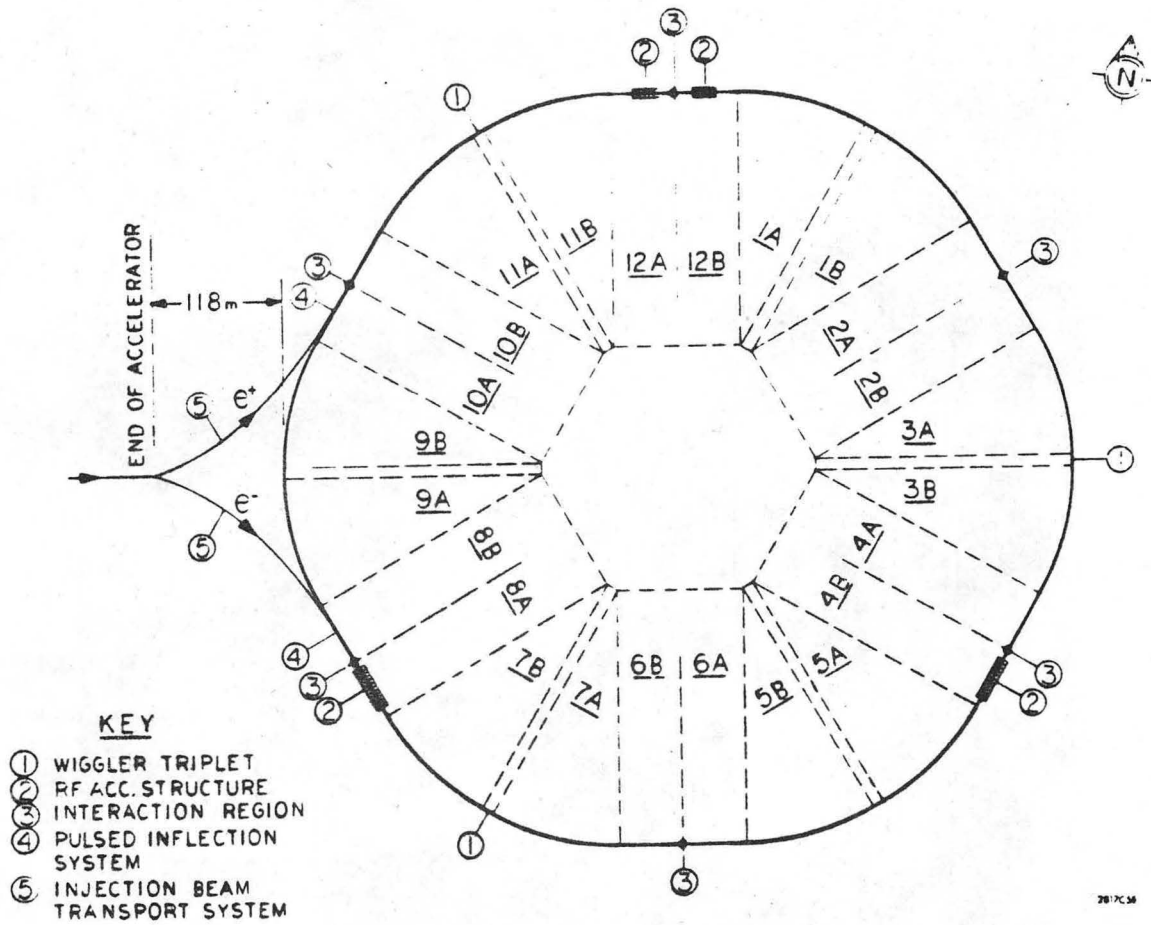
Fig. 2. A schematic view of the PEP electron-positron colliding beam storage ring. The physics experiments are located at the center of the interacting regions.

Many of the magnetic detectors for PEP and PETRA propose to cover a large solid angle (say 90% of 4π). Therefore, the magnetic detector should cover a spherical area from a disc perpendicular to the beam axis at the collision point (an angle of $90°$ from the axis) to an angle between 20 and $30°$ from the axis in both directions. The magnetic field is contained in a cylindrical region which has a length about twice its diameter.

The minimum outside diameter of the magnetic detector volume is determined by the quality of momentum resolution desired. The momentum resolution of particles improves with $D^2 B_o$ where D is the outer diameter of the detector and B_o is the average induction in the detector. The minimum momentum resolution of the detector is an inverse function of B_o and proportional to the minimum tracking tube diameter of the detector.

Small magnets are less expensive than large magnets. For a given central induction B_o the magnet cost will go up as D^2 or perhaps even faster. The construction of a detector magnet, as with any other endeavor, is a compromise between the money available and the scientific objective one is trying to achieve in the experiment.[12]

1.2. Why Use a Superconducting Solenoid?

Superconducting magnets are being considered for use in charged particle detectors in colliding beam machines for the following reasons: (1) The central induction of the magnet can be increased by a factor of three. This increase in central induction permits the momentum resolution to be increased for a given size magnet or it permits the magnet size to be reduced for a given momentum resolution. (2) The electric power and cooling water consumption of the magnet are reduced

if it is superconducting. As a result, the total cost of a supercon-
ducting magnet system is less in many cases than a conventional
magnet system. (3) Superconducting magnets can be operated at high
current densities. This allows interesting physics experiments to be
done outside the magnet coil. As a result, the physics experiments
become more flexible and less costly.

Three types of magnets can be considered for use in magnetic
detectors: (1) the dipole, (2) the toroid, and (3) the solenoid. All
three types of magnets can be used to analyze charged particles which
travel perpendicular to the flux lines generated by the magnet. The
three types of magnets are shown in Fig. 3.

The first type, the dipole magnet, is commonly used in conventional
spectrometers for momentum analysis. In an electron-positron storage
ring the dipole would be oriented so that the particle beam transverses
down the bore of the magnet. Since the magnetic field is perpendicular
to the direction of the electron-positron beams, the dipole will analyze
longitudinal momentum very well. Transverse momentum will be analyzed
well in one direction but not the other. The major disadvantage of
the dipole is its effect on the circulating beam of the machine. A
large dipole will adversely affect the orbit in any storage ring. As
a result, extensive first-order field compensation is required. In an
electron-positron storage ring, the field perpendicular to the direction
of beam travel will plague the experiment with synchrotron radiation.
As if the other disadvantages were not bad enough, superconducting
dipole magnets are difficult and expensive to build.

0 0 0 0 4 6 0 1 1 0 6

-7-
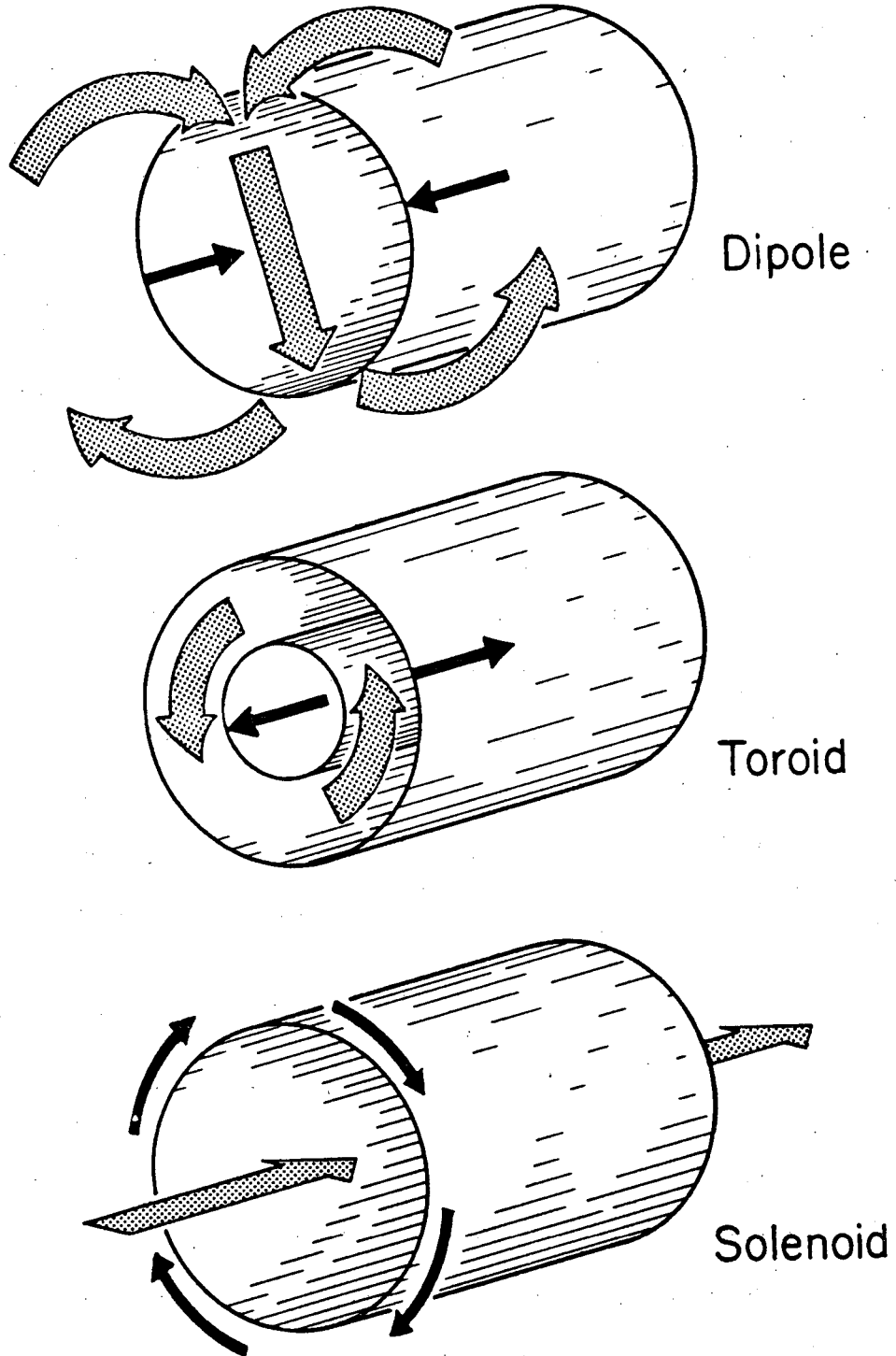
Dipole

Toroid

Solenoid

XBL 759-4190

Fig. 3. Types of magnets which can be used for magnetic
detectors (the dark lines show the current flow
direction; the shaded lines show the magnetic
flux direction).

The toroid, in theory, has no field in the region of the beam. The magnet offers good momentum resolution in both the longitudinal and transverse (radial) directions. However, it will have a coil interposed between the magnetic detector and the beam; this is undesirable. The field in a toroid is not uniform but instead varies inversely with radius. Like the dipole, the toroid is difficult and expensive to build.

The solenoid has its field parallel to the direction of the circulating particle beams. Full integral field compensation is required; but the second-order effects on the beam are small. There is almost no material between the colliding particle beams and the magnetic detectors. Transverse momentum is accurately resolved; longitudinal momentum is not accurately resolved. Superconducting solenoids are easy to build compared to the other types. As a result, nearly all of the proposed colliding beam experiment detector magnets will be solenoids which have the axis parallel to the direction of motion of the colliding beams.

1.3. Why Use a Thin Superconducting Solenoid?

The capital cost of magnetic detector experiments for PEP and PETRA is estimated to exceed six million dollars. While the magnet is estimated to be only about one sixth of the experiment's cost, the need to save money is prevalent. Substantial cost savings can be achieved if physics can be performed outside of magnetic field volume as well as inside the magnet. Also there are types of detectors, such as photomultiplyer tubes, which must be operated in little or no magnetic field. In order to achieve this, substantial numbers of charged and neutral particles must pass through or between the detector magnet coils.

Two approaches can be used to pass a substantial number of particles through the region occupied by the solenoid magnet coil: (1) one may lump the current in the solenoid into several discrete current lumps, or (2) one may make a uniformly thin coil. The viability of the lumped coil approach as compared to the thin coil approach depends on how thin the coil can be made.[13]

The advantage of the lumped coil is that there are regions between the coils which have almost no thickness at all. This is a distinct advantage in some kinds of experiments. Other experiments will be adversely affected by the thick coils which can impede particles from passing through about 25% of the solid angle. The thin coil approach permits particles to pass through the magnet at all solid angles, although the probability of particles passing through at low angles is less than the probability of their passing through at high angles. For many experiments, if both types of magnets have the same number of particles passing through the region occupied by the coil, one will choose the thin coil magnet. The reasons for this will become more apparent as we proceed.

The lumped coil magnet has a number of disadvantages over the thin coil magnet: (1) Since current is in discrete lumps, the peak field at the superconductor is always much higher than the central induction of the magnet.[14] A thin coil magnet has a peak induction in the coil which is only a few percent higher than central induction (if the magnet is bound at the ends by iron poles). (2) The magnetic field uniformity inside the lumped coil magnet is not as good as that in the thin coil magnet. (This is particularly true when iron poles are

used.)   (3) In order to gain advantage from a lumped coil detector, the region between the coils must be very thin from a radiation standpoint. The lumped coil magnet must really consist of many magnets, each with its own cryostat, or it becomes a single structure with many thin windows. In either case, the cryogenic system for the lumped coil magnet is considerably more expensive than the thin coil magnet. Studies at LBL[15] and the Rutherford High Energy Laboratory[16] indicate that the lumped coil system costs a factor of 1.5 to 2 more than a thin coil system for a magnet with a given useful volume.

Therefore, it can be argued that at least one of the magnetic detectors for PEP should be a thin solenoid with an approximate diameter of 2.0 meters and a length of 4.0 meters. The design central induction should be from 1.0 to 1.5 tesla; the radiation thickness of the super-conducting coil, and the cryogenic system, should be as low as possible in order to maximize the percentage of particles that will pass through the magnet without being converted to other particles or absorbed. Additionally, the thin solenoid magnet should have iron poles and an iron return path for the following reasons: (1) The number of ampere turns needed to generate the magnetic field is minimized; (2) the peak field rise in the coil is minimized; (3) the magnetic field uniformity inside the magnet is improved--this is very important for some kinds of detectors;[17] and (4) the field outside the coil is minimized. When the field outside the coil is low, photomultipliers and other sensitive electronics can be used in that region.

II. DEVELOPMENT OF A CONCEPTUAL DESIGN

The basic design concepts which will be employed in PEP and PETRA detector magnets were conceived during the last two months of 1974. P. Eberhard of Group A Physics at LBL asked if a low radiation thickness superconducting solenoid magnet could be incorporated into an experiment proposed for SPEAR. That experiment, called MINIMAG,[18] was to develop a large solid angle magnetic detector surrounded by lead glass counters to detect neutral gamma particles. It was felt that a superconducting magnet would result in a power saving and increased momentum resolution of the charged particles. Table 1 shows a comparison of conventional and superconducting MINIMAG magnet parameters.

The development of the MINIMAG superconducting solenoid required that three questions be answered: (1) How can one reduce the system radiation thickness to 0.33 radiation lengths or lower? (2) How can a large diameter coil be made to operate safely, yet be thin from a radiation standpoint? (3) How can the cryogenic problems which seem to plague large superconducting magnets be avoided?

Intuition played an important role in providing answers to the three questions. It was clear that the magnet and cryogenic system problems had to be solved together. This approach is not usually followed by superconducting magnet builders, who tend to assume that someone else will provide a vessel full of liquid helium for their magnets. Many failures and setbacks with superconducting magnets can be attributed to this attitude. As a result of answering the three questions as one, an integrated design concept emerged. This design concept has the following components integrated into a single unit:

Table 1. A comparison of conventional and superconducting magnets
         for the MINIMAG experiment.

Parameter	Conventional	Superconducting
Inside diameter (m)	0.9	0.9
Outside diameter (m)	1.1	1.1
Length between iron poles (m)	1.84	1.84
Central induction (T)	0.5	1.5
Induction outside coil (T)	<0.01	<0.01
Radiation thickness (Rad Len)	0.33*	0.33 **
Power consumption (MW)	1.6	<0.1

* Radiation thickness consists primarily of 30 mm of aluminum conductor.
  Total coil thickness including water cooling passages approaches 50 mm.

** Radiation thickness includes the superconducting coil and its
   cryostat.

(1) A high current density superconducting coil.

(2) A low resistance closely-coupled bore tube to control the

process of the magnet going normal.

(3) The two-phase helium tubular cooling system.

By February of 1975 a conceptual design for a superconducting

MINIMAG solenoid had emerged.[19] The MINIMAG Proposal was unfortunately

not accepted for a number of reasons, both scientific and nonscientific.

Fortunately, however, the Laboratory felt that the continued development

of a thin superconducting solenoid should proceed for future PEP detectors.

2.1. Low Radiation Thickness Means High Current Density Magnet Coils

The requirement of low radiation thickness has an important effect

on the design of the superconducting coil. Before proceeding, it

is useful to define the meaning of radiation thickness. One radiation

length of any material is enough material to convert about 63% of

high energy gamma rays to charged particle pairs. In general, the

number of particles Γ which pass through an amount of material unchanged

is a function of the original number of particles Γ_o and the radiation

thickness λ given in radiation lengths. To the first order the

functional relationship is

$$\Gamma = \Gamma_o e^{-\lambda} \quad . \tag{1}$$

In general, materials which are thin from a radiation standpoint

have low density and low atomic number. The thickness of one radiation

length of many materials may be found in Reference 20 or in Table 2.

Table 2. The thickness of various materials which equals one
radiation length.

Material	Density (g cm^{-3})	Thickness (mm)
Elemental Material		
Helium (liquid)	0.125	7450
Lithium	0.53	1560
Beryllium	1.85	357
Carbon	variable	~670
Magnesium	1.74	145
Aluminum	2.70	90
Iron	7.87	17.7
Copper	8.96	14.5
Tin	7.31	12.2
Lead	11.35	5.6
Uranium (238)	18.95	3.2
Metallic Alloys		
304 Stainless Steel	7.8	17.5
Niobium-Titanium (50% Ti)	~7	~18.9
Copper-Based Composite		
copper to S/C ratio 1-2	variable	15.2-16.2
Aluminum-Based Composite		
Al to S/C Ratio 1-2.5	variable	27-41
Magnesium Lithium Alloy	1.35	265
Brass	variable	11-13
Plastics and Plastic Composites		
Mylar	1.39	292
Polyethelene	0.95	490
Polystyrene	1.03	430
Epoxy-Dacron	variable	~360
Epoxy-Glass	variable	~180

Methods for calculating the radiation thickness of other materials
are found in Reference 21.

A typical copper-based superconductive composite consists of niobium,
titanium, and copper which have atomic numbers of 41, 22 and 29
respectively. The thickness of one radiation length of a copper-based
superconducting composite varies from 15.5 to 16.2 mm. The superconductor
cannot, as a rule, be over about 40% of the total radiation thickness
of the magnet and its cryostat. This means that the thickness of
a copper-based superconducting coils, alone cannot be over 2.2 mm
if the total system thickness is to be 0.33 radiation lengths. This
suggests that the coil will operate at high current densities.

An analytic expression for the minimum conductor current density J_{min}
is given by:

$$J_{min} \approx \frac{B_o}{\mu_o s} \qquad (2)$$

where B_o is the central induction of the solenoid, $\mu_o = 4\pi \times 10^{-7}$
(the permeability of air) and $S = 2.2 \times 10^{-3}$ m.

A minimum radiation length coil results from the superconductor
being used at maximum current density. This current density is a
function of both temperature and maximum field in the conductor.
A simple analytic expression for the maximum superconductor matrix
current density J_{max} in a solenoid with iron poles is given by:

$$J_{max} \approx \frac{1600 \; B_o^{-0.5}}{\mu_o} \qquad . \qquad (3)$$

Table 3 shows the minimum and maximum superconductor matrix current

densities for a copper-based superconducting magnet system which is

to be 0.33 radiation lengths thick.

Equations 2 and 3 are simplified, but actual coils which have been

proposed for thin detector magnets lie within the limits shown in

Table 3. The use of newly developed, but untested, aluminum-based

superconductor[22] will reduce the minimum current density by around

40 percent. It is clear that with either copper-based or aluminum-

based superconductors the current density in the coil will be high.

2.2. Stability of Superconducting Coils

Pure superconductors are very unstable when used in magnets.

They have a tendency to go normal spontaneously at currents which are

well below their critical current. Typically, once the superconductor

goes normal, the magnet quenches. In other words, the energy from

the magnetic field is dumped suddenly into the coil. Two methods

of stabilizing superconductors are commonly used; the first is cryogenic

stabilization and the second is intrinsic or adiabatic stabilization.

Cryogenic stability, introduced by Steckly[23] in 1965, requires that

the superconductor be able to carry all of its current in the normal

metal without heating the superconductor above its critical temperature.

Cryogenically stable coils do not quench (dump their magnetic energy)

because the current can leave the superconductor and return without

heating the superconductor. Since cryogenically stable magnets do

not quench, virtually all of the large superconducting magnets use

cryogenic stabilization. Before rushing to apply the principle of

Table 3 Maximum and minimum superconductor composite current density
        limits for thin superconducting solenoid coils as a function
        of central induction. ($\lambda =$ 0.33 with copper based super-
        conductor.)

Central Induction (T)	Current Density $(A\ m^{-2})$	
	Minimum	Maximum
0.50	0.18×10^9	1.80×10^9
0.75	0.27×10^9	1.47×10^9
1.00	0.36×10^9	1.27×10^9
1.25	0.45×10^9	1.14×10^9
1.50	0.54×10^9	1.04×10^9
1.75	0.63×10^9	0.96×10^9
2.00*	0.72×10^9	0.90×10^9

* Above 2.0 tesla central induction, the iron poles saturate. Extra
  ampere turns of superconductor are required in order to overcome
  the effects of iron saturation.

cryogenic stability to our thin solenoid problem, it is useful to look at the operating current densities J_{cs} for cryogenic stable magnets.

An expression for this current density is:

$$J_{cs} \approx \left[\frac{QA}{\rho}\right]^{1/2} \tag{4}$$

where Q is the heat flux transmitted to liquid helium such that the temperature in the superconductor is less than the critical temperature, (usually around 3,000 Wm^{-2}), A is the area of surface exposed to helium per cubic meter of superconductor (A is usually about 150 m^2), and ρ is the resistivity of the superconducting matrix when it is in the normal state (for copper $\rho \approx 1 \times 10^{-10}$ ohm m). Solving equation 4, one can see that $J_{cs} = 6.71 \times 10^7$ A m^{-2}. This is about a factor of three below the minimum current density required for a radiation thickness of 0.33 radiation lengths. Thus we find that cryogenically stable super-conducting coils are not suitable for thin detector solenoids.

Since cryogenic stability cannot be employed, one must use the principle of intrinsic or adiabatic stability. The principle of intrinsic stability, which was developed by Hancock,[24] Smith[25] and Chester,[26] requires that the superconductor be constructed in a special way. An intrinsically stable superconductor has the following characteristics: 1) The superconductor is divided into hundreds of small filaments which are less than 40 μm in diameter. 2) The fine superconducting filaments are co-drawn within a matrix which contains substantial amounts of low resistivity normal metal. 3) The superconducting filaments are

transposed or twisted so that normal metal to superconductor circulating currents do not develop. This twist pitch is typically only 10 to 20 times the diameter of the composite (the composite consists of both superconductor and the normal metal). 4) High current density intrinsically stable superconductors contain between one and two times as much normal metal as superconductor (this is called the normal metal to superconductor ratio.)

High current density magnets which are made from intrinsically stable superconductors can quench. If the stored energy of the magnet is low (the magnet is small), this is of no consequence. As the size and stored energy of the magnet grows, quenching becomes more of a risk. A PEP detector solenoid magnet is not supposed to quench; however, in the event that it does, it must survive the quench. For that reason, existing high stored energy magnets (say greater than 1 or 2 megajoules of magnetic energy) are all low current density cryo-genically stabilized magnets. Figure 4 shows the stored energy and current density of a number of superconducting magnets which have been built in the last 15 years. From this figure one can see that virtually all of the magnets follow a law which states that the higher the stored energy, the lower the current density. The PEP detector magnets, which will have a stored energy of more than 10 MJ, will have a current density in the superconductor of $0.8 - 1.0 \times 10^9$ Am^{-2}. This combination lies well out of range of normal practice for superconducting magnets. If the PEP detector magnets were built using normal techniques, the magnet would destroy itself during the first quench. The secret to preventing this destruction is the low resistance, closely coupled bore tube.
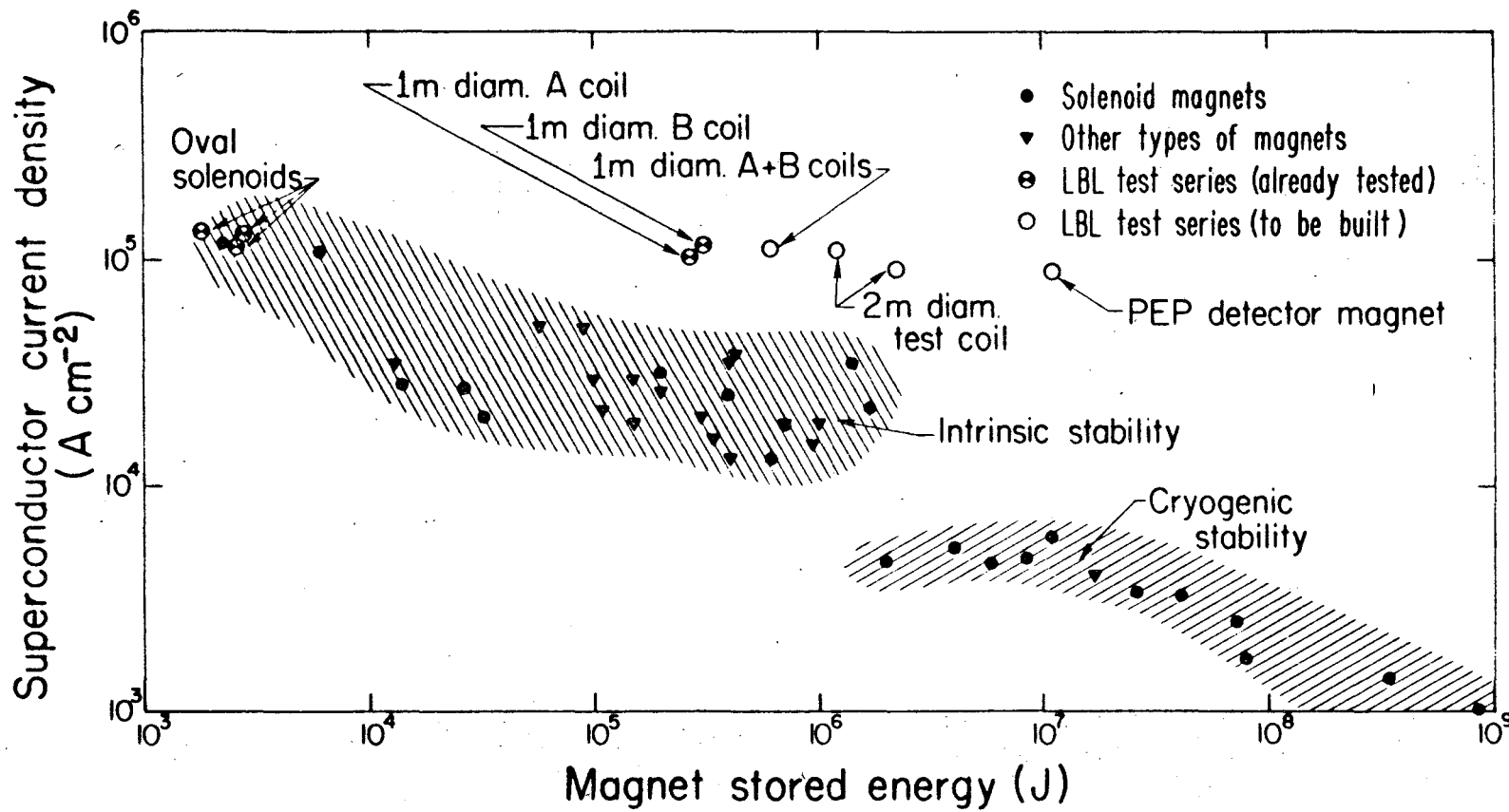
Fig. 4. A plot of current density in the superconductor of various magnets vs
the stored magnetic energy of that magnet. (Note the LBL thin magnet
series operates at current densities much higher than the state of the
art which is indicated by the shaded regions.)

XBL 769 4017

2.3. The Closely Coupled, Low Resistance Bore Tube to Control Magnet Quenching

Large thin coil detector solenoids are potentially subject to destruction during a magnet quench. The two primary causes of coil failure during a quench are: 1) Hot spots are formed in the coil due to the uneven distribution of quench energy in the coil. Normal regions propagate within a coil at finite velocities. Thus, part of the coil is superconducting while another part of the coil is normal. 2) There are excessive transient voltages due to the uneven resistance distribution within the coil. These transient voltages can cause substantial damage to the coil due to arcing. The formation of hot spots and transient voltages are usually directly related.

An upper bound estimate of the hot spot temperature can be found by assuming that a small section of superconductor is heated only by resistive heating and that there is no heat transfer out of that section. The Tollestrup[27] approximation is fairly valid once that small section of superconductor has reached a temperature of 30 K or above.[28] The Tollestrup approximation says that one can find the peak hot spot temperature by using the following integral expression:

$$ F(T) = \int_{T=0}^{T=T_{hot}} \frac{C(T)}{\rho(T)}\, dt = \int_{t=0}^{\infty} J(t)^2\, dt \qquad (5) $$

where for a typical copper-based superconductor

$$\rho(T) = \rho_{cu}(T) \frac{1 + r}{r} \tag{5a}$$

$$C(T) = C_{cu}(T) \tag{5b}$$

where $C_{cu}(T)$ is the specific heat per unit volume of copper as a function of temperature T; $\rho_{cu}(T)$ is the electrical resistivity of copper as a function of temperature, r is the copper to superconductor ratio; J(t) is the superconducting composite current density as a function of time t. The maximum hot spot temperature T_{hot} as a function of the integral F and r is shown in Figure 5.

It is clear from equation 5 that one must reduce J in the conductor as quickly as possible in order to minimize the hot spot temperature. The usual method for doing this is to put a resistor across the leads of the magnet. This reduces J and a portion of the energy of the magnetic field ends up in the external resistor instead of in the coil. The electrical circuit diagram for this scheme is shown in Figure 6a. The equation which describes the behavior of the circuit shown in Figure 6a is as follows:

$$L_1 \frac{di_1}{dt} + i_1 R_1 = 0 \tag{6}$$

where the resistance R_1 is the sum of the coil resistance R_c and the external resistance R_e.
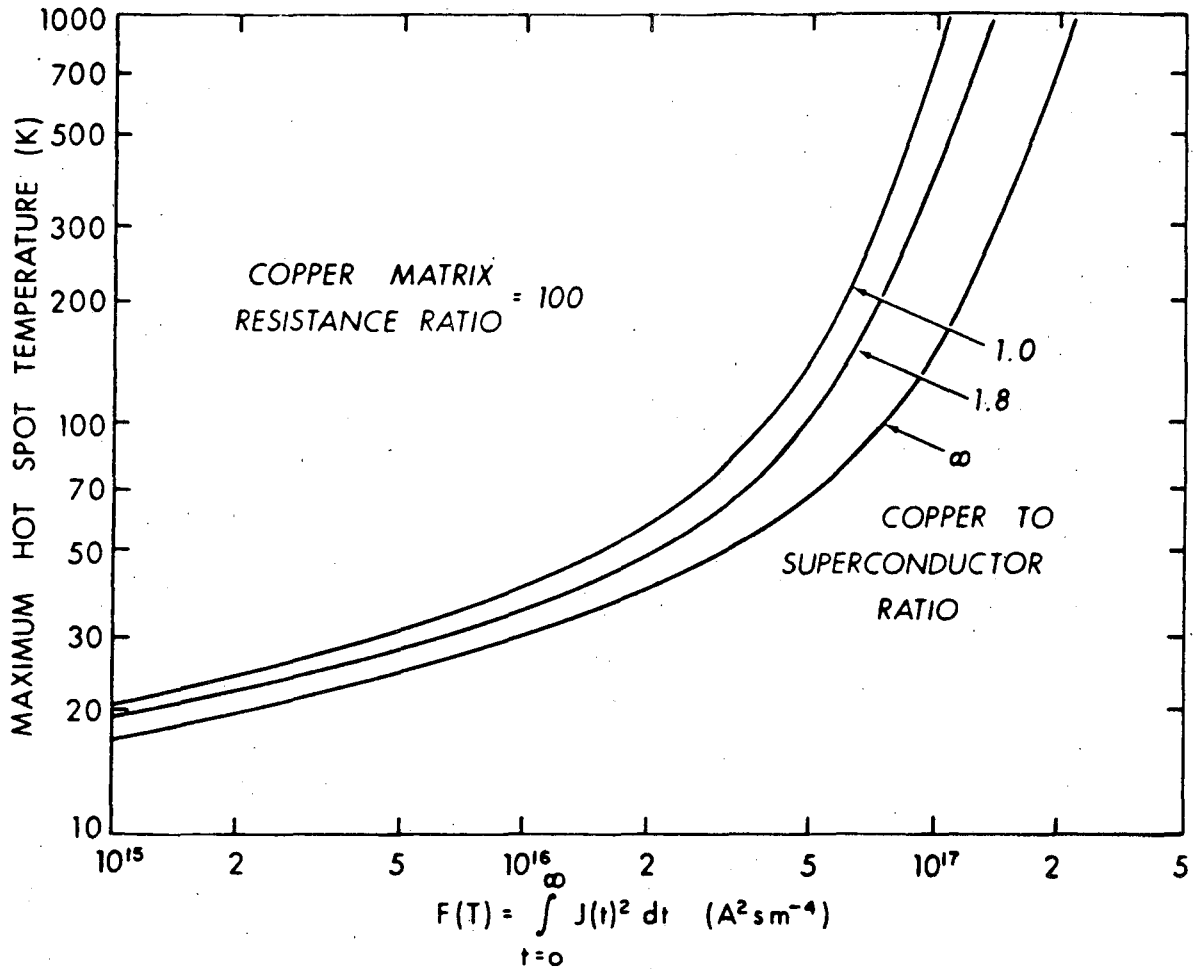
Fig. 5. The hot spot temperature vs the integral of current density squared with time for copper-based superconductors with copper (resistance ratio = 100) to superconductor ratios of 1.0, 1.8 and ∞.
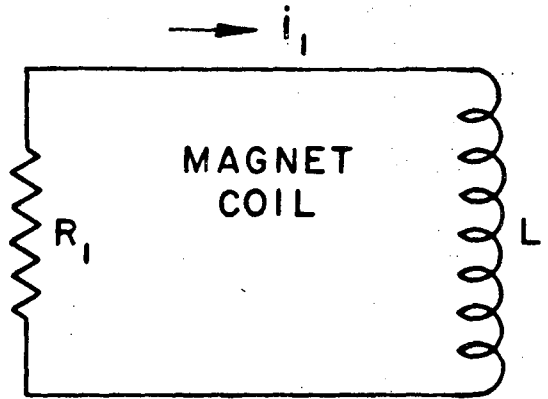
a) MAGNET COIL WITHOUT THE BORE TUBE
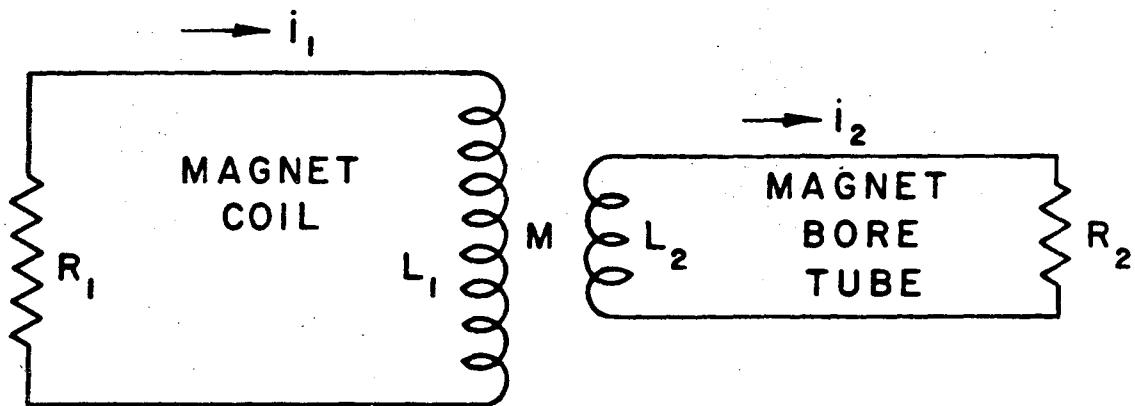
b) MAGNET COIL WITH THE BORE TUBE

XBL 773-7855

Fig. 6. The electrical diagrams of magnets without and
with conductive bore tubes.

$$R_1 = R_c(t) + R_e \qquad \qquad (6a)$$

and when i_1 is the coil current, L_1 the coil inductance, the initial condition for equation 6 is:

$$i_1 = i_0 \quad \text{when} \quad t = 0 \qquad \qquad (6b)$$

if one assumes that R_1 in equation 6 is constant with time. The solution to the differential equation takes the following exponential form:

$$i_1 = i_0 e^{-t/\tau_1} \qquad \qquad (7)$$

where

$$\tau_1 = \frac{L_1}{R_1} \quad . \qquad \qquad (7b)$$

The smaller τ_1 the faster the current in the magnet decays. Thus the larger the external resistance R_e the faster the current is removed from the conductor.

The external resistor quench control method works fairly well for moderate current density magnets which operate at high currents through the electrical leads. In high current density detector solenoids the external resistor approach has a number of faults: 1) the external resistor increases the magnetic flux change $d\phi/dt$, which aggravates an already bad transient voltage problem, and 2) in order for the external resistor quench control method to work, one must detect the

quench early so the external resistor can be put into the coil early. Such detection systems are prone to failure.

The external resistor approach was abandoned because it does not solve the quench problem in a fail-safe manner. Intuition suggested that another approach was possible. An external resistor could be coupled to the coil by a transformer. From there, the use of a low resistance bore tube closely coupled to the coil as a shorted turn secondary in a transformer became obvious. The circuit diagram for the scheme is shown in Figure 6b. The equations which describe the behavior of the circuit shown in Figure 6b are as follows:

$$L_1 \frac{di_1}{dt} + M_{12} \frac{di_2}{dt} + i_1 R_1 = 0$$

(8)

$$L_2 \frac{di_2}{dt} + M_{12} \frac{di_1}{dt} + i_2 R_2 = 0$$

where the coil circuit resistance R_1 and bore tube resistance R_2 take the form

$$R_1 = R_c(t) + Re$$ (8a)

$$R_2 = R_b(t)$$ (8b)

and where i_1 is the current in the coil; i_2 is the current in the secondary loop (the bore tube); L_1 is the coil inductance; L_2 is the

bore tube inductance; and M_{12} is the mutual inductance between the coil and the bore tube. The initial conditions for the above equations are:

$$i_1 = i_0$$

$$\text{(8c)}$$

$$i_2 = 0$$

at t = 0. The inductances L_1, L_2 and M_{12} are approximately as follows when the solenoid coil is bounded at the ends by infinite permeability iron poles:[29]

$$L_1 \approx \mu_o \pi a_1^2 N_1^2 / \ell_1 \tag{8d}$$

$$L_2 \approx \mu_o \pi a_2^2 / \ell_2 \tag{8e}$$

$$M_{12} \approx 2\mu_o \pi a_1 a_2 N_1 / (\ell_1 + \ell_2) \quad . \tag{8f}$$

The coupling of the system is supposed to be very good so we define coupling as follows:

$$\alpha = \frac{M_{12}^2}{L_1 L_2} \quad . \tag{8g}$$

The better the coupling, the closer α is to 1 as given by the definition in 8g.

When L_1, L_2, M, R_1 and R_2 are constants in equation 8, the solution takes the following form:

$$i_1 = \frac{i_0}{(\tau_L - \tau_s)} \left[(\tau_1 - \tau_s) \; e^{-t/\tau_L} + (\tau_L - \tau_1) \; e^{-t/\tau_s} \right]$$

(9)

$$i_2 = \frac{M_{12}}{L_2} \; \frac{i_0}{(\tau_L - \tau_s)} \left[(\tau_L + \tau_s - \tau_1) \; e^{-t/\tau_L} - (\tau_L + \tau_s - \tau_1) \; e^{-t/\tau_s} \right]$$

where the time constants τ_1, τ_2, τ_L, and τ_s are defined as follows:

$$\tau_1 = L_1/R_1$$

(9a)

$$\tau_2 = L_2/R_2$$

(9b)

$$\tau_L = \frac{\tau_2 + \tau_1}{2} \left\{ 1 + \left[1 - \frac{4\varepsilon\tau_2\tau_1}{(\tau_2 + \tau_1)^2} \right]^{1/2} \right\}$$

(9c)

$$\tau_s = \frac{\tau_2 + \tau_1}{2} \left\{ 1 - \left[1 - \frac{4\varepsilon\tau_2\tau_1}{(\tau_2 + \tau_1)^2} \right]^{1/2} \right\}$$

(9d)

where ε is nothing but one minus the coupling coefficient α. When ε is small τ_L and τ_s can be simplified to the following form:

$$\tau_L \approx \tau_1 + \tau_2 \qquad\qquad (9e)$$

$$\tau_s \approx \frac{\varepsilon \tau_1 \tau_2}{\tau_1 + \tau_2} \qquad\qquad (9f)$$

where

$$\varepsilon = 1 - \frac{M_{12}^2}{L_1 L_2} \qquad . \qquad\qquad (9g)$$

The solution to the coupled differential equations 8 given by equation 9 meets all of the initial conditions. The solution for small ε (good coupling between the coil and the bore tube) shows that i_1 drops very suddenly to a value which is less than the starting value. The bore tube current rises suddenly to a particular value which is less than $N_1 i_0$. Then the currents in the coil and bore tube decay slowly. Figure 7 compares the decay of i_1 with time for the two circuits shown in Figures 6a and 6b. The two longer time constants were chosen to be the same. The coupled bore tube current decay shows the characteristic sudden current drop. This is compared to the simple current decay characteristic of a simple resistor inductor circuit.

The magnetic flux in the magnet is the sum of fluxes generated by currents in the coil i_1 and by current in the bore tube i_2. When ε is small (when there is good coupling) the total flux contained in the magnet ϕ takes the following form:

$$\phi \approx \frac{M_{12} i_0}{(\tau_L - \tau_s)} \left[\tau_2 e^{-t/\tau_L} - \tau_s e^{-t/\tau_s} \right] \qquad . \qquad (10)$$
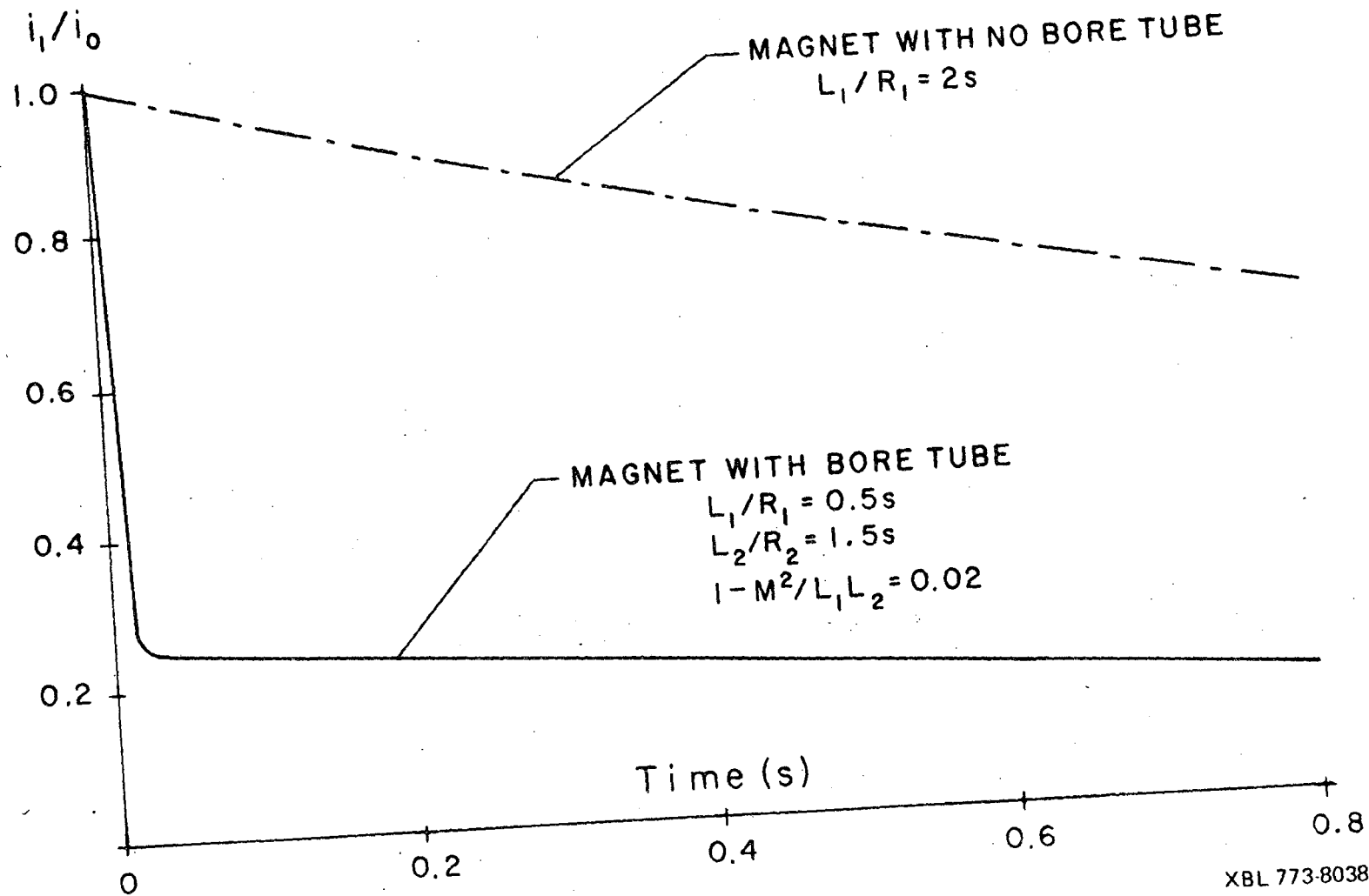
XBL 773-8038

Fig. 7. The ratio of current with starting current as a function of time for the two circuits shown in Fig. 6 (constant values of L_1, L_2, R_1, and R_2 are assumed).

From equation 10, one can see that flux in the coil decays with a time constant approaching the longer time constant τ_L while much of the current in the coil (equation 9) decays with a time constant approaching the shorter time constant τ_s. The transient voltages in the coupled system given by equation 8 go as $d\phi/dt$, not di_1/dt. Thus one can cause the current i_1 in the coil to drop quickly without creating large transient voltages.

The coupling between the coil and the bore tube should be better than $\alpha = 0.95$ ($\varepsilon = 0.05$). The resistance of the bore tube should be such that τ_2 is greater than τ_1 at all temperatures above 10 K. As a result, the well-coupled low resistance bore tube should affect the quench process in the following ways:

1) The bore tube behaves as a shorted secondary which causes a shift in current away from the coil to itself. The current in the coil is reduced, resulting in a reduction of the hot spot temperature.

2) The bore tube will absorb a substantial amount of the magnet stored energy during the quench process.

3) Since the time constant for magnetic flux decay is long compared to the time constant for the initial coil current decay, the transient voltages in the magnet coil system are greatly reduced. The bore tube, which is a single turn coil, has no transient voltage problem.

4) The bore tube causes portions of the coil to go normal which would not do so by ordinary quench propagation. This phenomena will be referred to as "quench back". The causes of quench back are described later.

The well-coupled low resistance bore tube controls the quench

process in a fail-safe manner. There are no unreliable electronic

components or switches to fail. To our knowledge, quench control

by the use of a well-coupled bore tube has not been done before.

Several years ago the Rutherford Laboratory in England had considered

the idea but they rejected it for fear it would not work.[30] As result

of our experimental work in November 1975, which showed that the concept

works, a number of laboratories are now considering the use of the

concept.[10,31]

2.4. The Two-Phase Helium Tubular Cooling System

A major problem with all large superconducting magnets is the

cryogenic and refrigeration system. All of the large magnets, which

are cryogenically stabilized, are cooled in a bath of boiling helium.

Nucleate boiling in liquid helium permits heat fluxes of 3000 Wm^{-2}

to be transferred with a temperature drop of less than 0.5 K.[32] The

bath-cooled magnet is difficult to cool from room temperature to 4 K.

Helium, which is a difficult fluid to use as a coolant because of

its low atomic weight, must flow into each region of the magnet;

if the flow in a section of the magnet is restricted, stratification

occurs and that magnet section remains warm.

Once the pool-boiled magnet is cold and the cryostat is filled

with liquid helium, the refrigeration problems are not over. Helium

has a very low heat of vaporization (20 Jg^{-1} at 4.2 K).[33] As a

result, the release of large quantities of magnet-stored energy during

a quench (in our thin coil system) will result in large quantities

of helium gas being flashed. For example, 1 MJ of energy will boil

400 liquid liters of helium into 286 m^3 (10,000 ft^3) of helium gas
at STP. The large amount of helium gas generated by a quench requires
careful design of the inner cryostat vessel and the relief valve system.
The thickness of a two-meter diameter pressure vessel which is designed
for at least three atmospheres is not trivial.

One is not restricted to bath cooling with an intrinsically stable
superconductor; it does not care how it is cooled as long as it is cooled.
Since heat generated in a dc solenoid is small (only the static heat
load and an eddy current heat load in the bore tube during charging
need be considered), a tubular cooling system will provide all of the
cooling that is needed. This system will also avoid all of the major
problems which are encountered in any large cryogenic system. The
advantages of the tubular cooling over an ordinary bath cooled system
are:

1) The cool down of the magnet is well-controlled because the
   helium flows in a well-defined path.

2) The mass of the tubular cooling system is less than that
   of a helium bath cryostat. The radiation thickness is also
   lower.

3) The amount of helium in direct contact with the magnet coil
   is minimized. Helium boil-off during a quench is orderly
   and well-controlled.

The tubular cooling system is not new. At least three superconducting
magnets use this system.[34,35,36] The Lawrence Berkeley Laboratory
system is different because it employs two-phase helium instead of
supercritical helium (the critical pressure of helium is 2.25 x 10^5

Pa; the critical temperature for helium is 5.19 K). The reasons for
choosing two-phase helium over supercritical helium are: 1) A two-
phase "boiling" helium system will operate at lower temperatures than
a supercritical helium system. Since the superconductor critical
current is a function of temperature, a lower operating temperature
will result in thinner coils. 2) The mass flow for a given amount
of refrigeration is lower for the two-phase system than for the supercritical
system. 3) The boiling two-phase system can transfer large local
heat fluxes without changing the temperature of the helium stream.

Stability of two-phase flow is achieved by choosing the right
flow regime. Here a bubble or froth regime was chosen, although the
two-phase flow system probably would have worked just as well in slug
or plug flow. A series of pressure drop calculations was done using
the Martinelli Nelson Technique.[37,38] Although the calculations agreed
with experiments, they turned out to be a waste of time. The much
simpler equation given below yielded almost the same results for round
tubes (the reason for this is that the density change across the two-
phase dome is less than a factor of 8).

$$\Delta P = \frac{0.8}{\pi^2} \frac{\dot{m}^2}{\rho} \left[1 + \frac{fz}{D} \right] \frac{1}{D^4} \tag{11}$$

where

$$f = 0.184\, Re^{-0.2} \quad \text{(tubulent flow smooth pipes)} \tag{11a}$$

and

$$Re = \frac{4\dot{m}}{\pi D \mu} \tag{11b}$$

and where m is the mass flow (kgs^{-1}), ρ is the average density of
the exiting helium (kgm^{-3}); Z is the tube length (m); D is the tube
diameter (m); μ is the helium gas phase viscosity (kgs^{-1}m^{-1}; note that
1 kgs^{-1}m^{-1} equals 10 poise); and ΔP is the pressure drop along the
tube (Nm^{-2} or Pa). (Note that 1 bar = 10^5 N m^{-1} = 10^5 Pa = 14.55 psi.)

2.5. Other Features of the Conceptual Design

The high current density thin superconducting coil, the low resisti-
vity, well-coupled bore tube and the tubular cooling system should be
cast into a single integrated system. The coil should be uniformly thick
along its length. All of the cryogenic services and the current services
should be in the end regions which may be thick from a radiation standpoint.

The cryostat supports should also be in the end region. The support
system should be self-centering during the cool down so that the position
of the magnet center remains unaltered.[39] Also, the support system should
be designed to support gravity loads and asymmetric magnetic forces which
can occur during operation or a quench. Shields and support points which
are at 80 K can be used in the end region where radiation thickness is
not important. The central part of the magnet could be covered by about
100 layers of multi-layer superinsulation inside and outside the coil
to reduce the heat leak; no 80 K shield in this region is needed.

The outer cryostat vacuum vessel must have minimum radiation thick-
ness, yet safety dictates that it must also resist buckling. Thus a
honeycomb or composite material, which is thin from a radiation standpoint,
is warranted. The inner part of the vacuum vessel ordinarily sees only
hoop tensile forces, yet safety dictates that it too must be designed
to resist buckling.

III.   THE ONE-METER DIAMETER TEST SOLENOID MAGNETS

Calculations of the conceptual design suggest that it should
be possible to build a large thin superconducting solenoid detector
magnet. But since the conceptual design has two unusual features, one
or more test coils should first be fabricated to test it. The Lawrence
Berkeley Laboratory chose to build two one-meter diameter test coils.

The diameter of the test coil was selected for very practical
reasons. LBL already had a cryostat in its warehouse with an inside
diameter of 1.118 m (44 inches). Since the cryogenic vessel already
existed at the "right price", the outside diameter of the magnet was
set to be about 42 inches (1.067 m). Except for the superconductor,
the two LBL test coils are identical. The reasons for building two
magnets are: 1) One can test the electrical and magnetic coupling
between the two coils. An understanding of the coupling process is
important for the development of modular lumped or thin coil solenoids.
2) One can test superconductors which have different characteristics.
For example, is it better to use a low copper to superconductor ratio
conductor or a high copper to superconductor ratio conductor?
3) Fabrication mistakes can be corrected on the second prototype.
As a result, one should be able to estimate the fabrication cost of
future superconducting thin solenoids.

As stated above, the two one-meter test solenoids are identical
except for the superconductor. The two magnets are wound on identical
bore tubes; both magnets have essentially identical tubular cooling
systems. There are minor differences in the insulation and in the
fabrication technique. The second coil (the B coil) benefited

considerably from the experience gained in building the first coil

(the A coil). The primary difference between the two coils is their

copper to superconductor ratio: the A coil uses a 1.8 to 1 copper to

superconductor ratio conductor; the B coil uses a 1 to 1 copper to

superconductor ratio conductor. Both superconductors have the same

nominal diameter. This section describes the following about the

LBL one-meter test magnets: 1) the superconductor, 2) the fabrication

of the magnet coils, 3) the instrumentation of the test coils, and

4) the physical and electrical parameters of the two solenoids.

3.1. Superconductor Parameters and Tests

The superconductors used in the two thin solenoid phototypes

are described and the testing procedures are discussed. This sub-

section describes 1) the physical properties of the superconductor,

2) the short sample superconductor, and 3) oval solenoid tests. The

superconductor used in the two solenoids is typical of the kind of

multifilament superconductors which are readily available in the United

States from four manufacturers.

a) Physical Properties of the Superconductor

Two superconductors were ordered, one from Magnetic Corporation of

America (MCA), and one from Supercon. Both superconductors are about

1.00 mm in diameter. The total length of each order was 3000 m, and

each was delivered in three pieces. Both superconductors consist

of niobium-titanium alloy co-drawn in a copper matrix. The composition

of the MCA niobium-titanium is about 55% niobium and 45% titanium.

The Supercon material is 52% niobium and 48% titanium. In both conductors,

the pinning centers are created predominantly by heat treatment rather than by cold working. (The heat treatment of both superconductors is a trade secret.) Although both conductors were developed within the last 18 to 24 months, they represent the kind of superconductor which is readily available from the American superconductor industry. The composition and heat treatment of the niobium-titanium has been optimized for use at induction levels of 5 to 6 tesla. The composition of the superconductor is not optimized for use in magnets which have peak inductions of 2 to 2.5 tesla, but the superconductor is available at a reasonable price.

The structure of the superconductor is typical of modern 2000 to 3000 filament conductors. It is a stacked conductor consisting of 15 to 20 bundles of superconducting filaments. (there are between 100 and 200 filaments in each of the bundles) which are in a high conductivity copper matrix (the copper had a resistivity ratio of at least 200 before it was processed). Table 4 shows the mechanical properties of the superconductors.

The superconductor was supplied insulated by the manufacturer. The specification called for a polyvinal-formal insulation which is 0.05 mm thick, laid down in accordance to NEMA Standard MW-1000, Section MW15-C (Triple) Polyvinal Formal Resins. The specification also called for the insulation to be laid down in at least three passes. Visual inspection and an electrical buzz test of the insulation found some holes and cracks in the coating, though these were infrequent; they were repaired by varnishing the suspect region of the wire. Over most of its length, both superconductors were properly insulated.

Table 4. Mechanical properties of the superconductors used in the large solenoid experiment.

	MCA Superconductors	Supercon Superconductors
Matrix Diameter (mm)	0.99	1.00
Copper to Superconductor Ratio	1.8 to 1	1.0 to 1.0
Number of Filaments	2300	2700
Filament Diameter (μm)	12.3	13.6
Filament Twist Pitch (mm)	10	10

Visual inspection of the superconductor (the insulation was stripped away on several samples of each type of conductor) showed that the conductor was sound. There was no evidence of superconducting filament protrusion through the copper. Although there was evidence of the twisting process, the surface of the conductor was smooth. Visual inspection was also extended to the superconducting filaments themselves. Because the niobium-titanium filaments are impervious (or nearly so) to the effects of nitric acid, the copper was etched away with strong nitric acid. There was no evidence of filament breakage. (A few filaments were broken but not many. A superconductor which has few broken filaments will usually pass the current test.) The twist pitch of the conductor was measured and found to be correct. Microscopic examination of the filaments showed that there was no change in filament diameter along the short lengths examined.

b) Short Sample Superconductor Tests

The superconductor was tested using the LBL short sample technique. This technique uses a relatively long sample which permits one to measure the resistivity of the superconductor as a function of current and magnetic induction.

The short sample consisted of a loop of superconducting wire about 500 mm long which was wound around a small fiberglass-epoxy spool in a bifilar fashion. Several tries had to be made to mount the sample correctly so that there was no wire motion in the magnetic field. The external magnetic field was generated by a small superconducting solenoid with a bore diameter of 50 mm and a length

of 100 mm. The sample was positioned in the center of the solenoid. The expected external field variation due to imperfections in the coil of the magnet is only about one percent. In addition to the external field, the sample also saw the self-field generated by the current in the conductor itself. The self-field is a major source of error only when the external field is below 1 tesla. A first order correction for self-field is included in the data presented here.

Resistance data was taken at external fields (as measured at the center of the superconducting solenoid) of 0, 1, 2, 3, 4, and 5 tesla. Since our test magnets will be operated at peak inductions in the coil of below 2 tesla, data above 5 tesla was not necessary. (An approximation of the high induction points can be found by extending a linear line from the 5 tesla point until it intercepts zero current at between 10 and 11 tesla.) The resistance data was taken in a helium bath at a temperature of around 4.25K. (The pressure in the dewar was slightly above atmospheric.)

The resistivity of the wire was derived by measuring the voltage developed across the sample and current put in the sample.[40] Knowing the current I, the voltage V, the sample length ℓ between voltage taps, and the superconductor matrix diameter d, one can calculate the superconductor resistivity ρ using the following formula:

$$\rho = \frac{V\pi d^2}{4I\ell} \quad . \tag{12}$$

Measured data points were taken at resistivities as low as $10^{-16}\Omega m$ and at up to resistivities approaching $10^{-13}\Omega m$. The measured data is shown on log plots in Figures 8 and 9. The curves are nearly vertical, which is an indication that the superconducting material is good.[40] A bad multifilament superconductor shows a very definite slope away from vertical. In most cases this nonvertical slope is caused by broken or uneven filaments in the matrix. In theory, broken filaments should be independent of the material metallurgy; in practice, however, bad metallurgy will often mean broken filaments.

Table 5 shows the $10^{-14}\Omega m$ current at various external inductions. Superconducting magnets are designed to be operated so that the maximum resistivity of the superconductor in the magnet is less than $10^{-14}\Omega m$. Most high current density intrinsically-stable solenoids quench when the superconductor resistivity is just above $10^{-14}\Omega m$.[41] The superconductor current density column in Table 4 suggests that the Supercon and MCA conductors are metallurgically similar. The heat treatment process used in the two materials must be similar because the higher induction superconductor critical current densities are similar. The primary difference between the current carrying capacity of the two conductors is the difference in copper to superconductor ratio.

c) Oval Solenoid Tests

It is normal that the new superconductor be tested in a small magnet in order to determine whether it is stable. Normally, a small round solenoid would be used for the test. In this situation, the solenoid winding is well supported so that there is no wire motion
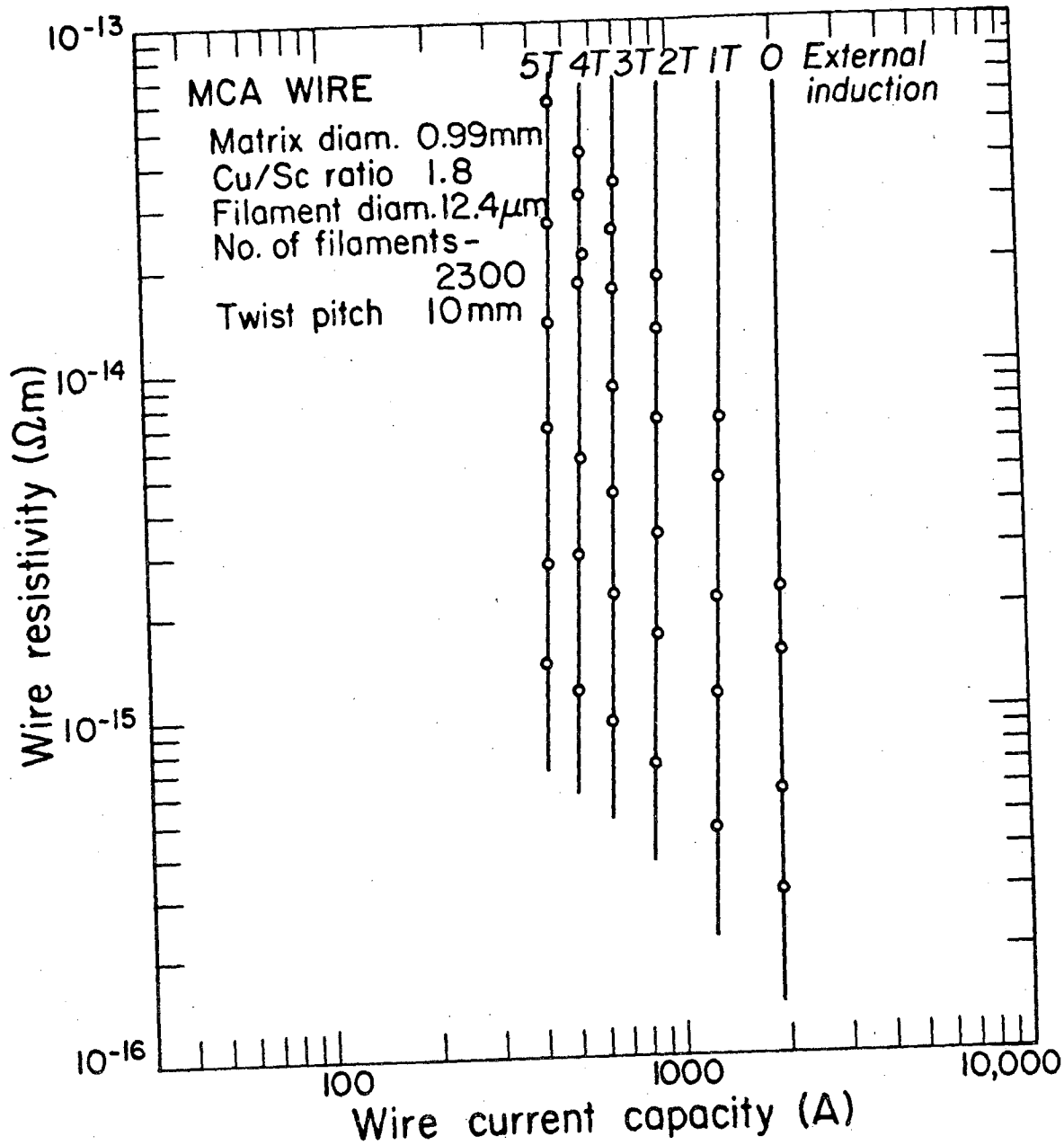
Fig. 8. Superconducting wire resistivity as a function
of current and magnetic induction near sample
of MCA superconductor.
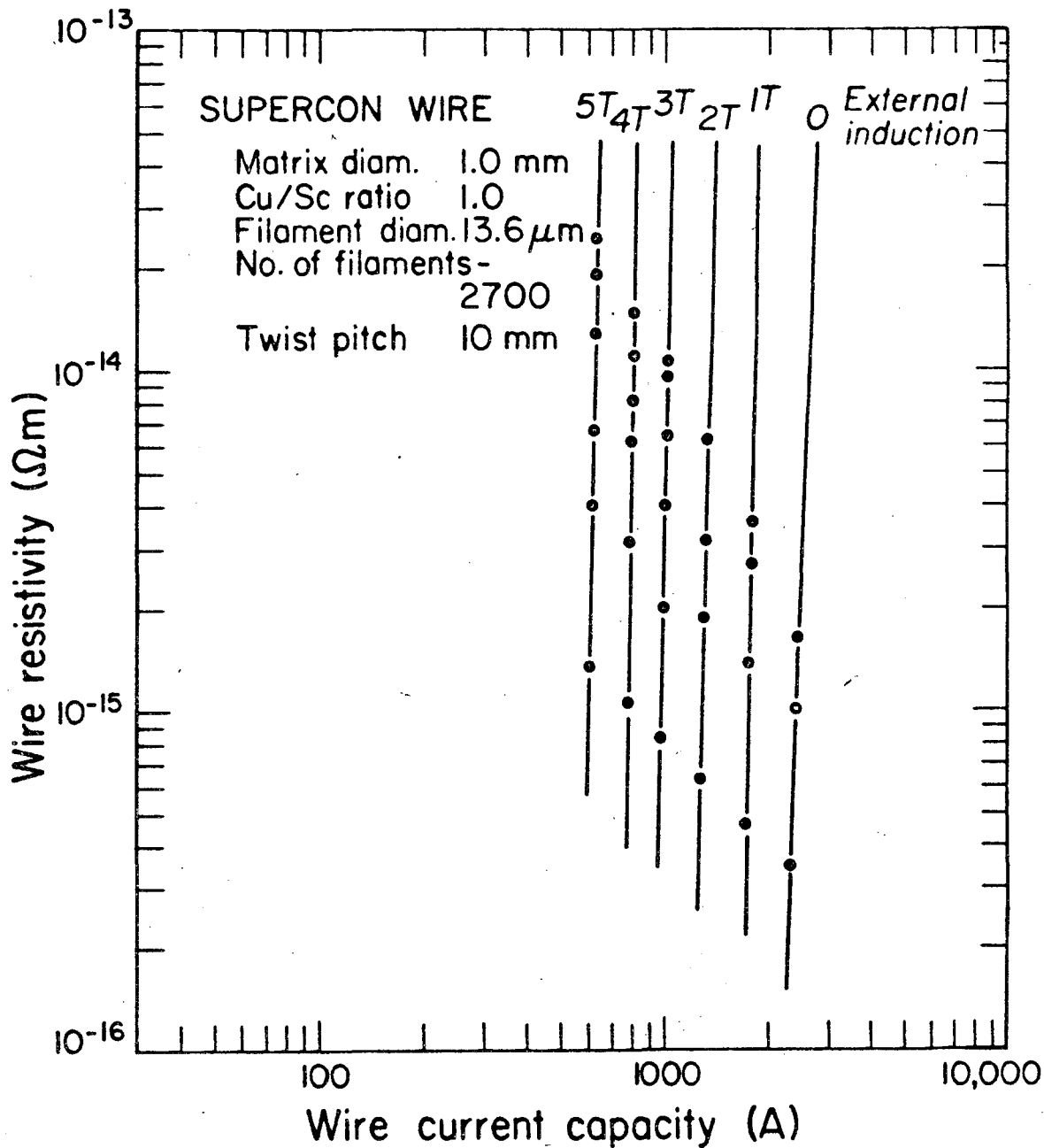
XBL 759-4187

Fig. 9. Superconducting wire resistivity as a function
of current and magnetic induction near a sample
of Supercon superconductor.

XBL 759-4188

Table 5. The 10^{-14} ohm m critical current density versus induction.

Induction (T)	Matrix Current Density (Am^{-2})		Superconductor Current Density (Am^{-2})	
	MCA	Supercon	MCA	Supercon
0.0*	2.60×10^9	3.34×10^9	7.27×10^9	6.67×10^9
1.0	1.74×10^9	2.30×10^9	4.87×10^9	4.60×10^9
2.0	1.17×10^9	1.73×10^9	3.27×10^9	3.46×10^9
3.0	0.87×10^9	1.28×10^9	2.43×10^9	2.57×10^9
4.0	0.70×10^9	1.02×10^9	1.96×10^9	2.05×10^9
5.0	0.57×10^9	0.79×10^9	1.58×10^9	1.58×10^9

*The corrected induction for the MCA wire is 0.5 tesla; corrected induction for the Supercon wire is 0.7 tesla.

inside the magnet. Previous experience plus successful physical and short sample tests made the simple round solenoid test unnecessary (in our opinion). We decided, instead, to wind the conductor onto an iron-shielded oval solenoid form. (The oval solenoid tests are similar to the ones performed with rectangular conductors in March and May of 1975.)[42] An oval solenoid test permits the testing of the superconductor under reasonable conditions of induction (comparable to the worst case in the final one-meter diameter magnets), and at rather high stress-levels. In addition, the magnet forces cause the conductor to move. This permits one to see the effects of wire motion and training.

There were two test oval solenoids wound on the same coil form that was described in reference 42. Both oval coils contained two layers of 90 turns each, and had iron pole pieces so they behaved like infinite solenoids. The physical dimensions of the oval solenoids are shown in Table 6.

The oval solenoid tests are designed so that high magnetic stresses are put into the superconductor (about 4×10^8 Nm^{-2}). As a result, the superconductor deforms elastically, then plastically, causing conductor motion which may manifest itself as training. The magnet with its iron shield is cooled in a bath of liquid helium at a temperature of 4.25 K. The magnets are quenched at various charge rates in order to test for training behavior and charge rate sensitivity.

The MCA solenoid, which was tested in July of 1975, showed considerable training (quenching prematurely due to wire motion), but eventually reached the critical current of the superconductor which was around 900 A. (The superconductor critical current in a

Table 6. Physical characteristics of the oval solenoids.

Solenoid Length	101.5 mm
Major Axis Diameter	202.5 mm
Minor Axis Diameter	70.0 mm
Maximum Radius of Curvature	500.0 mm
Minimum Radius of Curvature	33.0 mm
Number of Turns	180
dB/dI	0.00224 T/A

magnet was by definition the 10^{-14} ohm m resistivity current.) The

peak current that was obtained in the magnet was 910 A. This corresponds

to an induction in the wire of 2.0 tesla. There was little or no charge

ratio sensitivity. Using methods given in reference 42, we estimated

that the peak stress in the conductor at 910 A was 3.5 x 10^8 Nm^{-2}

(51,000 psi). See reference 43 for more data on this test.

The Supercon solenoid, which was tested in August of 1975, showed

much worse training than the MCA solenoid. The lower copper to super-

conductor ratio in the Supercon conductor made it much more sensitive

to wire motion (during the tests, wire movement of as much as three

millimeters was observed.) The Supercon oval solenoid did not reach

the critical current of the superconductor. The peak quench current

reached was 1036 A. This corresponds to a current density of

1.32 x 10^9 Am^{-2} in the matrix at an induction 2.3 tesla. (LBL had

on a previous occasion run a small test solenoid at current densities

of 1.45 x 10^9 Am^{-2} at a peak induction of 1.8 tesla.[44]) The estimated

stress in the conductor was about 4.2 x 10^8 Nm^{-2} (61,000 psi).[42,43]

The oval solenoid tests showed considerable wire motion. They

also showed that the superconductor will operate at high current densities

while being subjected to high levels of stress.[45] The Supercon material

with its 1 to 1 copper to superconductor ratio was more sensitive

to wire motion. Both materials, while sensitive to wire motion, should

perform reasonably well in large potted solenoids which will restrict

wire motion.

3.2. Fabrication of the Large Solenoids

The two one-meter diameter thin solenoids were fabricated in the Lawrence Berkeley Laboratory assembly shop. The first coil was made between June and October of 1975; the second coil was fabricated in January and February of 1976. The first magnet was the first superconducting magnet ever manufactured by the main assembly shop. All of the previous magnets built at LBL were made by specially-trained technicians.

The fabrication of the large solenoid consisted of five primary steps:[46] 1) the central bore tube fabrication, 2) the superconducting coil winding, 3) the aluminum cooling tube winding, 4) vacuum impregnation of the coil, and 5) the assembly of the leads and cooling tubes.

a) The Magnet Bore Tube

Three aluminum bore tubes were fabricated together. The magnet bore tubes had an inside diameter of 1021 mm and an overall length of 500 mm. The bore tube consisted of a barrel and two end flanges. The outside diameter of the barrels was 1034 mm; the outside diameter of the flanges was 1070 mm. The barrels were fabricated from 1/4 inch thick 1100 aluminum plates; the flanges were fabricated from 1 x 3/4 inch 6161 aluminum bars.

The plates were cut, rolled up, and welded end-to-end with a single seam weld. The bars were rolled up and welded to the barrels by J welds. The welds were then ground flat to permit winding of the coil, and plate jig fixtures were made so that the coil could be held round (to about 1 mm) while mounting, drilling, machining, and coil winding.

After rolling, welding and rough machining, all three bore tubes were annealed at 350°C (650°F) for 15 minutes in the paint shop oven. Four test samples were sent to the Bureau of Standards, in Boulder, Colorado, for resistivity measurements.[47] (We decided later to anneal two of the bore tubes for one hour at 350°C. This had to be done off the LBL hill. The bore tube used for Coil A had only the paint shop anneal.) When the anneal was finished, holes in the flange were drilled and taped and the finish machining was completed. The strain gages were applied when bore tube fabrication was finished.

One mistake made on the bore tubes was in not specifying vacuum-tight welds, which meant we had to epoxy the bore tubes in order to vacuum impregnate the coil. The second and third bore tubes were vacuum checked before the coils were wound on the tubes. A second mistake was the failure to specify the weld differently in order to cut the amount of machining in the corners. Just before winding the superconductor, the bore tube was sandblasted. A photo of the finished bore tube is shown in Figure 10.

b) Coil Winding

Each coil consists of over 830 turns of Nb-Ti multifilament superconductor wound in two layers between the flanges on the outside of the bore tube barrel. The insulated conductor diameter is 1.1 mm. The specific properties of the conductor have been discussed previously. The insulation to ground, which separates the winding from the bore tube, consists of 1/16-inch thick glass epoxy resin spacers at the flanges and a layer of half lapped tape 0.007 inch thick; 3/4 inch wide glass cloth tape is used between the coil and the bore tube barrel.
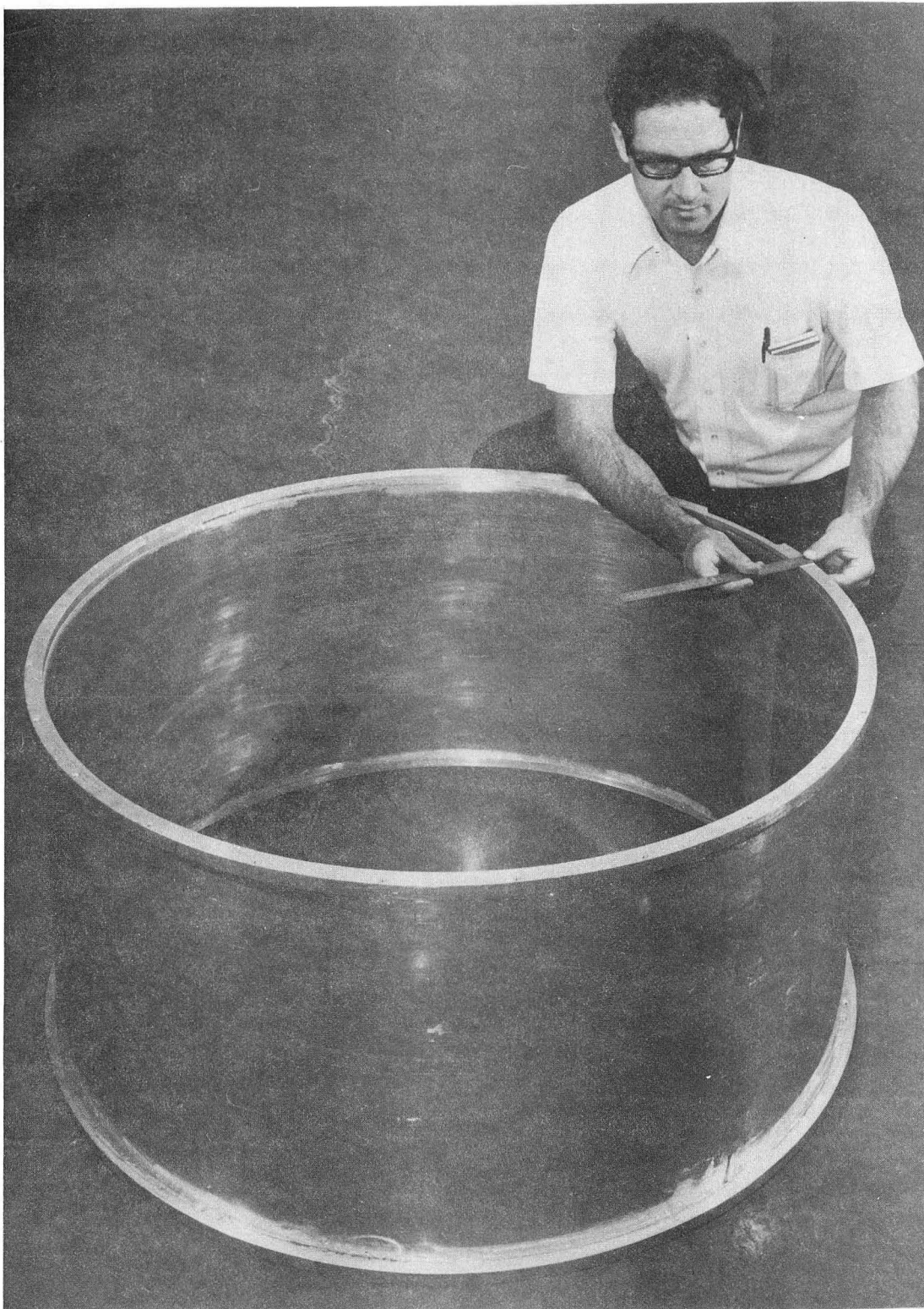
CBB 757-5223

Fig. 10. A one-meter diameter test solenoid 1100-0
aluminum bore tube.

The total thickness between the barrel and the coil is 0.35 mm (0.014 inches). Layer to layer insulation consists of the same half lapped tape (0.35 mm thick). The insulation between the coil and the aluminum cooling tube is also the half lapped 0.007 inch tape.

Before winding the coil, a 5-m long section piece of 18-gage copper wire was spliced to the superconductor. A special soldering iron tip was developed to make long soft solder splices, using a 62% Sn, 2% Ag and 36% Pb solder. All splices were covered with glass sleeving. The spliced conductor at the ends was passed through a hole in the flange so that about 1.8 m was left outside the flange. The holes in the flange had an epoxy fiberglass plug in them. The magnet conductor with copper wire soldered to it was passed through a hole in the plug; then it was epoxied in place.

The A coil was wound on one of the large lathes in the main machine shop. A coil up to 1.5 m in diameter could have been wound on that lathe. The B coil was wound on the LBL large magnet coil-winding machine, which allows us to wind coils up to 3.0 m in diameter. The wire was maintained at a tension of 130 N (29 pounds) by a tensioner borrowed from the Lawrence Livermore Laboratory. The pretension in the wire is required in order that the thermal contraction coefficients between the superconductor and the bore tube be matched.[48]

The coil was wound with the turns laid carefully next to one another. Occasionally a soft-face epoxy hammer was used to jog the turns into position. The A coil had splices in the 388th turn and the 647th turn. The B coil had splices in the 404th turn and the 784th turn. The splices were made with the specially designed soldering

gun tip. Each splice, 3.2 m long (one turn around the coil), was
then covered by fiberglass sleeving and wound into the magnet
coil. Figure 11 shows the B coil being wound on the LBL large magnet
winding machine.

After the last turn was tied down (to maintain tension in the
coil) the lapped fiberglass tape was wound around the coil to insulate
it from the cooling tube. The two pieces of spliced superconductor
which would eventually form the coil leads were coiled and put out of the
way for later work. A cross-section of the magnet with its bore tube,
superconductor, and cooling tube is shown in Figure 12.

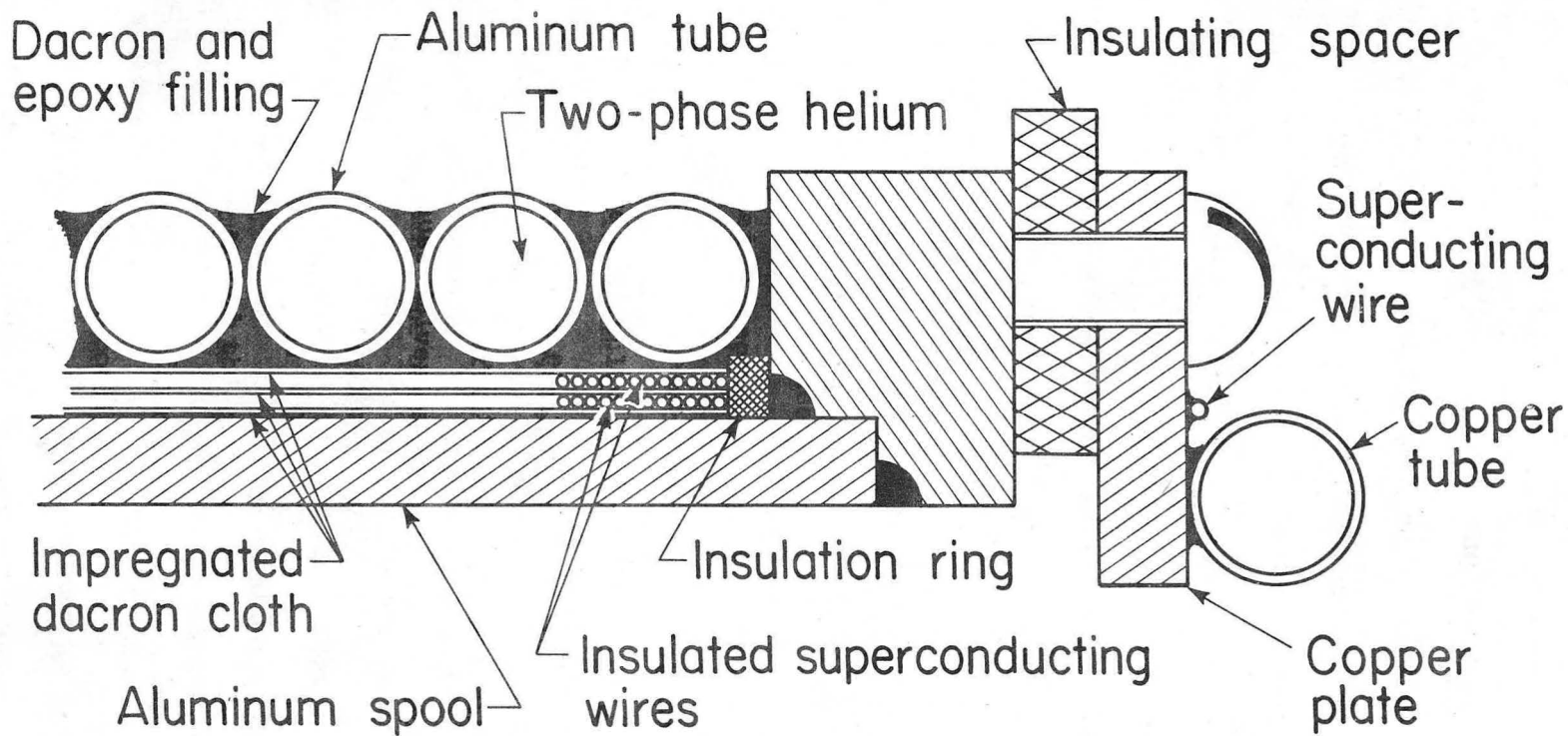### c)   The Aluminum Cooling Tube Winding

The cooling tube, which is used to carry two phase-helium,[39] is
wound over the insulated superconducting coil. The tube has a
12.7 mm (0.5 inch) outside diameter with a 1.1 mm (0.042 inch) wall
thickness. We had some difficulty finding the tube in long continuous
lengths, but one of our buyers finally found it in three 600-foot
lengths at the Wolverine Tube Division of Universal Oil Products in
Decatur, Alabama. Because Wolverine was about to scrap it, we paid
the bargain price of 7 cents per foot for it. The tube is quite soft
and is made from almost annealed 3003-0 aluminum alloy.

The tube was wound around the coil on the large conventional
magnet winding machine. Thirty-five turns of tubing were wound around
each coil, and total length of cooling tube in the coil assembly
was just over 117 m (384 feet). Since the tube is round, it will
withstand much higher pressures than a square tube with the same wall
thickness. There are small spaces between the tubes, which are

-54-
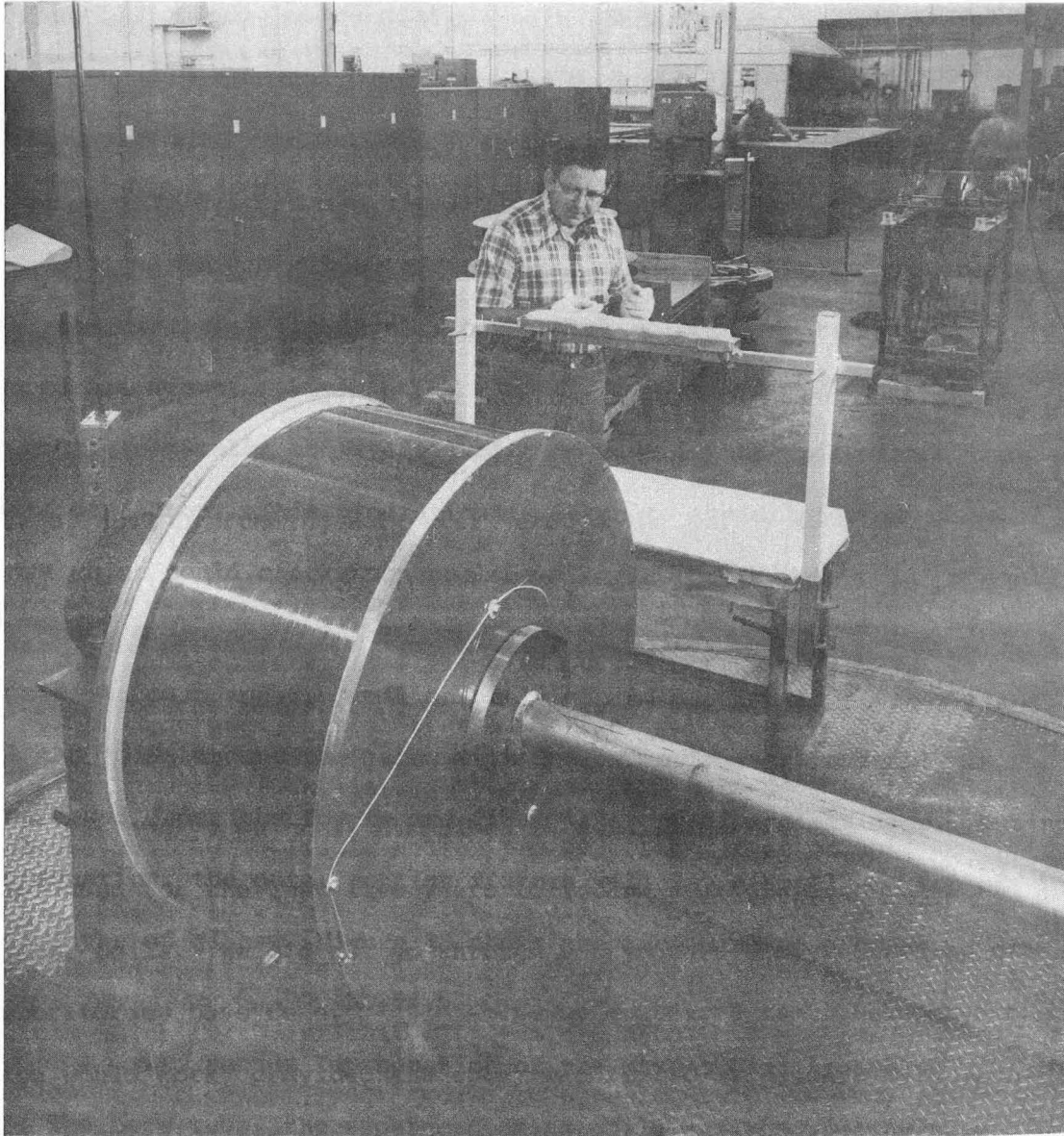
CBB 761-273

Fig. 11. The winding of the 1.1 mm diameter super-
conducting wire on the B magnet bore tube
in the Lawrence Berkeley Laboratory main
shops.

Fig. 12. A cross section of the one-meter diameter test solenoid magnet.

Labels in figure:
- Dacron and epoxy filling
- Aluminum tube
- Two-phase helium
- Insulating spacer
- Super-conducting wire
- Copper tube
- Impregnated dacron cloth
- Insulation ring
- Copper plate
- Aluminum spool
- Insulated superconducting wires

XBL 757-3453

filled with dacron roving. There were spaces at the end of the tube layer where we could not quite get in another tube turn: these were also filled with roving. The A magnet has one quench-inducing coil located at the end of the magnet just under the tube. The B magnet has four quench coils mounted under the tubes. Two coils are located near the center of the magnet; one quench coil is located at each end of the magnet.

Care was taken to fill all of the voids in the coil with either glass or dacron. This precaution is taken to avoid large expanses of epoxy which could crack upon cool down. (In theory, the coil assembly is designed for rapid cool down--one should be able to dunk the coil in liquid nitrogen and the coil assembly should survive.) After filling all the voids around the tubes with dacron roving, the assembly is compressed under the fourth and final layer of fiberglass tape. During impregnation, the outer potting fixture will lay directly on top of this layer of glass. Figure 13 shows the tube winding process.

d) Vacuum Impregnation of the Magnet Coil Assembly

The bore tube, the superconducting coil, and the cooling tube are cast together to form a single rigid unit. We chose to vacuum impregnate the coil because experience at Rutherford and at Karlsruhe[49] shows that a solid void-free structure can be created this way. Vacuum impregnated superconducting magnets, especially solenoids, have performed very well. Further, vacuum impregnated conventional coils have been built for years at LBL; the techniques are well understood by our assembly shop.
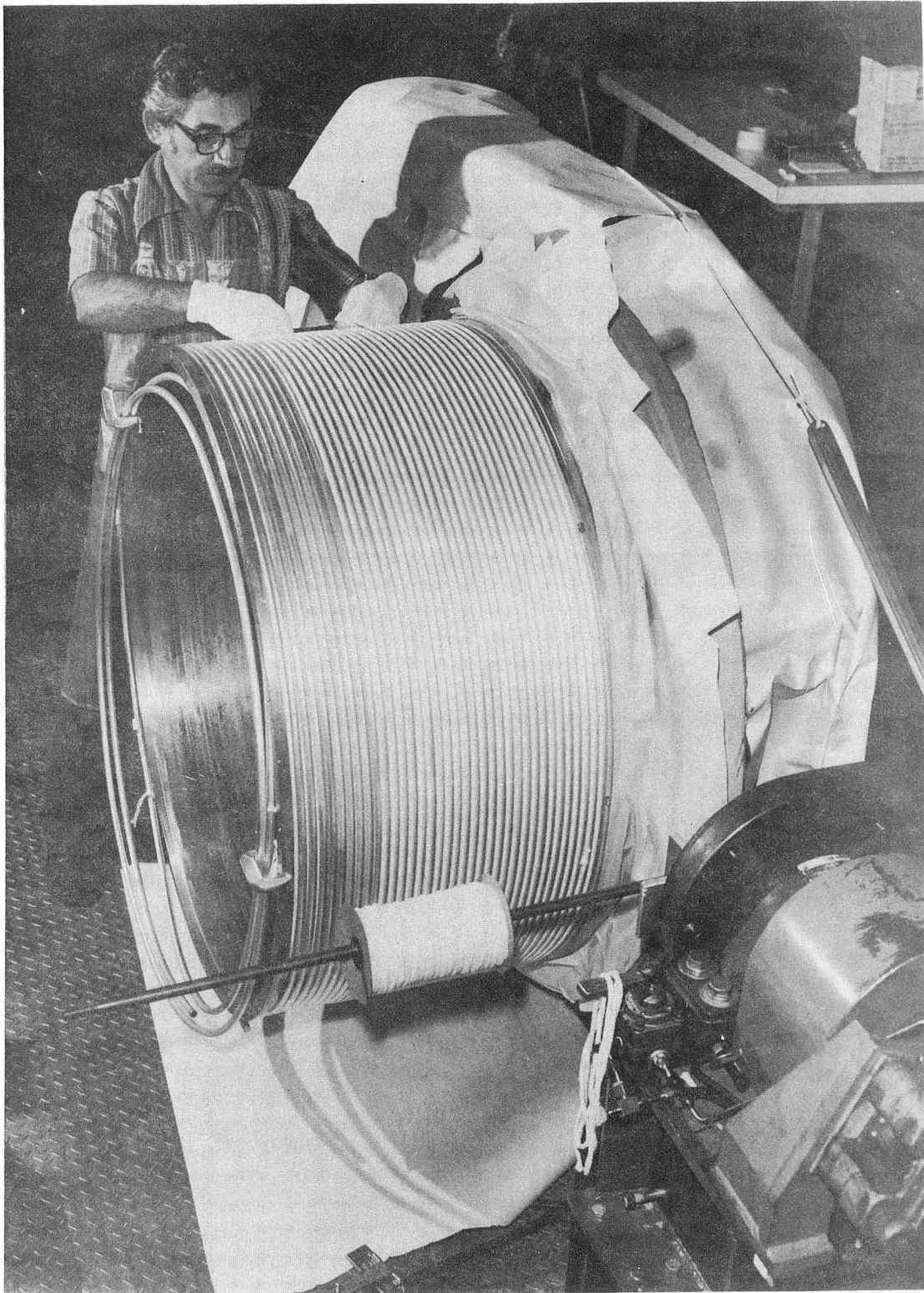
CBB. 759-6794

Fig. 13.   The winding of the aluminum cooling tube
           on the A solenoid magnet.

A steel potting shroud, with vacuum pump out ports and the epoxy fill ports in it, was built by the sheetmetal shop. Other parts were also built to make the coil assembly vacuum tight. Vacuum leaks were filled with bits of aluminum and silicone rubber. We found that the bore tube welds leaked; they were painted with epoxy. Repeated mass spectrometer vacuum checks were made. There was more patching with bath tub caulk, epoxy and "dux seal" until a vacuum tight structure was obtained.

The plastic shop controls the potting temperature of a conventional coil by running hot water through the hollow conductor. We used the aluminum cooling tube for the same purpose while we potted our coil. The plastic shop has a cam-controlled water temperature controller to regulate the temperature of the assembly during potting and curing the epoxy.

The epoxy, which is described in detail in reference 50, has been used for the last five years to vacuum impregnate conventional magnet coils. We did not go through a cryogenic epoxy search as other laboratories have done.[51,52,53] We were assured that the epoxy formulation would work, provided the epoxy was filled with glass or dacron. The formulation has the following properties which make it ideally suited for vacuum impregnation: 1) low viscosity (500 C poise at 25°C), 2) long pot life (~6 hours at 50°C), 3) good wetting power, 4) a moderate cure schedule (about 24 hours with a final cure temperature of 80°C, and 5) good vacuum properties.

The first coil took nearly seven hours to pour. Apparently there were no clear passages for the epoxy to enter the coil. The second magnet (the B coil) took only an hour and a half to pour, at a pouring

temperature of 50°C. After the pour was completed, the temperature
was raised to 60°C, and the cure was started. Eight hours were spent
at 60°C, then the coil temperature was slowly raised to 80°C. The cure
proceeded for about twelve more hours after which the temperature was
allowed to drop to room temperature. The casting equipment is shown
in Figure 14.

e) Leads and Cooling Tubes and the Final Assembly

After the coils were taken from the molding fixture they were
voltage tested to ground at at least 1000 V. The current flow measured
had to be less than 50 μA. An assembly consisting of copper bars,
copper tubes and various fitted preassembled parts was fabricated.
The copper bars with copper tubes soldered to them carry the current
from the coil to the electrical leads. They are cooled by the two-
phase helium leaving the magnet cooling coil.

Since the coil cooling tube is at ground potential and each of
the leads to the magnet may be at any arbitrary voltage, the copper
bus bars on top of the magnet must be insulated from the grounded
cooling coil and the return line to the refrigerator. The two copper
bus bars must be insulated from each other as well. Figure 15 shows
an electrical and gas flow diagram of the copper bus bar and coil
assembly. The insulators used were made of vacuum-tight ceramic with
kovar sleeves brazed to them. They will stand off at least 10 kV
and can be used at cryogenic temperatures. A commercial aluminum
to stainless steel transition was used to connect the aluminum tube
to the copper bar assembly. Figure 16 shows a photograph of the completed
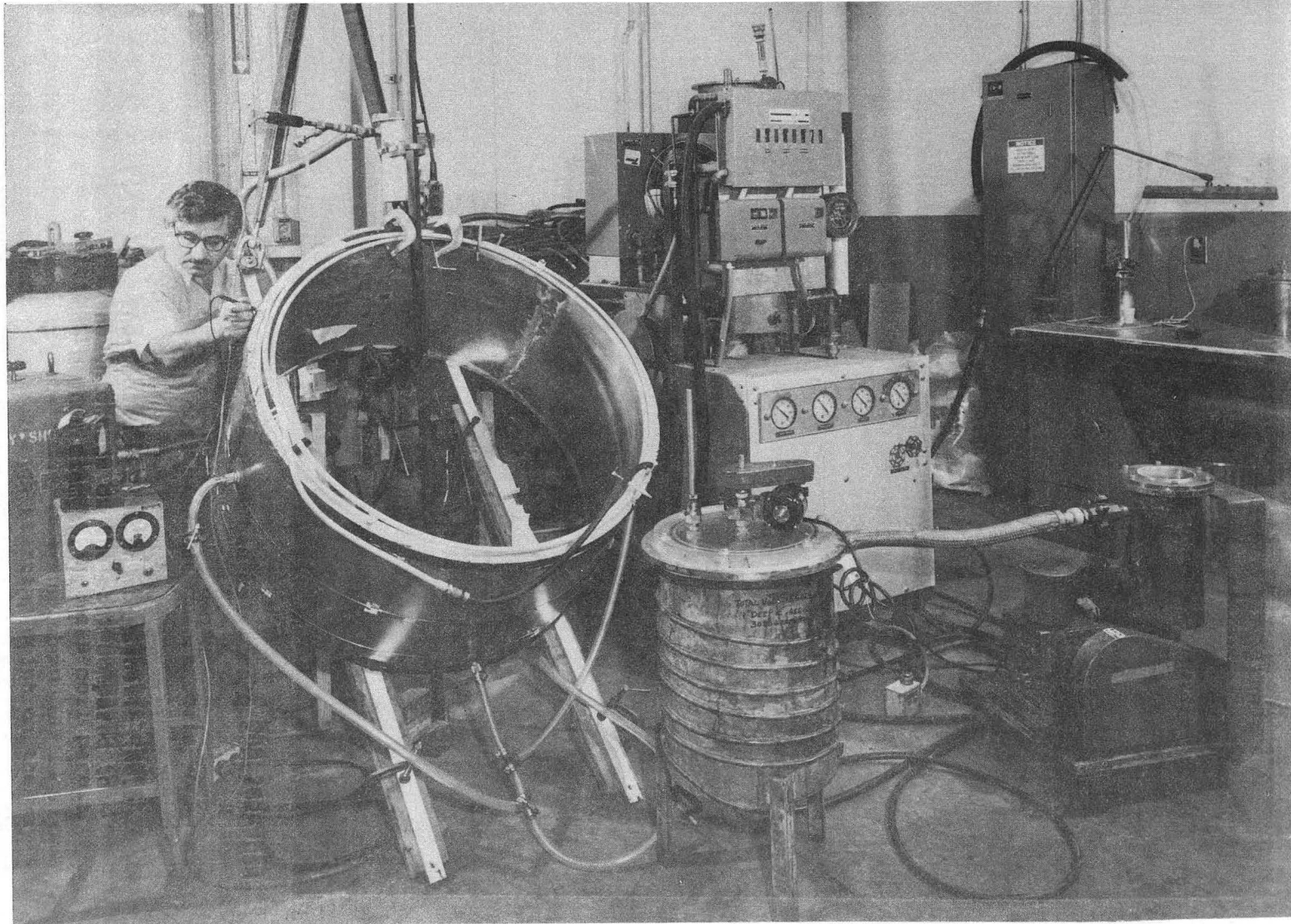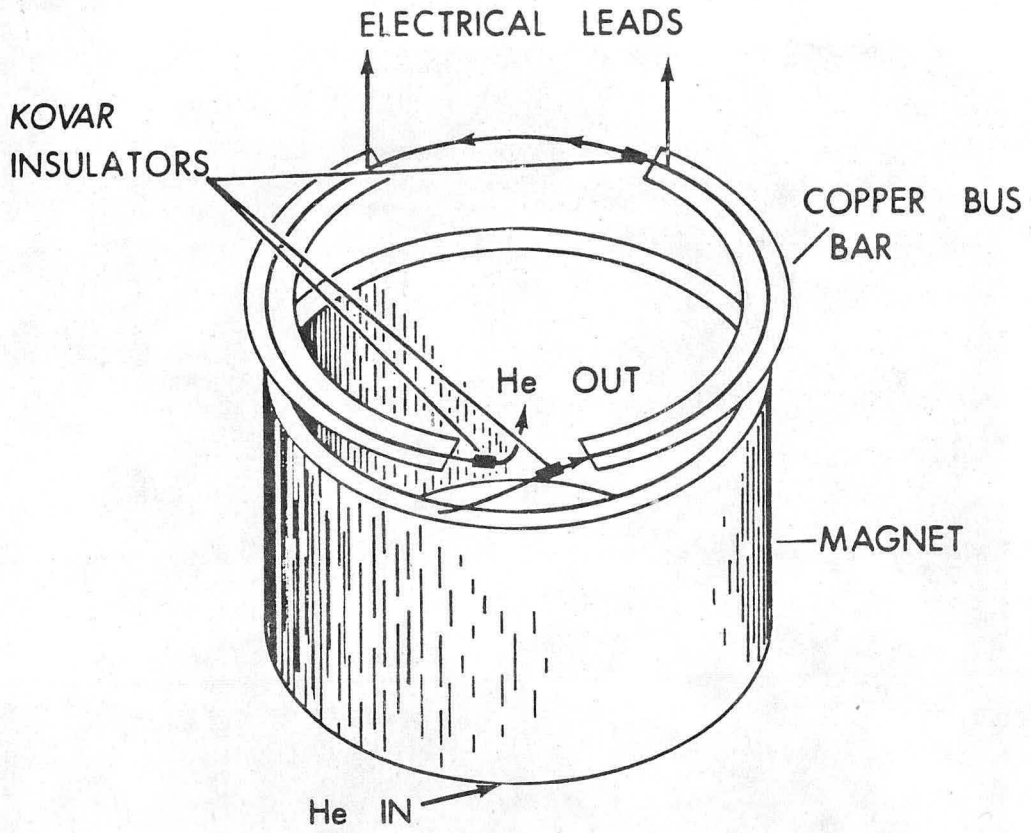assembly.

Fig. 14.   Vacuum impregnation of the A magnet in the Lawrence Berkeley plastic
shop.   The equipment just to the right of the magnet controls the epoxy
temperature during pouring and curing.

CBB 7510-7378

a) Two Phase Helium Flow.
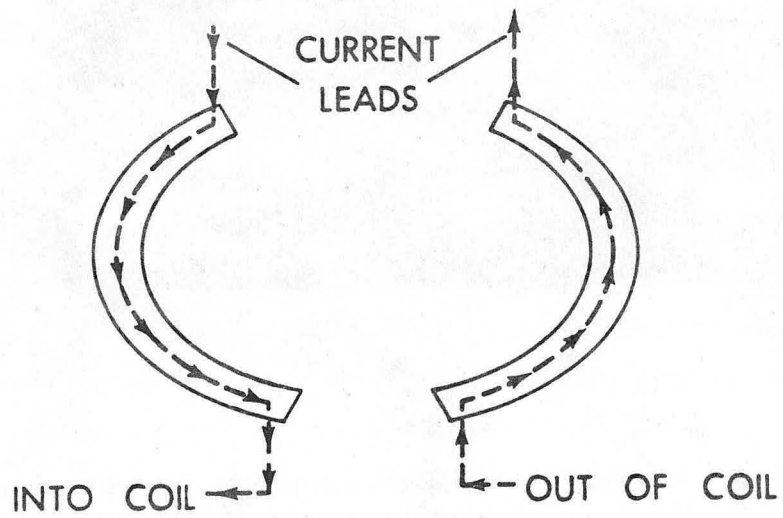
b) Electric Current Flow.

XBL 774-8448

Fig. 15. Flow diagrams for two phase helium and electric current into and out of the test magnets.

CBB 762-2054

Fig. 16. The finished B solenoid magnet. (Note
the thickness of the coil compared to
the magnet diameter.)

---

of the solenoid coil going normal at low currents without the risk of
burning the magnet. In order to induce a quench, one must heat up a
small region of the superconductor in the coil to a temperature which is
above the superconductor critical temperature. Two methods were tested:
a resistance heater which drives the superconductor normal, and a pulsed
coil which heats the superconductor by changing the magnetic field.
We found that pulsing the field locally was the easiest and most reliable
method for inducing quenches.[55]

The pulsed magnetic field technique (from here on known as the $\dot{B}$
technique) requires that a small coil be attached to the main super-
conducting magnet coil. The coil is connected to receive the discharge
of a capacitor. This discharge causes a fast and local change in
magnetic induction B. The magnetic field variation ($\dot{B} = dB/dt$) makes
the superconductor warm up and turn normal. The advantages of this
technique are: 1) the quench inducement is nearly instantaneous (within
1 ms); 2) the normal region formed is small (about 50 to 100 mm^2);
3) the heat is induced in the conductor itself; and 4) quenches
produced by the $\dot{B}$ technique appear to model spontaneous quenches well.

The location of the quench inducing coils on the main superconducting
coils is shown in Figure 17. The A coil has only one quench-inducing
coil located at its end. The B coil has four quench coils--one is
located at each end of the coil and two are located at the center
of the coil. The additional quench points in the B coil permit
one to measure the effect of the quench starting point on the way
magnets go normal. In addition, one can induce quenches at multiple
points in the coil.
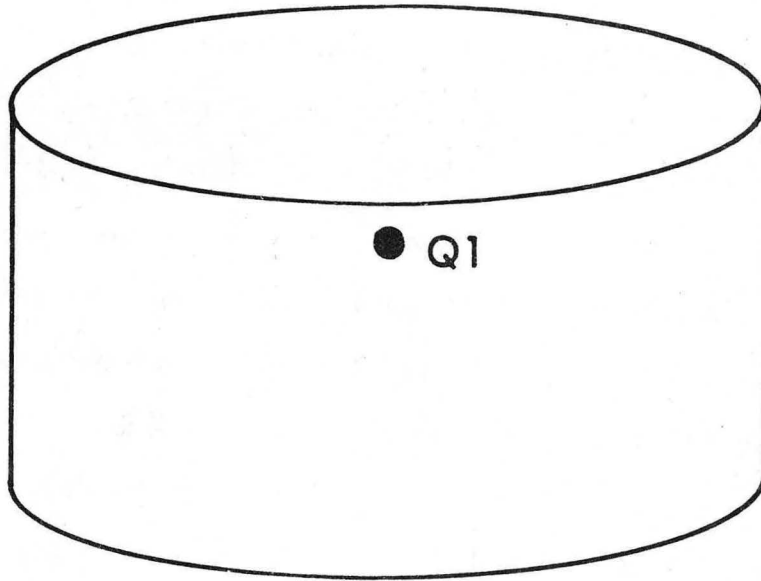
a) Quench Coil on the A Magnet.
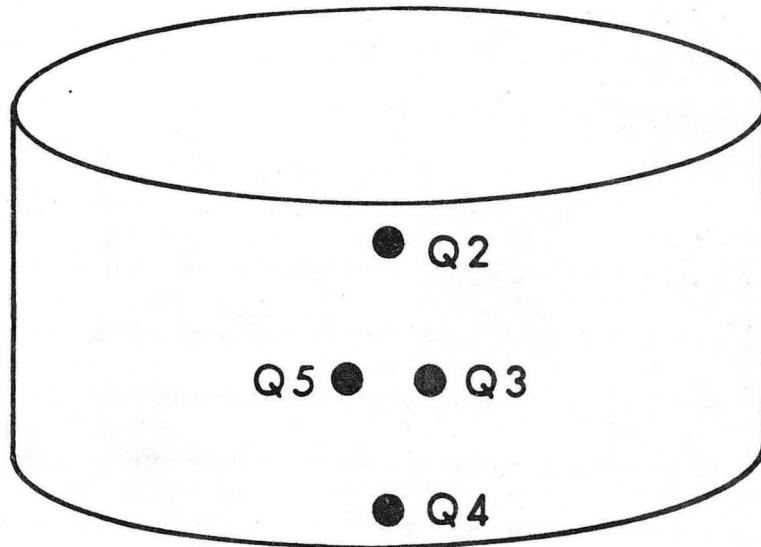
b) Quench Coils on the B Magnet.

XBL 774-8316

Fig. 17. The location of the small coils for
inducing quenches in the A and B magnets.

The circuit for firing the quench coils (shown in Figure 18) is a simple capacitor discharge circuit. A 1000 μF capacitor is charged to a set voltage. The charge is dumped into the small coils which are cast into the magnet. These coils, which come from a television set, have an inductance of around 1.0 mH. The time constant for the quench coil and all of its circuitry varies depending on the length of the leads between the capacitor and the quench coil. Time constants of 1.5 to 3.0 ms are typical for the LBL experiments. The heating of the superconductor is due almost entirely to coupled ac losses in the superconductor.[56,57,58] Only about 1 kJ m^{-3} is required to drive the superconductor normal. The energy required to drive the coil normal is a function both of the current and the local field (proportional to the current) in it. The quench energy as a function of current is shown later.

b) Magnetic Flux Measurement Coils

The changes of magnetic flux within the solenoids are measured by coils which are wound around the magnets. The voltage generated by these coils is proportional to the rate of flux change[59] ($d\phi/dt$) which is proportional to the rate of total current change. The use of a $d\phi/dt$ coil permits one to see the shift in total current from the magnet coil to the magnet bore tube.

The A magnet has a single $d\phi/dt$ coil wound around the finished magnet (outside the cooling tube). It is wound about 100 mm from one end. This is probably not the best position for a $d\phi/dt$ coil, because the coupling to the magnet coil is estimated to be only about 85 to 90 percent. (The $d\phi/dt$ coil is shown in Figure 19.)

RELAY
SWITCH

R ≈ 50 Ω

VOLTAGE
SOURCE
0 - 500 V

V

VOLTMETER

STORAGE

CAPACITOR

C ≈ 1000 μF

QUENCH
INDUCING
COIL
L ≈ 1mH

-67-
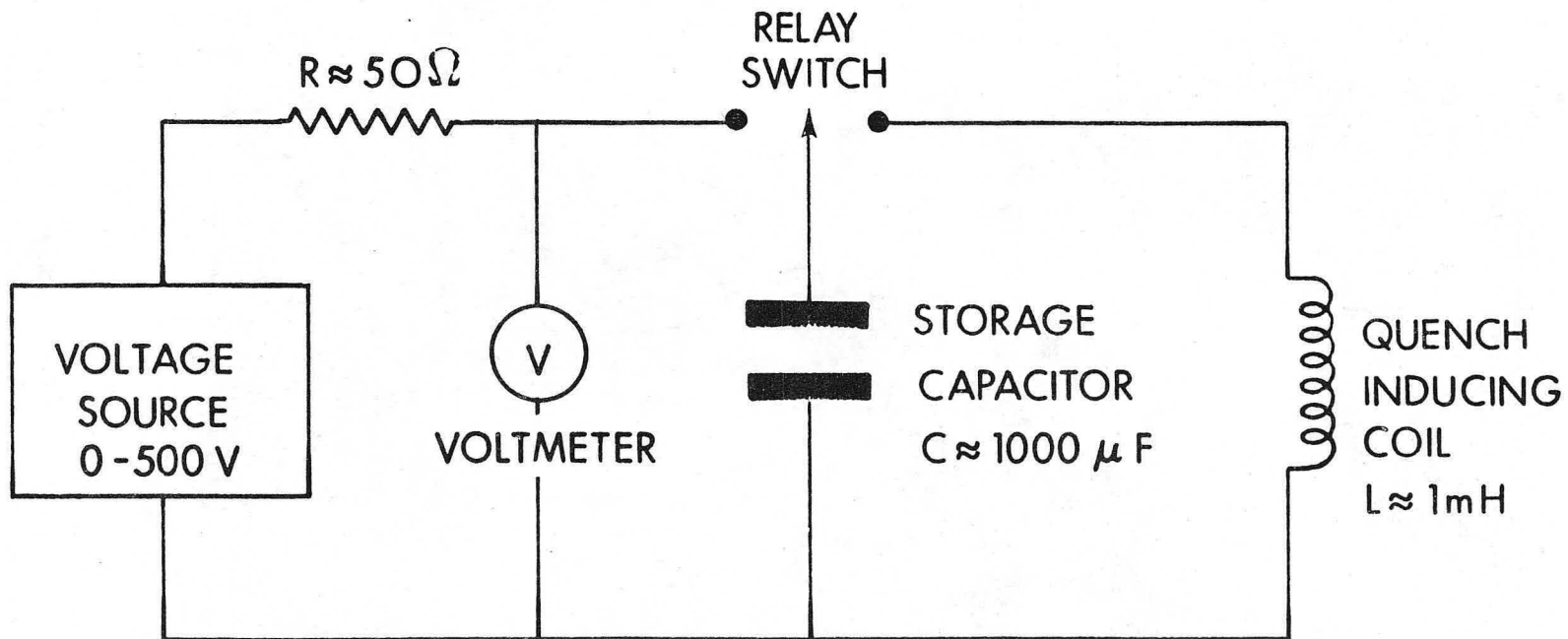
XBL 774-8474

Fig. 18. The electrical circuit diagram for the
quench inducing circuit (see Fig. 17 for
the location of the quench coils).
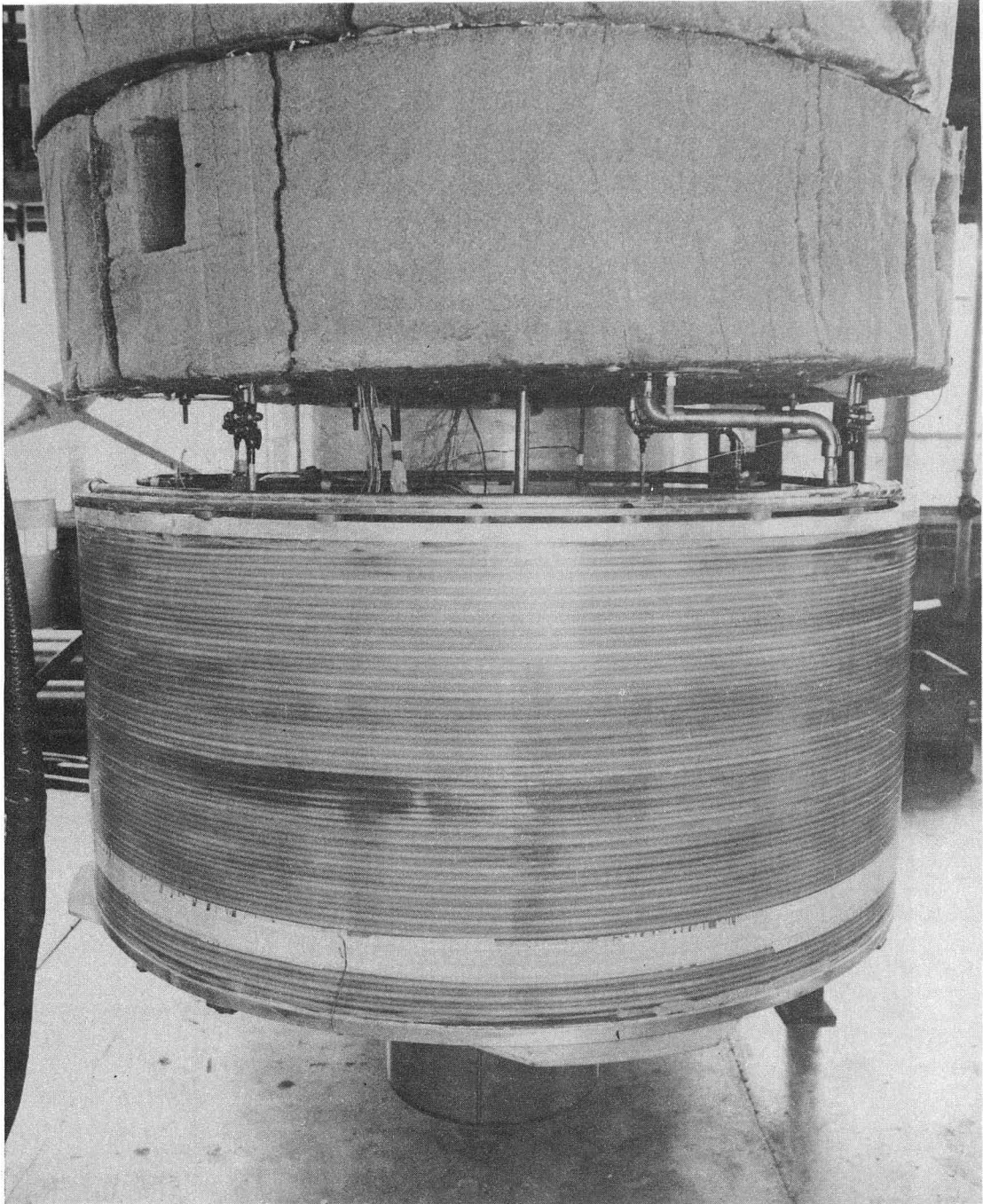
CBB 7512-8784

Fig. 19. The finished A magnet just before the
March 1975 test. The white band about 8 cm
from the bottom of the magnet is a 37-turn
P coil for measuring the change in the magnet.

The B magnet has two $d\phi/dt$ coils. One is wound directly over
the magnet coil between the superconductor and the cooling tube.
This coil is split into two parts with 20 turns each. (One turn makes
the transition between the two coils; the total number of turns in
the coil is 41.) The center of this $d\phi/dt$ coil corresponds to the
center of the superconducting magnet coil within about ±0.5 mm.
The coupling between it and the magnet coil is estimated to be better
than 99 percent. The second $d\phi/dt$ coil is identical to the first
except that it is located outside the cooling tubes. Figure 20 shows
the second $d\phi/dt$ coil which also corresponds to the superconducting
coil center within about ±0.5 mm.

The two $d\phi/dt$ coils in the B magnet will permit one to directly
measure the effect of the cooling tube on the magnet's quench performance.
The inner and outer $d\phi/dt$ coils can be bucked; the signal remaining
corresponds to the current induced in the cooling tube during the
quench process. The central location of the B magnet $d\phi/dt$ coil should
result in better measurements of the coupling between the superconducting
coil, its bore tube and its cooling tube.

c) Temperature Sensors

The first test of the first one-meter diameter solenoid lacked
accurate measurements of coil and bore temperature. Copper-constantan
thermocouples were used during the cool down. This type of thermocouple
is completely useless below 25 to 30 K. We found that a lack of good
temperature measurements while the magnet was operating at or near
its operating temperature was a real handicap. Other methods had
to be used to measure temperatures at or near 4 K.
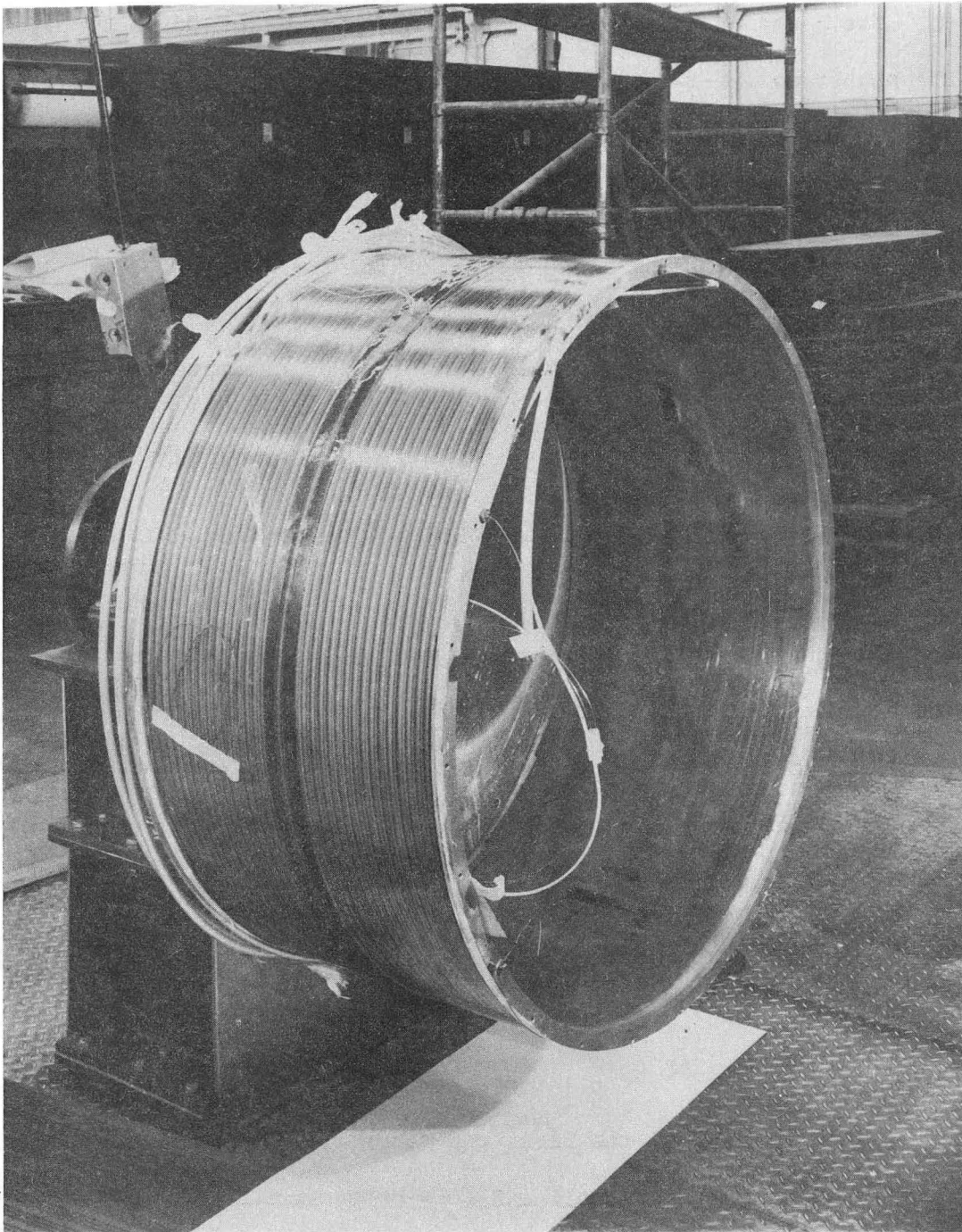
CBB 762-1385

Fig. 20. The finished B magnet. The double dark
band at the center of the magnet is a 41-turn
P coil for measuring the rate of change of
magnetic flux in the magnet.

A number of the common methods for measuring 4K temperature was rejected. Our laboratory has had bad luck with ordinary carbon resistors; therefore this method was ejected. (Operation of carbon resistors in a vacuum is particularly risky.) The vapor bulb thermometer was also rejected, for two reasons: 1) the temperature range is limited to between 2.5 and 20 K; and 2) the thermometers are bulky and have a long thermal time constant.

Before choosing our silicon-diode thermometers we looked at platinum resistance thermometers, capacitance thermometers, gallium arsenide thermometers and glass-ceramic carbon resistors.[60] We felt that the silicon-diode offered the best combination of cost and reliability for a sensor which could be used over the entire range of temperatures from 4 to 400K. The major disadvantage of the silicon-diode is its magnetic field sensitivity. However, we found that we could calibrate the diode to get rid of this effect.

The silicon-diode has very good sensitivity at low temperatures. The signal from the sensor is about 2.4 volts at 4.2K, 0.9 volts at 77K, and 0.35 volts at room temperature. Figure 21 shows the voltage output of the silicon-diode as a function of temperature. The silicon-diodes are powered by a LBL-built 10 μA power supply.[61] The total power dissipated in the sensor at 4.2K is around 25 μW. This low rate of power dissipation is important when the sensor is operating in vacuum.

Each silicon-diode is mounted on an aluminum plug which can be screwed into the magnet experiment. The plug serves as a platform for the diode and as a heat sink for the electrical leads which go to the diode. The thermal time constant for the diode and plug is about 100 ms at
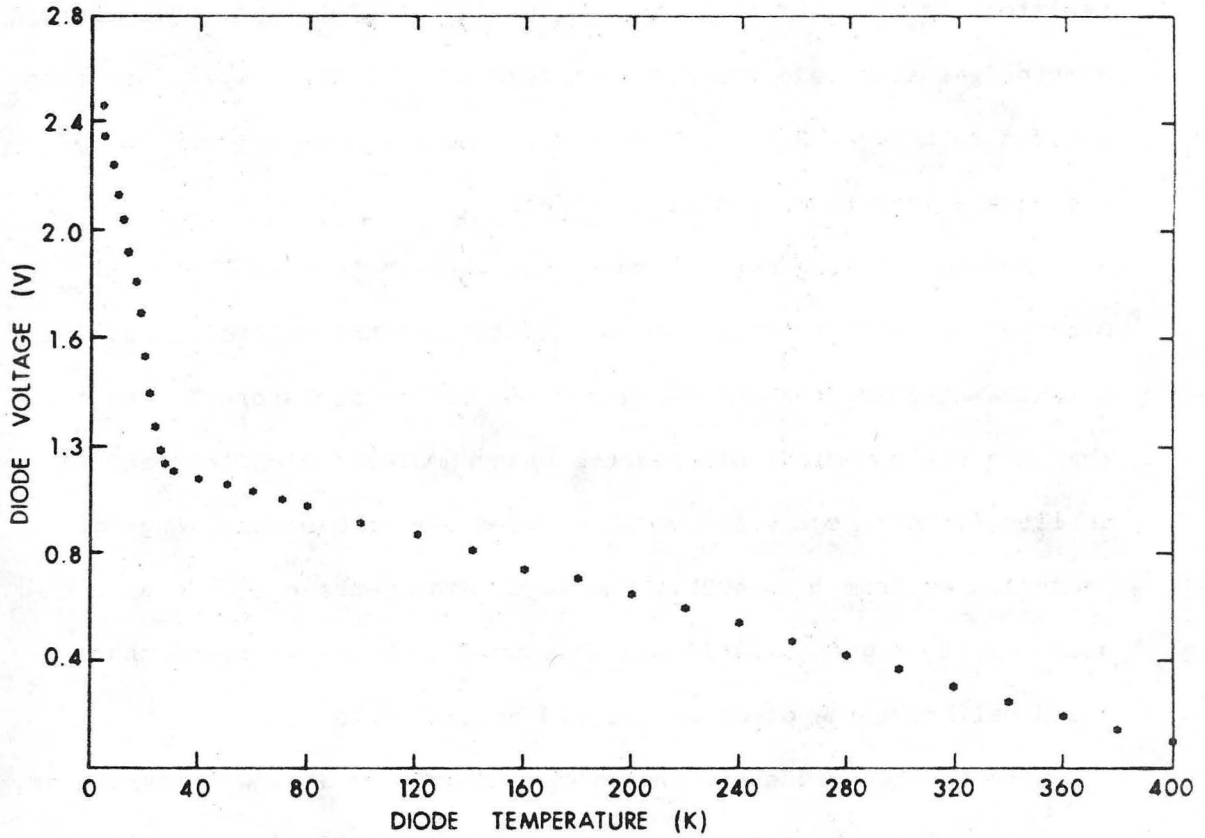
XBL 774-8449

Fig. 21. The voltage generated by the silicon-
diode thermometer as a function of
temperature (this is a typical
calibration curve).

4K, and increases to several seconds at 77K. The diode temperature
sensor system time constant is about a factor of three faster than
the time constant for heat removal from the magnet.

Each magnet bore tube had three temperature diodes on it. There
were two uncalibrated diodes (these had been calibrated only at 4.2,
20, 77, and 300 K) at each end inside the bore tube (on
the flange). There was one calibrated diode (calibrated over the
full temperature range by Lakeshore Cryotronics[62]) at the center of
each bore tube. In addition to the magnet diodes there was one uncalibrated
diode located on the helium inlet tube from the refrigerator. Each
experiment used from four to seven silicon diodes. Figure 22 shows
the location of the silicon diodes on the magnet bore tube.

d) Bore Tube Strain Gages

The one-meter diameter thin superconducting solenoid magnets
can potentially put the superconducting wire under large stresses.
However, other components of the magnet, such as the bore tube and the
cooling tube, can carry part of the magnetic forces so that the super-
conductor operates at much lower levels of stress. One can learn
how the magnet behaves as it is energized by measuring the strain
in the bore tube as we put current in the coil. Strain gages, which
are capable of operating at 4K, were used to measure the bore tube
strain.

The magnet experiment operated at a temperature of 4.5K. The
magnetic induction on the gage varied from 0 to 2 tesla. The maximum
strain one would expect to measure in the aluminum bore tube was less
than 0.5 percent. The properties desired for these gages were as
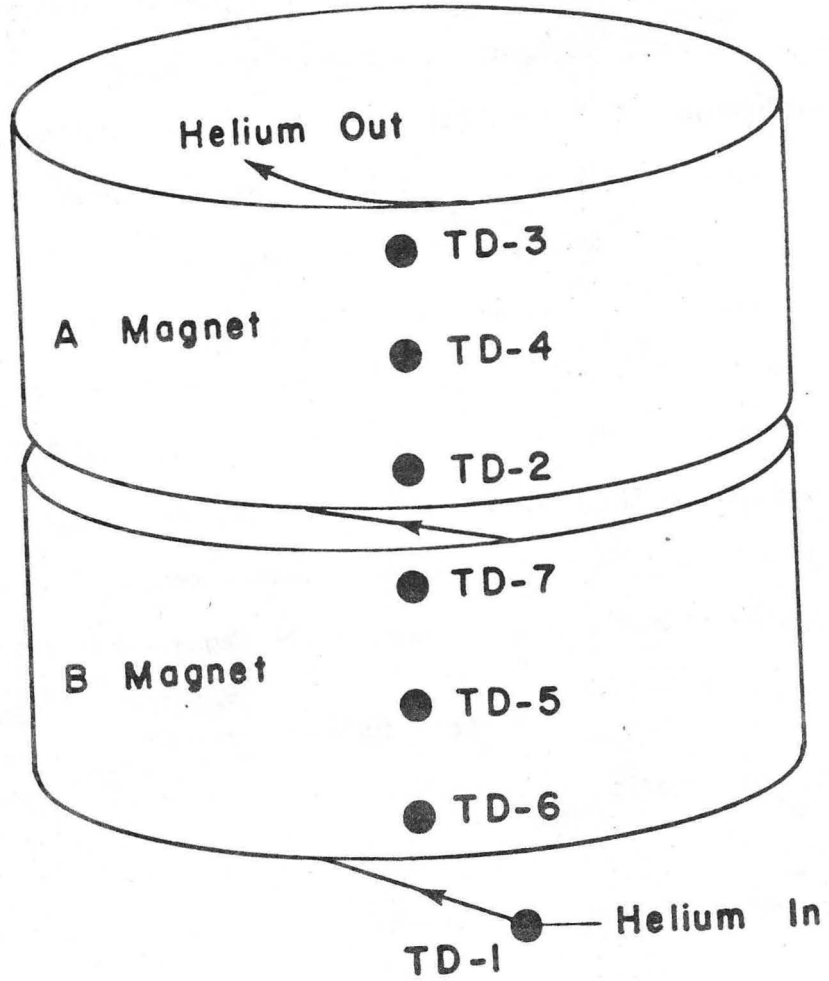
Fig. 22. The location of the silicon-diode
thermometers of the A and B magnet
bore tubes and the helium pipe
entering the magnet (this set-up was
applied during the July 1976 test).

follows: 1) the gage should operate at 4K, 2) there should be little
or no change in resistance as the temperature changes; 3) there should
be little or no change in resistance as the magnetic environment changes
4) the contraction coefficient of the gage should match that of the
aluminum it is applied to; and 5) one should be able to cool the gage
while it is mounted on the bore tube without having it come unglued.
The gage chosen for use in the thin coil experiment was the Micro-
Measurement WK-13-250 BF-120 gage. This gage meets all of the objectives
given above, except the change of gage resistance with temperature.
More detailed information on the strain gages may be found in reference
63 or in the data sheet provided by the manufacturer.

The strain gages were mounted on the aluminum bore tubes before
the coil was wound. Since strain gages are affected by over twenty
different environmental factors (the most important are temperature
and magnetic field), the use of dummy gages to buck out extraneous
environmental factors was justified. A dummy tab with unstrained
gages was mounted so that it saw the same environmental factors (except
strain) as the gages mounted on the magnet bore tubes. The dummy
strain gage and the active strain gage were mounted in a bridge circuit
(see Figure 23). The bridge was balanced; the relative strain between
the bore tube and the dummy tab was measured. (A commercially available
strain gage bridge box owned by LBL was used in our experiment.)

The A magnet had two gages mounted on its bore tube. They were
mounted at the center of the tube such that they measured strain in
the transverse or hoop direction (see Figure 24). The B magnet had
four gages mounted on its bore tube. Two of these gages were mounted
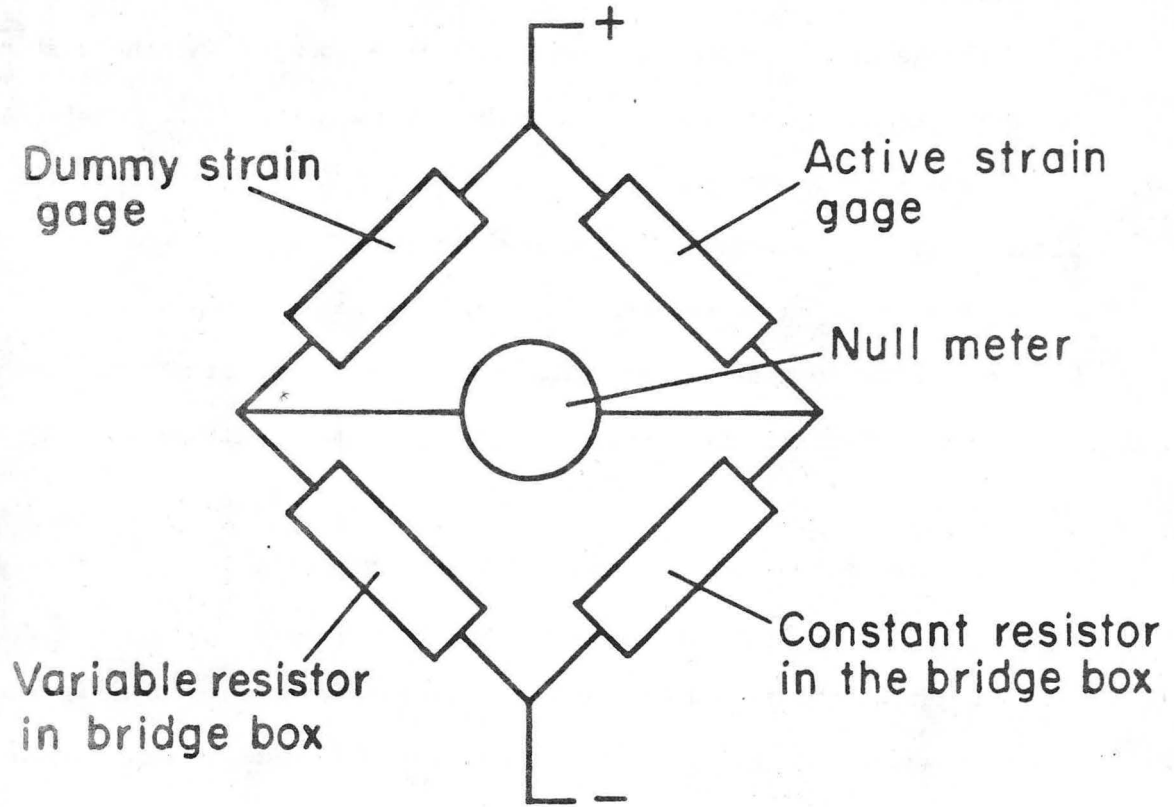
Fig. 23. A simple bridge circuit for the strain gages. The dummy strain gage compensates for temperature and magnetic field sensitivity.

XBL764-5485 A
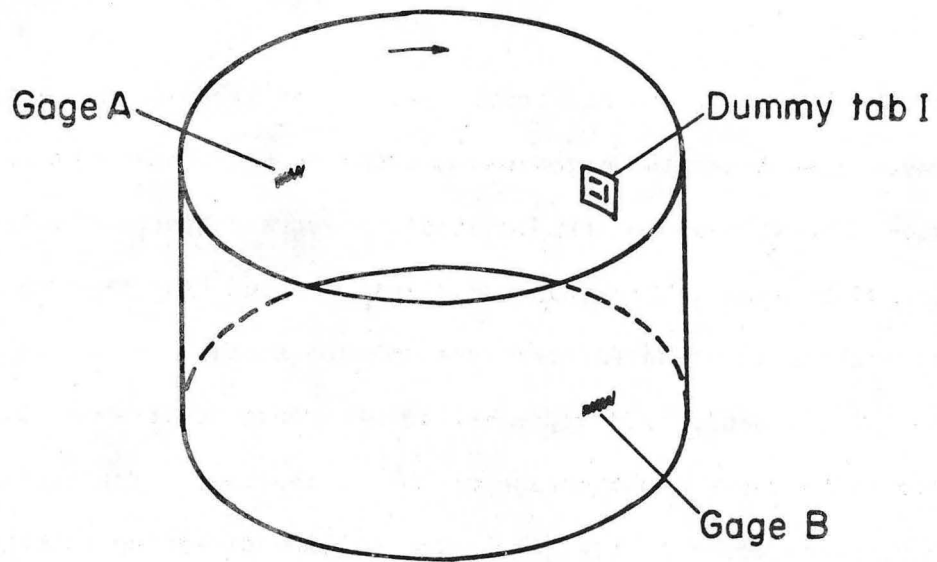
a) A magnet strain gages and dummy tab.
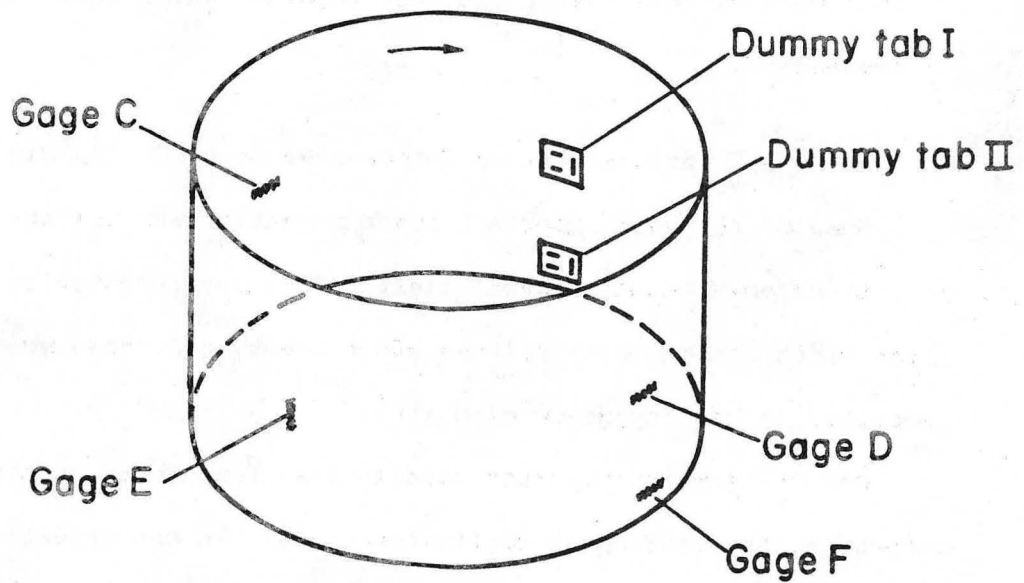
b) B magnet strain gages and dummy tab.

XBL764-5383A

Fig. 24. The location of the active and dummy
strain gages on the A and B magnets.

on the center of the bore tube just as the gages on the A magnet.
One of the other two gages was mounted on the center of the bore tube
such that it measured the longitudinal strain (perpendicular to the
loop direction). The fourth gage was mounted near the edge of the
bore tube; it measured transverse (hoop) strain.

Three separate dummy tabs had been made for the magnet experiments.
Figure 25 shows a photograph of one of the tabs. The tab had two gages
which were mounted parallel to the rolling direction (the hoop direction
in the magnet) and one gage mounted perpendicular to the rolling direction.
The dummy tabs were mounted inside the magnet bore tube but not touching
it; also, they were mounted so that the temperature, magnetic field
strength, magnetic field direction, rolling direction, and degree
of cold work matched that of the active gages which they were supposed
to compensate.

e) Instrumentation Not Mounted In or On the Magnet

Some of the most important instrumentation was not mounted on
or fabricated with the magnet itself. This instrumentation included
those which measure coil voltage and current, and those which measure
pressures in the cryogenic circuitry.

One of the most important single measurements to be made on the
magnets as they are operating is the current in the magnet coil.
Current in the coil is taken by measuring, with a digital voltmeter,
the voltage across a 1.066 m ohm water-cooled shunt which carries the
full current into the coil. The coil voltage to be measured is taken
from voltage taps which are mounted directly to the ends of the super-
conducting portions of the coil. (The voltage drop across the electrical
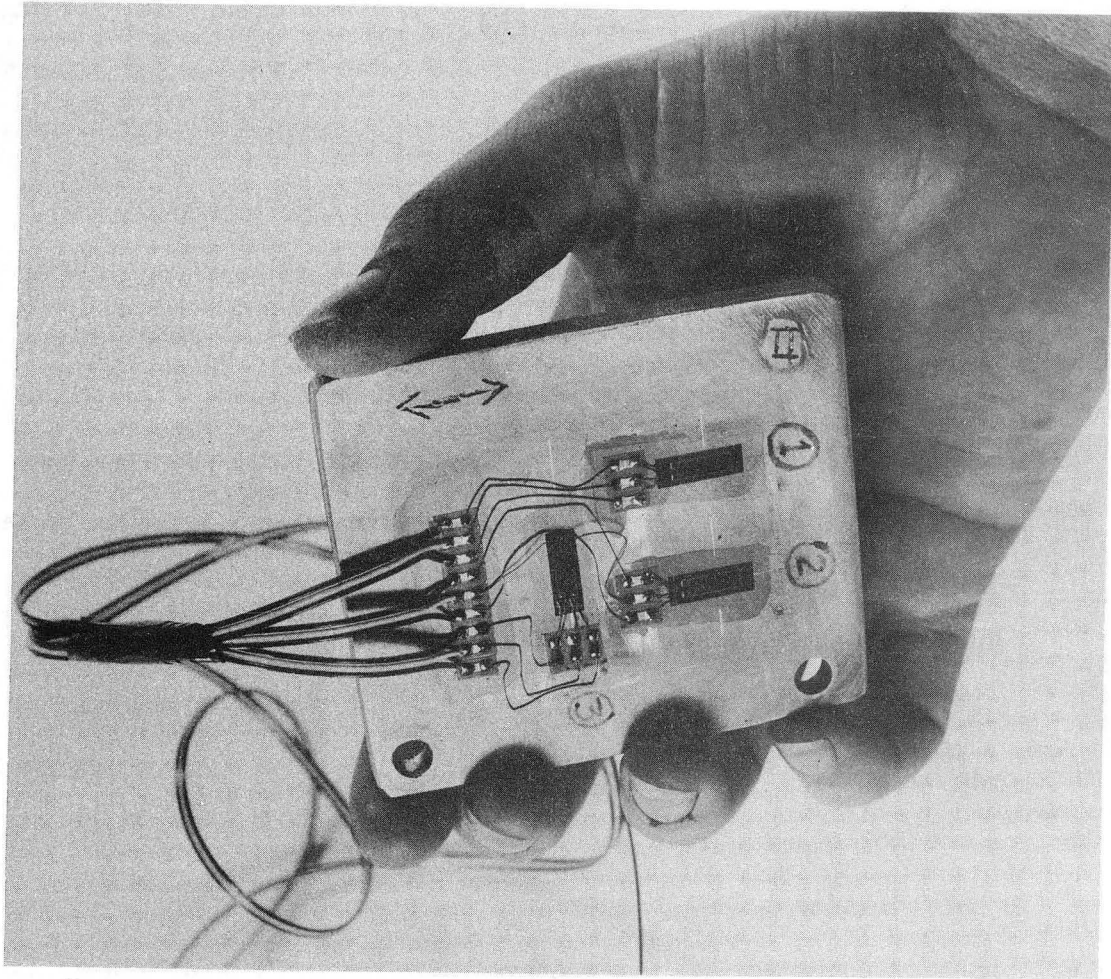
CBB 764-3036

Fig. 25. The dummy tab used for strain gage
compensation. The arrows show the
hoop or rolling direction.

leads at 1000 A is about 50 mV.) One cannot measure coil voltages across room temperature electrical lead ends.

Pressures in the refrigeration circuitry are measured directly by room temperature pressure gages which are connected to the point in question by capillary tube. Oscillation in the pressure gages is eliminated through the use of needle valves which snub out the oscillations. We measured differential pressures with magnahelic differential pressure gages between the two pressure taps in question. Magnahelic gages may be pegged to the maximum value without destroying the gage itself. This is an important feature because differential pressures will vary about two orders of magnitude as the experiment is cooled down. The location of the various pressure gages is shown in the next section of this report.

Other instrumentation in our experimental apparatus included various copper-constantan thermocouples on the liquid helium and liquid nitrogen circuits. An American Magnetic temperature sensor was mounted in the control dewar. This sensor is not very sensitive at 4K. (The silicon-diode sensor is far superior to the American Magnetic thermometer at temperatures below 20K.) An American Magnetic liquid helium level gage was also mounted in the control dewar.

The last piece of sensing apparatus was several small coils mounted inside the solenoid. These coils permitted us to make an approximate field map inside the solenoid. They played an important role during the time we were calibrating the experiment, and were used as a check for measuring the self inductance of the magnet.

3.4. Physical and Electrical Parameters of the Magnets

This section deals with the mechanical and electrical parameters of the finished magnets. Table 7 shows these basic dimensions. The magnet bore tube, coil, and cooling tube assembly are about 1.4 mm thinner than the flange of the coil. The Fiberglass standoff buttons between the copper bus bar and the coil bore tube extend beyond the edge of the coil. The largest overall diameter of the coil is about 1080 mm. The mass of the coil assembly is broken down in Table 8. Table 9 shows an estimate of the radiation thickness of the magnet assembly.

The electrical parameters of the magnet were calculated using a computer program called HENRY,[64] which uses elliptic functions to calculate the field in the coil, the inductances and the stored energy. The procedure for calculating the electrical parameters is discussed elsewhere.[65,66,67]

The load line for the A and B magnets is shown in Figure 26. This figure shows the peak induction in the coil versus the current in the superconductor. It also shows the critical current in the A coil and B coil superconductor as a function of induction and temperature. (Temperatures of 4.2 K and 5.0 K are shown). The critical current line is defined by a resistivity of 10^{-14} ohm m. The design current for the A magnet is 700 A; the design for the B magnet is 880 A. The electrical parameters of the two magnets are given in Table 10.

One can understand the electrical behavior of the magnet coil and its bore by looking at relative time constants of the coil and

Table 7. Finished magnet dimensions.

	Dimension (mm)	
	Coil A	Coil B
Inside diameter	1021	1021
Ouside diameter	1070	1070
Magnet thickness	24.5	24.5
Magnetic coil length	460.9	464.1
Magnet spool length	500	500
Overall assembly length	~600	~600
Thickness of the various components		
Bore tube	6.35	6.35
Superconducting coil	3.25	3.25
Cooling tube assembly	13.50	13.50
Flange thickness	24.50	24.50

Table 8. A breakdown of the mass of various magnet components.

	Mass (kg)	
	Coil A	Coil B
Aluminum bore tube	34.0	34.0
Insulated superconductor	17.5	16.0
Fiberglass	1.5	1.5
Dacron and other plastic parts	0.8	0.6
Refrigeration tube	12.2	12.2
Epoxy	9.2	8.5
Sub Total	75.2	72.8
Copper bar assembly	6.0	6.0
Total Cold Mass	81.2	78.8

-84-

Table 9. A breakdown of the radiation thickness in a coil.

Component	Radiation Thickness*	
	Average through the coil	Through the end flange
Superconductor	0.100	--
Aluminum bore tube	0.071	0.271
Aluminum refrigeration tube	0.033	---
Glass, dacron and epoxy	0.029	---
TOTAL RADIATION THICKNESS	0.233**	0.271*

* Given in radiation lengths.

**The average radiation thickness over the whole coil including the end flanges is less than 0.24 radiation lengths.
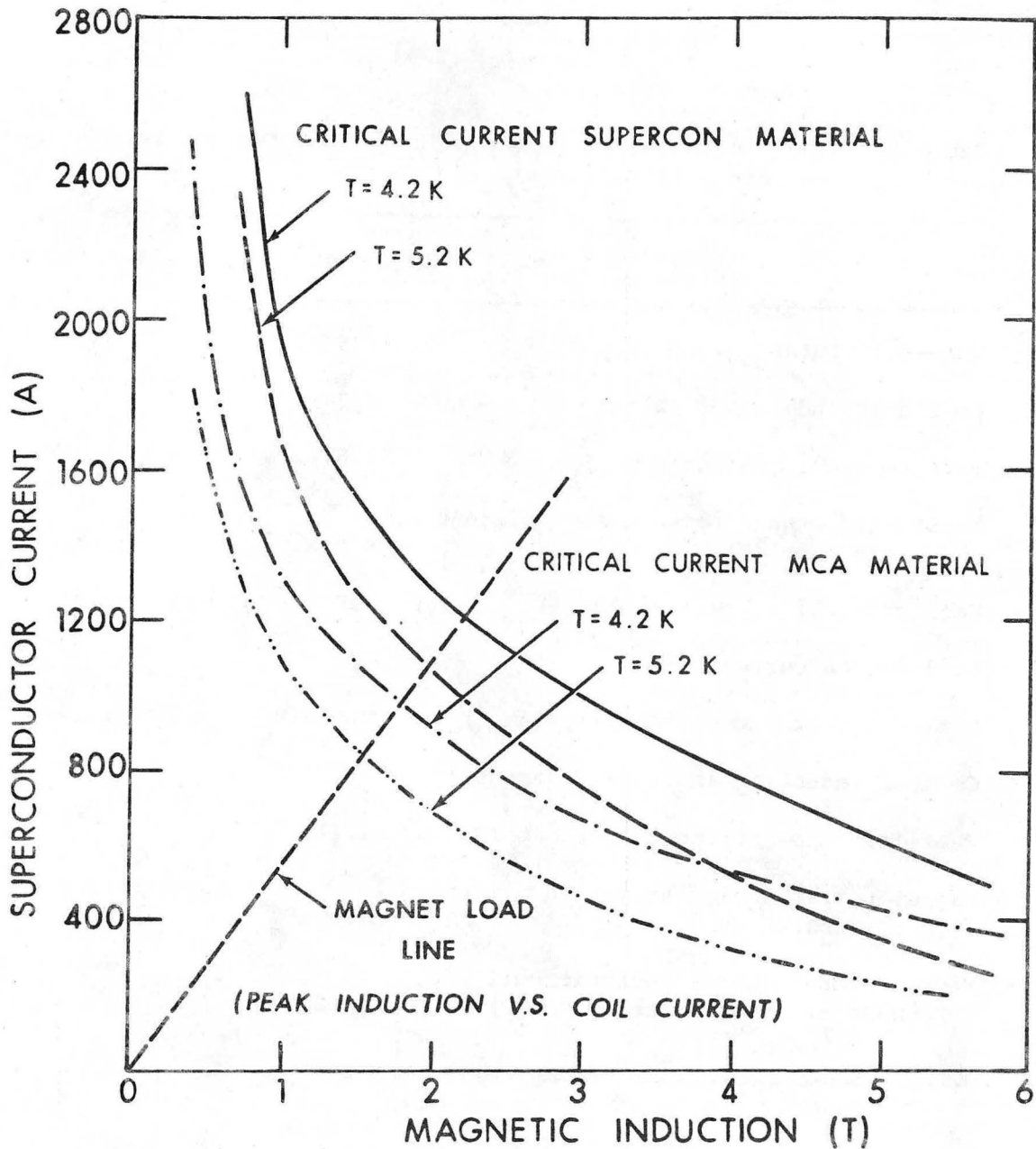
Fig. 26. The peak magnetic induction in the
magnet superconductor vs magnet current
(the load line), and the critical current
for the MCA and Supercon superconductors
as a function of magnetic induction. The
intersection of the load line with the
superconductor performance curve determines
the critical current for the magnet.

Table 10. The electrical characteristics of the two LBL test
magnets (without iron).

	A Magnet	B Magnet
Number of turns	835	832
Coil self inductance (H)	0.789	0.782
Bore tube self inductance (H)	1.014×10^{-6}	1.014×10^{-6}
Mutual inductance between the coil and bore tube (H)	8.97×10^{-4}	8.92×10^{-4}
Coil critical current at 5 K (A)	910	1160
Coil design current (A)	700	880
Design matrix current density (Am^{-2})	0.91×10^{9}	1.12×10^{9}
Central induction at design current (T)	0.65	0.77
Peak induction at design current (T)	1.11	1.40
Magnet stored energy at design current (J)	1.93×10^{5}	3.03×10^{5}
Magnet stored energy per unit coil mass at design current (Jg^{-1})	11.2	18.9

the bore tubes. In all cases, the superconductor was assumed to be in the normal state. The time constants shown in Table 11 are defined by equations 9a and 9b.

From Table 10 one can predict that a substantial portion of the magnet-stored energy will end up in the bore tube after a magnet has quenched. The B magnet should dump more energy into the bore tube than the A magnet. The magnet and bore tube combination should fulfill the objectives of the conceptual design. Section 5.3 of this report shows that the bore tube does behave as it should. Tests on the magnet coils show that the parameters given in Tables 10 and 11 are correct.

Table 11. Current decay time constants for the LBL coils and bore tubes as a function of temperature.

Temperature (K)	Bore Tube* Same for Both Magnets	MCA Coil[†]	Supercon Coil[††]
10	537	610	398
20	537	610	398
30	519	610	398
40	446	325	249
50	365	155	109
70	242	60.2	42.4
100	154	32.6	22.9
150	87.8	18.2	12.8
200	60.4	12.6	8.9
250	44.3	9.4	6.5
300	35.4	8.1	5.7

* Based on resistance ratio 15.3 aluminum. 300K resistance of the bore tube is $2.89 \times 10^{-5}\Omega$.[48]

† Based on a resistance ratio of 75 superconductor, 1.8-1 Cu to s/c ratio. The 300K resistance is 92.5 Ω.

†† Based on a resistance ratio of 70 superconductor, 1-1 Cu to s/c ratio. The 300K resistance is 132 Ω.

IV.   REFRIGERATION OF THE LBL TEST SOLENOIDS

The LBL test solenoids are designed to be cooled by two-phase helium which circulates in the cooling tube around the magnet coil. It is desirable that the liquid helium used be of lowest quality. (Quality, in this case, is defined in the same sense as it is for steam. A quality of 0 is saturated liquid; a quality of 1 is saturated vapor. Qualities between 0 and 1 define where the fluid is in the two-phase region.) Low quality helium in the cooling tube reduces the pressure drop in the system for a given mass flow, and there is more heat of vaporization available for cooling when it is used. The LBL system uses the heat vaporization of the helium. This drops the operating temperature and minimizes the temperature change across the system.

Two kinds of systems can be used to circulate low quality helium through the magnet cooling tube. They are: 1) a liquid helium pump used as a circulator, or, 2) the refrigerator compressors used as a circulator. Both systems use a heat exchanger to insure that the helium will enter the system at or near the saturated liquid line. Figure 27 shows schematic diagrams of the two approaches.

The helium pump loop system shown in Figure 27a has the following advantages: 1) The refrigerator is completely decoupled from the load. In theory, one could substitute liquid helium from a storage dewar for the refrigerator. 2) The mass flow through the system is limited by the capacity of the pump, not the capacity of the refrigerator. The two disadvantages of the use of a helium pump system are: 1) The pump work is put into the helium, and therefore extra refrigeration
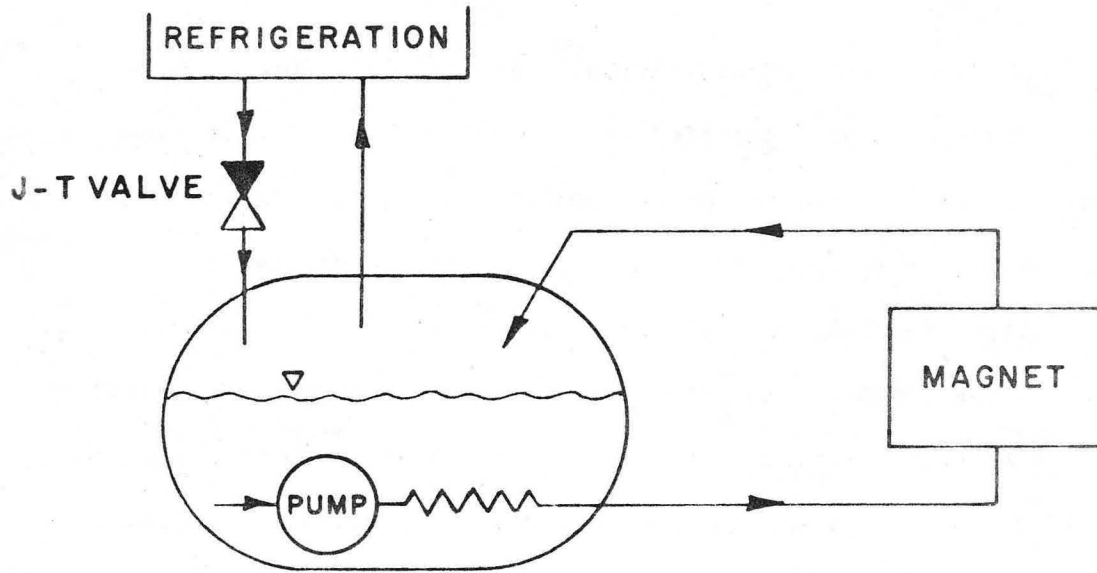
a) LIQUID HELIUM CIRCULATION WITH PUMP
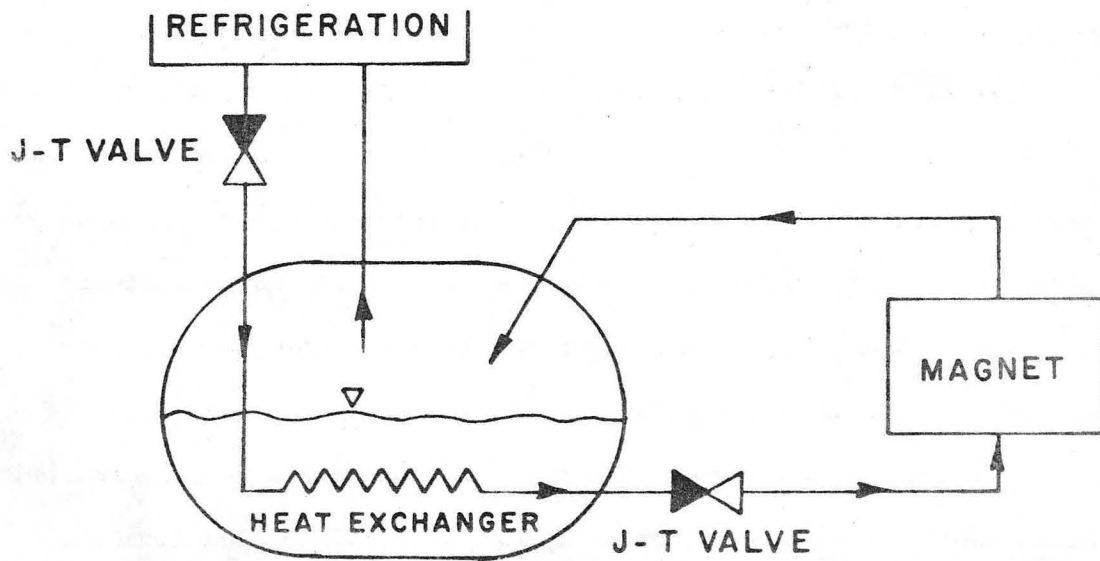
b) LIQUID HELIUM CIRCULATION WITH REFRIG. COMPRESSOR

XBL 773-7856

Fig. 27.   Two types of two-phase helium circulation
systems for tubular cooled superconducting
magnets.

must be supplied to overcome the work which goes into pumping.

2) The simple pump loop system shown in Fig. 27a cannot be used to cool the magnet down from room temperature; one must connect the magnet cooling system directly to a refrigerator.

The refrigerator compressor can be used as a circulator provided a heat exchanger is used in an accumulator. The function of this heat exchanger is to reduce the inlet quality to the magnet cooling tube. The quality change across the magnet remains the same for a given mass flow in the circuit. The circuit shown in Fig. 27b has two Joule Thompson valves (J-T valves) which expand the gas in two stages. The first J-T valve expands the gas to a pressure of about 5 bar. The gas is heated while it is being expanded from 15-18 bar to 5 bar. The heat is transferred to the boiling liquid helium in the accumulator tank as the gas flows through the heat exchanger. Expansion of the gas from 5 bar to the final inlet pressure of the load will result in an inlet quality at the load which approaches zero. If there were no heat exchanger the inlet quality at the load would be around 0.4; the pressure drop in the tubular cooling system would be a factor of 2 to 3 higher.

The system shown in Figure 27b is analyzed from a thermodynamic standpoint in reference 39. This system is capable of being operated at 30 to 40 percent over the capacity of the refrigerator for short periods of time. (The amount of time is dependent on the amount of excess liquid helium in the accumulator). It can be cooled down by the refrigerator directly, provided one bypasses the gas back to the compressors after that gas has passed through the load being cooled

down. Although this system was chosen for use in the LBL test coils,
it is likely that a hybrid system (a combination of Figure 27a and
Figure 27b) will be used in the final magnets to be built for PEP.
The hybrid system is expected to offer maximum reliability.

The LBL test coils were tested at two different locations, using
two different refrigerators. Substantial improvements were made in
the cryogenic system as these tests proceeded. The first two tests
(November of 1975 and March 1976) were made using a cryogenic technology-
incorporated (CTi) Model 1200 refrigerator liquifier located in LBL's
Building 64. The last test (July 1976) was performed in Building 58 using
a CTi Model 1400 refrigerator.

4.1. Refrigeration for the Building 64 Tests

The first two tests of the large solenoids were done in a small
superconducting magnet laboratory located at the north end of
Building 64 at LBL. This laboratory is equipped with a 500 Incorporated
(the company name has since been changed to Cryogenic Technology
Incorporated--CTi) Model 1200 refrigerator. The refrigerator is a
Claude cycle machine based on designs originated by Sam Collins of
MIT.[68] The LBL Model 1200 machine developed 35 watts at 4.5K or
10 liters per hour of liquid helium[69,70] in 1969 when it was installed
at Berkeley. The performance of this machine has degraded after a
number of years of use,[70,71] and it currently will deliver about
18 W at 4.5K or $8\ell h^{-1}$ of liquid helium. This refrigerator was used
to cool down the experiment when it operated in Building 64.

The magnet cryostat was salvaged from the LBL Howard Terminal warehouse in Oakland. The cryostat, which was originally built in 1965, was not in very good condition. However, since its price was right, we could afford to spend a little money to repair and refurbish it. The cryostat has about 20 layers of super-insulation around its stainless steel inner vacuum vessel. We used about 80 cm of foam to insulate the neck of the vessel. After refurbishing and vacuum pumping, the dewar heat leak was about 12 watts. This heat load could be cut down some by bleeding large quantities of boil off helium out of the top plate. This procedure could cause the main vacuum system O ring to freeze.

The cryostat, which is 2.2 m high and 1.3 m in diameter, could not be used in the Building 64 laboratory because the building ceiling is only 3 meters. The doorways are even smaller. Therefore, the experiment was located in back of Building 64 about 2 m from the building wall. A flexible co-axial transfer line was built to connect the refrigerator to the cryostat. This transfer line, which has a flexible section about 7 m long, can be bent to a curvature with about 0.5 m radius. The inside diameter (cold diameter) is 10.9 mm; the vacuum shell diameter (the outside of the flexible hose) is about 40 mm. Refrigeration is sent out to the experiment through a small inner line (its ID is about 4.5 mm); the cold gas is returned to the refrigerator through the annular space between the OD (7.9 mm) of the inner line and the 10.9 mm ID of the transfer line itself. The co-axial system behaves like a heat exchanger, so proper care must be exercised during cool

down. The construction and test of the flexible transfer line used
in this test is described in Reference 72.

a)   The November 1975 Test

The large cryostat was used as a cryostat for the November 1975
test. The magnet with all of its plumbing was sitting in a helium
gas atmosphere. (It was felt, at the time, that we could save a lot
of money by using this arrangement. We were wrong.) Cold gas (hopefully
two-phase helium) from the refrigerator would circulate through the
magnet coil and provide cooling for two gas-cooled electrical leads.
The two-phase helium (if the were any) would drop into a small pot where
phase separation would occur and cold helium gas would then flow back to
the refrigerator through the annular space in the transfer line. The
system shown in Figure 28 would work provided the total refrigeration
load did not exceed the capacity of the refrigerator. This was not
the case, as the reader will see later.

The gas-cooled electrical leads used for this experiment and
the two later experiments were the standard LBL "Tampax" leads. These
electrical leads are very easy to build and perform well. They have
superconductor soldered to the outside, and consist of a 19.1 mm
(3/4 inch) ID type K copper pipe. Helium gas flow in it is laminar,
so the heat transfer from the tube wall to the gas is not very good.
The insertion of an epoxy fiberglass rod (the Tampax) into the tube
creates a 0.5 to 0.7 mm annular space between the tube and the epoxy-
fiberglass rod which improves the heat transfer from the copper tube
to the helium by at least a factor of twenty. This in turn improves the
performance of the electrical leads considerably.
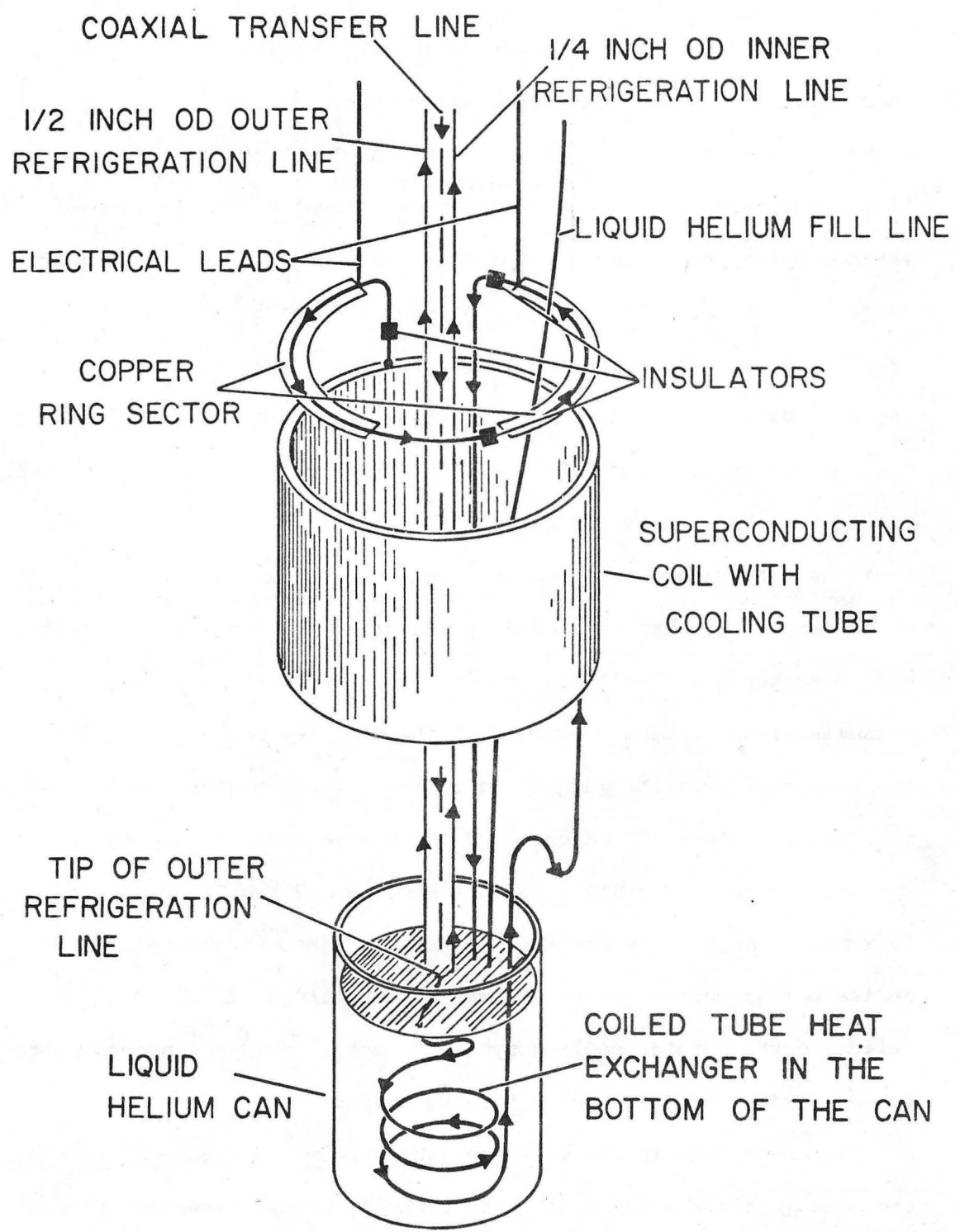
Fig. 28. A schematic view of the cryogenic cooling
system used on the November 1975 test of
the A magnet.

XBL 774-8545

The Model 1200 refrigerator cooled the experiment from 300K to 50K in about twelve hours. The bypass was opened so that helium did not return to the refrigerator through the annular space in the transfer line. The temperature of the magnet was measured by copper-constantan thermocouples (they are not good below 40K) and by measurements of the magnet resistance. The magnet cool down stopped at about 50K. The total heat load exceeded the capacity of the refrigerator. In addition, the refrigerator reacted poorly with the gas volume around the magnet.

Liquid helium from a 500 ℓ dewar was used to cool the magnet from 50K to 6K. The liquid was added to the collection pot. The flow from the refrigerator removed the remainder of the heat from the magnet, whose temperature was monitored by measuring its resistance. This method worked quite well down to about 9.5K when the superconductor became superconducting. Below 9.5K the only way one could estimate the temperature in the magnet was to measure the pressure drop across the cooling tube in the magnet. Using this method, it was estimated that the magnet temperature was between 6 and 7 K. Two-phase liquid flow in the magnet was never established. Since the magnet operated at its design current at an estimated temperature of 6.5 K, liquid helium in the tubular cooling system is not a necessary prerequisite for successful operation of a thin solenoid.

The major difficulty with the system shown in Figure 28 is that the load (estimated to be between 35 and 40 watts) exceeded the capacity of the refrigerator (estimated to be between 15 and 20 watts). Every time the magnet went normal, the gas volume around the magnet was heated. This gas rushed out of the system through the relief valves

and was lost. The total gas volume around the magnet was estimated

to be 1400 liters. This volume requires about 250 liters of liquid

helium to fill it at 6K. The refrigerator does not react well with such

a large gas volume, and small changes in temperature easily change

the flow conditions in the refrigerator. In any event, the system

shown in Figure 28 was the wrong one to use. It cost the experimenter

nearly 2000 liters of liquid helium to find out the effectiveness

of quick and cheap cryogenic solutions.

b) The March 1976 Test

As a result of previous experimental experience, a number of

changes were made in the cryogenic system. These included: 1) accurate

temperature measurement below 50K, 2) reduced cold gas volume in

contact with the Model 1200 refrigerator and 3) a number of changes

in cryogenic components so that the cryogenic system used for the

March 1976 test (and later ones as well) closely resembled the system

shown in Figure 27b. Temperature measurements were made using the

silicon-diode thermometers described in the previous section.

The large cryostat was converted into a vacuum vessel. The plumbing

for the magnet was made vacuum tight. In many cases soft-soldered

joints were replaced by hard-soldered or welded joints. The

transfer line was rebuilt to reduce its losses.[72] A transition piece

was made to separate the inner and outer parts of the co-axial transfer

line. Figure 29 shows a schematic diagram for the cryogenic system

used for the March 1976 test. Figure 30 shows the vacuum tight plumbing

which is a part of this cryogenic system.
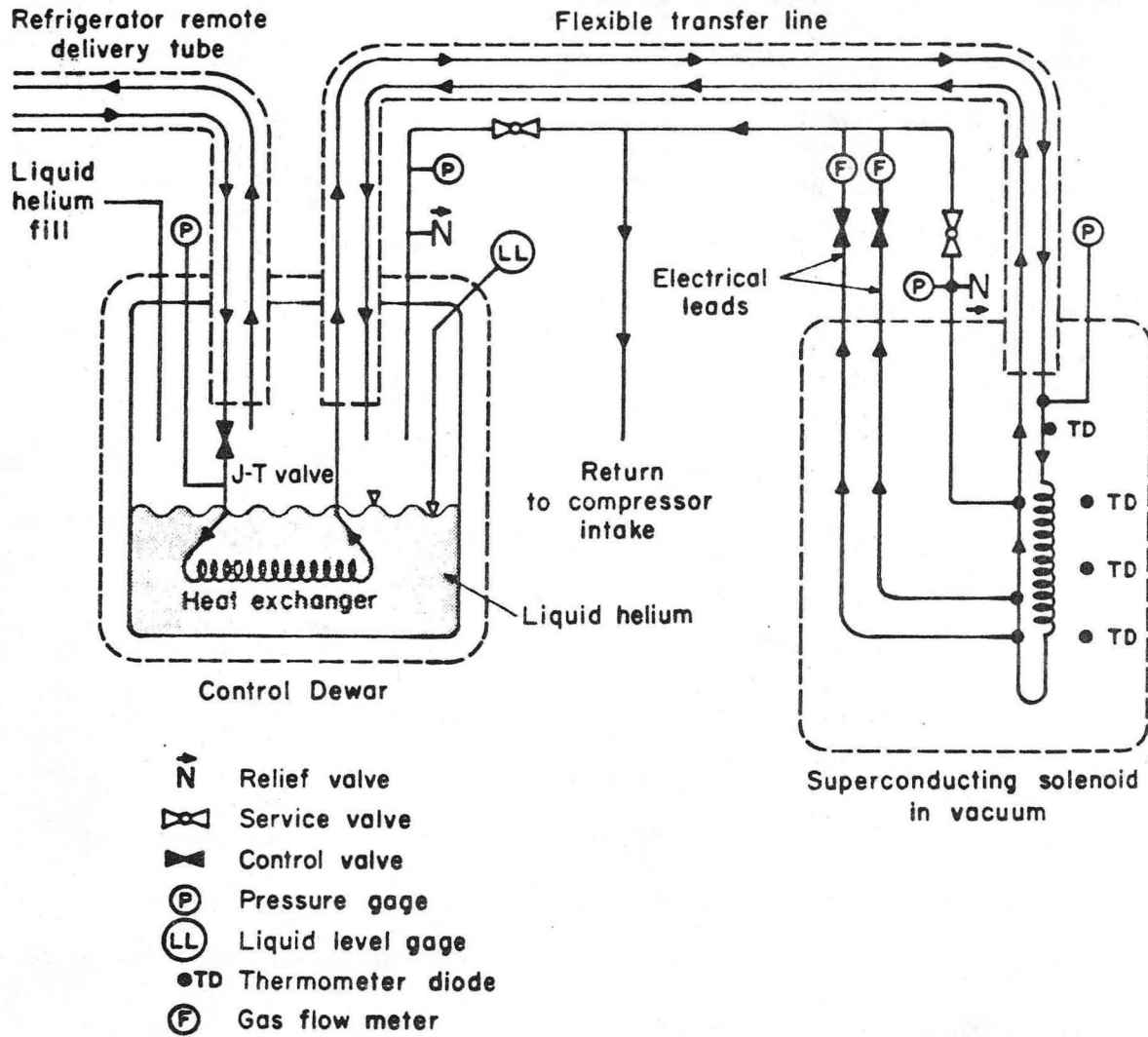
Fig. 29. A schematic diagram of the cryogenic cooling system used for the March 1976 test of the A magnet. The July 1976 test of both magnets has a cryogenic system with a similar schematic diagram.
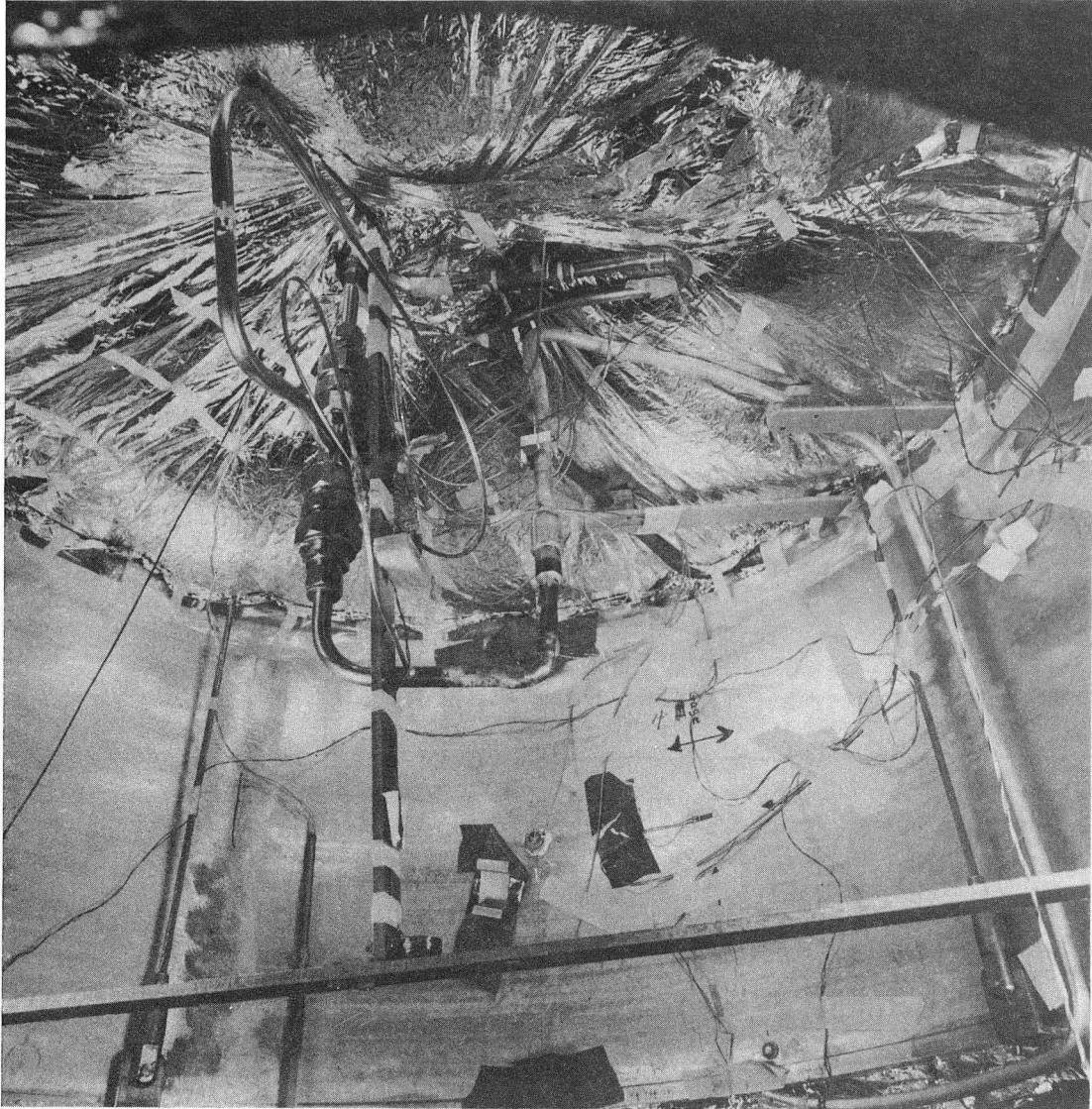
CBB 673-2832

Fig. 30. The cryogenic plumbing system of the
A magnet used during the March 1976
test. (Note all of the plumbing is
in a vacuum and it is at 4.6 K.)

The magnet with its tubular cooling system was shielded by a nitrogen temperature shield, and by multilayer insulation. The liquid helium, which is in contact with the magnet, was limited to about 11 liters (the volume of the tubular cooling system). Control of the refrigeration process and phase separation was achieved by using a separate 25.4 cm (10 inch) inside diameter control cryostat containing heat exchanger which helped lower the quality of the two-phase helium entering the co-axial transfer line to the magnet. The control dewar held around 40 liters of liquid helium. Figure 31 shows the Model 1200 refrigerator connected to the control dewar. Figure 32 shows the large cryostat located outside Building 64, a temporary shack. The flexible transfer lines, cables, helium service lines, and electrical leads passed from the Building 64 superconducting magnet laboratory to the magnet cryostat through a window in the building.

The cool down of the experiment, which had a cold mass of about 150 kg, took around 12 hours to reach 70K. From 70K down the cool down was very slow. During the early phase (above 120K), there was a temperature gradient of about 40 Kelvin degrees from end to end in the magnet (see Figure 33). The rate of cool down was limited primarily by the mass flow of helium. The refrigerator delivered 1.5 to 2.0 g s^{-1} of helium and this rate was nearly constant during the entire cool down of the magnet. The reasons for constant mass flow are: 1) The refrigerator heat exchanger cools down much more rapidly than the experiment. 2) The high pressure side of the heat exchanger is designed to have a low pressure drop. The pressure drop across the magnet was measured and found to be nearly linear with the magnet temperature (see Figure 34).
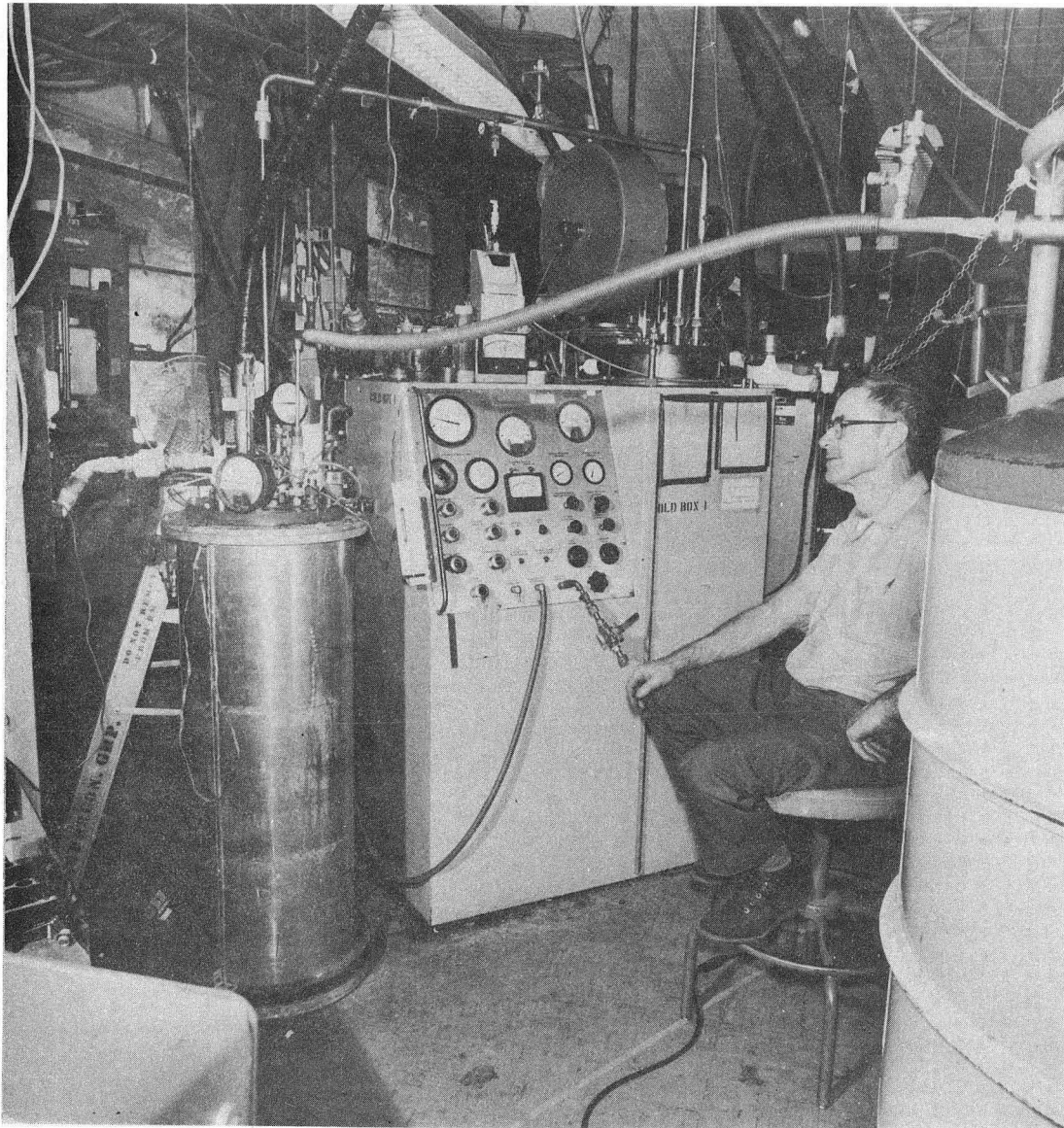
CBB 763-2356

Fig. 31. The refrigerator and control dewar
used in the March 1976 test in Bldg. 64. The
control dewar is at the left, the model 1200
refrigerator is in the center; and the 500 liter
storage dewar is to the right. The black line
rising straight above the control dewar is a co-
axial transfer line to the magnet which is
located outside Bldg. 64.
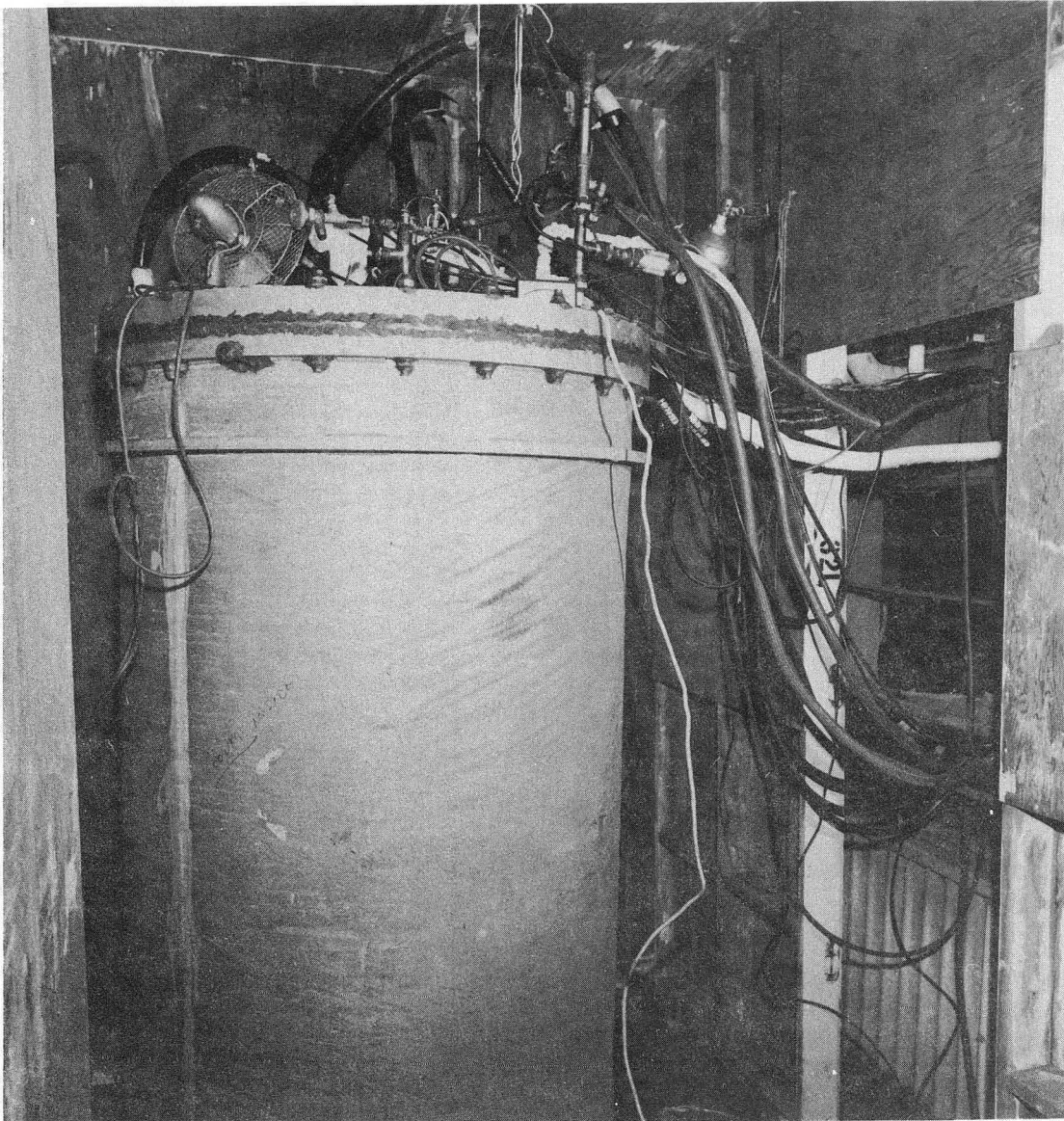
CBB 763-2354

Fig. 32. The magnet cryostat located outside the
          window of Bldg. 64 during the March 1976
          test. (A temporary shack was built
          around the magnet cryostat.)
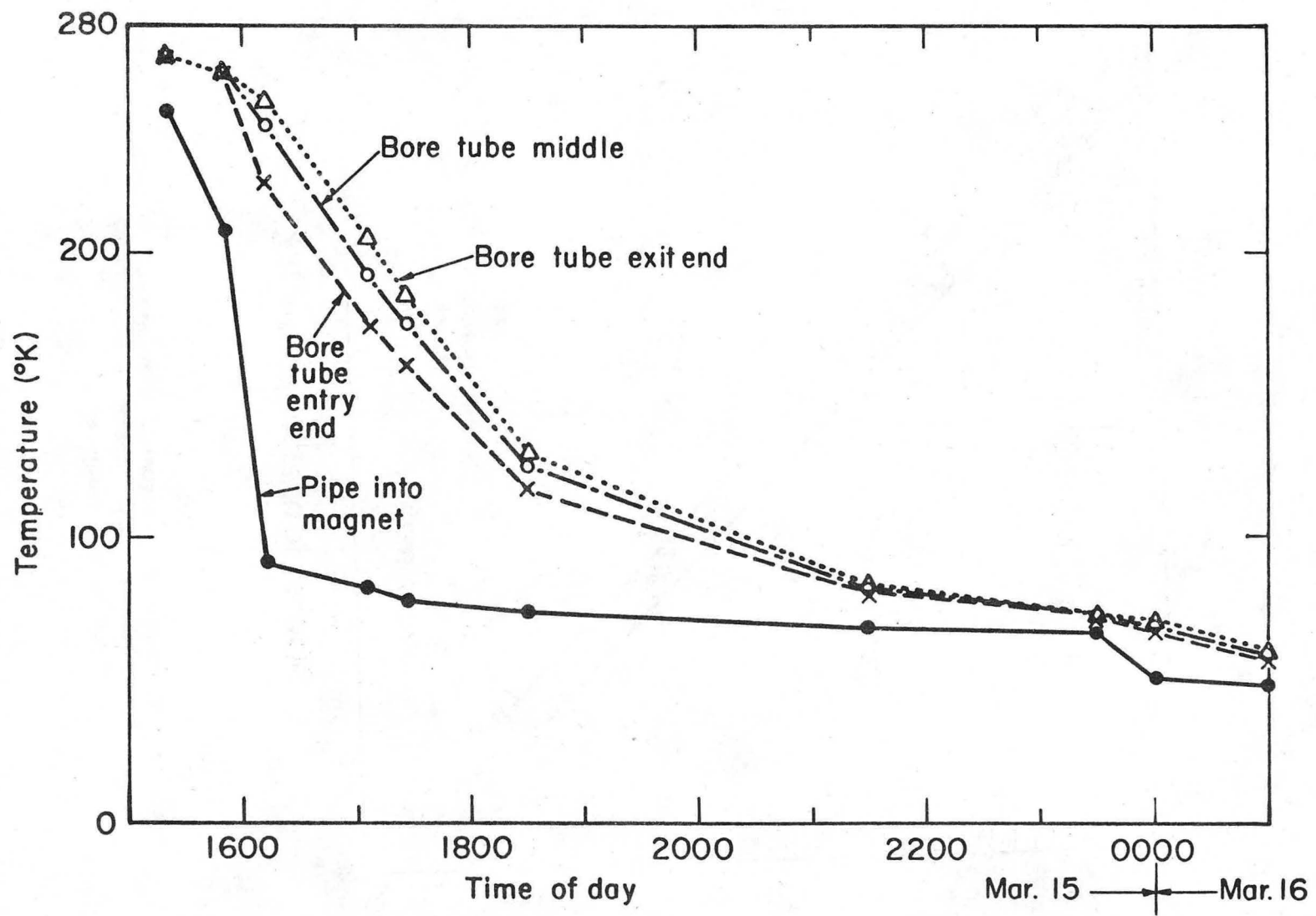
Fig. 33. The temperature at various points on the magnet as a function of time during the magnet cool down of March 1976.
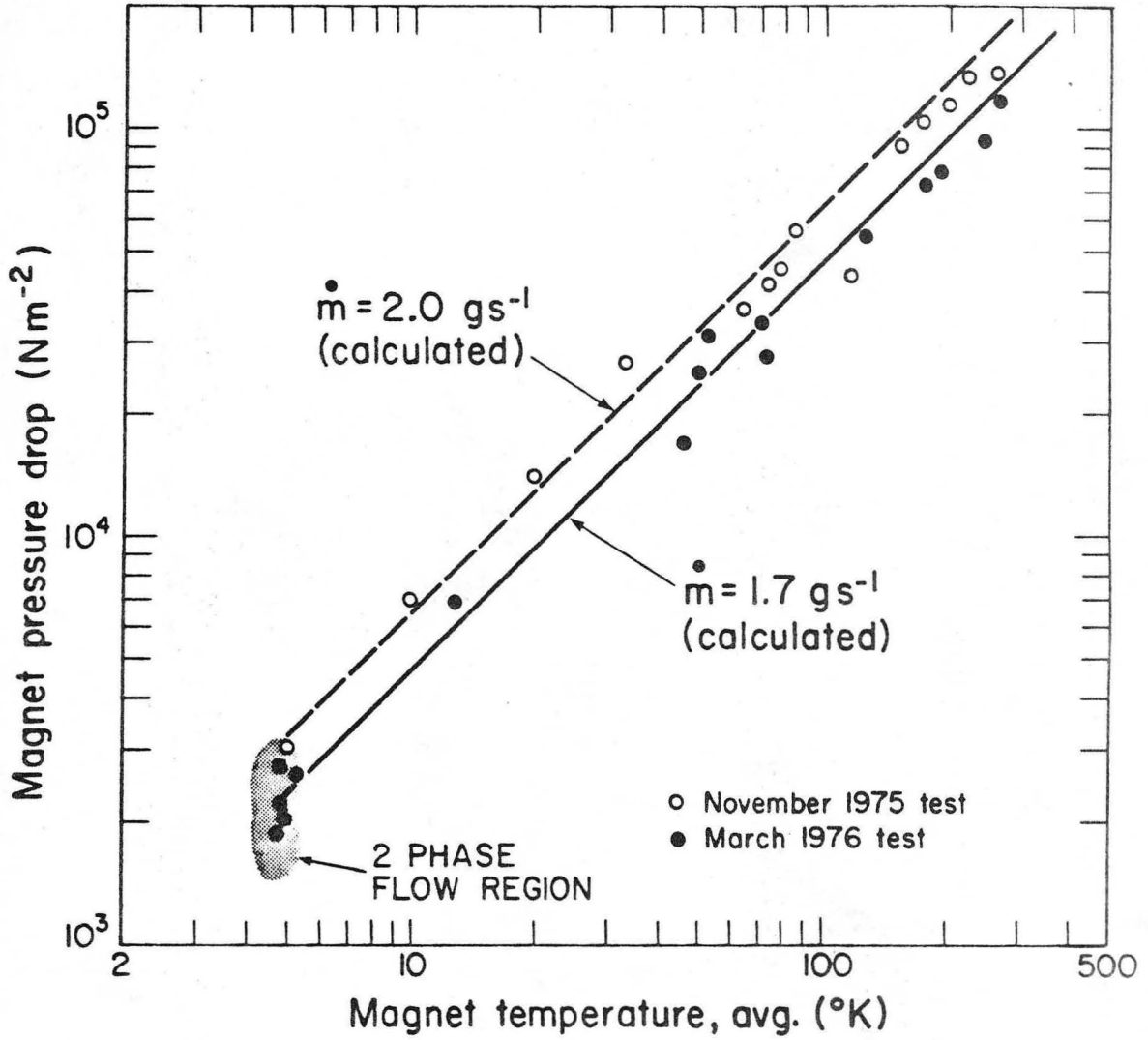
Fig. 34. Pressure drop across 117 meters of 10.8-mm
diameter cooling tube as a function of
average magnet temperature.

0 0 0 0 4 6 0 1 1 5 4

The refrigerator could not cool the load below 50K. The estimated load was about 30 W, which is 10 t 15 W more than the refrigerator can deliver. It should be noted that a helium refrigerator can deliver considerably more refrigeration at higher temperatures. (At 50K the Model 1200 machine should be delivering 50 to 60 watts of refrigeration. A second factor that inhibited the cool down was vacuum. The vacuum was quite poor (about 100 μm of Hg); the superinsulation had considerable conductive heat transfer through the gas. A temperature of 50 to 60K is too high for effective cryogenic pumping (the vapor pressure of nitrogen is above 100μ.)

Liquid helium was added to the control dewar to cool the magnet below 50K, to its operating temperature. The amount of liquid used was greatly reduced over the previous test. The magnet was superconducting within 40 minutes and two-phase flow through the magnet was established as soon as the magnet temperature dropped below 5 K. The onset of two-phase flow was marked by a sudden reduction of pressure drop across the 117 m of cooling tube surrounding the magnet. The flow of two-phase helium was very stable; there was no evidence of slug or plug flow in the tubular cooling system.

Once two-phase flow in the cooling tube started, steady state operation was quickly established. The helium in the control dewar boiled off at the rate of 0.17 g s^{-1} (about 4.9 ℓ h^{-1}). This is a refrigeration deficit of around 12 W. The magnet was not affected by the lack of refrigeration as long as liquid helium remained in the control dewar.

A magnet quench was followed by a pressure rise when the heat was transferred to the liquid in the 117 m cooling tube. After about 20-30 seconds the pressure dropped back to the normal operating range. When there was liquid in the control dewar and when the helium bypass valve was open for a minute, the magnet returned to its normal operating temperature quite quickly.

Refrigerator operation during the second test (March 1976) was an improvement over the previous test (November 1975). The control dewar served as buffer between the magnet and the refrigerator and the magnet was able to operate as long as the control dewar contained liquid helium. It was decided that the July 1976 test would be performed using the CTi Model 1400 refrigerator in Building 58. The use of this refrigerator permitted long term steady state operation.

4.2   Refrigeration for the Building 58 Magnet Tests

The July 1976 test was performed after much delay. While the experiment was being moved to Building 58 in order to get adequate refrigeration, a leak in the helium system opened up which had not manifested itself in the previous two tests. The leak, which was due to a badly soldered joint that had survived the previous two tests, was fixed. An attempt to test the magnets was made in June 1976; this ended in failure because of bad vacuum. Several causes for possible vacuum failures were found and corrected. In addition, the superinsulation system for cryostat was improved in preparation for the test during the latter part of July 1976.

a)   Modification of the Experiment

The system had a number of modifications, the most important of which was having both magnets in the same cryogenic vessel. This required modification of both the electrical and cryogenic systems. The liquid nitrogen shield was extended and more superinsulation was added to the vessel. Additional instrumentation was installed for the second magnet.

The two magnets were placed back-to-back with the electrical leads (this experiment has three electrical leads); bus bar assembly for the A magnet was placed at the top while the B magnet bus bar was at the bottom. (Figure 35 shows the two magnets mounted together.) The two-phase helium stream enters magnet B along its bus bar (only one lead is supplied with cold gas from this bus bar). The helium flows through magnet B and from there into magnet A. Then it exits from the system through the A magnet bus bar. (The A magnet bus bar supplies two electrical leads with cold helium.) Figure 36 shows the piping assembly for the two magnets in series. Figure 37 shows the two magnets fully superinsulated and ready to install in the vacuum vessel. The control dewar arrangement is the same as the control dewar arrangement shown in Figure 29.

Electrically, the two magnets were hooked up in series. They were supposed to have been hooked up so that the directions of their solenoidal fields coincided. Unfortunately, this did not occur; instead, the magnets were hooked backwards so that their magnetic fields were opposite, forming a solenoidal quadrupole.[65] The error was not discovered until just before the experiment was to be superinsulated. Since the one-week delay involved in correcting the error would have put us in
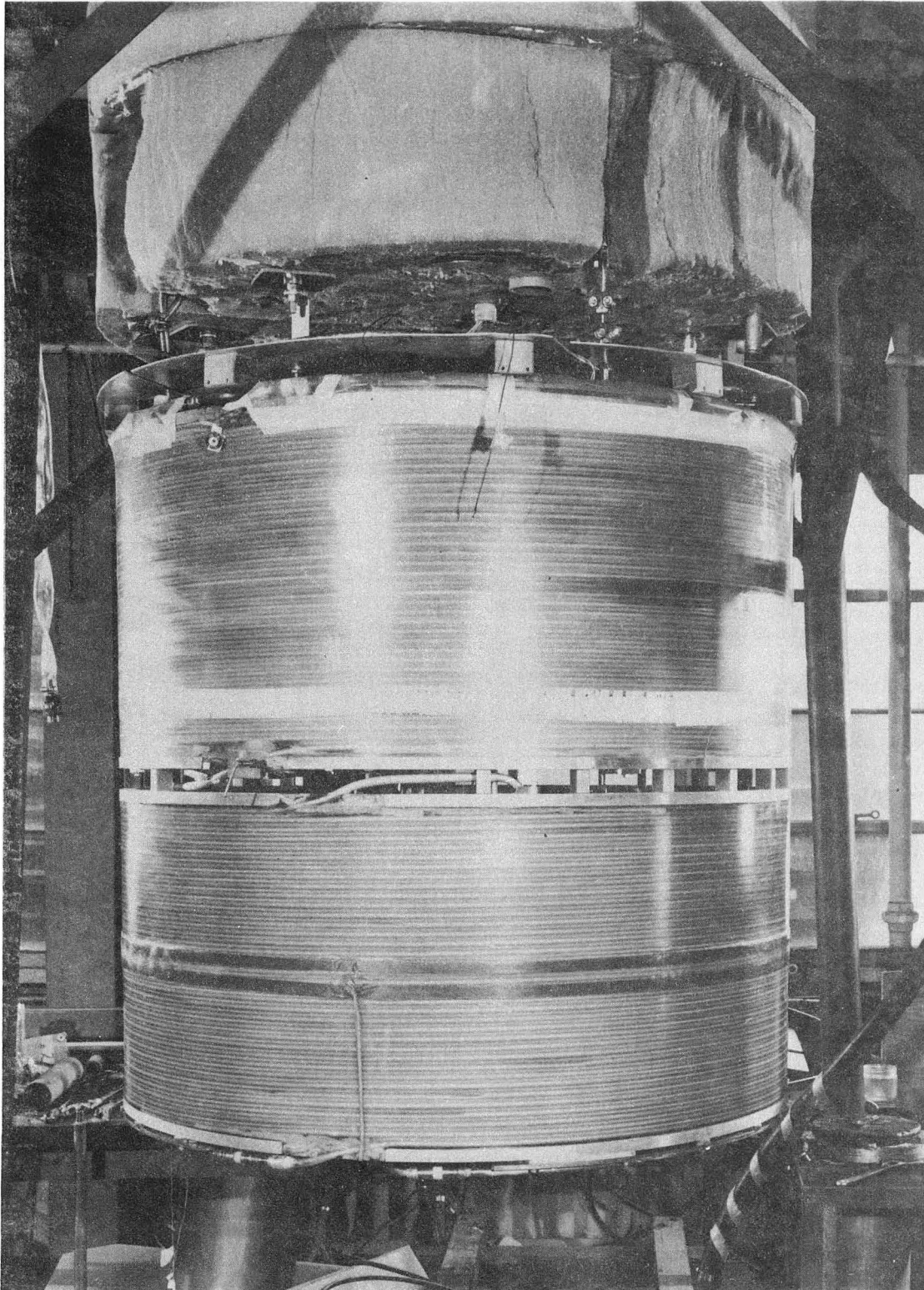
CBB 765-4874

Fig. 35. The A magnet (above) and the B magnet
mounted together prior to the July 1976
test.
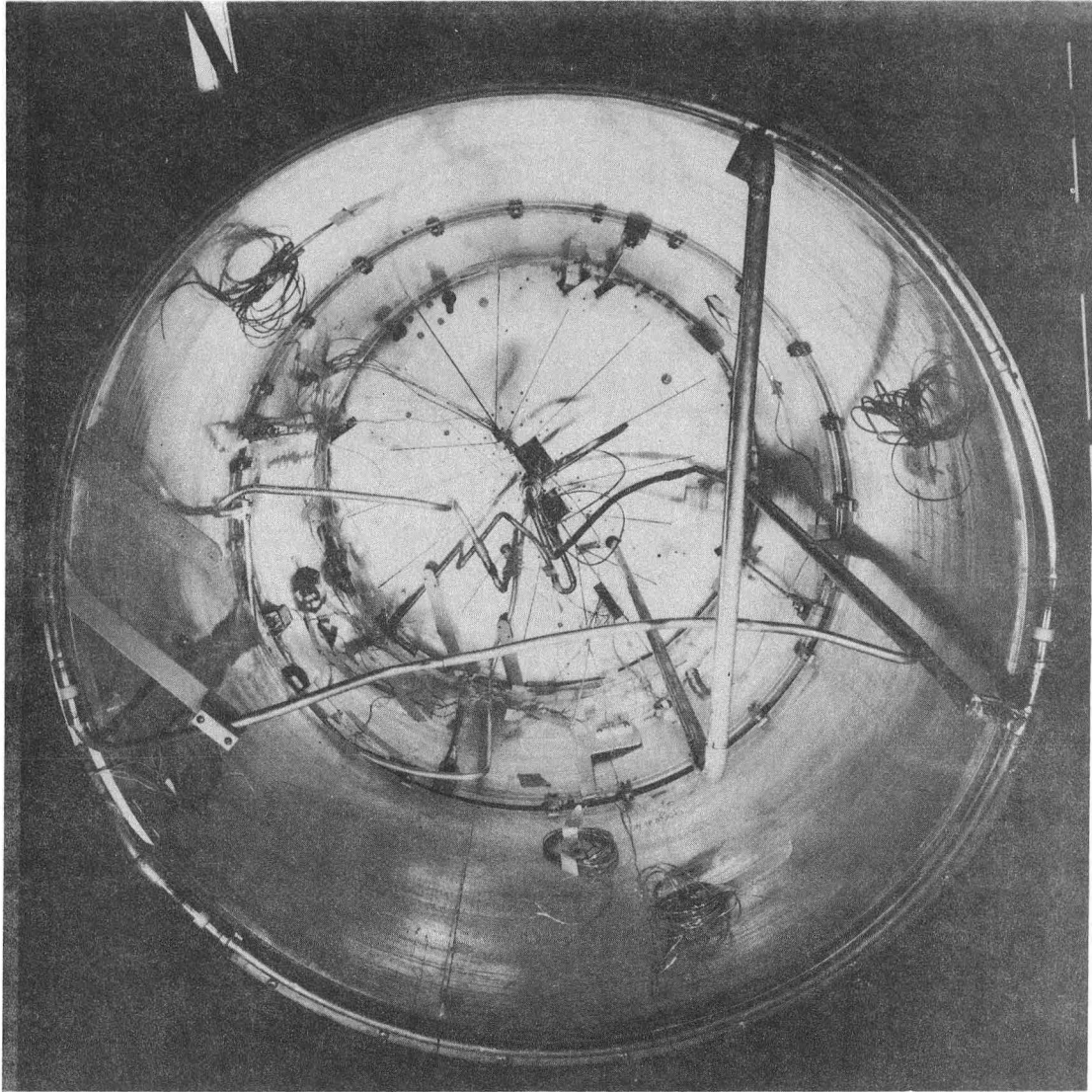
CBB 765-4876

Fig. 36. The cryogenic plumbing of the A and B
magnets hooked together for the
July 1976 test.
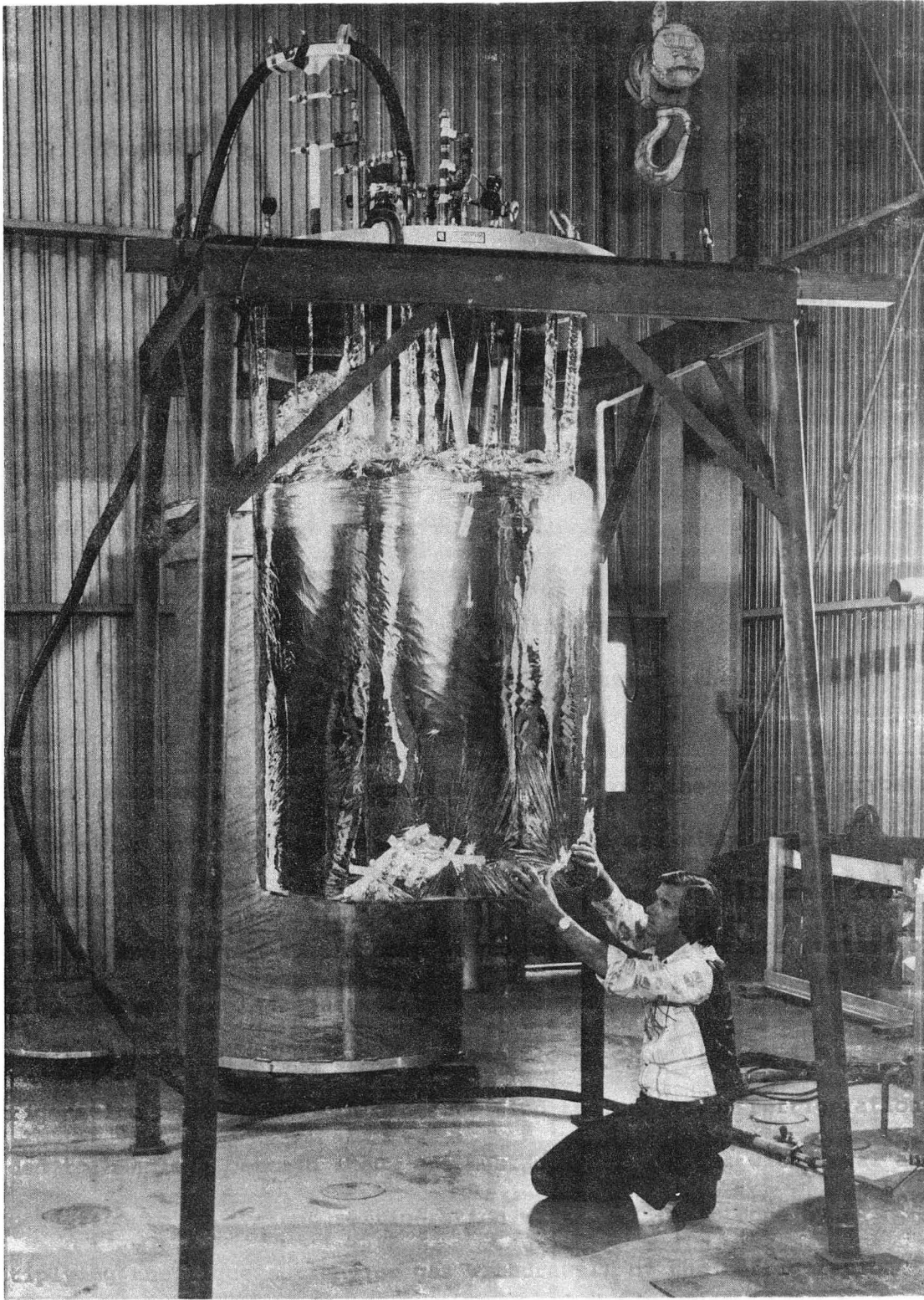
CBB 769-8355

Fig. 37. The A and B magnets fully insulated and
shielded just before insertion into the
vacuum tank. (The photo was taken just
before the July 1976 test.)

direct conflict with a high priority ESCAR magnet experiment, we
decided to test the magnets even though they were hooked up backwards.
Most of the information we hoped to gain from the two magnet series
could be learned with the two magnets hooked in opposition.

After the magnets were hooked together electrically and mechanically,
about 40 layers of superinsulation were put on the outside of the coils.
All pipes entering the magnets were electrically insulated with Mylar
film, then superinsulated. Care was taken that the superinsulation
did not short the magnets electrically. The same care was taken with
the twisted pair instrumentation leads.

The liquid nitrogen shield, which was in three parts, was installed
around the magnets. Both the inside and outside of the shield was
superinsulated. The styrofoam previously used for insulation at the top
of the cryostat was replaced with about 10-15 layers of superinsulation
between the room temperature cryostat lid and the liquid nitrogen shield.

The support system between the magnet and the cryostat consisted
of stainless steel cables and fiberglass epoxy rods. The cables carry
the gravity load plus downward magnetic forces. The fiberglass epoxy
rods carry the upward magnetic forces in compression.

The cables and compression rods contributed about 2.5 W heat load
to the helium system. The total radiation heat load over an area
of 5.5 m^2 was estimated to be around 1.5 watts. The transfer line
losses were estimated to be 3.5 W. The control dewar heat leak (mostly
through its styrofoam plug) was around 2.5 W. The total heat leak
into the experiment was around 10 W.

b)   Characteristics of the Model 1400 Refrigerator

The Model CTi 1400 refrigerator in Building 58 was purchased by LBL
in 1972. The machine has two compressors, each of which deliver gas at
the rate of 5 g s^{-1} at a pressure of 17.5 bar (240 psig). The refrigera-
tor is equipped with a liquid nitrogen precooler, which uses about
9 g s^{-1} (40 ℓh^{-1}) of nitrogen during normal operation. When the
refrigerator was new, it was supposed to deliver 70W of refrigeration
at 4.5K or liquify 0.69g s^{-1} (20 ℓh^{-1}) of helium.[73] The machine
is now four years old. It delivers a maximum of 55W at 4.5K or it
liquifies 0.60 g s^{-1} (17.3 ℓh^{-1}) of helium.

The refrigeration-liquefaction curves for mixed mode operation are
shown in Fig. 38. The curves result from the recent calorimeter tests on
the Model 1400 in Building 58.[74] Table 12 summarizes the important
information given in Figure 38.

Gas withdrawal through electrical leads or off the top of a cryostat
is equivalent to helium liquefaction (1 g s^{-1} of gas withdrawal is
equivalent to 1 g s^{-1} of helium liquefaction). The gas withdrawn from
the system is returned to the compressors at room temperature instead of
passing through the refrigerator heat exchanger. For every gram per
second of gas withdrawn, the refrigerator loses a portion of its
refrigeration capability. In order to find the amount of refrigeration
needed to handle a certain load, one must convert the gas withdrawal and
liquefaction to equivalent refrigeration watts. This is done by
multiplying the liquefaction (or gas withdrawal) by the refrigeration
liquefaction coefficient. The refrigeration load is around 10 W. The
total liquefaction plus gas withdrawal capability left is 0.45 g s^{-1}.
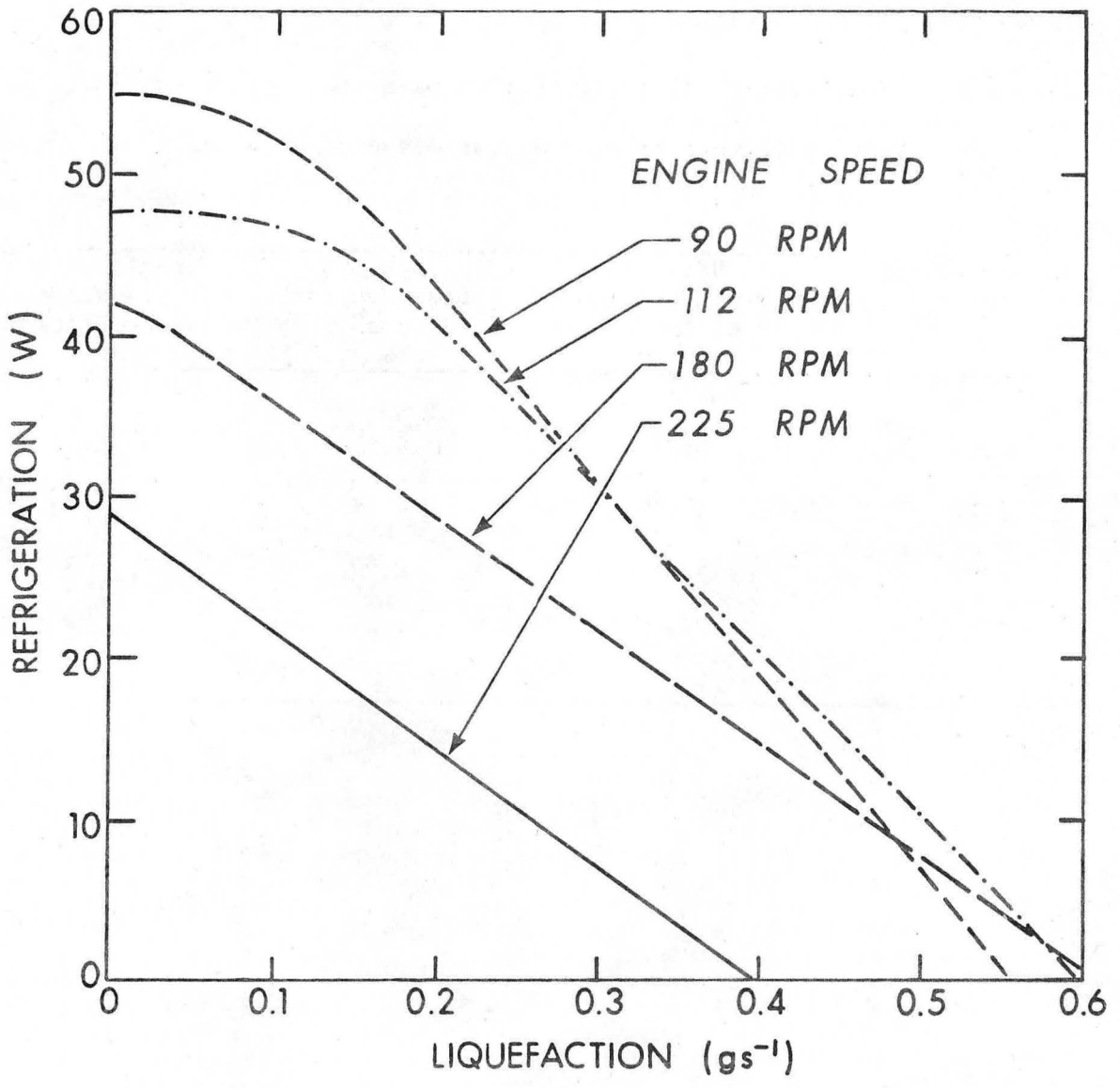
Fig. 38. Measured curves of liquefaction vs
refrigeration at various engine speeds
for the Bldg. 58 Model 1400 refrigerator.

XBL 774-8478

Table 12   Liquefaction and refrigeration parameters of the Building

Model 1400 refrigerator at various engine speeds

Engine Speed (RPM)	Maximum Refrigeration at 4.4 K (W)	Maximum Liquefaction (g s^{-1})	Refrigeration Liquefaction Coefficient J g^{-1}
90	55	0.55	125
112	48	0.59	107
180	41	0.60	72
225	29	0.39	74

This is equivalent to 56.3 W of refrigeration. Table 13 shows a breakdown of the heat and gas loads for the experiment.

c)   The Cool Down of the Magnets

The general procedure for cooling down the magnet system is as follows:

1)   The service valve which bypasses helium around the refrigerator is opened. During the cool down, cold helium is taken from the refrigerator and fed into the warm magnets. The helium is warmed up to nearly room temperature as it cools the magnets and therefore must not be allowed to return through the co-axial transfer line. It is taken from the cryostat and returned warm to the compressor intake.

2)   As the magnets cool, the helium bypass (through the service valve) is kept open. Internal bypasses within the refrigerator are opened to help cool the refrigerator heat exchanger. This increases the mass flow of cold helium delivered to the magnet.

3)   As the magnets approach liquid helium temperature, the sevice valve may be throttled down, allowing part of the helium to flow back to the refrigerator heat exchangers. When the magnets become superconducting (at 9 K), the service valve can be closed entirely. Joule-Thompson cooling will cool the magnet further until liquid helium begins to collect in the control dewar.

Table 13. A breakdown of refrigeration and liquefaction loads during the March 1976 and July 1976 tests.

	March 1976 Test With No Current	July 1976 Test	
		No Current	800 A
Direct Refrigeration			
Radiation heat load (W)	~6.0	~1.5	~1.5
Support heat load (W)	~2.0	~2.5	~2.5
Transfer link heat leaks (W)	~3.5	~3.5	~3.5
Control dewar heat load (W)	~0.6	~2.5	~2.5
TOTAL DIRECT REFRIGERATION (W)	~17.5	~10.0	~10.0
Gas Withdrawal Liquefaction Load			
Electrical leads (gs^{-1})	0.14	0.17	0.26
Top of control dewar (gs^{-1})	0.02	0.01	0.01
TOTAL GAS FLOW (gs^{-1})	0.16	0.18	0.27
Equivalent Refrigeration in the Gas Withdrawal (W)	11.2[*]	22.5[**]	33.8[**]
TOTAL REFRIGERATION NEEDED (W)	28.7	32.5	43.8
Type of Refrigerator	CTI 1200	CTI 1400	CTI 1400
Net Liquefaction in Control Dewar (gs^{-1})	-0.17	0.27	0.18
Surplus Refrigeration (W)	-11.9	33.8	22.5

[*] Refrigeration liquefaction coefficient is 70 Jg^{-1}.

[**] Refrigeration liquefaction coefficient is 125 Jg^{-1}.

This procedure is used any time one wants to cool superconducting magnets using a refrigerator and was used to cool the experiment during the July 1976 test.

The Model 1400 refrigerator cooled the 220 kg of magnets, transfer line and control dewar to 4.8 K in just under 48 hours. Figure 39 shows the temperatures of Magnet A and Magnet B (measured with the calibrated diodes at the center of the magnet bore tubes). The B magnet cooled from 290 K to 130 K in four hours. The A magnet, which is downstream from the B magnet, sat at 210 K after four hours. During the first night, the cool down stopped. The following morning the cool down resumed after the bypass valve was closed down, permitting the refrigerator to slightly cool internally. The two magnets were superconducting 24 hours later.

The Model 1400 refrigerator has quite different cool down charac- teristics from the LBL Model 1200 refrigerator. The Model 1400 refrigerator heat exchanger takes a long time to cool down. Refrigerator temperature tends to follow that of the load; the mass flow of gas delivered from the refrigerator to the load increases as the temperature of the load decreases. Figure 40 shows the mass flow rate through the tubular cooling system as a function of the average magnet temperature. Figure 41 shows the pressure drop across both magnets as a function of temperature. The jump in mass flow and pressure drop at a temperature of 130 K reflects the changes made in the operation of the refrigerator on July 24th at 10.00 a.m.
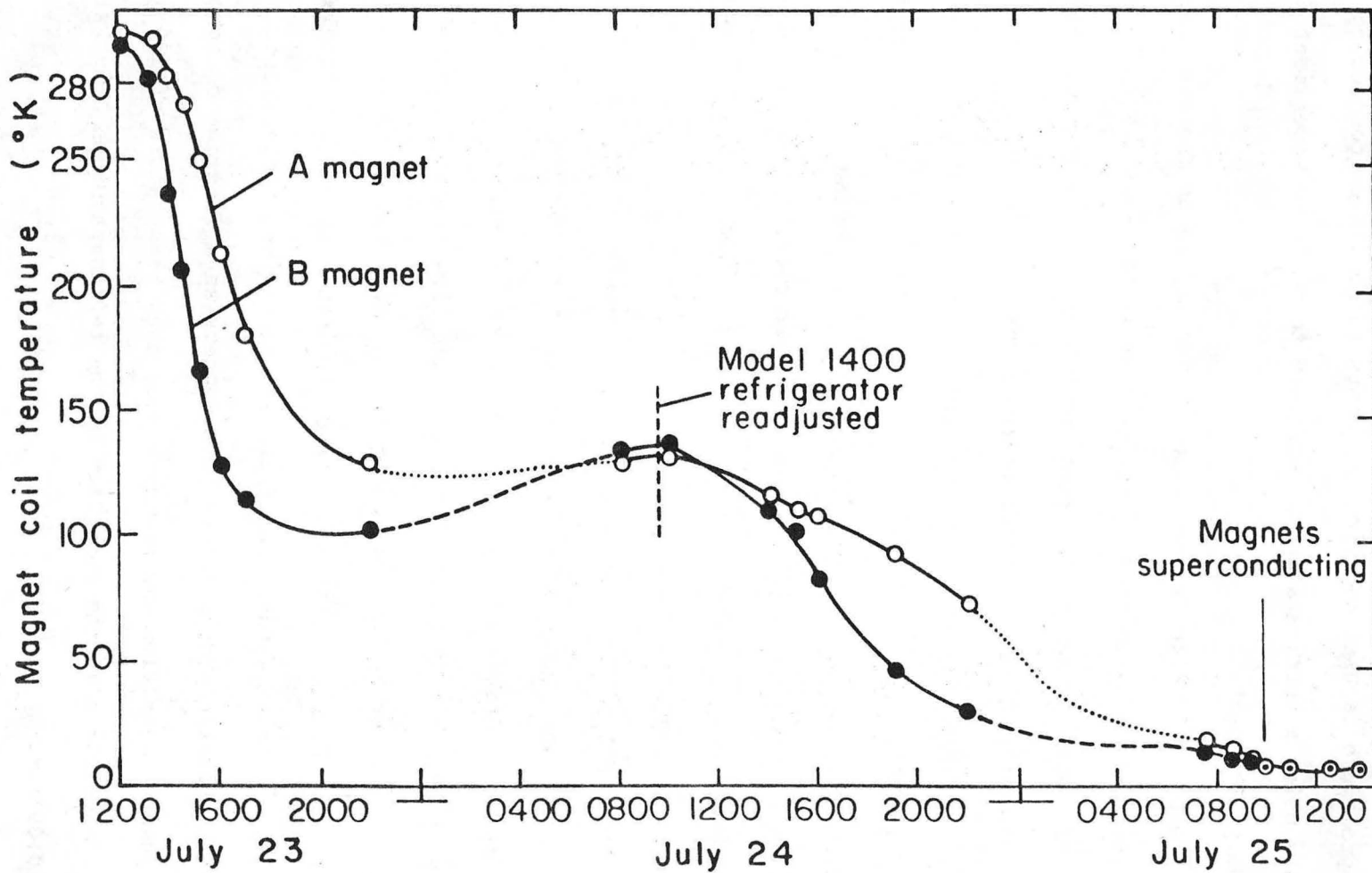
Fig. 39. The average temperature of the A and B magnets vs time of day during the magnet cool down of July 1976.

XBL769-4080
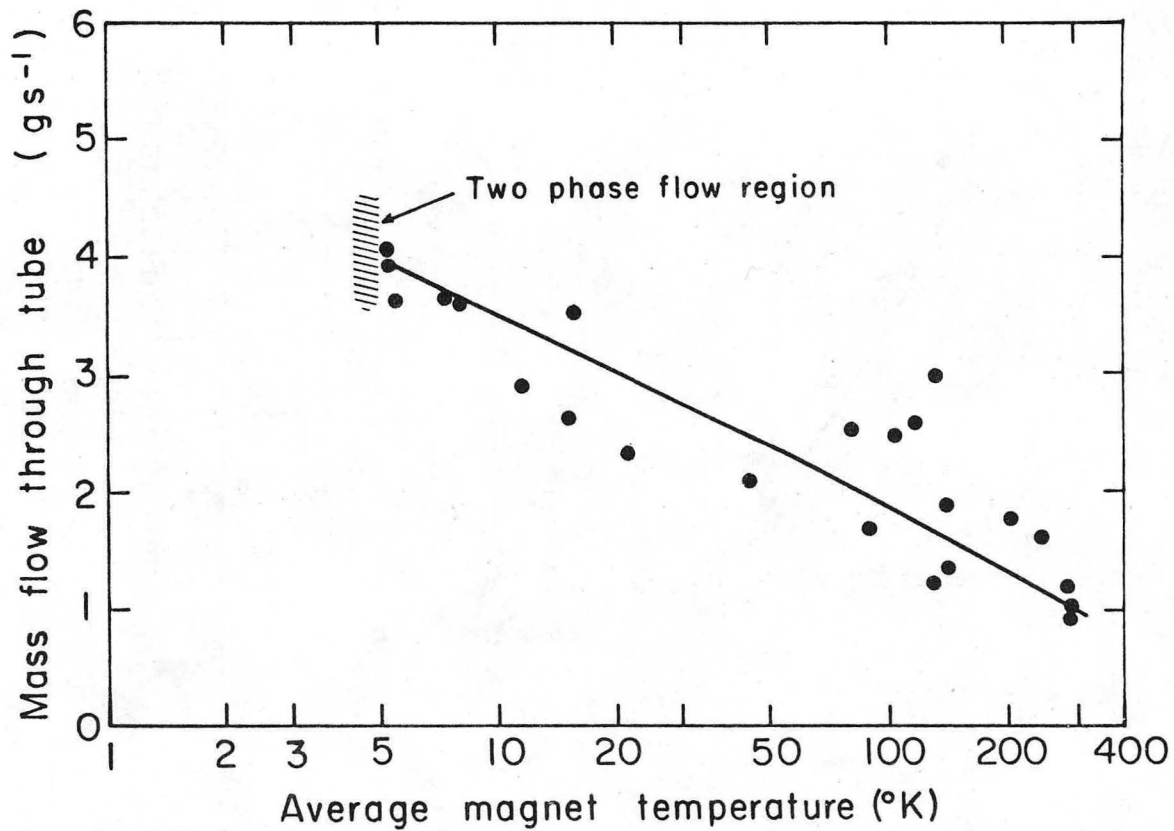
Fig. 40. Mass flow rate through 235 meters of cooling tube as a function of average magnet temperature (in both magnets) during the July 1976 test cool down.
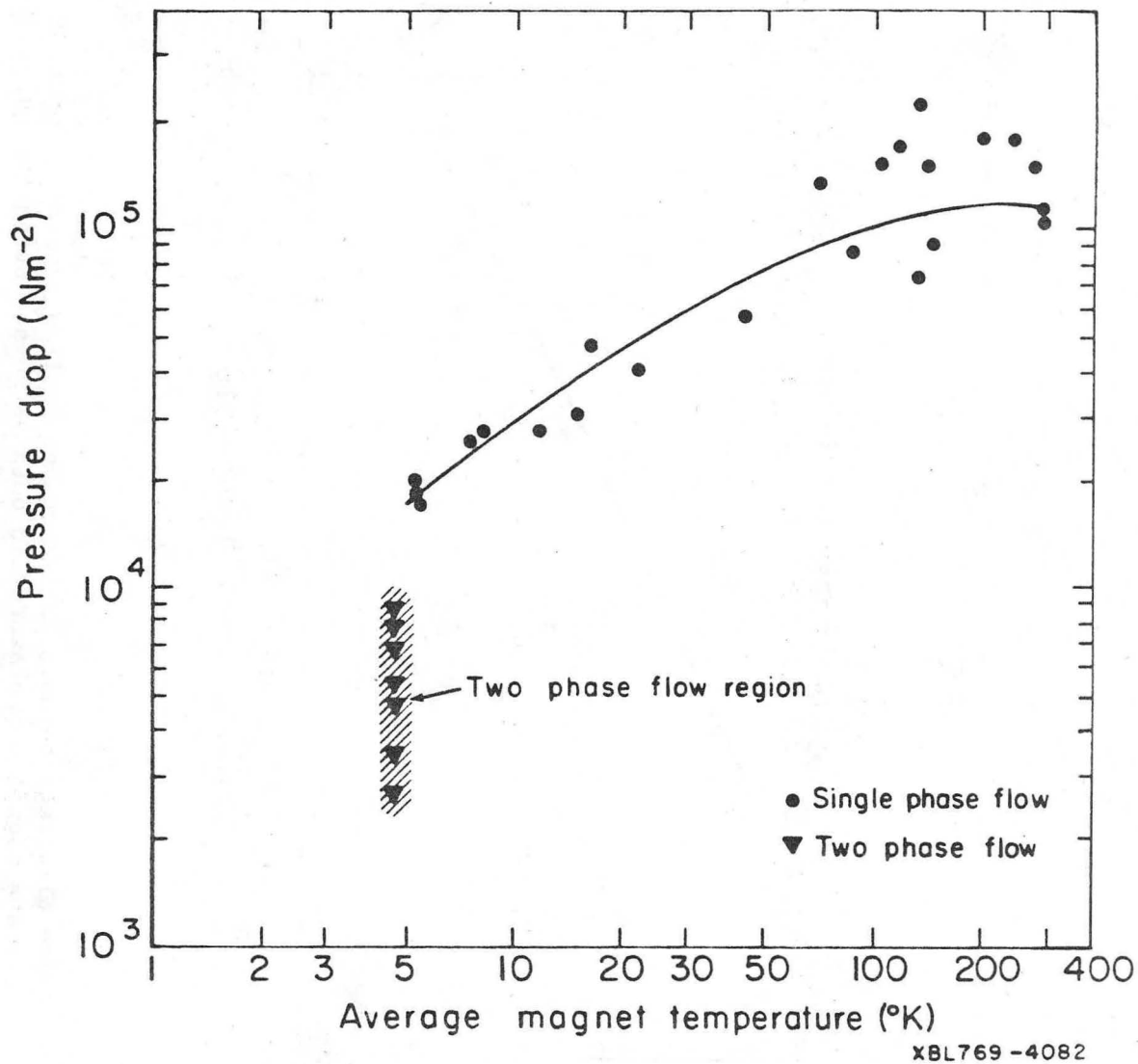
Fig. 41. Pressure drop through 235 meters of 10.8 mm
ID tube as a function of average magnet
temperature (both magnets). (Note the
dramatic change in pressure drop when two-
phase flow is established.

d) Steady State Operation of the Magnet System

Once the temperature of the magnet dropped below 5.0 K, liquid helium was formed filling the control dewar. Two-phase helium flow was established, and pressure drop across the two magnets suddenly fell by at least a factor of two. This pressure drop through 235 m of 10.9 mm ID aluminum tube varied from 0.028 to 0.060 bar. The average quality of the helium in tube varied from 0.05 to about 0.40, depending on operating conditions of the system.

During most of the magnet run, the cooling tube carried between 80 and 90 percent liquid helium. Only once did we see oscillations in pressure drop across the magnets (we are not sure whether this was due to flow oscillation or due to oscillations in the capillary tube between the magnahelic differential pressure gauges and the cold helium). The oscillations observed were small in magnitude (less than 0.005 bar). The top of the large cryostat is shown in Figure 42. The two magnahelic gages that were used to measure differential pressure can be seen.

During steady state operation of the magnet system, when there is no current in the magnets, the refrigerator was producing liquid helium in the control dewar at the rate of 0.27 g s^{-1} (7.8 liquid liters per hour). When the magnet had 800 A flowing in it, the liquefaction rate was reduced to 0.18 gs^{-1} (5.2 ℓh^{-1}). Table 13 compares the performance of the refrigeration system during the March 1976 test with the performance during the July 1976 test. A breakdown of the various heat and gas withdrawal loads is given.
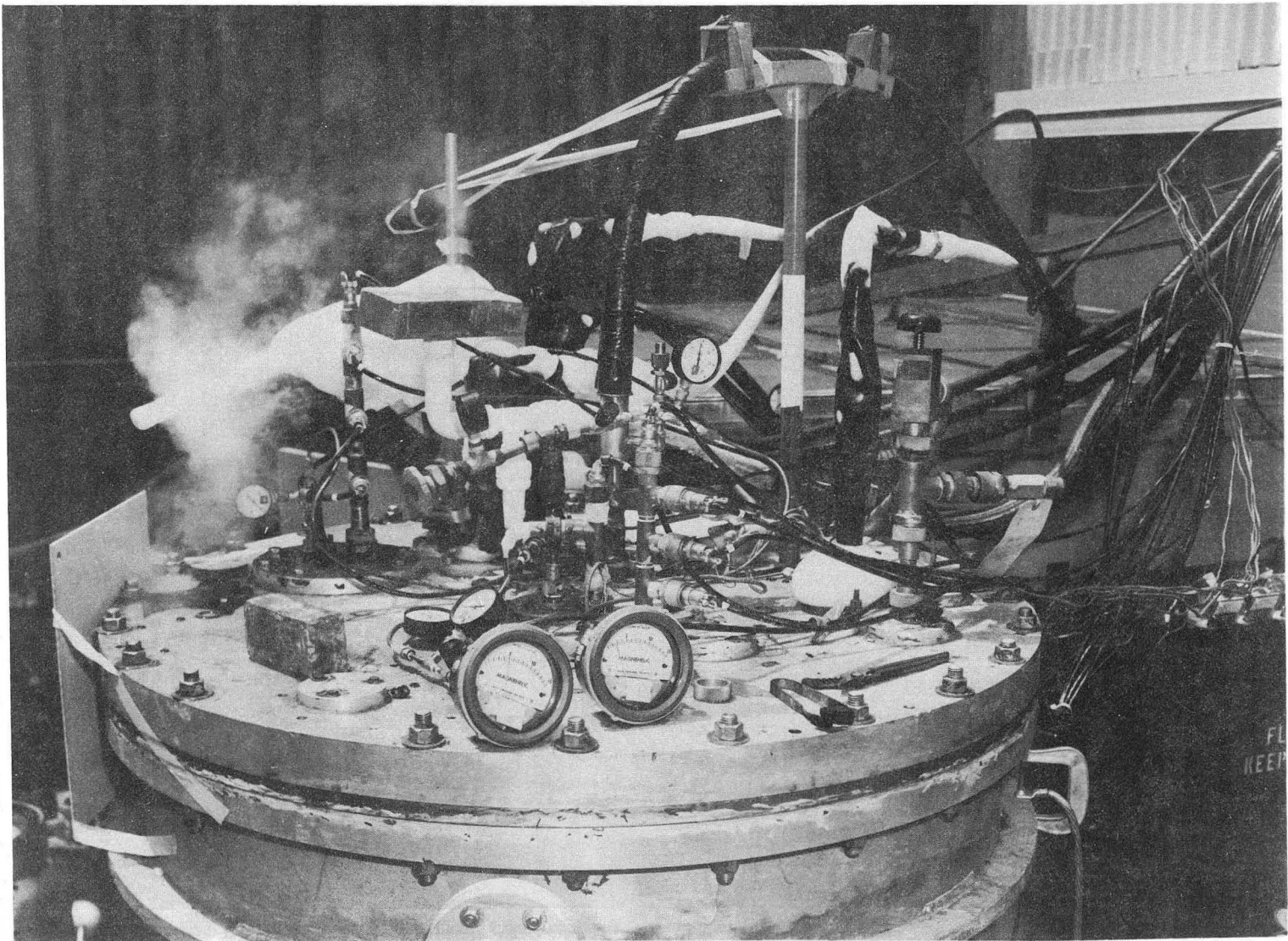
CBB 767-6702

Fig. 42.   The top of the magnet cryostat during the July 1976 test. (Note the
magnahelic gages close to the camera. Both gages read on scale
indicating two-phase flow in the magnet.)

e)   The Refrigeration System's Response to a Quench

The tubular cooling system around the magnets has a volume of 22 liters, capable of containing around 1.5 kg of helium during normal operation. When the magnet or magnets quench, thermal energy is dumped into this helium, which boils until it becomes supercritical. The pressure rises, expelling much of the gas.

At currents below 400 A, which correspond to a magnet energy of 59 kJ, the refrigerator could make the system recover within a few minutes provided there was liquid helium in the control dewar. At higher currents, the bypass valve has to be opened in order to help the magnet recover. During the experiment, high-stored energy quenches boiled away considerable helium from the control dewar (roughly 40 ℓ per 100 kJ). The highest current quenches, where the magnet-energy was over 250 kJ, required a liquid helium transfer to the control dewar from a 500 liter storage dewar (see Fig. 43) after nearly every quench.

The pressure in the tube rose with a much longer time constant than quench itself. Pressures as high as 14 bar (190 psig) were seen during an 800 A quench of the magnet. The peak pressure during a 400 A quench (the coil dumped one quarter the energy of the 800 A quench) was just under 11 bar (145 psig). The pressure in the tubular cooling system reached its peak 10-20 seconds after the magnet was quenched, which in itself took just over one second. For all practical purposes, the process of putting the magnet-stored energy into the coil and bore tube is decoupled from the heat transfer process.

Once the cooling system pressure reached its peak, the pressure dropped back to near normal in about 30 seconds. It took 10 to 20
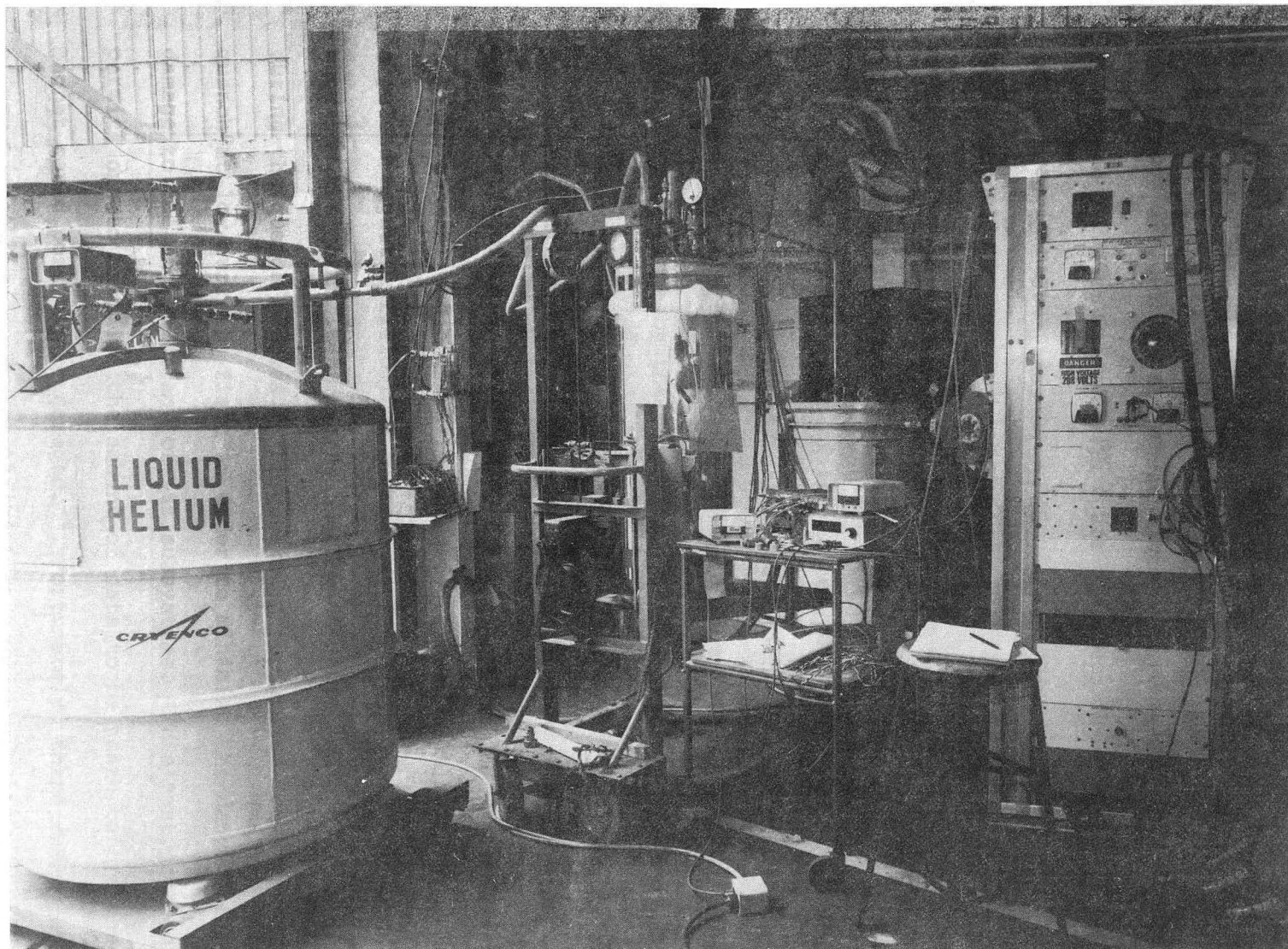
Fig. 43. The refrigeration system for the July 1976 test. (Far left is a 500 liter storage dewar. In the center is the control dewar. Just right of center in the back is the Model 1400 refrigerator. To the far right is the magnet's 1000 A power supply.)

CBB 767-6706

minutes for the magnet system to reach a stable operating condition after being quenched while containing 200 kJ or more of stored energy. (This process takes longer if a helium transfer to the control dewar is required.)

The July 1976 test established that the magnets could be cooled down and operated using the Model 1400 refrigerator. The quench process was well-behaved. During the test, the magnet was left operating unattended overnight on the refrigerator with 400 A flowing through the coil. The B magnet was operated on the refrigerator (in the closed cycle mode) with currents as high as 920 A. The magnet was quenched at this current, depositing 314 kJ of magnetic energy as heat into the super-conducting coil and bore tube. The July 1976 test verified the viability of the tubular cooling system.

V. THE ONE-METER DIAMETER TEST COIL EXPERIMENTS

The two one-meter diameter test coils were tested in November 1975, March 1976 and July 1976. These tests will be henceforth known as tests 5, 6, and 7. (Tests 1 through 4 are a series of tests done on small oval solenoid magnets.) The A magnet was tested during all three tests; the B magnet was tested only during July 1976 (test 7). Section 4 described the refrigeration of the magnets during the three tests; this section describes the tests themselves.

The following aspects of the magnet tests and test procedures are discussed: 1) the method of data acquisition and transfer to the computer; 2) the calculations which are done off line by the computer and the plots made by the computer; 3) the results of the magnet experiment; 4) the results of the strain gage measurements which are correlated with spontaneous quenching in the magnets (this spontaneous quenching is often referred to as training).

In general, quenches were induced in the magnet coil by putting a pulsed magnetic field into a small section of the magnet. The experiments show how the normal region grew and how the coil and bore tube interacted during the quench process. The general procedure followed was to quench at low currents first in order to minimize the danger of permanent damage to the magnet or any of its subsystems. This test procedure permits one to maximize the amount of data to be taken before the magnet could possibly be damaged.[54] Fortunately, there was no evidence of any magnet damage even at the highest currents at which the experiment was operated.

5.1 The Method of Data Acquisition

The magnet coil has a number of instrumentation points on it (see subsection 3.3 of this report). This instrumentation includes: 1) small coils for inducing quenches, 2) magnetic flux measuring coils, 3) temperature sensors on the magnet bore tube, and 4) strain gages mounted on the bore tube. In addition, there is instrumentation for measuring the current flowing in the coil conductor. (One may also measure the resistance of the coil as it cools down.)

a) Inductance and Field Mapping

Before the magnet could be powered for quench testing the following procedure was followed: 1) The temperature of the bore tube and the resistance of the coil was monitored. Figure 44 shows the resistance of each magnet as a function of temperature. 2) When the magnet temperature dropped below 15 K, the electrical performance of the quench-inducing coils was checked. The magnet insulation was checked at this temperature also. 3) Once the magnet was cold and superconducting, the various inductances (self and mutual) for the various coils were measured. A crude field map as made using small coils.

Field mapping was done with small coils which have a diameter of about 10 mm. The magnet was powered from 0 to 50 A. The signal from the coil was passed through an analog integrator and became directly proportional to the induction changes at the center of the measuring coil. The induction component measured was the component parallel to the axis of the magnetic measurement coil. Figure 45 shows the location and axis direction of each of the measuring coils. The field map of the A coil being powered was measured during test 6 (March 1976).
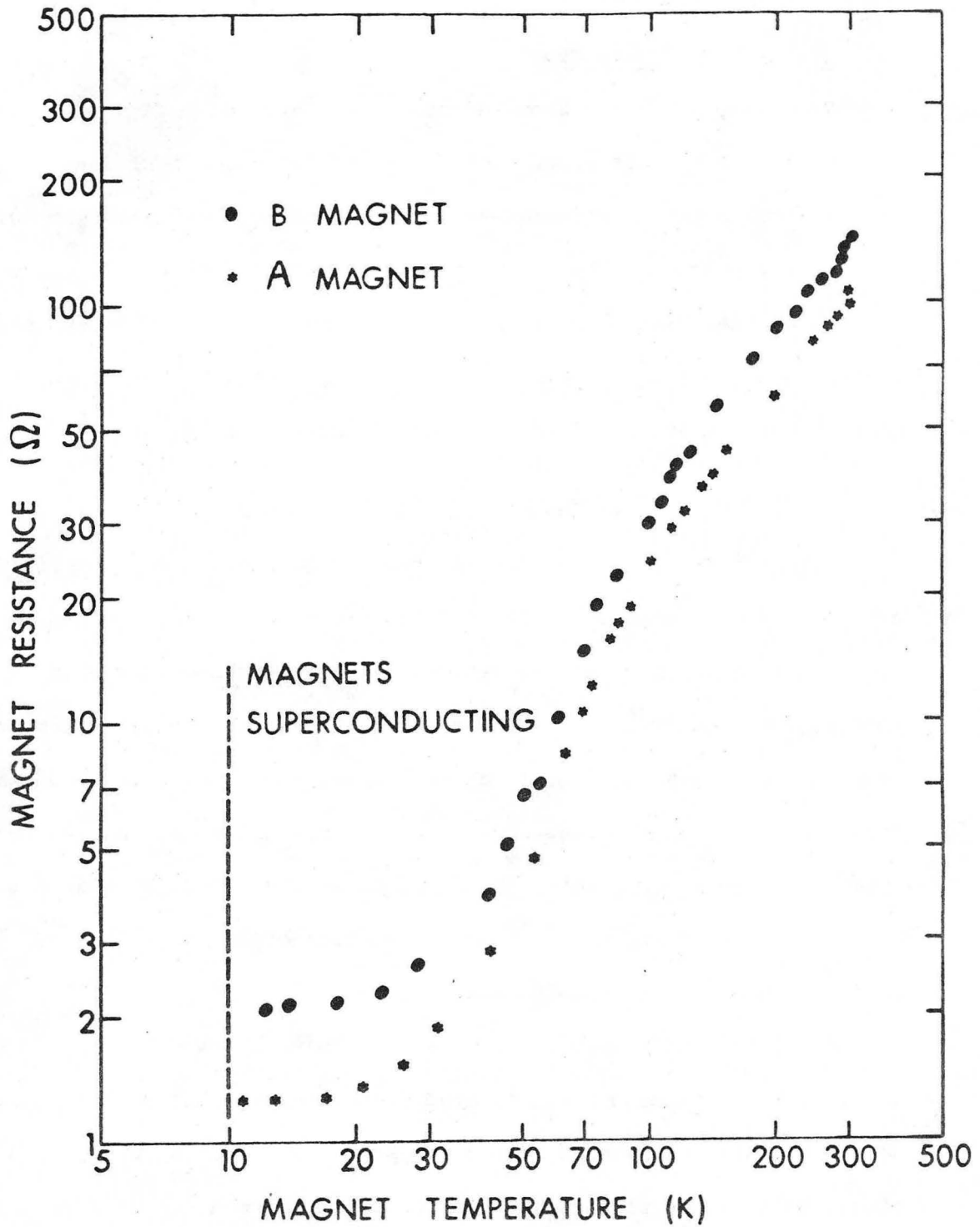
XBL 774-8445

Fig. 44. The measured resistance of the A and B
magnets as a function of their average
temperature.
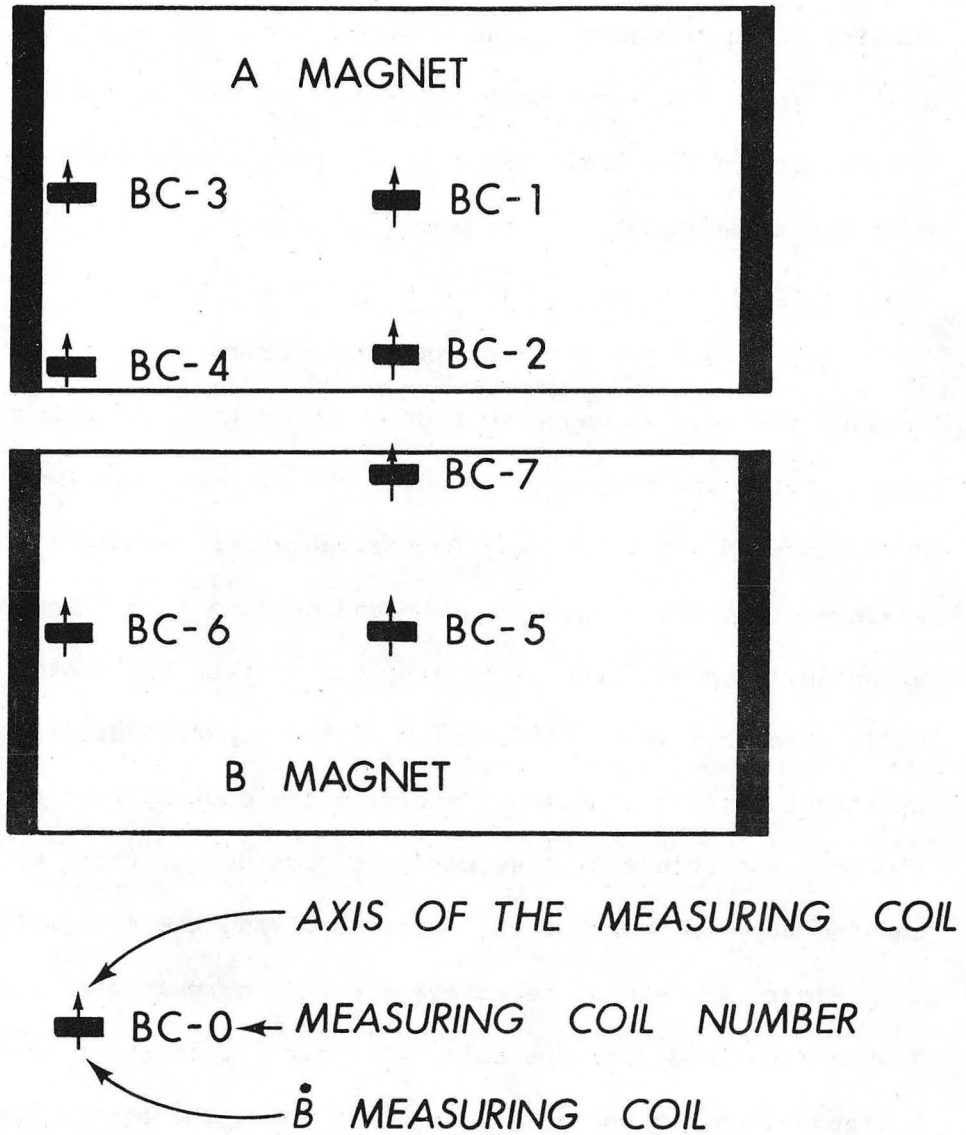
Fig. 45. The location of the small coils which
measured the magnetic field. (The
arrow direction indicates the direction
in which the magnetic field is measured.)

Coils 1 through 4 measure the field in the A magnet due to current flowing in the A magnet. The B magnet field map was made during test 7 (July 1976). All seven coils were used to map the field. Table 14 shows the results of the field mapping. It should be noted that the field map data has an error of between 5 and 10 percent, due primarily to integrator drift coupled with a very small signal.

Each of the two magnets has pickup coils wound around them which measure the rate of magnetic flux change within the pickup coil. These pickup coils are closely coupled to the magnet. The A magnet pickup coil, located about 130 mm from the center of the magnet, has 37 turns which enclose the coil, bore tube and cooling tube. The B magnet pickup coils, with 41 turns each, are located over the center of the magnet coil. One coil is located on top of the superconducting coil under the cooling tube; the other coil encloses the cooling tube as well as the coil and bore tube. We used the pickup coil which was under the cooling tube for most of the tests involving the B magnet.

Figure 46a shows the active electric circuit used for tests 5,6, and 7 which involved just one coil. The circuit in the figure shows just the A magnet (tests 5 and 6). Figure 46b shows the active electric circuits of both magnets being hooked in series. In both Figures 46a and 46b, the bore tube circuit is left out. Three kinds of data are taken from the magnet. They are: 1) the voltage across the current shunts, 2) the voltage across the leads of the A and B magnets V_A and V_B, and 3) the $d\phi/dt$ signals from the pickup coils for the A and B magnets P_A and P_B.

Table 14. A crude field map* of the magnets when current is carried
in the A magnet and the B magnet.

Measuring point	Current in the A magnet (test 5 and 6)		Current in the B Magnet (test 7)	
	dB/dI (TA^{-1})	Induction at 700 A (T)	dB/dI (TA^{-1})	Induction at 700 A (T)
1	8.9×10^{-4}	0.62	3.6×10^{-4}	0.25
2	6.9×10^{-4}	0.48	6.7×10^{-4}	0.47
3	14.9×10^{-4}	1.04	---	---
4	9.9×10^{-4}	0.69	6.4×10^{-4}	0.45
5**	---	---	9.2×10^{-4}	0.64
6**	---	---	15.0×10^{-4}	1.05
7**	---	---	7.2×10^{-4}	0.51

* The accuracy of this field map is probably only around 10 percent.
** Point 5 in the B magnet is equivalent to point 1 in the A magnet.
Point 6 in the B magnet is equivalent to point 3 in the A magnet.
Point 7 in the B magnet is equivalent to point 2 in the A magnet.
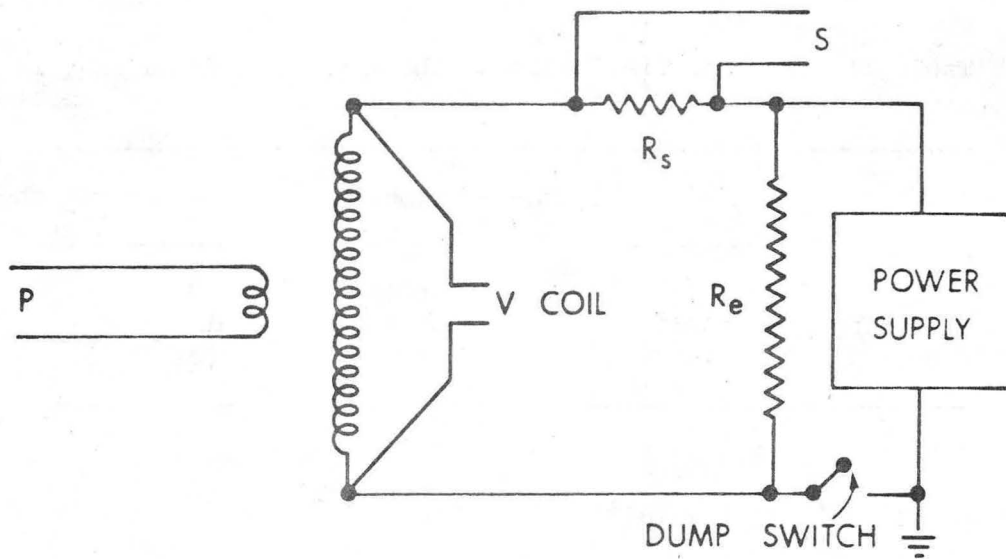
a) SINGLE COIL HOOKUP.
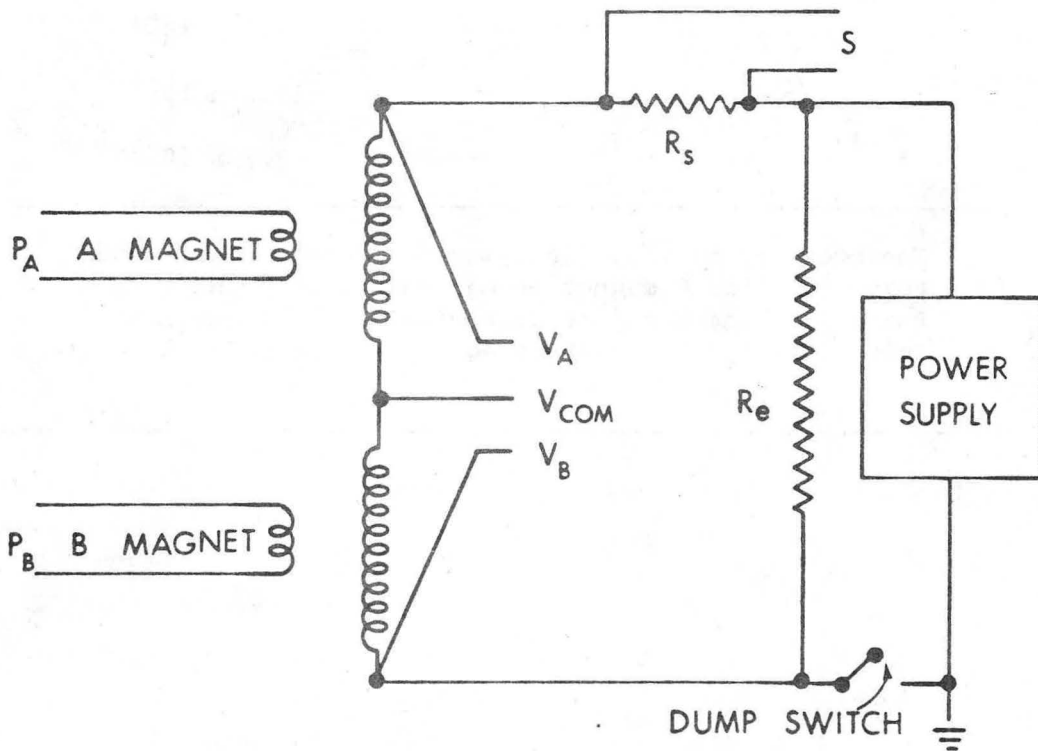
b) A AND B MAGNETS HOOKED IN SERIES.

XBL 774-8473

Fig. 46. Electric circuit diagrams of the magnet
with its measuring coils, shunt resistor,
voltage taps, and power supply.

The simple circuit shown in Figure 46a has two inductances which are important. They are the self inductance of the magnet coil (L_1 or, to differentiate between the A and B magnets, L_A or L_B) and mutual inductance between the pickup coil and its magnet ($M_{A,PA}$ or $M_{B,PB}$). The circuit shown in Figure 46b has several important inductances. There are three self inductances, depending on which magnets are hooked to the power supply. They are L_A, L_B and L_{A+B}. The mutual inductances include the following: $M_{A,PA}$, M_{B,P_B}, $M_{A,PB}$, M_{B,P_A}, M_{A+B,P_A}, $M_{A+B,PB}$, $M_{A+B,A}$, $M_{A+B,B}$ and of course $M_{A,B}$. The preceding symbols are defined in the list of symbols.

The inductances were measured at the start of each test. In general, the method was to measure the voltage generated across each of the coils as the magnet or magnets in question was being charged at a specific rate of current change. For example the self inductances of the coils are:

$$L_A = \frac{V_A}{dI_A/dt} \qquad\qquad\qquad (13a)$$

$$L_B = \frac{V_B}{dI_B/dt} \qquad\qquad\qquad (13b)$$

$$L_{A+B} = \frac{V_A + V_B}{dI_{A+B}/dt} \; . \qquad\qquad\qquad (13c)$$

The other inductances can be calculated similarly by taking the ratio of the coil voltage in question with the voltage across the coil with which the mutual inductance is being taken. The ratio is multiplied by the appropriate self inductance given above.

Table 15 shows the various self and mutual inductances associated with the circuits shown in Figures 46a and 46b. The A and B magnets shown in Fig. 35 were hooked up backwards with their fields in opposition (like a quadrupole) instead of in the same direction. The self inductance of these two coils in series was less than the sum of the two magnet self inductances. (If the magnets had been hooked up so their fields were in the same direction, the self inductance of the two magnets in series would have been larger than the sum of the two individual magnet self inductances.)

The time constants of the coil system were measured by dumping the coil across an external resistor. The resistor chosen was made from a bifilar coil of wire which had a resistance of 0.25 ohm. The coil was discharged through the resistor at currents of 50, 100, 200 and 300 A. The long time constant measured on the A coil at the 50, 100, and 200 A currents was 3.8 s. At 300 A the time constant was reduced because the current in the bore tube caused the coil to go normal. This was the first time we observed quench back. The time constant was measured on the B magnet with the resistor in place; we measured a long time constant of 4.3 s. No measurements of the short time constant were taken on the A magnet. The measured short time constant on the B magnet was around 2 ms, which is quite a bit shorter than the expected value of 4 or 5 ms.

Table 15. Measured self and mutual inductance for the A and B magnets and their pickup coils.

		Measured	Calculated
Self Inductances			
A magnet	L_A	0.79 H	0.789 H
B magnet	L_B	0.78 H	0.782 H
A + B magnet (field opposing)	L_{A+B}	1.15 H	1.193 H
A + B magnet (field together)	L_{A+B}	---	1.949 H
Mutual Inductances			
A to B magnet	$M_{A,B}$	0.19 H	0.189 H
A magnet to A pickup	$M_{A,PA}$	31.0 mH	---
A magnet to B pickup	$M_{A,PB}$	11.0 mH	---
B magnet to B pickup	$M_{B,PB}$	38.0 mH	---
B magnet to A pickup	$M_{B,PA}$	13.0 mH	---
A+B magnet to A pickup	$M_{A+B,PA}$	20.0 mH	---
A+B magnet to B pickup	$M_{A+B,PB}$	34.0 mH	---
A+B magnet to A magnet	$M_{A+B,A}$	0.60 H	---
A+B magnet to B magnet	$M_{A+B,B}$	0.59 H	---

b)   The Set Up for Quench Operation

The quench data from the magnet is recorded on the screens of four tectronic storage oscilloscopes. Figure 47 shows a photograph of the data recording set up for the July 1976 test. Pictures were taken of these screens. These pictures were digitized on one of the LBL scanning tables, and the digitized data were then processed by the LBL 7600 computer. The oscilloscopes which can record three or four signals simultaneously were triggered by the circuit which induces the quench in the magnet itself. This signal provided a zero time mark and started the sweep of the appropriate oscilloscopes (from here on referred to as scopes).

Scopes A, B and D recorded time on the x axis. Scopes A and B displayed the voltage across the quench coil (showed the trigger pulse), the current shunt signal S, and the pickup coil signal P. Scope D displayed the same signals as A and B during test 5 (the November 1975 test) and part of test 7 (the July 1976 test). Scopes A, B and D were run at various sweep rates so that certain kinds of information could be recorded about the magnet.

Scope D during test 6 (the March 1976 test) and part of test 7 (the July 1976 test) displayed the signal from three of the silicon-diodes. Since the response time of the diodes was not instantaneous, the only thing that was successfully recorded on the scope pictures was the time constant of the silicon-diodes and their mounting lugs. (This time constant was 5 to 10 seconds.)

Scope C, which required no trigger, displayed σ versus S, P vs S, and ψ vs S, σ, P, ψ and S are defined as follows:
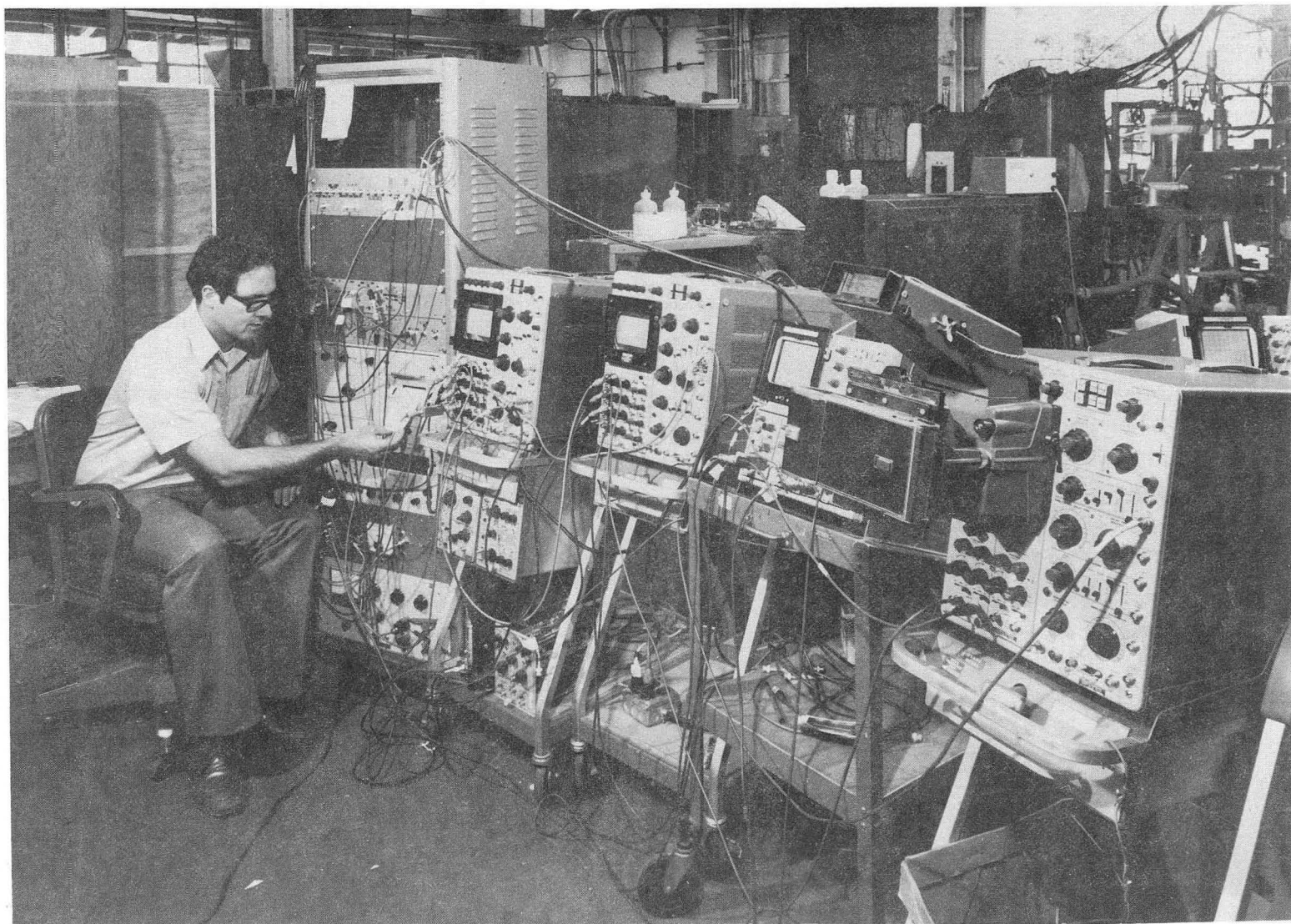
Fig. 47. The oscilloscope set up used to measure quenches during the July 1976 test in Bldg. 58.

$$\sigma = \frac{1}{\tau_{I1}} \int_{t_o}^{t} S(t) \, dt \tag{14a}$$

$$\psi = \frac{1}{\tau_{I2}} \int_{t_o}^{t} P(t) \, dt \tag{14b}$$

where

$$S(t) = R_s I(t) \tag{15a}$$

$$P(t) = -\frac{N_p}{N_1} \frac{d\phi}{dt} \tag{15b}$$

where t is time; t_o is the starting time; τ_{I1} and τ_{I2} are the time constants of integrators to which the current shunt signal S(t) and the pickup coil signal P(t) are connected; R_s is the shunt resistance in series with the magnet coil; N_p is the number of turns in the pickup coil; N_1 is the number of turns in the coil; ϕ is the magnetic flux which passes through the loop of the pickup coil and I(t) is the current in the coil. (Note that t, t_o, τ_{I1}, τ_{I2} are in seconds; ϕ is given in webers; I is given in amperes; and N_1 and N_p are dimensionless.)

The picture from scope C could be measured directly to obtain the integral of current squared with time. Using a polar planimeter or some other method one can measure the area of the σ vs S curve on the oscilloscope picture. From that area and the use of appropriate constants (see Reference 75) one can directly obtain the expression given in the right half of Equation 5. Using Figure 5 it is possible to estimate the worst case temperature which might occur within the magnet coil. With this information, one can estimate what a safe operating current for the next quench might be.

The picture from scope C may be used to estimate the amount of energy which is dumped into the bore tube relative to the total energy contained by the magnet before the quench was initiated. ψ, which is proportional to the magnet flux ϕ, does not decrease in the same way that S, which is proportional to the current I, does. When much of the coil current I has decayed, there is still much flux within the coil bore tube structure. By measuring the area under the ψ vs S curve and comparing that area to a triangle with the same end points, one can find the fraction of the magnet energy which ends up in the coil and in the bore tube. The scope C picture is shown in Figure 48a. Figure 48b shows the appropriate area for calculating the integral of current density squared with time. Figure 48c shows the appropriate areas for calculating the fraction of the energy which ends up in the coil bore tube.

5.2 The Computer Analysis of the Experimental Data

The experimental data of the magnet quench tests were recorded on polaroid film from the screen of storage oscilloscopes. These
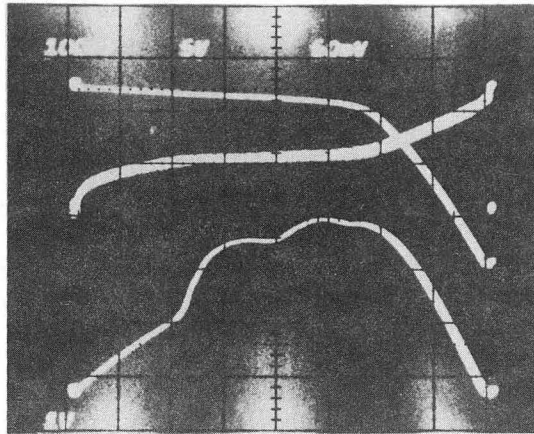
(a) The oscilloscope picture.
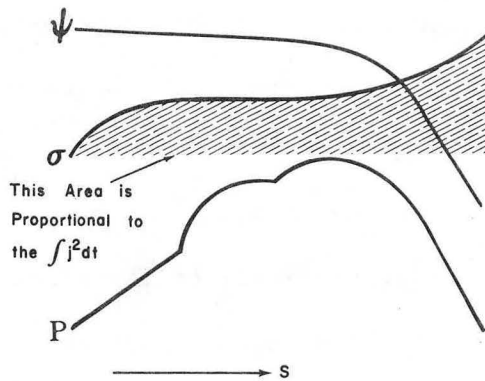
(b) The method used for calculating $\int j^2 dt$.
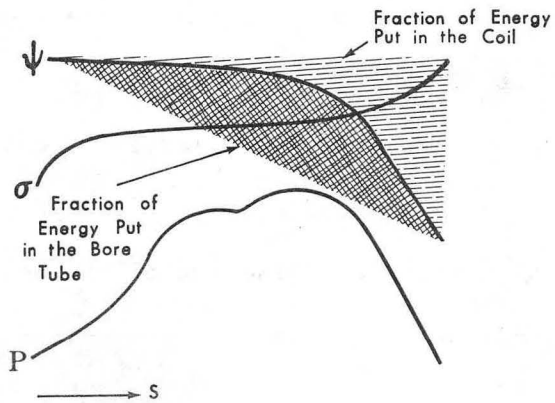
(c) The method used to calculate the energy
fraction which ends up in the coil and
bore tube.

XBB 774-2988

Fig. 48. The C oscilloscope picture and its
interpretation

pictures were digitized by scanning them with a bubble chamber photo
scanning table similar to the one shown in Figure 49. The photos from
scopes A and B were scanned. The position of the scope trace could
be determined within a fraction of a millimeter. Figure 50a shows
a photograph of the scope screen after a magnet quench. Figure 50b
shows the position of lines which represent the S and P traces as
well as the quench coil trigger pulse as a function of time.

The S and P signals as a function of time are sent to the computers.
The current $I(t)$ is obtained thus:

$$I(t) = \frac{S(t)}{R_s} \; . \tag{16}$$

The inductive voltage across the main coil is defined as:

$$V(t) = \frac{N_1}{N_P} P(t) \; . \tag{17}$$

The flux contained in the main coil as a function of time t is:

$$\phi(t) = \frac{L_1 I(o)}{N_1} - \frac{1}{N_1} \int_0^t V(t) \, dt \tag{18a}$$

where L_1 is the coil self inductance and $I(o)$ is the initial current
in the coil. The magnetic flux within the magnet which is due to
current in the coil is:

CBB 769-8903

Fig. 49. The bubble chamber scanning table to
scan the oscilloscope picture. The
scanning table digitized the data
for use in the CDC 7600 computer.
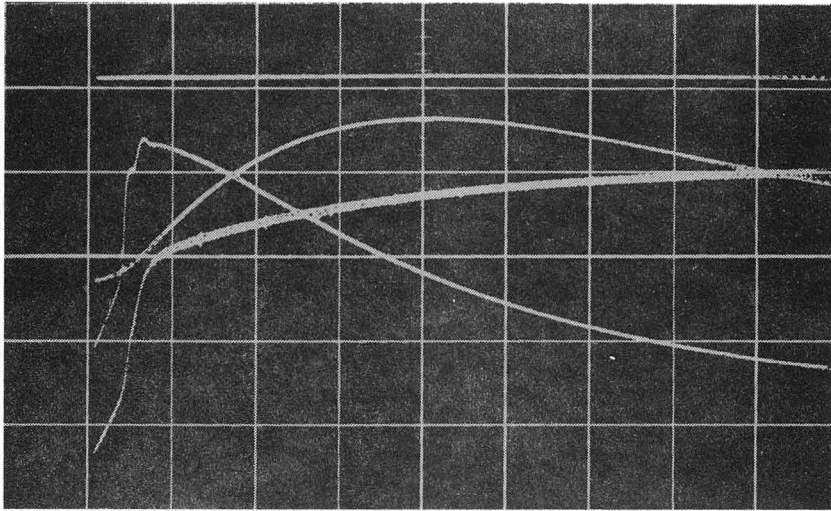
Test 7, Run 38
Q_z in B magnet
    I = 384

time (s)

0   0.2   0.4   0.6   0.8   1.0   1.2   1.4   1.6

Q

V_A

P_B

S

t = 0.2 s cm⁻¹
Q = 20 V cm⁻¹
P_B = 5 V cm⁻¹
S = 100 m V cm⁻¹
V_A = 20 V cm⁻¹

0
1
cm
2
3
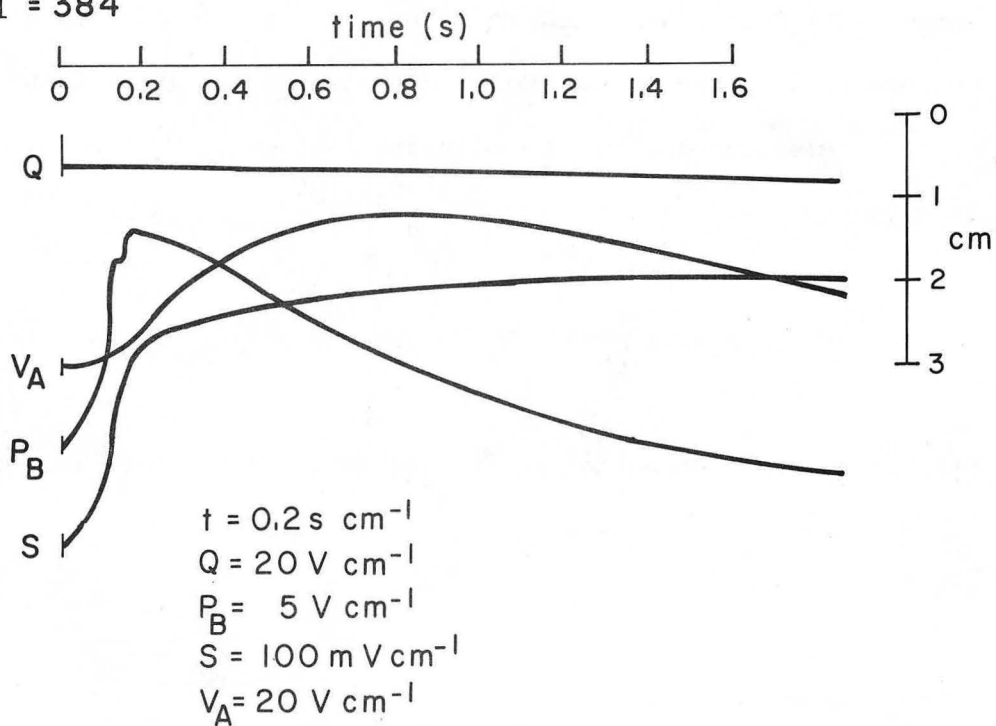
XBL 772-300

Fig. 50.   A typical oscilloscope picture of a quench
(taken on the A scope). Interpretation of
the picture is given below.

$$\phi_c(t) = \frac{L_1 I(t)}{N_1} \quad . \tag{18b}$$

The magnetic flux due to current flowing in the bore tube is:

$$\phi_{AL}(t) = \phi(t) - \phi_c(t) \quad . \tag{18c}$$

Once the flux ϕ, ϕ_c and ϕ_{AL} have been determined one can determine the current which is carried by the bore tube as a function of time:

$$i_2(t) = \frac{N^2 \phi_{AL}(t)}{L_1} \tag{19}$$

where $i_2(t)$ is the bore tube current as a function of time t; N_1 is the number of turns in the coil and L_1 is the magnet self inductance.

The electromagnetic energy in the coil as a function of time is given by:

$$E(t) = \frac{\phi(t)^2}{2L_1} \quad . \tag{20}$$

The energy transformed to heat in the coil and the bore tube circuits, due to resistance in those circuits, is

$$E_H(t) = \frac{1}{2} L_1 I(o)^2 - E(t) \quad , \tag{21a}$$

the heat energy dissipated in the coil circuit alone is

$$E_{HC}(t) = \int_o^t V(t)\ I(t)\ dt \qquad , \qquad (21b)$$

and the heat energy which is dissipated in the bore tube alone is

$$E_{HAL}(t) = E_H(t) - E_{HC}(t) \qquad . \qquad (21c)$$

The computer further defines the terms R_I, the ratio of the current with the initial current, and R_ϕ, the flux or total current ratio:

$$R_I = \frac{I(t)}{I(o)} \qquad (21a)$$

and

$$R_\phi = \frac{\phi(t)}{\phi(o)} = \frac{I_2(t) + N_1 I(t)}{N_1 I(o)} \qquad . \qquad (21b)$$

The time constants for coil and bore tube current decay can also be defined from the data fed into the computer:

$$\tau(t) = N_1 \frac{\phi(t)}{V(t)} \qquad\qquad (23a)$$

$$\tau_c(t) = \frac{N_1 \phi_c(t)}{V(t)} \qquad\qquad (23b)$$

$$\tau_{AL}(t) = \tau(t) - \tau_c(t) \qquad\qquad (23c)$$

where τ is the total circuit decay time constant (note this changes as a function of time). Note that ϕ, ϕ_c, ϕ_{AL}, and V have been defined previously.

The time constant of the coil and the bore tube are inversely proportional to the resistance of the coil R_1 and the bore tube R_2. If the coil self inductance L_1 and the bore tube self inductance L_2 are known, then

$$R_1(t) = \frac{L_1}{\tau_c(t)} \qquad\qquad (24a)$$

and

$$R_2(t) = \frac{L_2}{\tau_{AL}(t)} \qquad . \qquad \text{(24b)}$$

Last but not least, the integral of current density squared with time as a function of time can be determined directly:

$$F(t) = \frac{4}{\pi d^2} \int_0^t I^2(t) \, dt \qquad \text{(25)}$$

where $F = F(t)$ (see Equation 5) and d is diameter of the superconductor matrix. $F(t)$ may be converted into hot spot temperature by the use of Figure 5.

The information, which was fed into the computer in the form of S and P as a function of t, came out of the computer in graphical form. For example, plots of R_I and R_ϕ as a function of t yielded a great deal of information. The most dramatic series of plots shows ϕ, ϕ_c and ϕ_{AL} as function of t. The plot, which shows how the current shifts from the coil to the bore tube, will be shown and discussed in the next subsection. The graphical form of the computer output data greatly facilitated our understanding of the kind of processes which go on within the thin superconducting magnet system.

5.3   The Results of the Quench Tests

The primary purpose of the three tests was to observe the response of the magnets to induced quenches. The A magnet, which was quenched during all three tests, was quenched at a single point. The B magnet, which was quenched only during test 7, was quenched at four different points.

Quench tests were made in graduated steps with quenches being induced at low currents first.[54,75] This procedure was followed in order to get as much experimental data as possible before the magnet might be destroyed. Both magnets were operated at current densities in excess of 10^9 Am^{-2} without apparent damage. The quench tests performed the following functions: 1) quench propagation velocities were measured; 2) the limiting hot spot temperature in the superconductor was estimated; 3) a shift in the current from the coil to the bore tube was measured; 4) the amount of magnetic energy which was deposited in the coil and bore tube was estimated; and 5) quench back from the bore tube back to the superconducting portions of the coil was demonstrated.

Tables 16, 17, and 18 summarize the experimental data on a run by run basis. Table 16 covers data from test 5 (Nov. 1975); Table 17 covers data from test 6 (March 1976); and Table 18 covers data from test 7 (July 1976). The three tables show what transpired during the various runs of the three tests. Included in the tables are: the current in the magnet at the time of quench, the type of quench, the limit value of coil temperature, the final bore tube temperature, the fraction of the magnetic energy dumped inside the bore tube, the quench back time, and remarks which may add to the description of the run. The data shown in Tables 16 through 18 provide the bases from which the conclusions of this section are drawn.

a) Quench Propagation Velocities

The quench tests showed that the coil resistance grew as time squared early in the quench process. The quench propagates along the wire at velocities as high as 35 ms^{-1}. The propagation of the

Table 16. Summary of experimental data for test 5 (November 1975).

Run	Current (A)	Quench* Type	Quench Back** Time (ms)	Energy Fraction in Bore Tube	Remarks
8	50	none	NQB	—	dump across a 0.25 ohm resistor
9	50	none	NQB	—	dump across a 0.25 ohm resistor
10	50	none	NQB	—	dump across a 0.25 ohm resistor
11	50	none	NQB	—	dump across a 0.25 ohm resistor
12	50	none	NQB	—	dump across a 0.25 ohm resistor
13	100	none	NQB	—	dump across a 0.25 ohm resistor
14	200	none	NQB	—	dump across a 0.25 ohm resistor
15	300	QB	—	—	dump across a 0.25 ohm resistor
16	300	Q_1	—	—	
17	100	Q_1	NQB	0.40	
18	100	Q_1	NQB	—	
19	200	Q_1		—	
20	200	Q_1	520-600	—	
21	300	Q_1	260-320	—	
22	300	Q_1	—	0.56	
23	400	Q_1	180-220	0.65	
24	500	Q_1	160-190	0.68	
25	525	spon	—	—	spontaneous quench due to high temperature 7.6 K
26	200	none	—	—	field map at 200 A
27	541	spon	85-110	—	spontaneous quench due to high temperature 7.2 K
28	300	none	NQB	—	charge rate sensitivity to 4 V, no quench
29-30	699	spon	65-80	0.73	temperature at coil high, about 6.5 K
31	300	Q_1	280-340	—	40 V quench, near threshold
32	300	Q_1	280-340	—	30 V quench, near threshold
33	300	Q_1	240-340	—	100 V quench
34	300	Q_1	220-280	—	200 V quench
35-38	300	none	NQB	—	quenches inside bore tube, no quench
39	300	none	NQB	—	heater on for 60 S at 37 W, total energy 2220 J, no quench
40	580	spon	—	—	spontaneous quench due to high temperature
41	360	spon	—	—	spontaneous quench due to high temperature

* Quench type symbols:
Q_1 = quench coil imbedded in the magnet
spon = spontaneous quench
none = no quench
QB = quench back induced quench

** Quench back time:
NQB = no quench
— = quench back time not known

Table 17. Summary of experimental data for test 6 (March 1976).

Run	Current (A)	Quench* Type	Upper Coil T (K)	Quench back** Time (ms)	Bore Tube Temperature (K)	Energy Fraction In Bore Tube	Remarks
21	50	none	--	NQB	—	--	through the 1/4 resistor
22	50	none	—	NQB	—	--	
23	50	none	—	NQB	--	--	
25	100	none	--	NQB	—	--	1.0 V charge, no quench
27	100	none	—	NQB	--	--	5.5 V charge, no quench
28	200	none	--	NQB	--	--	5.5 V charge, 0.8K bore tube T rise
29	200	none	--	NQB	--	--	2.15 V charge, no temperature rise
30	100	none	—	NQB	-..	.--	no quench at 100 V
31	200	Q_1	--.	--	--	0.44	
32	200	Q_1	76	700-800	25.7	0.45	
33	300	Q_1	81	350-450	34.2	0.54	
34	500	Q_1	170	130-170	46.1	0.65	
35	597	spon	--	--	52.5	0.63	training quench
36	200	Q_1	—	700-800	25.4	0.44	70 V quench
37	200	Q_1	78	700-800	25.3	0.43	threshold 63 V
38	300	Q_1	100	340-440	33.7	0.55	43 V quench threshold
39	300	Q_1	100	360-460	--	0.56	40 V quench threshold
40	300	Q_1	100	360-440	—	0.55	70 V quench
41	500	Q_1	175	150-190	46.1	0.64	28 V quench threshold
42	500	Q_1	200	150-200	—	0.62	70 V quench
43	600	Q_1	240	130-160	50.6	0.62	25 V quench threshold
44	600	Q_1	235	130-170	—	0.64	70 V quench
45	654	spon	230	110-140	53.0	0.66	18 V quench threshold
46	696	spon	235	100-120	56.0	0.64	training quench
47	700	Q_1	380	75-110	55.1	0.64	18 V quench threshold
48	100	Q_1	—	NQB	—	—	125 V quench
49	100	Q_1	--	NQB	—	--	150 V quench
50	100	Q_1		NQB /	—	--	150 V quench
51	300	Q_1	110	340-420	33.4	0.53	70 V quench
52	300	none	--.	--	—	--	try to quench through bore tube
53	300	Q_1	110	320-400	33.5	0.54	150 V quench
54	300	Q_1	--	340-420	33.8	--	70 V quench
55	700	yes	--	80-100	54.6	0.66	bore tube rapped by exploding coil, quench
56	733	spon	290	70-90	60.0	0.66	training quench
57	773	spon	240	70-90	57.5	0.67	training quench

* Quench type symbols:
none = no quench
Q_1 = quench in coil imbedded in magnet
spon = spontaneous quench
yes = quench from another source

** Quench back time
NQB = no quench back
-- = quench back time not known

Table 18. Summary for data from test 7 (July 1976).

Run	Powered Magnet Coil	Starting Current (A)	Quench Coil*	Quench** Voltage (V)	Upper Limit Coil Temp. (K)	Quench Back Time*** (ms)	Bore Tube Temperature (K) A	Bore Tube Temperature (K) B	Energy Fraction in Bore Tube	Remarks
12	B	195	Q_2	T120	90	700-800	--	--	--	data here questionable
13	B	195	Q_2	T120	85	700-800	5.7	21.8	--	data here questionable
14	B	292	Q_2	120	240	320-400	13.1	29.4	0.61	
15	B	30^	Q_2	120	--	300-360	13.5	30.2	--	
16	B	292	Q_2	120	195	320-390	13.1	36.7*	0.60	hot spot effect seen
17	B	389	Q_2	120	--	22(-270	14.5	40	0.65	
18	B	389	Q_2	120	170	200-280	--	38.4	0.64	
19	B	389	Q_2	120	290	200-260	--	38.3	0.64	
20	B	389	Q_2	120	195	240-270	14.5	38.3	0.64	
21	B	389	Q_3	120	195	200-260	14.5	44.1#	0.64	hot spot effect seen
22	B	389	Q_3	120	195	200-260	14.5	43.8#	0.63	hot spot effect seen
23	B	389	Q_2	120	195	210-270	14.5	37.9	0.65	
24	B	389	Q_4	120	170	200-270	14.5	38.0	0.63	
25	B	389	Q_5	120	195	200-250	14.5	43.5#	0.64	hot spot effect seen
26	B	389	Q_2+Q_4	120	170	170-220	14.5	37.9	0.65	
27	B	389	Q_2+Q_5	120	170	190-230	14.5	43.5#	0.64	hot spot effect seen
28	B	389	Q_2	T80	195	210-250				
29	B	97	Q_2	T200	--	NQB	6.0	17.8	0.40	
30	B	97	Q_4	T180	50	NQB	6.0	15.3	0.38	
31	B	195	Q_3	120	95	560-640	--	26.6#	0.55	hot spot effect seen
32	B	292	Q_4	120	--	300-270	--	29.1	0.60	
33	B	97	Q_2	T190	--	NQB	5.8	16	0.40	
34	B	195	Q_4	T120	--	560-540	9.1	25	0.54	
35	B	195	Q_3+Q_4	120	--	520-600	9.1	23.8	0.53	
36	B	195	Q_2	T120	115	570-680	9.1	23.6	0.55	
37	B	389	Q_2	200	200	190-250	14.5	38.0	0.64	
38	B	389	Q_2	200	--	195-240	--	37.8	0.63	
39	B	389	Q_2	200	170	195-240	14.2	37.9	0.64	
40	B	389	Q_2	T70	170	220-270	14.5	35.9	0.63	
41	B	97	Q_2	200	56	NQB	15.3##	14.5##	0.42	
42	B	97	Q_3	T230	50	NQB#	18.1##	15.1##	0.43	the hot spot effect
43	B	97	Q_4	200	54	NQB	15.3##	#19.1##	0.4?	apparent heat transfer
44	B	97	Q_4	T170	56	NQB	15.3##	#19.0##	0.42	from coil hot spot to
45	B	97	Q_2+Q_4	200	48	NQB	17.7##	#17.8##	0.48	the coil bore tube
46	B	97	Q_3+Q_5	240	50	NQB#	18.2##	15.3##	0.45	
49	A+B	97	Q_2	T190	58	NQB	--	16.4	0.25	
50	A+B	97	Q_2	T185	58	NQB	11.9	16.4	0.25	
51	A+B	97	Q_3	T250	58	NQB	11.9	18.8#	0.25	hot spot effect seen
52	A+B	97	Q_3	T250	58	NQB	11.9	18.7#	0.28	hot spot effect seen
53	A+B	97	Q_4	T180	65	NQB	11.7	16.0	0.24	
54	A+B	97	Q_2+Q_4	200	56	NQB	11.7	16.2	0.26	
55	A+B	97	Q_1	T240	80	NQB	17.1	--	0.18	very slow quench in A coil
56	A+B	97	Q_1	250	80	NQB	17.1	7.7	0.17	
57	A+B	107	Q_1	250	65	NQB	18.3	9.6	0.20	
58	A+B	195	Q_1	150	125	1000-1200	23.4	19.9	0.45	

Table 18. Continued.

Run	Powered Magnet Coil	Starting Current (A)	Quench Coil*	Quench** Voltage (V)	Upper Limit Coil Temp. (K)	Quench Back Time*** (ms)	Bore Tube Temperature (K) A	B	Energy Fraction in Bore Tube	Remarks
59	A+B	195	Q_1	T140	125	1000-1200	23.2	19.8	0.49	
60	A+B	195	Q_1+Q_2	170	91	720-840	22.4	21.7	0.53	
61	A+B	195	Q_2	170	125	800-900	21.8	22.5	0.53	
62	A+B	292	Q_2	170	100	420-500	20.8	27.3	.59	
63	A+B	292	Q_1	170	140	500-600	28.8	26.5	0.57	
64	A+B	292	Q_1+Q_2	170	120	3.7-460	28.8	27.1	0.56	
65	B	97	Q_2	200	--	NQB	5.7	14.7	--	
66	B	97	Q_2	200	--	NQB	5.9	14.7	0.40	
67	B	486	Q_2	T70	310	160-200	16.2	41.7	0.66	
68	B	584	Q_2	T60	350	130-165	18.1	44.5	0.68	helium bottle disturbs magnet, no quench
69	B	778	Q_2	T45	500	90-100	21.6	51.8	0.74	
70	B	864	Q_2	T45	580	80-90	23.4	54.9	0.75	
71	B	920	Q_2	T45	780	72-80	25.3	59.0	0.75	
72	B	560	spon	--	--	60-70	--	--	0.71	very fast charge, hot bore tube
73	B	904	none	--	--	no data	--	--	--	2 volt charge up, no quench
74	A	97	Q_1	T220	--					
75	A	97	Q_1	250	--	NQB	15.6	5.2	--	
76	A	100	Q_1	T210	--	NQB	15.8	5.2	--	w/o filter
77	A	195	Q_1	T140	118	800-960	24.2	6.8	0.48	
78	A	200	Q_1	T140	86	740-900	24.6	7.0	0.48	w/o filter
79	A	292	Q_1	T100	125	440-500	30.5	9.5	0.52	
80	A	389	Q_1	T80	185	260-310	39.0	11.8	0.60	
81	A	486	Q_1	T70	280	170-220	44.3	13.6	0.62	
82	A	804	spon	--	--	no data	51.7	19.8	0.68	training quench

* Q_1, Q_2, Q_3, Q_4, and Q_5 are the coil from which quenches are induced; none is non quench, and "spon" is a spontaneous quench

** T before the voltage indicates a threshold test.

*** NQB is no quench back; "no data" is no quench back data available.

$ Temperature on bore tube elevated due to hot spot in coil next to bore tube.

$$ TA corresponds to temperature at center of B coil bore tube; TB corresponds to temperature at edge of bore tube under quench coil Q_4. This symbol only applies in Runs 41 through 46.

normal region (or quench) from wire to wire is much slower than the propagation along the superconducting wire. The growth of the magnet resistance with time early in the quench can be represented as follows:

$$R_1(t) = R_{con} \; \alpha \; V_Q^2 t^2 \tag{26}$$

where $R_1(t)$ is the resistance of the magnet as a function of the time t since the quench was induced. V_Q is the velocity of normal region propagation along the superconducting wires; α is the ratio of wire-to-wire propagation velocity to propagation velocity along the wire; R_{con} is a constant which relates the normal region area to the resistance of the coil at time $t = 1$.
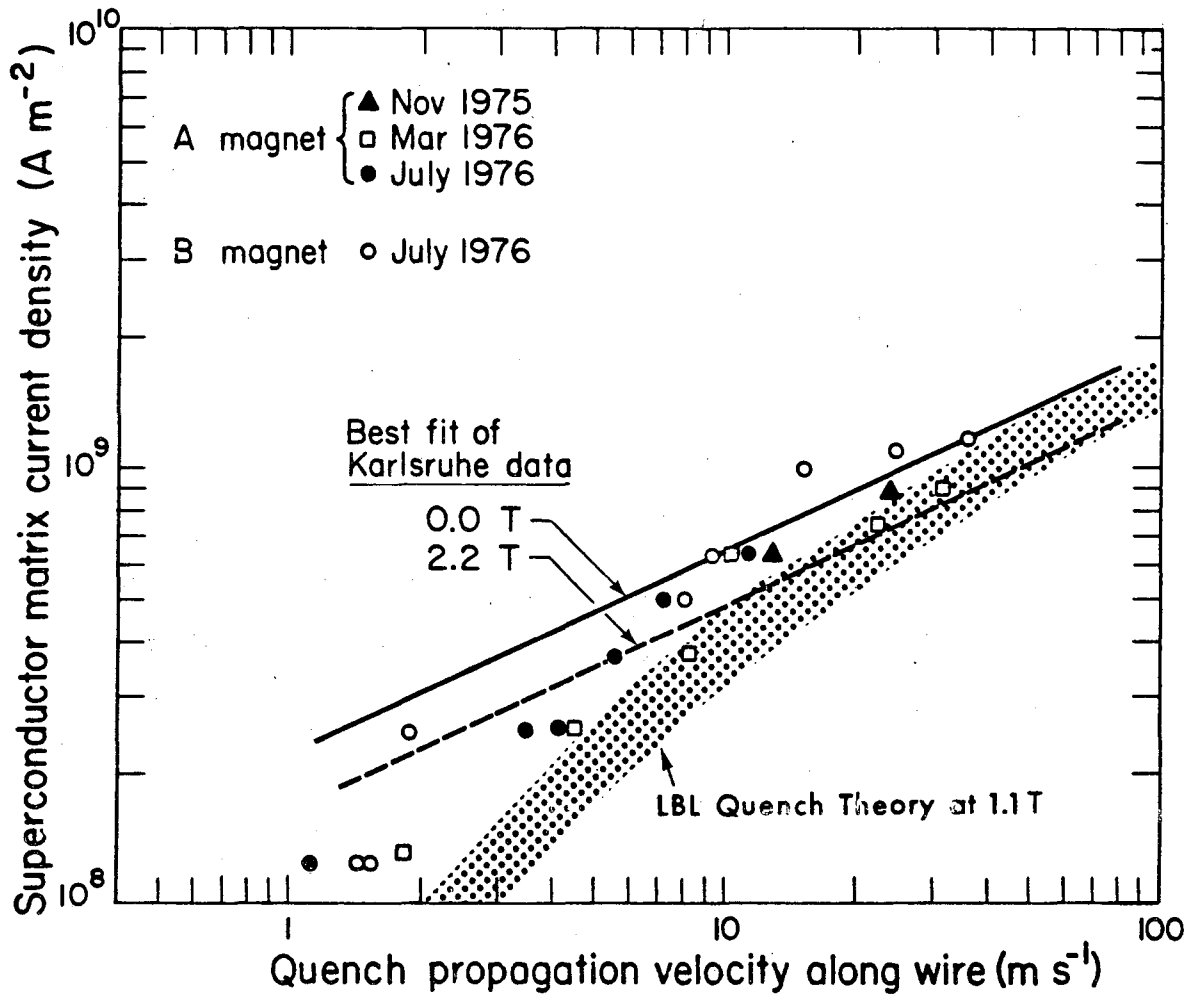
The longitudinal quench velocity V_Q has been theoretically derived by a number of investigators.[76,77] In general, these models make too many simplifying assumptions and do not agree with the measurements which have been made. Recently here at LBL a new theory was developed by Eberhard and Green.[28] This theory can be used to predict the velocity of normal region propagation in the absence of transverse heat transfer from the superconducting wire (the only direction heat is transferred is along the wire proceeding in the normal zone.) The velocity of normal region propagation V_Q can be represented as follows:

$$V_Q = 0.548 \; J \left[\frac{\alpha_{cu} \rho_{cu}}{H_{CRT} - H_o} \right]^{1/2} \tag{27}$$

where v_Q is the longitudinal normal region propagation velocity (ms^{-1}), J is the matrix current density (Am^{-2}), α_{cu} is the thermal diffusivity of copper at the temperature the superconductor becomes normal (m^2s^{-1}), ρ_{cu} is the electrical resistivity of copper at the temperature the superconductor becomes normal (Ωm), H_{crt} is the enthalpy per unit volume of the superconductor matrix at the temperature the super-conductor becomes normal, and H_o is the enthalpy per unit volume of the superconductor matrix at the starting temperature. The temperature at which the superconductor becomes normal is a function of the matrix current density J and the local magnetic induction B.

The above equation shows no dependence of copper to superconductor ratio in the matrix (there is a slight dependence which is found in the H_{crt} term but the dependence is small). To the first order quench wave velocity V_Q is dependent only on J and B. The J dependence of V_Q is not linear. At low current densities V_Q goes as $J^{1.5}$. At high current densities V_Q goes as J^n where $n \geq 2$. Measurements of quench propagation velocity in isolated well-cooled wire samples show a J^2 dependence.[78] It is believed that heat transfer retards the quench velocity at low J; hence the J dependence does not change to $J^{1.5}$ as the LBL theory indicates. The Karlsruhe measurements show that V_Q depends only on J and B. There is no discernible dependence on matrix copper to superconductor ratio.

Figure 51 shows the results of the LBL quench velocity measurements. These measurements are compared to a best fit of the Karlsruhe measure-ments[79] and to the LBL quench theory. The LBL measurements which were made in a magnet agree in magnitude with the Karlsruhe single.
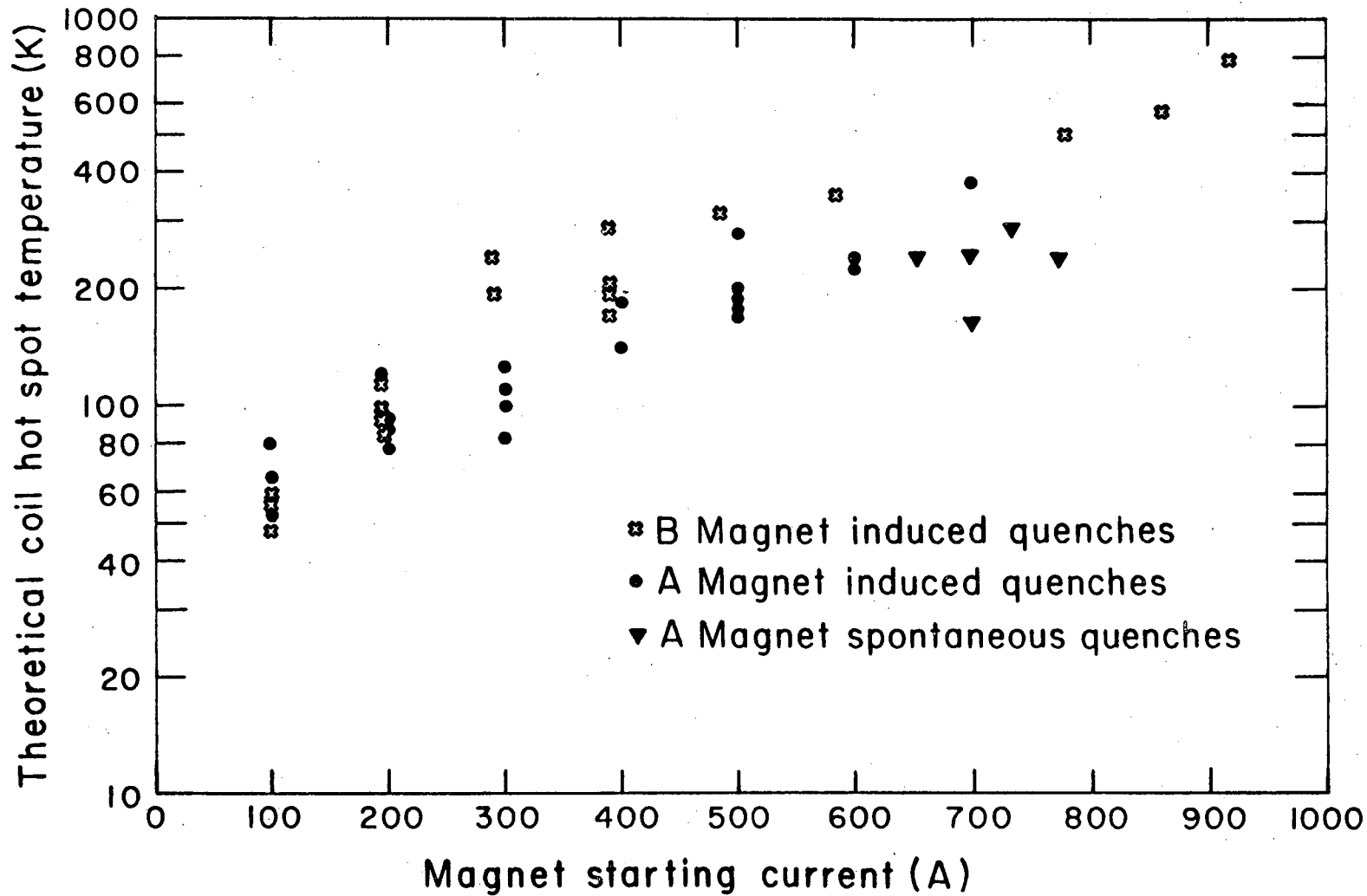
Fig. 51. Measured quench velocities along the wire
in the A and B magnets as a function of
current density in the wire. (The measure-
ments are compared to the LBL theory with no
heat transfer. Also shown are best fits of
bare wire measured data taken by P. Turowski
at the Institut für Experimentelle Kernphysik
the Kernforschungszentrum, Karlsruhe, W. Germany.

wire data. However, the LBL quench theory yields results which are high. The shape of the V_Q vs J curve is the same for the measurements and theory. The measured velocities are believed to be influenced by transverse heat transfer. The ratio of transverse quench velocity to the quench velocity along the wire is calculated to be 0.02 to 0.025, $R_{con} \approx 1.5$ ohm m^{-2} for the A magnet and $R_{con} \approx 2.5$ ohm m^{-2} for the B magnet.

b) The Maximum Temperature Possible in the Magnet Coil

The maximum temperature possible in a superconducting magnet is a function of the integral of the matrix current density squared with time. A doubling of this integral when it is low results in only a small temperature change. When the integral is large (say, corresponding to a temperature of 140 K) a doubling of the integral of J^2 with time will result in a very large temperature change. (If the integral of J^2 dt is doubled from a starting value which corresponds to 140 K, the final temperature will be around 1000 K.) The reason for the high sensitivity of temperature with the integral is the fact that the resistivity of the metal changes much faster than the specific heat. (See Equation 5 and Figure 5.)

The integral of J^2 dt was calculated from the scope C picture, and also from the computer data. There was reasonable agreement between the two calculations. From Figure 5 one can calculate the maximum possible temperature in the superconductor. This temperature is plotted against coil current in Figure 52, which also shows data points for Magnet A and Magnet B. Theoretical hot spot temperatures as high as 800 K were recorded.

Fig. 52. Measured theoretical hot spot temperature (taken from measurements of the integral of current density squared with time) as a function of starting current in the A and B solenoid magnets.

XBL 772-298

In general, the highest current runs exceeded the maximum safe operating quench temperature of about 400 K. The theoretical hot spot temperature was higher for the B magnet than for the A magnet, the reason being that $(r+1)/r$ (r is the copper to superconductor ratio) has a greater effect on the final temperature than does the faster quench back in the B magnet. It was interesting to note that spontaneous quench, which often occurs in the center of the coil, will cause lower hot spot temperatures than induced quenches which occur at the edge of the coil. The magnet resistance does not grow as quickly from a quench at the coil edge as it does from a quench at the coil center. Quenches which were induced by two separate coils had lower theoretical hot spot temperatures than quenches induced by one coil. A and B magnet powered together had a higher hot spot temperature than quenches induced in the magnets when they were powered separately.

Maximum theoretical hot spot temperatures of up to 800 K were calculated from the integral of J^2 dt. The insulation begins to char when its temperature reaches 400-450 K. The theoretical hot spot temperatures were in some cases very high, yet there is absolutely no evidence of damage to either of the magnet coils. It can be safely assumed that heat transfer from the superconductor matrix to the surrounding insulation and the bore tube reduced the hot spot temperature and the resistance of the coil. Indeed, there is evidence that suggests that this heat transfer is quite considerable. The bore tube temperature was measured with the silicon-diodes, and was shown to be considerably hotter under the portions of the coil in which the quench was induced than under other parts of the coil. Thus it appears that the LBL

magnet design is inherently safer than the simple theory would suggest.

c)   The Shift in Current from the Coil to the Low Resistance Bore Tube

The shift of the current from the magnet coil to the low resistance bore tube was noticed from the very beginning of the experiments.[80,81,82] Figure 53 illustrates the shift in the current. This figure shows the total magnetic flux ϕ, the magnetic flux due to current in the coil ϕ_c and the magnetic flux due to current in the bore tube ϕ_{AL} as a function of time. The total current (between the coil and the bore tube) remains constant for some time. Yet the current flowing in the coil drops dramatically and the current in the bore tube rises just as dramatically.

The shift in the current from the coil to the bore tube is inherent, as shown in the basic coupled equation 8; it starts almost as soon as the primary circuit becomes resistive. The time constant of this shift is the short time constant τ_s discussed in Section 2. As the coil resistance increases, more current is forced into the bore tube. The sudden drop in coil current, which occurs between 80-110 ms, is caused by quench back which will be described later in this section. Quench back, however, is not necessary in order to achieve a dramatic shift in the current from the coil to the bore tube, as illustrated in Figure 54. The difference between what is shown in Figures 53 and 54 is due to the initial current at which the quench started. Both figures show that once the bore tube current reaches its peak value, both currents will decay almost exponentially with a time constant τ_L which is discussed in Section 2.

The shift in current from the superconductor to the bore tube has the effect of reducing the integral of J^2 dt and hence the hot

AA01, TEST 6, LOG 2, RUN 47.
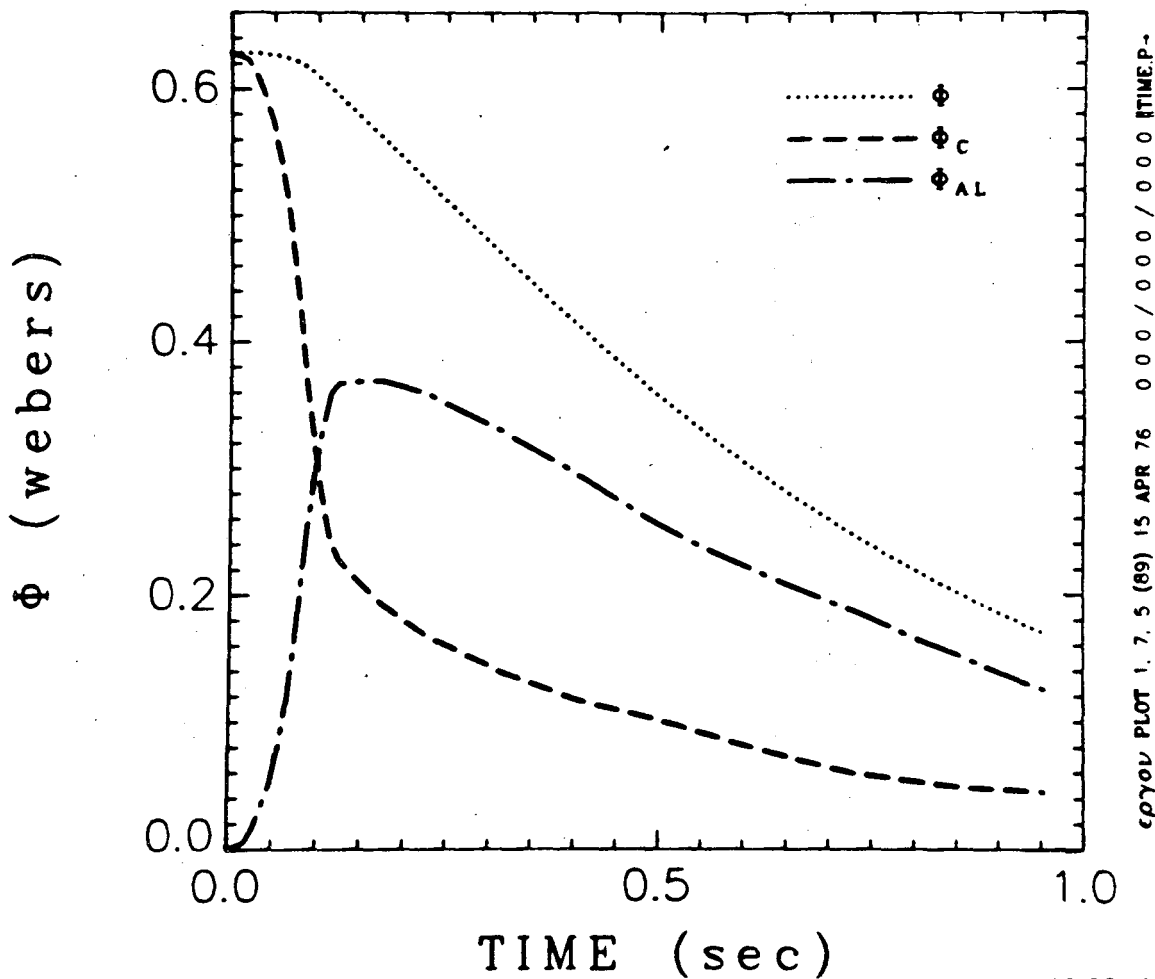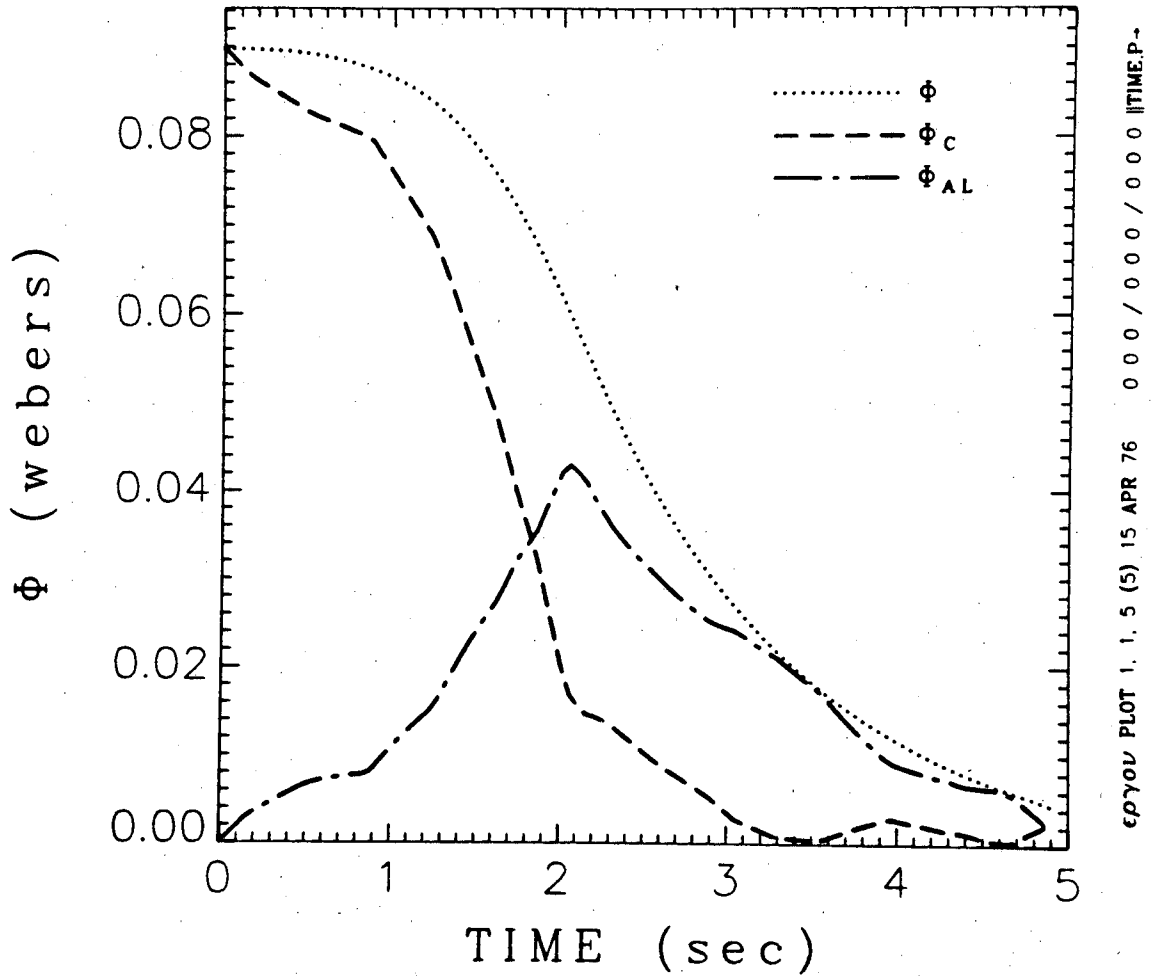
$I_0 = 700$, $U_Q = 18$

Fig. 53. Measured magnetic flux during a 700 A
quench of the magnet due to current in
the coil ϕ_c, current in the bore tube
ϕ_{AL} and the total current ϕ vs time (the
shift of current from the coil to the
bore tube can be seen. Quench back is
evident at 700A).

XBL 768-8944

AA01, TEST 6, LOG 2, RUN 50.

$I_0 = 100$, $U_Q = 150$

XBL 773-8049

Fig. 54. Measured manetic flux during a 100 A quench of the A magnet due to current in the coil ϕ_c, current in the bore tube ϕ_{AL}, and the total current ϕ vs time (there is a shift in current from the coil to the bore tube, but there is no quench back at 100 A).

-162-

spot temperature in the coil. The decrease in the current does not

result in large changes to total magnetic flux. Hence the inductive

voltages in the coil system which are proportional to $d\phi/dt$ are kept

within reasonable bounds. Figure 53 graphically illustrates the role

of the bore tube. The shift in current to the conductive bore tube

is further aided by quench back.

d) Quench Back to the Magnet Coil

The bore tube causes the entire coil to go normal before the

normal region propagation occurs in the quench along the wires

and from wire to wire. Figures 55 and 57 show a sudden drop in the

coil current at all currents above 100 A. These figures, which are

normalized current plots with time, illustrate that high current

quenches take less time than low current quenches. The break in the

current is due to the sudden shift of the current from the coil to the

bore tube, caused by a sudden increase in coil resistance. This is

the process we call "quench back"; it is nothing more than the whole

coil becoming normal at once.

The current break shown in the normalized current curves of

Figures 55 and 57 should be contrasted with the lack of a break in

the magnetic flux which is shown in the normalized flux versus time

curves of Figures 56 and 58. (Figure 55 and 56 belong to the A magnet;

Figures 57 and 58 belong to the B magnet.) A further comparison between

Figures 53 and 54 show that the magnet coil becomes normal rather

suddenly and its current drops suddenly. The drop in coil current

when there is no quench back is far less dramatic; hence, there is no

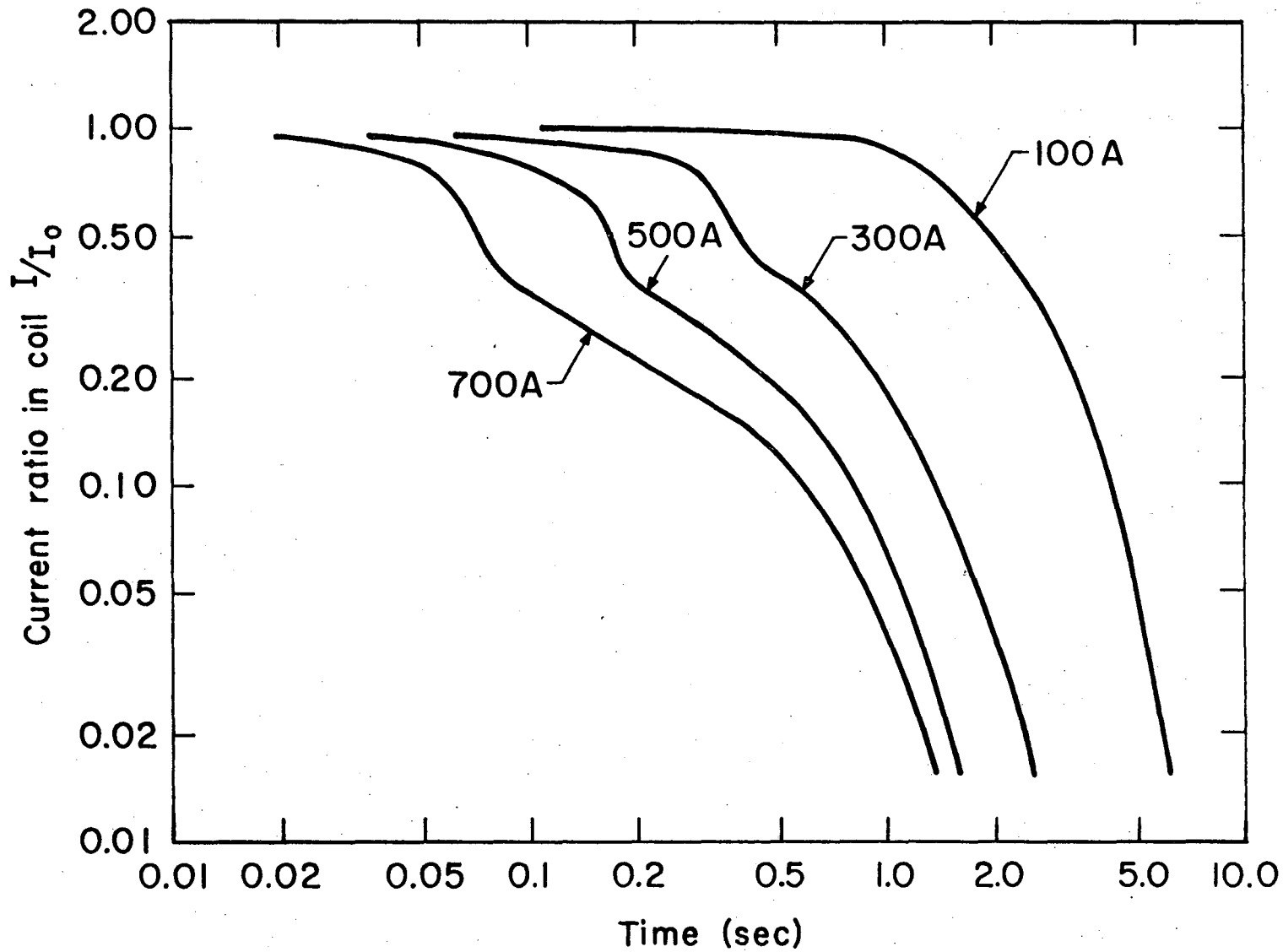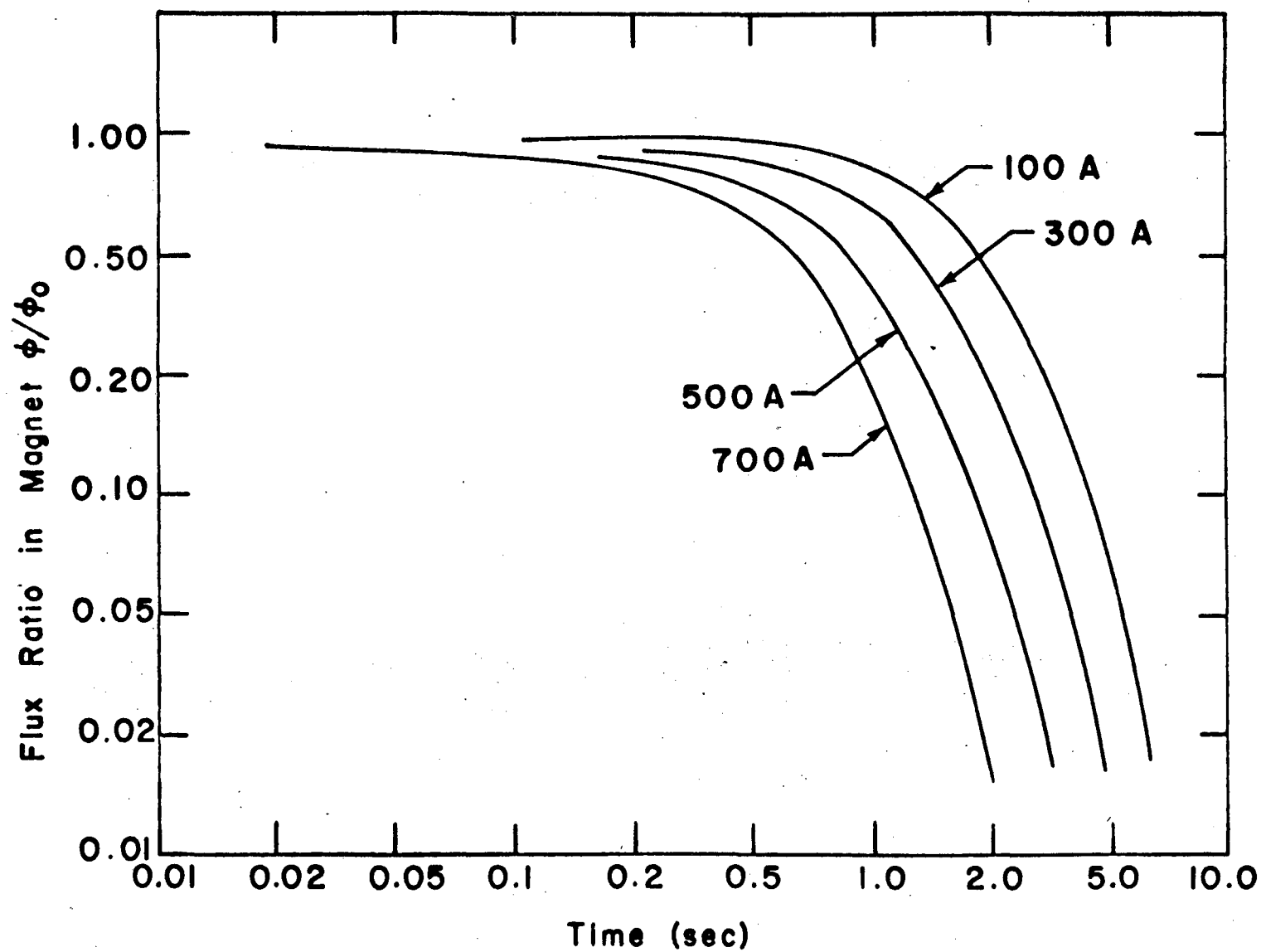characteristic break. The limit for the start of the quench back

Fig. 55. The ratio of the current to the starting current vs time for quenches induced at various starting currents in the A magnet. (The 100 A curve has no break because there is no quench back.)

XBL 764-1391

Fig. 56. The normalized total current vs time in the A magnet for various starting currents. (Note there is no break in the curves. Note the much longer time constant for the total current decay. Compare with Fig. 55.)

XBL 774-8236

-164-

Fig. 57. The ratio of current to starting current vs time for various starting currents in the B magnet. (Note there is no break or quench back in the 100 A curve.)

XBL 769-4081

XBL 774-8279

Fig. 58. The normalized total current vs time for various starting currents in
the B magnet. (Note the much longer time constants for total currents.
Note there is no break in the curves. Compare this with Fig. 57.)

phenomena occurred when the initial coil current was between 100 and 200 A.

There are two ways that quench back can be initiated. The first, which occurs at low rates of di/dt, is initiated by the current in the bore tube. This current heats the bore tube which in turn heats the coil in thermal contact with the bore tube. This method of quench back has a couple of time constants attached to it.[84] There is a characteristic time for the bore tube to heat up, and a characteristic time for the heat to be transferred to the coil. The second method of quench back, which occurs at high rates of di/dt, is initiated by the high rate dB/dt associated with quick current shifts to the bore tube.[56,57,58] This method of quench back will occur even when there is no thermal contact between the bore tube and the coil. Once a high enough value of dB/dt has been achieved, quench back will occur very quickly. The LBL measurements of quench back indicate that the first method (the thermal quench back) appears to dominate at low currents. At high currents both methods of quench back could be important. The second method (the magnetic method) will be dominant whenever the current is dropped suddenly (shifted to the bore tube) by putting an external resistor into the coil circuit which results in a large voltage across the coil.
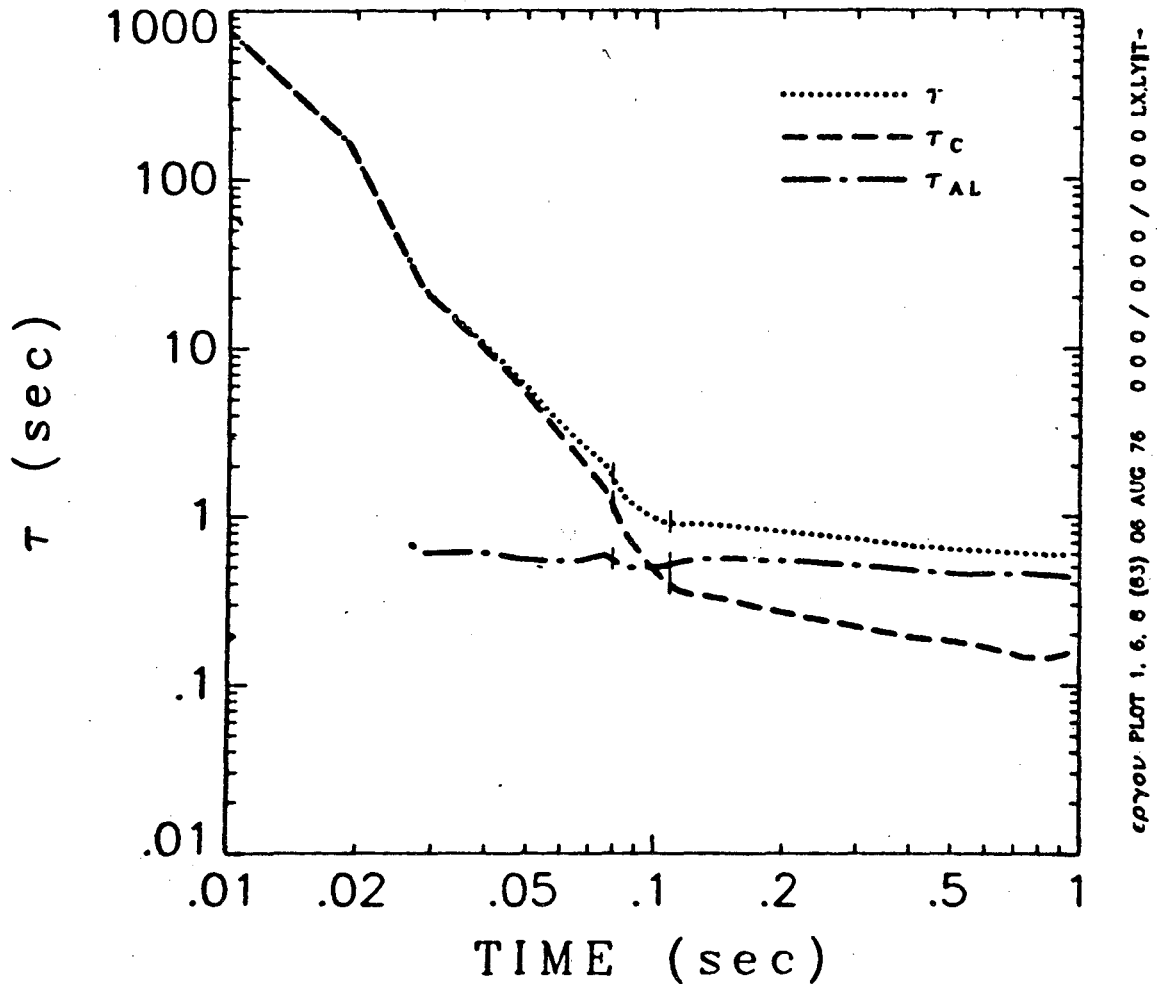
Quench back divides the quench process into two distinct periods. In period 1, the current in the bore tube increases largely as the current in the coil decreases; it ends in quench back. The total flux in the magnet decays very little during this process. The analysis of period 1 shows that the coil resistance increases quadratically.

This is shown in Figure 59 by a quadratic decrease in the coil time constant τ_c (see Equation 23b in this section). Before quench back only a portion of the coil turns normal, as evidenced by high values of τ_c. Figure 60 shows the coil resistance change vs time at various currents in the coil. Quench back has started when the coil resistance change with time varies from a t^2 to a t^n relationship where n is greater than 3. Figure 61 shows that relatively little magnetic energy has turned to heat by the time quench back starts. (The fact that ϕ in Figure 53 remains constant is also evidence of this.) When the coil is entirely normal at the end of quench back, period 2 starts. This period is characterized by the exponential-like decay of the current in the coil and the bore tube (see Figure 53).

Quench back appears to start when the current in the coil drops to around 70 percent of the original current in the coil. Once started, it proceeds rapidly until the coil current drops to about 30 percent of its original value. Figure 62 shows the quench time as a function of the starting current in both the A and B magnets. The width of the band represents the time over which the coil becomes entirely normal through the quench back process. At low currents the A magnet requires more time to quench back than does the B magnet. An explanation for this is that the B magnet conductor has low copper to superconductor ratio. Superconductor has a higher normal resistance as the quench propagates, driving the current into the bore tube sooner and thereby causing quench back sooner. A quench induced in the B magnet at two separate points causes a faster quench back than one induced at one point.

AA01, TEST 6, LOG 2, RUN 47.

PAGE 76 $I_0 = 700$, $U_Q = 18$

XBL 768-8955

Fig. 59. The time constant of the magnet τ_c, the
time constant of the bore tube τ_{AL}, and
the total time constant τ as a function
of time. (This is the same 700 A quench
of the A magnet shown in Fig. 53.)

Fig. 60. Magnet resistance vs time during quenches
at various starting currents in the A magnet.
(Note that coil resistance grows as time
squared early in the quench. Quench back
causes a faster resistance growth rate.)

XBL 764-1527

AA01, TEST 6, LOG 2, RUN 47.

$$I_0 = 700, \quad U_Q = 18$$

XBL 768-8943

Fig. 61. The magnet time constant τ_c, the bore tube
time constant τ_{AL} and the total time constant
τ as a function of total magnet energy turned
to heat. This is the same 700 A quench of the
A magnet shown in Fig. 53 and Fig. 59.

XBL 768-3252

Fig. 62.   Quench back time vs starting current in the A
magnet and the B magnet. (The lower line of
the shaded area shows the start of quench back,
the upper line shows the finish of quench back.)

The duration of period 1 is extremely important since it is the most likely time when patterns for magnet overheating and burnout are established, provided that τ_1 is smaller than τ_2. In both the A and B magnets, period 1 was found to decrease as approximately as $i_0^{-3/2}$, where i_0 is the starting current in the coil. Efforts in reducing the quench problem in thin magnets must be aimed at reducing the duration of period 1. Methods for doing this will be discussed further in Section 7.

e) The Final Bore Tube Temperature and the Distribution of Energy between the Coil and the Bore Tube

The silicon-diodes measured the temperature of the bore tube as the quench process proceeded. Silicon-diode thermometry had a typical time constants of 5 to 10 seconds; these thermometers were not useful for showing the fine structure of bore tube temperature change. The time constant for heat removal from the bore tube is typically greater than 10 seconds (particularly when the magnet is quenched at high currents). The silicon-diode thermometers proved to be somewhat useful for measuring the local temperature maxima on the bore tube.

This temperature can be correlated with the energy which has been deposited in the bore tube by current. Figure 63 shows a plot of bore tube enthalpy as a function of temperature.[85,86] The total energy deposited in the bore tube from the magnet is:

$$E_{AL} = V_{AL} \left[H_{AL} (T) - H_{AL} (4.5) \right] \qquad (28)$$

where E_{AL} is the heat energy deposited in the bore tube, (J) V_{AL} is the volume of the bore tube m^3, $H_{AL}(T)$ is the enthalpy of the aluminum

Fig. 63. The enthalpy of aluminum as a function of absolute temperature (zero enthalpy occurs at absolute zero).

XBL 774-8480

-174-

at a temperature T ($J\ m^{-3}$), and H_{AL}(4.5) is the enthalpy of the aluminum
at a temperature of 4.5 K (Jm^{-3}). There is about 29 kg ($1.07 \times 10^{-2}\ m^{3}$)
of 1100-0 aluminum in the bore tube. Most of the bore tube energy
will end up in the 1100-0 aluminum. The 5 kg of 6061 aluminum in
the bore tube end will not absorb much of this energy because its
resistivity is too high. The fraction of the magnet's energy which
ends up in the bore tube is given by:

$$ f = \frac{2\ E_{AL}}{L_1 I_o^{2}} \tag{29} $$
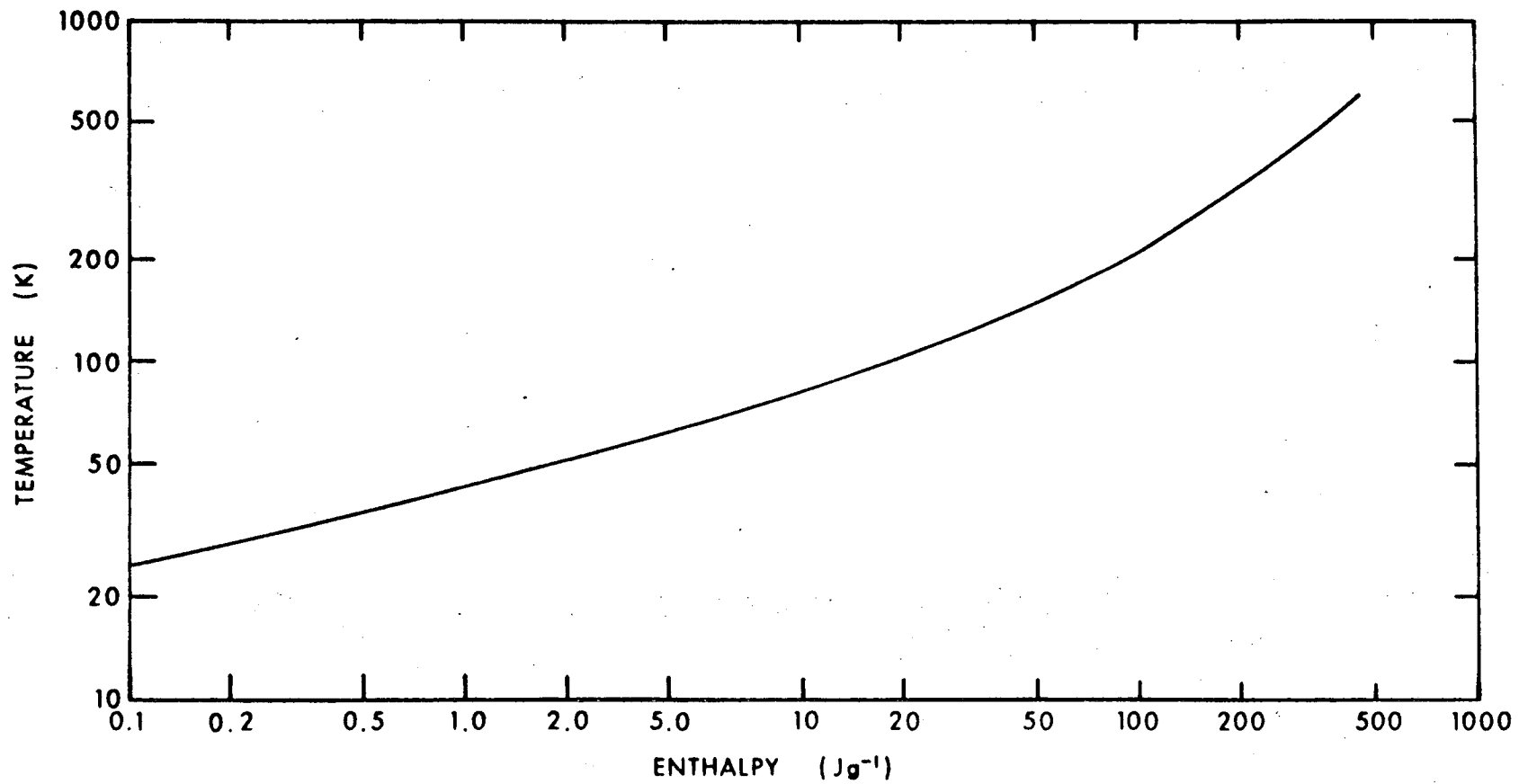
where f is the fraction of the energy ending up in the bore tube
L_1 is the inductance of the coil (H), I_o is the starting current in
the magnet and E_{AL} is as previously defined.

Figure 64 shows the final bore tube temperature as a function
of time in the A and B magnets. One can see the effect of thermal
diffusivity in the thermometry, which results in an error of several
degrees in the temperature measurement. Figure 65 shows the final
bore tube temperature as a function of current in the A and B magnets.
This figure is based on direct temperature measurement with the silicon-
diodes. In all cases the diodes used are located away from the region
where the quench was induced.

Three methods can be used to estimate the fraction of magnetic
energy which ends up in the magnet bore tube. They are: 1) direct
measurement of the areas under the ϕ curve in the scope C pictures
(see Figure 48c), 2) the determination of the change in enthalpy of
aluminum bore tube by temperature measurements with the silicon-diodes

XBL 772-297

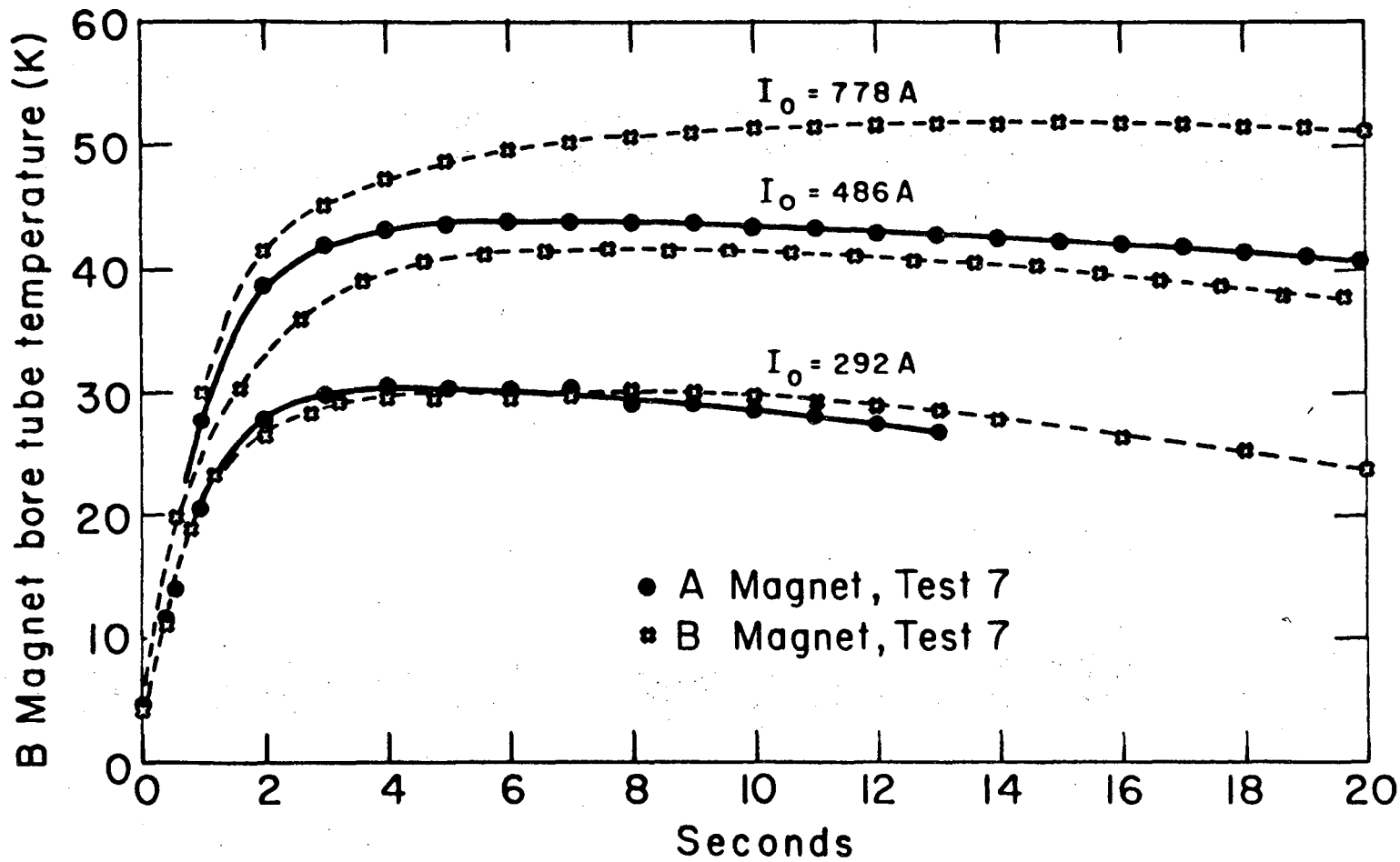Fig. 64. The indicated bore tube temperature measured in
diodes TD-4 and TD-5 as a function of time
after the start of the quench and the starting
current in the magnet. (Note the temperature
measure time lag is greater for the B magnet
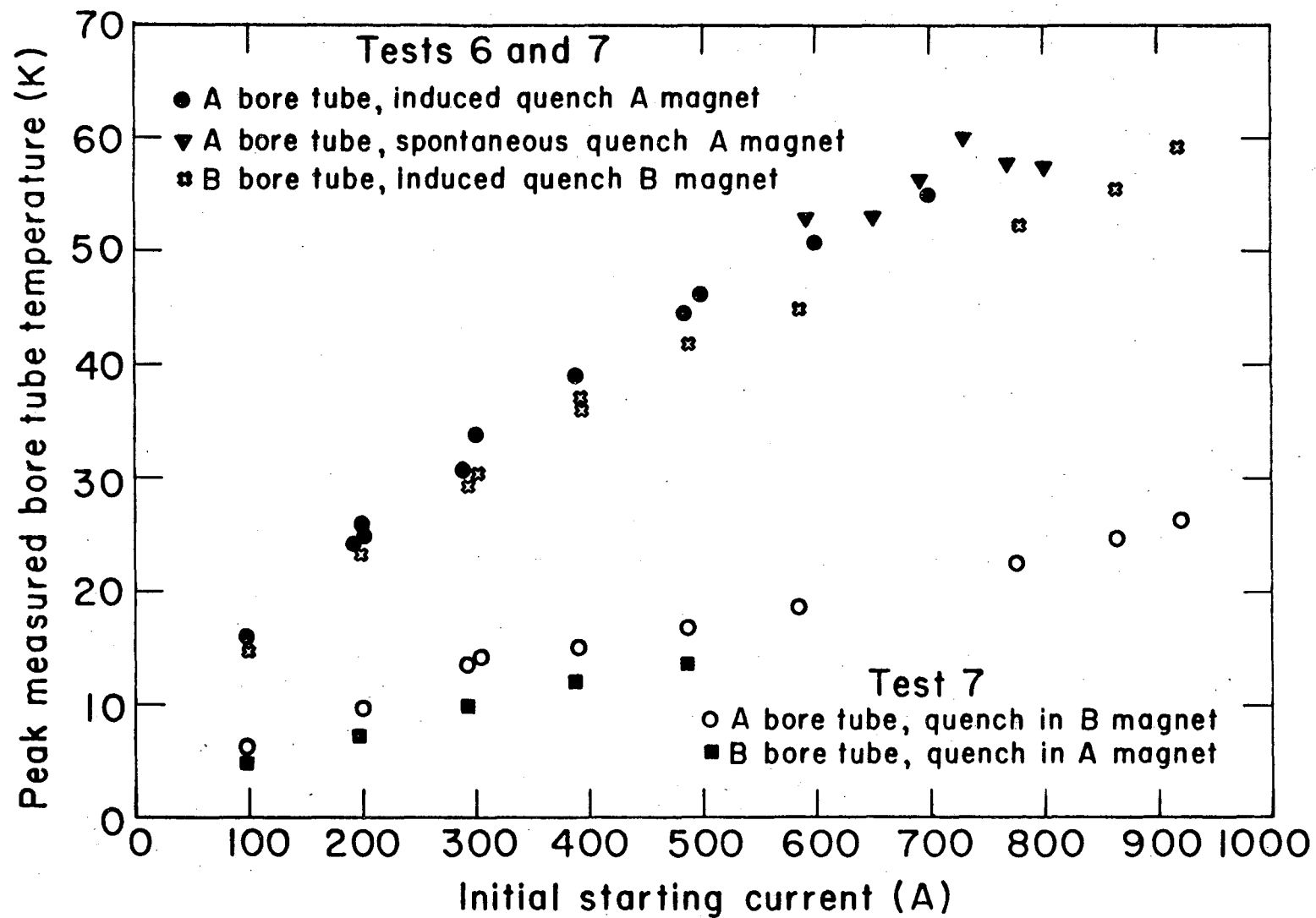sensor TD-5 than for the A magnet sensor TD-4.)

Fig. 65. The peak measured bore tube temperature after the magnet has quenched vs the starting current of the magnet.

XBL 772-295

(see Figure 63), and 3) the calculation of E_H and E_{HAL} with the computer from the scan of pictures from scope A. Figure 66 shows the fraction of the magnet energy which ends up in the bore tube of the A and B magnets as a function of the initial current in the magnet. In all cases the method used to calculate f was the first method described previously.

The three methods for estimating the fraction of the magnetic energy that ends up in the bore tube are compared in Table 19. The two electrical methods (measurement of the scope C picture and the direct calculation of E_{HAL} and E_H with the computer) compare reasonably well. The temperature method does not correlate well at all with the two electrical methods. There are two reasons for this: 1) the time lag in the thermometry is long so that the bore tube has cooled by the time the thermometer measures maximum temperature, 2) and other circuits, such as the helium cooling tube and other aluminum parts, absorb part of the energy. Of the two reasons, the dominant one causing disagreement appears to be the time lag in the thermometer which causes the temperature reading to be about 4 degrees low. The resulting error in the temperature measurement leads to large errors in the bore tube enthalpy change estimate. A correction of the final bore tube temperature was made in some of the runs in test 7. This was done by extrapolating the temperature decay slope back to a time of 1.5-2.5 seconds in a plot similar to Figure 64. This corrected temperature was used to calculate a corrected fraction of energy which ends up in the bore tube. The corrected value in Table 19 correlates much better with the electrical measurements.

Table 19 and Figure 66 show that most of the magnetic energy in a quench will end up in the bore tube. The highest current runs result in 70 percent or more of the energy being deposited in the bore tube. In most cases, and as shown in Figure 61, the magnet is entirely normal after less than ten percent of the magnetic energy has been converted to heat. Above 35 K the bore tube time constant τ_2 is a factor of 4 to 6 greater than the coil time constant τ_1. As a result of the longer time constant, the bore tube will absorb the bulk of the magnetic energy. Energy which it absorbs does not get absorbed by the coil, and as a result, the coil hot spot temperature is reduced.

The bore tube absorbs energy differently than does the coil. More energy becomes deposited in its cold parts than in its hot parts so that its temperature evens out. On the other hand, energy deposited in the superconducting coil tends to gravitate to the hot spot, making it worse.

f) The A and B Magnets Powered in Series

During test 7, the A and B magnets were tested together. These magnets were electrically hooked together in series. The hookup of the helium system between two coils was such that the superconductor connecting them could not transport a normal zone between the two coils. These magnets were run to a maximum current of 300 A. The current had to be restricted because the two magnets had been hooked together with their magnetic fields in opposition.

Runs 49 through 64 of test 7 experimented with the two magnets together. Quenches were initiated in each of the two coils and then

Table 19. A comparison of various methods for determining the fraction of magnetic energy which ends up in the bore tube as heat.

Run	Current (A)	Scope C Method	Computer Method	Temperature Method	
				Uncorrected	Corrected
Test 5, Magnet A					
17	100	---	0.40	---	---
20	200	---	0.53	---	---
22	300	---	0.56	---	---
23	400	---	0.65	---	---
24	500	---	0.68	---	---
Test 6, Magnet A					
36	200	0.44	0.48	0.25	---
33	300	0.54	0.53	---	---
39	300	0.56	0.59	0.40	---
41	500	0.64	0.68	0.47	---
42	500	0.62	0.68	---	---
43	600	0.62	0.70	0.53	---
44	600	0.64	0.70	---	---
47	700	0.66	0.70	0.54	---
Test 7, Magnet A					
77	195	0.48	---	0.23	0.42
78	200	0.48	---	0.23	---
79	292	0.52	---	0.26	0.48
80	389	0.60	---	0.45	0.56
81	486	0.62	---	0.46	0.57
82	804	0.68	---	0.46	---

Table 19. Continued.

Run	Current (A)	Scope C Method	Computer Method	Temperature Method	
				Uncorrected	Corrected
Test 7, Magnet B					
66	97	0.40	0.43	0.18	---
36	195	0.55	0.50	0.19	0.42
15	292	---	0.56	0.28	0.45
67	486	0.66	0.66	0.36	0.58
68	584	0.68	0.70	0.32	---
69	778	0.74	0.73	0.33	0.57
70	864	0.75	---	0.37	---
71	920	0.75	---	0.40	0.58
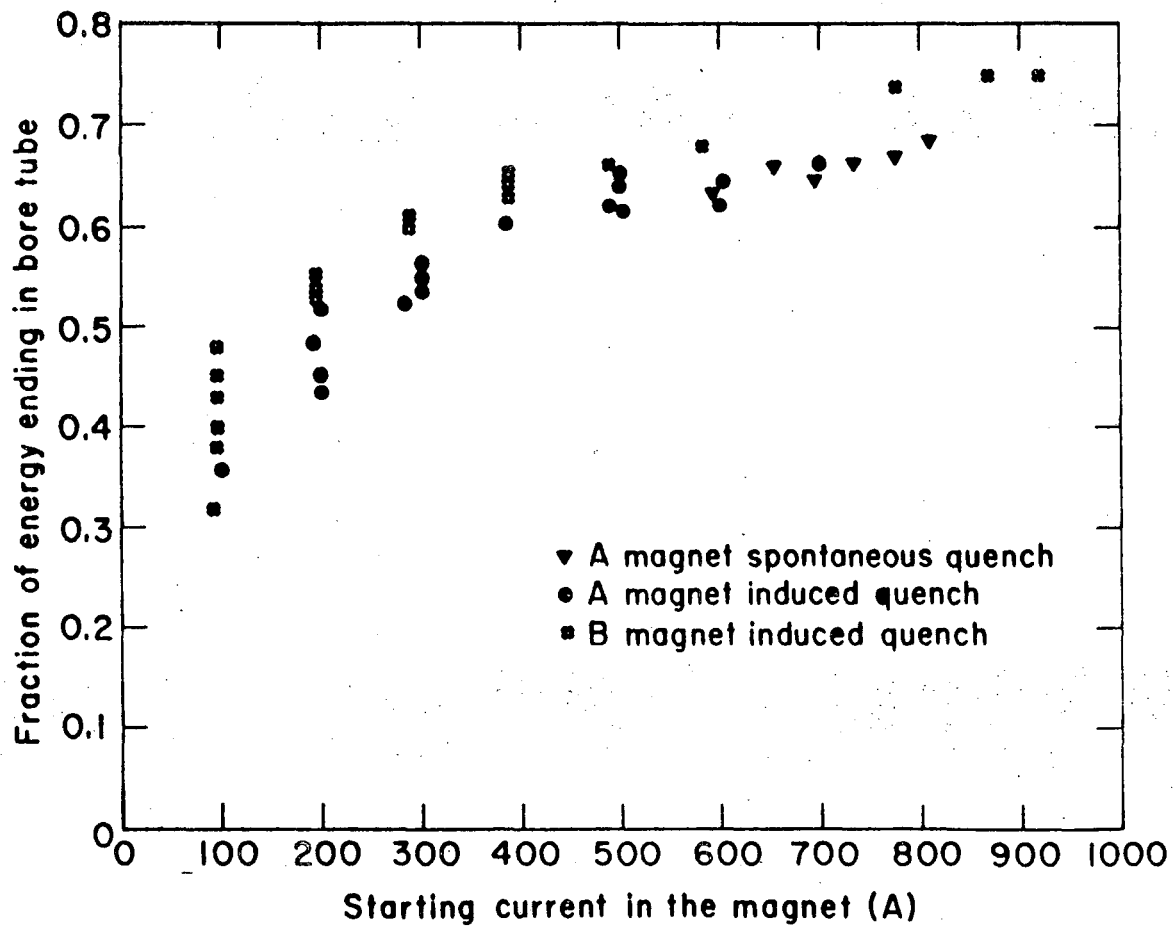
Fig. 66. The fraction of the total magnetic energy which becomes heat in the bore tube as a function of the starting current in the magnet. (Note the data was taken by analyzing the scope C pictures.)
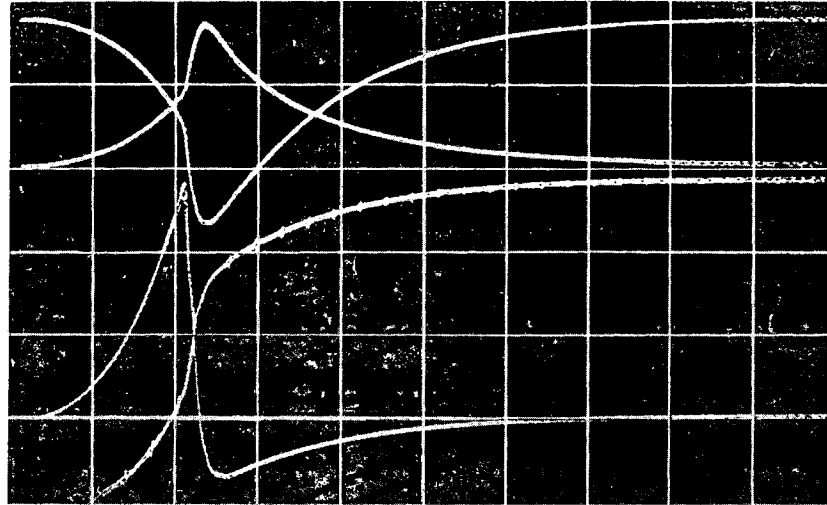
in the two coils together. At 97 A the coils did not quench easily. When one coil was quenched, the other coil never became normal. The coil in which the quench was induced experienced no quench back. At 195 A quench back occurred in both coils. This effect is dramatically seen in Figure 67. The value of V_{com}, the voltage to ground on the lead between the two coils (see Figure 46b), goes positive as the A coil becomes resistive. Suddenly V_{com} decreases and becomes negative. This sudden decrease in voltage is caused by the second coil going normal through quench back. The characteristic trace of P_A and P_B compares with the P trace in Figure 50. The current trace in Figure 67 compares with the current trace in Figure 50.

In general, the following can be said about the two coils in series: 1) The quench in the first coil will cause the second coil to go normal through quench back. 2) The quench back time for two coils in series is longer than the quench back time for either coil alone. 3) If the quench is induced in both coils simultaneously, the quench back time is shorter than inducing quench in one coil by itself. 4) The temperature of both bore tubes is nearly equal when quench back occurs. When no quench back occurs, the bore tube under the coil in which the quench was induced will be warmer than the coil bore tube which has not gone normal. 5) The coil hot spot temperature will be hotter when the two coils are series than when one coil is quenched alone.

5.4. Strain Measured on the Magnet Bore Tube and Its Correlation to Magnet Training

Strain gages were mounted on the aluminum bore tubes in order to measure the strain as the magnet was powered. The method of mounting

-184-

Test 7, Run 59
Q_1 in A coil
$I = 195\,A$

Quench back in B coil

$t \approx 0.5\,\mathrm{s\,cm^{-1}}$
$P_A \approx 2.0\,\mathrm{V\,cm^{-1}}$
$P_B \approx 2.0\,\mathrm{V\,cm^{-1}}$
$V_{com} \approx 20\,\mathrm{V\,cm^{-1}}$
$S \approx 50\,\mathrm{m\,V\,cm^{-1}}$
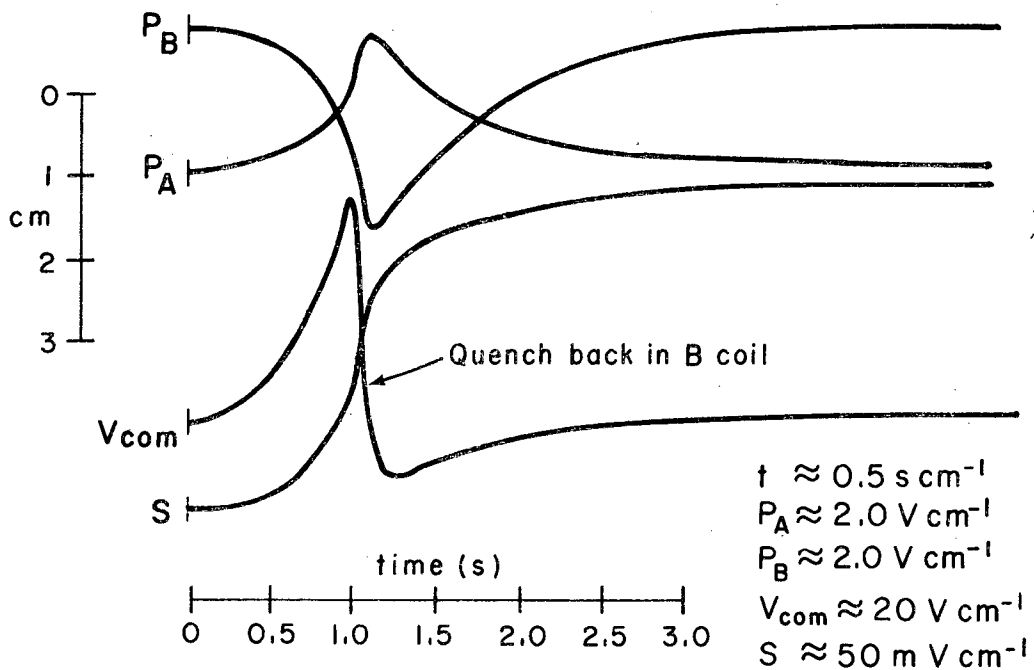
XBL 772-299

Fig. 67   An oscilloscope picture of quench when the
A and B magnets are hooked up in series.
(Note the V_{com} reverses in sign when quench
back occurs in coil B.)

the strain gages and the method of strain measurement is described

in Section 3.3. The A magnet has two strain gages mounted on it

(gages A and B); the B magnet has four strain gages mounted on it

(gages C, D, E and F). Figure 24 shows the location of the strain

gages on the two magnet bore tubes.

The magnetic force on an individual conductor is the cross product

of the current and induction vectors. Since the magnitude of the

magnetic induction at the wire is directly proportional to current,

the magnetic force on the wire is directly proportional to the magnet

current squared. Since stress is proportional to force, the stress

in the magnet wire is directly proportional to the magnet current

squared. Figure 68 shows the direction of the magnetic forces in

one of the magnet coils when it is being powered alone. The length

of the arrows in Figure 68 is proportional to the magnitude of the

force.

The magnetic force on the coil winding is transmitted to other

parts of the magnet system. The integrity of the epoxy determines

which parts see the magnetic force. Thus measurement of the bore

tube strain is useful for diagnosing the condition of the interface

between the coil and the bore tube. Training, which is defined as

premature spontaneous quenching due to coil motion or cracking (the

usual cause) can be correlated to the condition of the epoxy joint

between the bore tube and the current carrying coil. The strain gages

mounted on the A magnet show the effect of a broken interface between

the coil and the bore tube. Magnet B, which showed no sign of breakage,

shows an entirely different pattern of strain gage behavior.
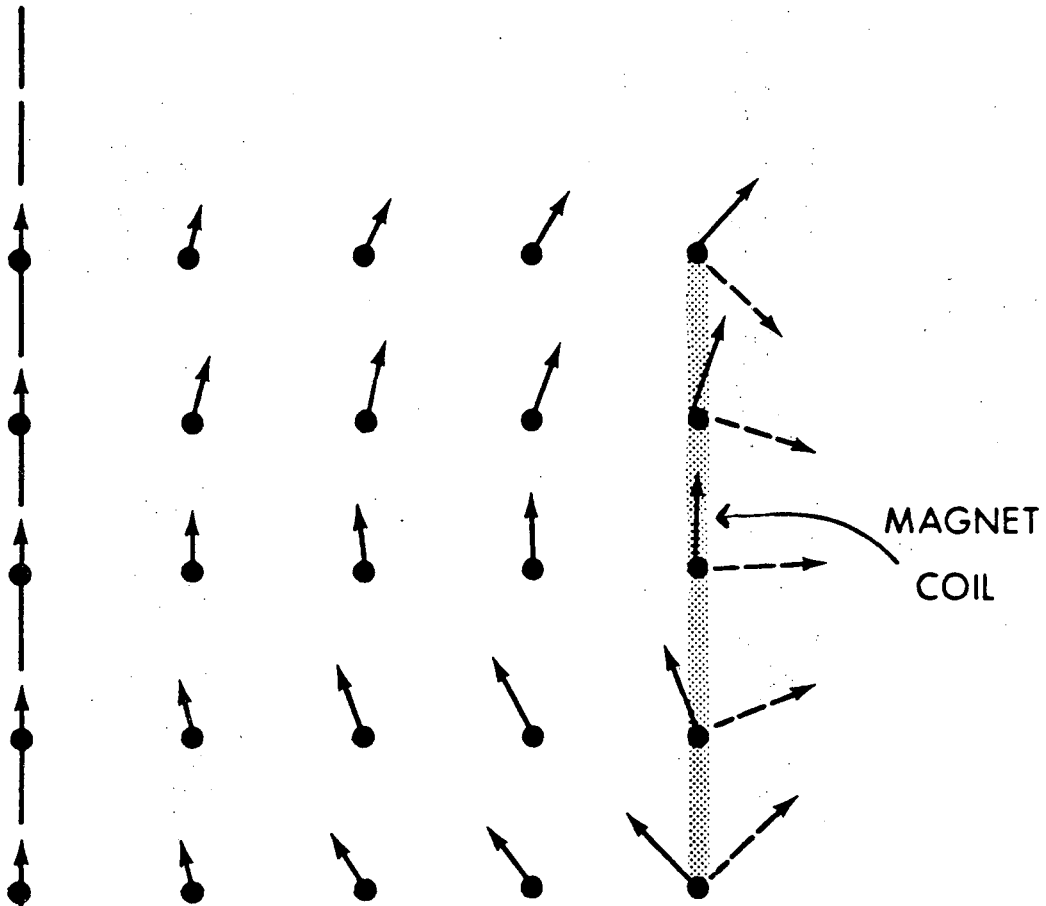
Fig. 68. The direction and magnitude of the field and
magnetic forces in the magnet when it has
current in its windings.

a)   Strain Gage Measurement on the A Magnet

The first test of the A magnet in November 1975 (test 5) showed

little or no evidence of coil separation from the bore tube. Figure

69 shows the stress versus strain curve for the bore tube during test

5 as measured by strain gage A. The B strain gage curves overlay the

A strain gage curves almost precisely. (The B strain gage measurements

are within 10μ strain of the A strain gage measurements. Note the

$10^4\mu$ strain is one percent strain.) The A magnet strain gage measurements

during test 5 showed a classic plastic-elastic behavior characteristic

of a well designed composite system. (See Reference 63).

Figure 69 shows that there is a plastic deformation line and

an elastic deformation line. The magnetic force which is proportional

to the current squared caused the bore tube to deform plastically

when the coil was charged the first time. When the coil current was

reduced, thus reducing the magnetic force, the strain in the bore tube

was reduced along an elastic deformation line. Subsequent charging

of the coil showed elastic deformation until the previous charging

current limit had been reached. Once beyond this previous current

limit, plastic deformation was resumed. The important factor in the

first A magnet test was the fact that both strain gages behaved in

an identical way.

The March 1976 and July 1976 tests showed different strain gage

behavior. The responses of the two presumably identical strain gages

were not the same. The A strain gage measurements shown in Figure

70 (taken during the March 1976 test) shows behavior which is similar

to the elastic behavior found in the November 1975 test. This indicates
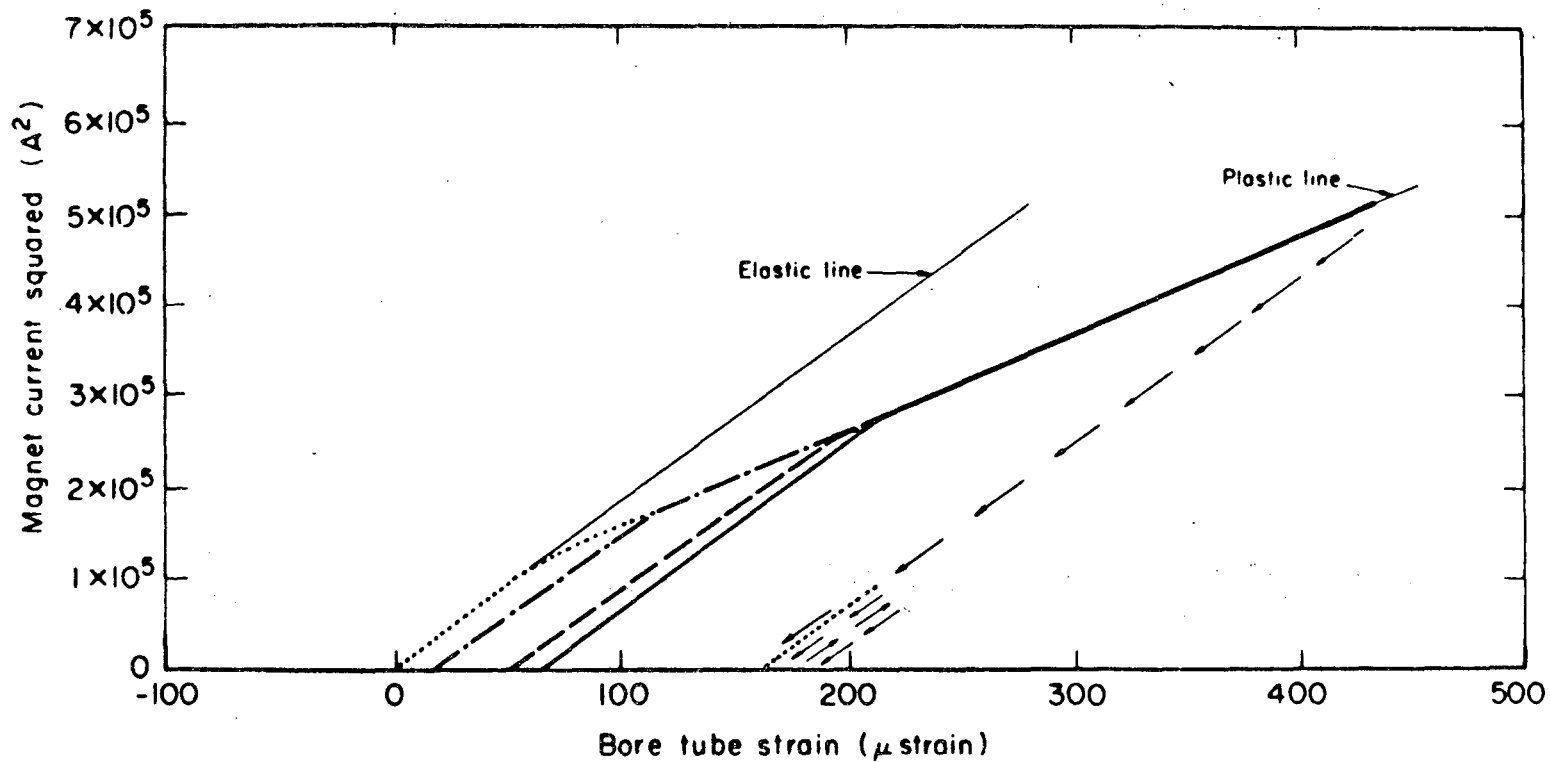
XBL 764-5489A

Fig. 69. Measured bore tube strain vs current squared as measured by the A and
B strain gages on magnet A during test 5 (November 1975) before the
epoxy bond between the coil and bore tube broke.
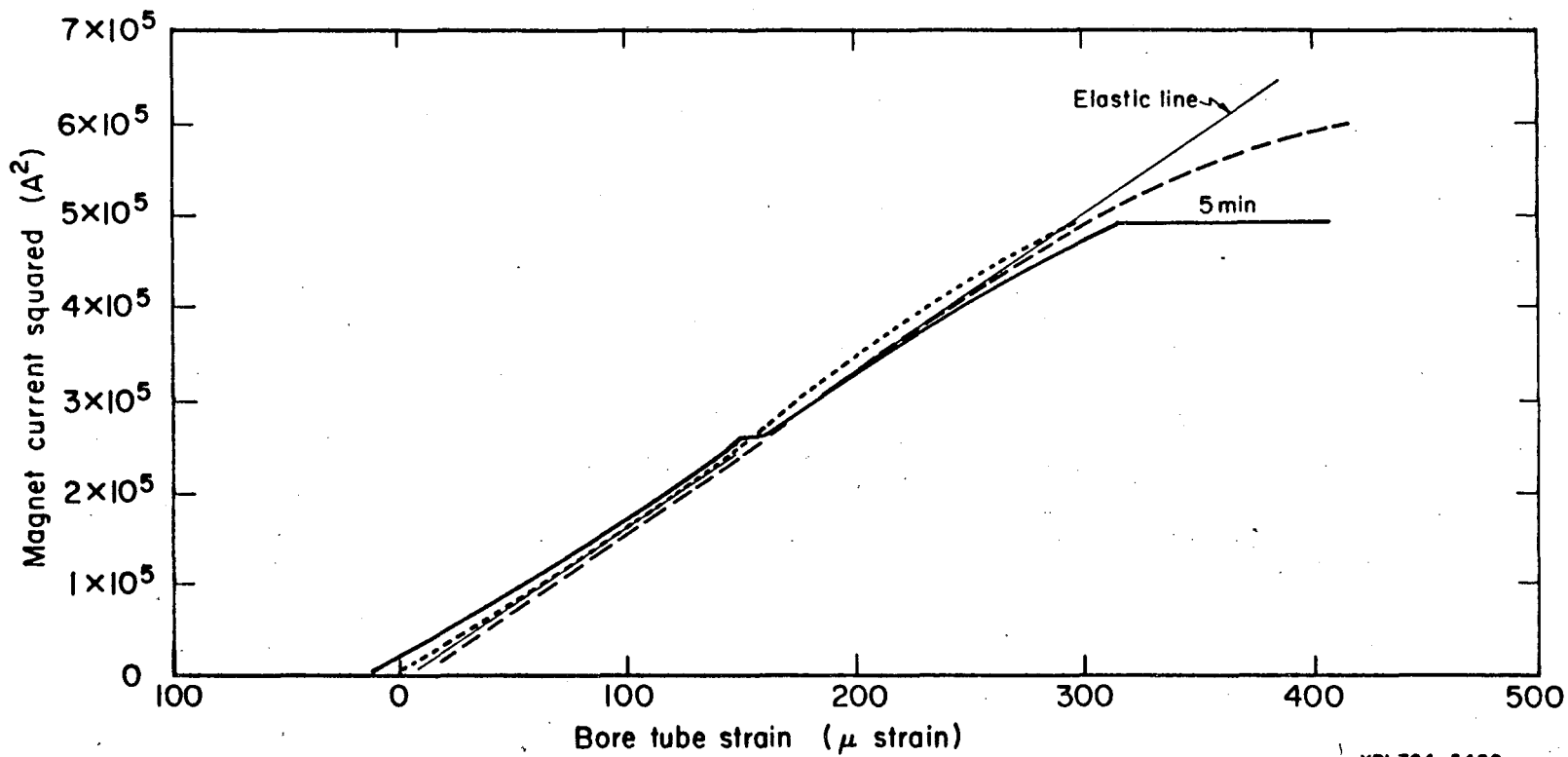
Fig. 70. Measured bore tube strain, as measured by the A strain gage on magnet
A during test 6 vs the magnetic current squared. (There is evidence
of epoxy breakage. Compare this figure with Figs. 69 and 71.)

XBL764-5488

the bore tube and coil are straining together. The B strain gage measurements taken during the March 1976 tests (see Figure 71) show marked differences from th A strain gage measurements. The gage would show elastic strain up to a certain magnetic force level. Above this level the rate of strain versus magnetic stress would be reduced (like a sudden increase in modulus). In some cases the bore tube strain would be reduced as stress was applied. This behavior was indicative of the coil lifting away from the bore tube above a certain level of magnetic stress. The July 1976 test showed further deterioration of the coil bore tube interface in the region of the B strain gage (see Figure 72).

b) Spontaneous Quenching and Training

Spontaneous quenching was observed in all three tests of the A magnet. It is believed that spontaneous quenches during test 5 (November 1975) were due to poor cooling. Pressure drop measurements across the magnet cooling tube indicate that the magnet probably was never cooled below 6 K, and thus the A magnet probably operated near its critical current (which is a function of the local magnetic field and temperature). During test 6, the magnet was well cooled. Its operating temperature was always below 5 K. There was immediate evidence that something was wrong with the coil bore tube interface at or near the B strain gage.

Cracking apparently occurred between the bore tube and coil, caused in part by thermal stresses during the second cool down of the magnet. The coil started to peel away from the bore tube, forming shear points at the boundaries of each region, which further continued
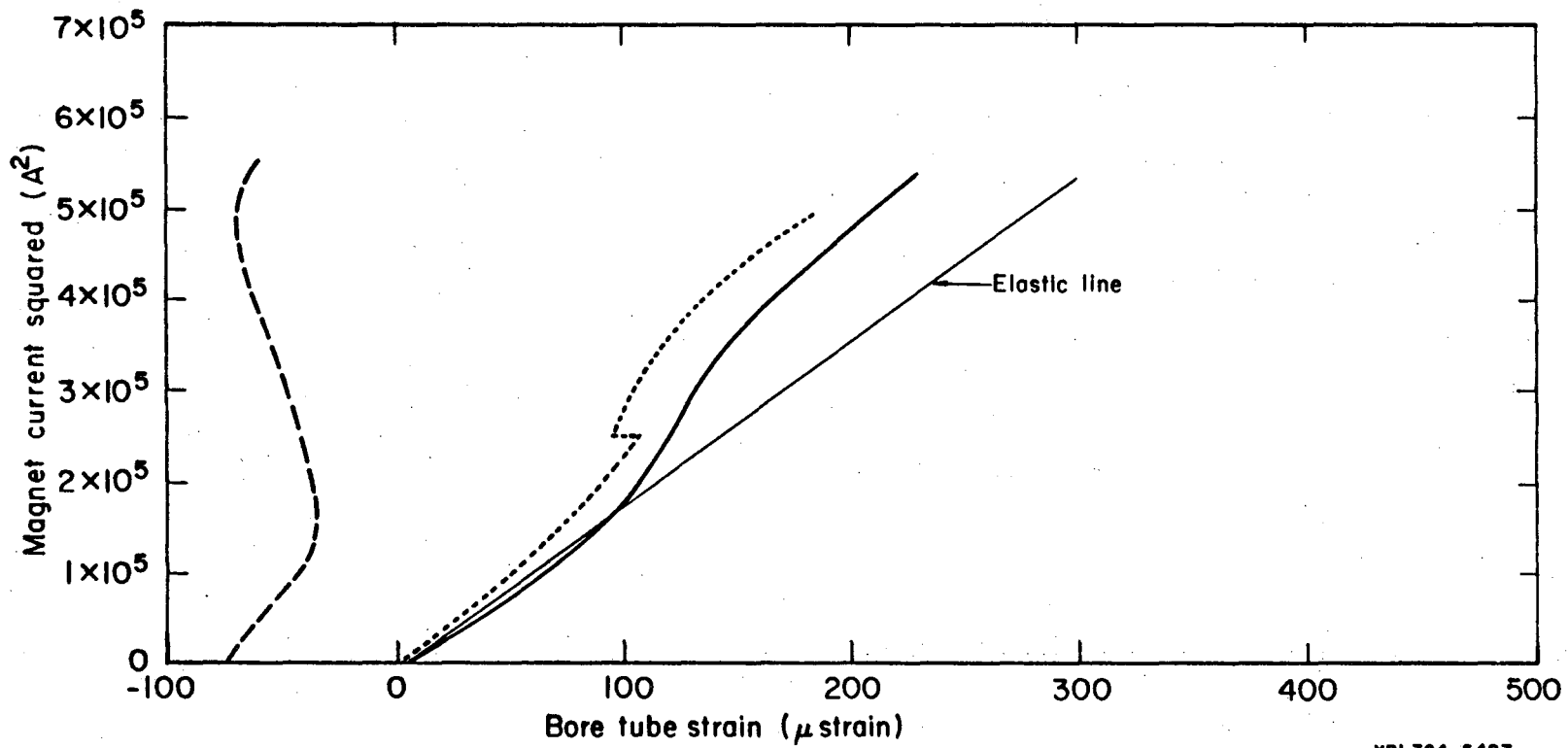
Fig. 71. Measured bore tube strain vs magnet current squared as measured by the B strain gage on magnet A during test 6. (The epoxy bond between the coil and the bore tube was broken.)
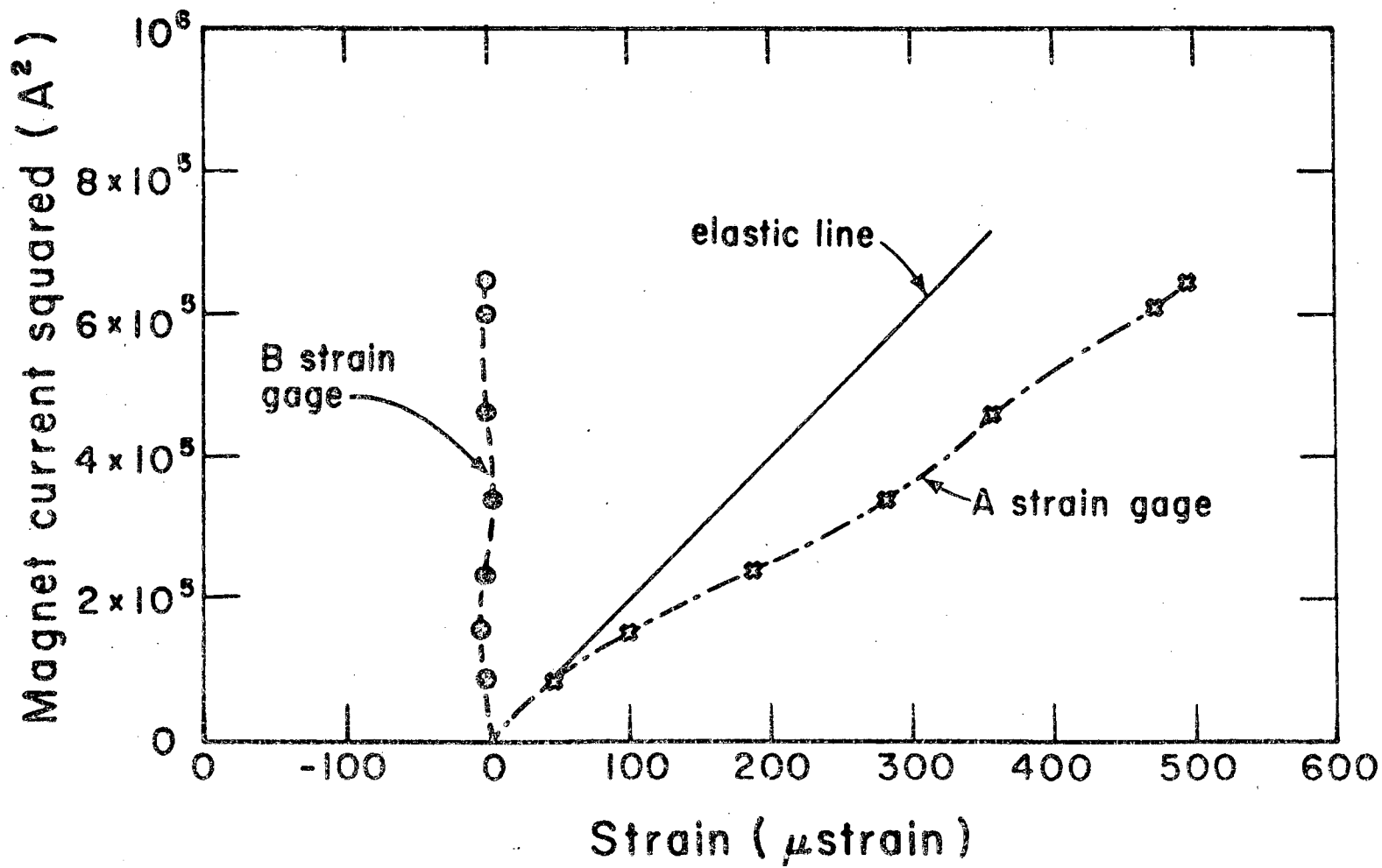
XBL 772-293

Fig. 72. Measured bore tube strain vs current squared as measured by the A and
B strain gages in magnet A during test 7. (The curves are
characteristic of epoxy breakage between the coil and the bore tube.)

the separation process. (Epoxy is quite strong in tension but weak in shear, so it was effective in preventing separation.) The coil separation from the bore tube did not occur smoothly but rather, in a series of jerks. The radial motion of the coil was less than 50 μm or so, but this motion occurred suddenly. The superconductor saw a high rate of magnetic flux change, causing ac loss and heating the wire which then drove the superconductor normal. Once a normal region is established in the superconductor, it will propagate quenching in the entire magnet. The sudden movement of a small portion of the coil as it broke away from the bore tube is believed to be the cause of training observed during tests 6 and 7.

Spontaneous quenches in magnet A during tests 6 and 7 show what appears to be progressive training. Figure 73 shows the spontaneous quench history of the A magnet. The current at which spontaneous quenches occurred during test 5 was quite erratic. A reasonable explanation for this is temperature variation, since there was no evidence of coil break away from the bore tube. The progressive increase of the spontaneous quench current during tests 6 and 7 is typical of training. Dipole magnets built by Karlsruhe in Germany,[87] the Rutherord Laboratory in England,[88] Brookhaven National Laboratory in the USA,[89] Fermi Laboratory in the USA[90] and the Lawrence Berkeley Laboratory[91] all show similar behavior. The causes of training in the magnets are believed to be due to wire motion and epoxy breakage. When the coil was well supported, less training was observed.

Training quenches at 597, 654, 696, 733, 773, and 804 A have been observed. The A magnet is expected to train further in future
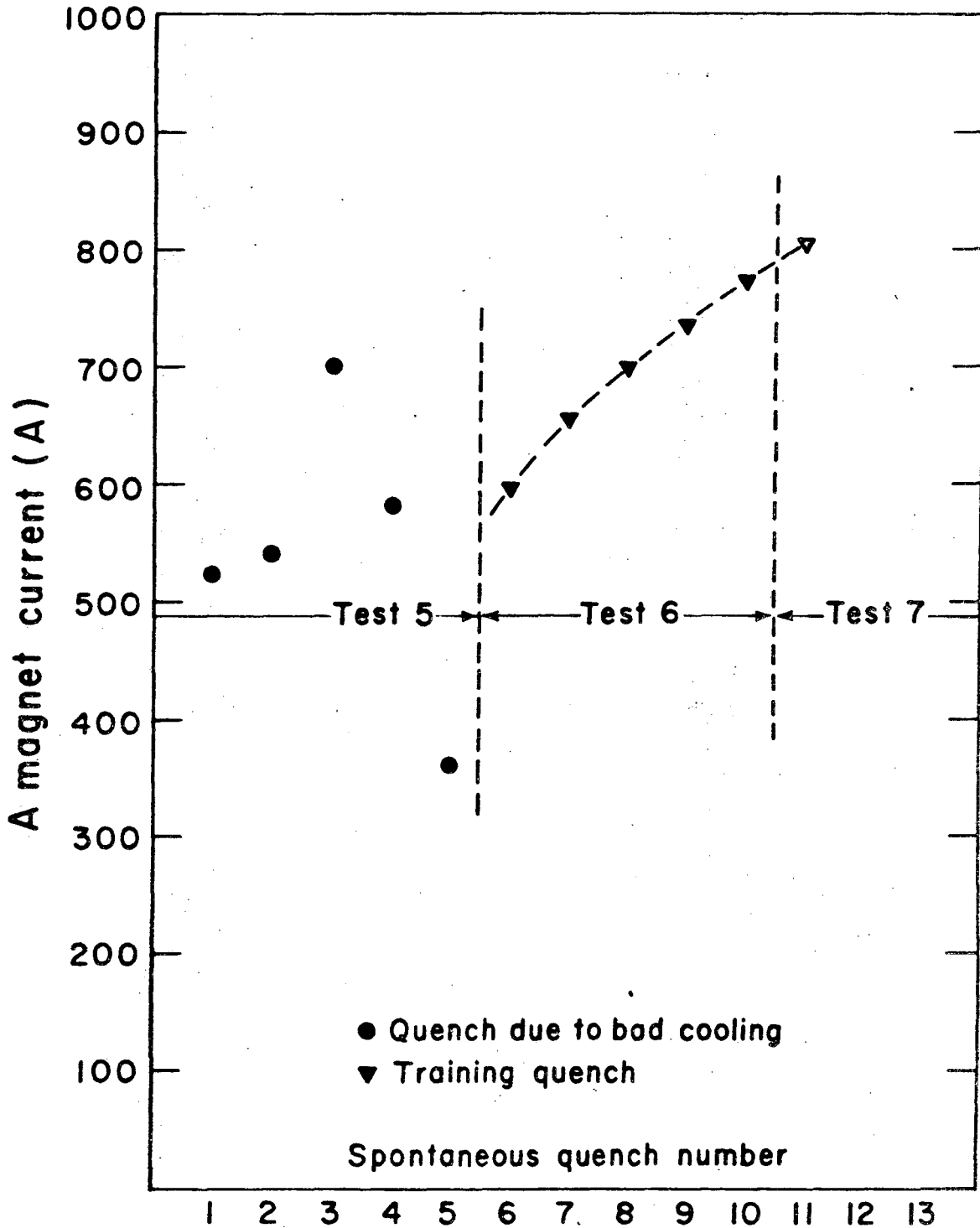
Fig. 73. The spontaneous quench history of the A magnet. (Test 5 had inadequate cooling; tests 6 and 7 showed training.)

XBL 772-294

tests. The cool down of the magnet is believed to be contributory
to the breaking of the epoxy bond between the cool coil and the bore
tube. However, the warm-up and subsequent cool down of the magnet
appears to have no effect on the progressive nature of training in
that magnet. No training has been observed in the B magnet, which
has only been cooled down once. A second cool down of the B magnet
may find that cool movement and training will become a problem in
the future. However, since the B magnet epoxy impregnation was better
than the A magnet, there may be no training. Further testing of
the B magnet is needed in order to resolve this point.

c) Strain Gage Measurements in the B Magnet

The B magnet was tested for the first time during test 7. There
was no evidence of coil separation from the bore tube. Figure 74,
which is a plot of bore tube strain at gage C versus the current squared
in the B magnet, resembles Figure 69 very closely. The strain measurement
at strain gage D very closely resembled Figure 74 and 69. Thus the
B magnet strain gage measurements showed the plastic-elastic behavior
of composite structures where one component is plastically deformed
and the other components are elastically deformed. The elastic
strain of the magnet without the bore tube closely resembles the plastic
deformation slope shown in Figure 74.[63] Figure 74 shows only the
results of three higher current runs (runs 68, 69 and 70). The break
from elastic to plastic behavior occurred in run 68 at a current of
486 A, to which the magnet had been previously charged (run 67).

The strain in the E and F strain gages during runs 68, 69, and
70 is shown in Figure 75. The E gage which measures longitudinal
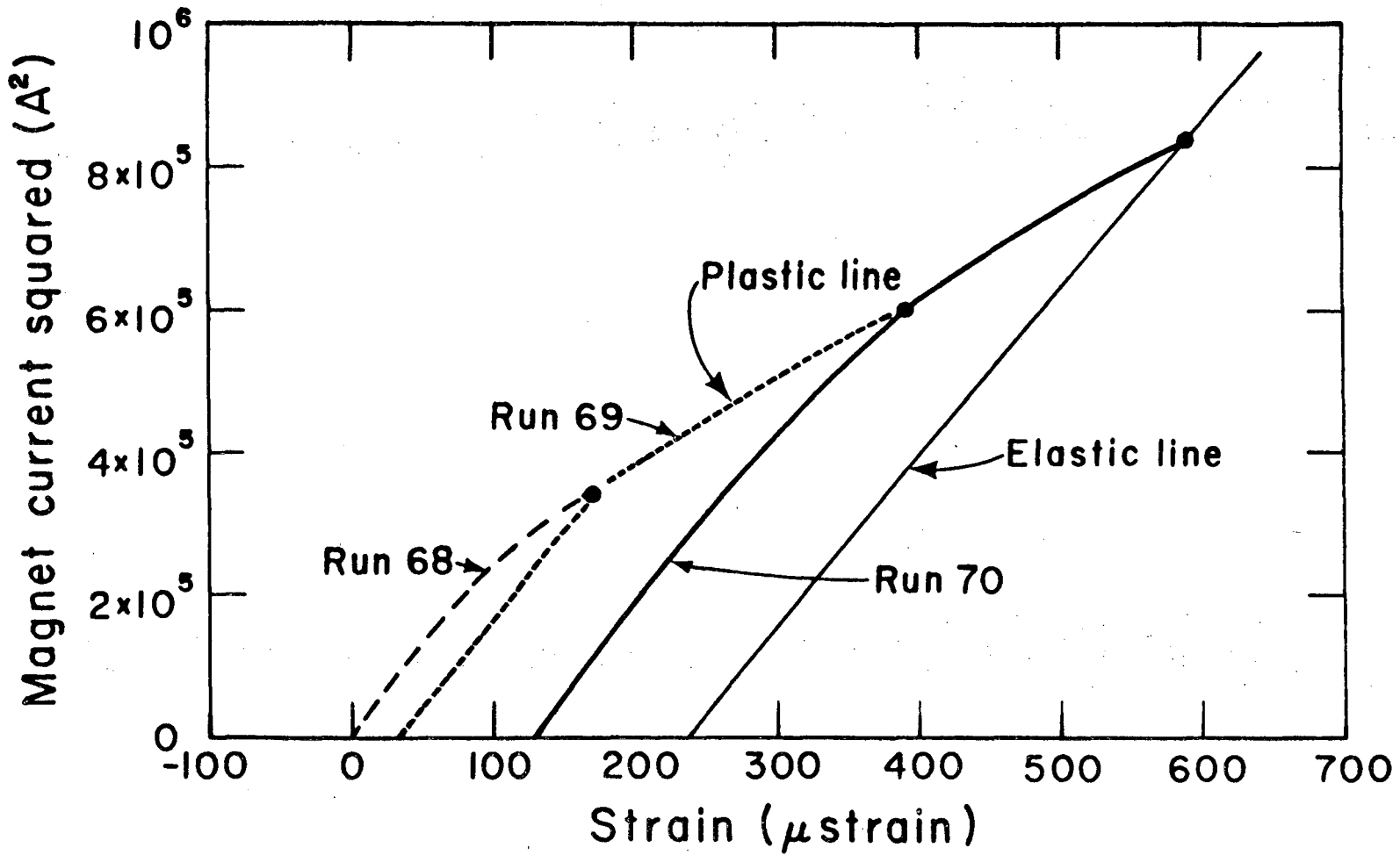
Fig. 74. Measured bore tube strain vs magnet current squared as measured by strain gages C and D on the B magnet during test 7 (there is no evidence of epoxy breakage between the coil and the bore tube).
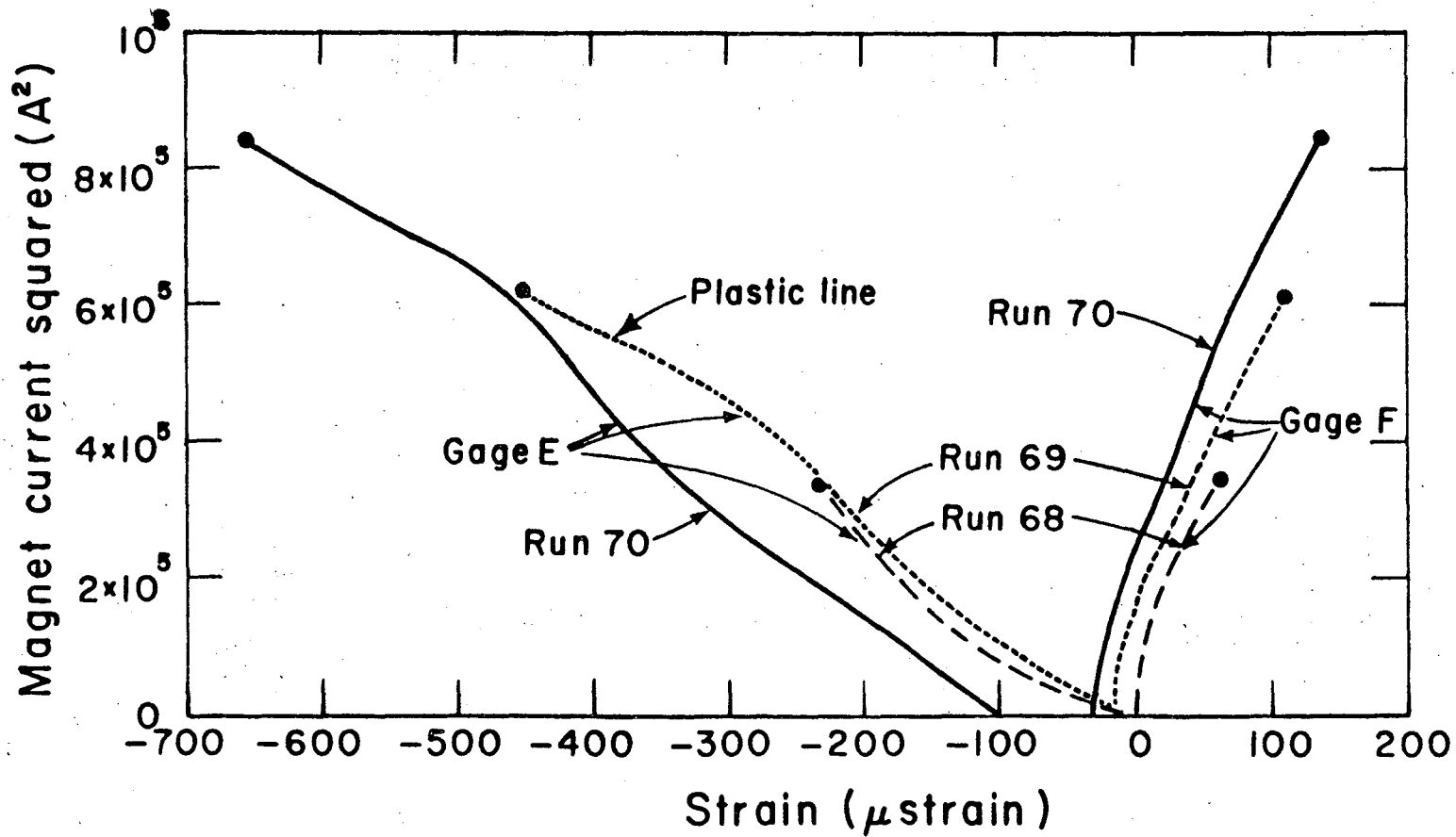
XBL 772-302

Fig. 75. Measured strain vs the magnet current squared as measured by gages E and F on magnet B during test 7 (negative strains are compressive, positive strains are tensile).

strain in the bore tube, shows that the bore tube is put into compression by the magnetic forces. There are two factors which come into play: 1) There is a direct magnetic force carried for the most part by the bore tube alone, that puts it in compression. 2) There is a Poisson ratio effect due to the hoop strain of the bore tube in the transverse direction. The combined effect of the two factors is a large compressive strain. The F gage, which measures hoop strain at the edge of the bore tube, shows that the bore tube is strained in tension. The tensile strain at the edge of the bore tube is much smaller than the tensile strain at its center. The plastic deformation measured by gages E and F is compressive, but only slightly so.

As magnet B is charged with current the bore tube becomes barrel-shaped. An exaggerated view of this change is shown in Figure 76. Due to plastic deformation of the bore tube, the magnet assumes a permanent barrel shape. A charge from 0-920-0 A will permanently deform the magnet so that the diameter of the magnet at the center is about 0.3 mm larger than the diameter at the ends of the magnet. When the magnet is at a current of 920 A, the diameter at the magnet center grows almost 0.65 mm. (This includes the plastic and elastic deformation.) The edge diameter grows only about 0.15 mm (this also includes the plastic and elastic deformation. In most cases, the change of solenoid shape is of no consequence.

5.5. A Summary of the A and B Magnet Test Results

The three tests of the two one-meter diameter solenoid magnets achieved all of their objectives. The following were the primary results:
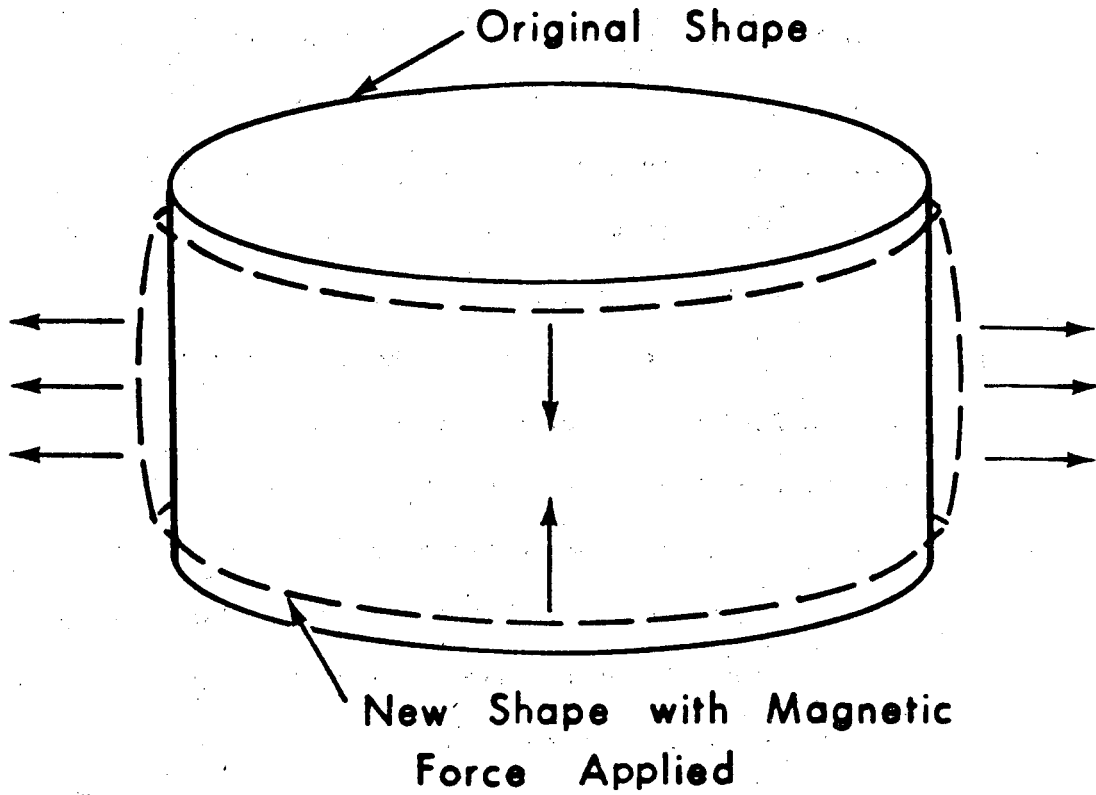
Fig. 76. The change of bore tube shape as magnetic
forces are applied. (Note the shape change
is greatly exaggerated.)

1. Both magnets operated above their design current. Both magnets operated at superconductor matrix current densities in excess of 10^9 Am^{-2}.

2. The magnets operated at full design current while being cooled with two-phase helium which flows through a tubular cooling system. The helium was supplied to the tubular cooling system by a closed helium refrigerator.

3. Quench velocities were measured. The measured values agree with the theory within a factor of two.

4. As the magnet resistance grew, the current flowing in the coil shifted to the low resistance bore tube.

5. The shift of the current from the coil to the bore tube caused superconducting portions of the magnet coil to go normal through the "quench back" process. The increased resistance of the coil caused less current to flow in it, thus reducing the hot spot temperature.

6. The bore tube absorbed up to 75 percent of the magnetic energy in the form of heat. This energy did not end up in the superconductor.

7. When both magnets were powered in series, a quench in one magnet caused the other magnet to go normal through quench back.

While the primary objectives of the magnet tests were met, the magnet tests results cannot be called 100 percent positive. The following information will be useful for the construction of the next generation of superconducting magnets:

1.   The epoxy joint between the superconductor and the bore

     tube broke, causing training in the A magnet.

2.   The normal region did not grow fast enough to cause quench

     back soon enough to insure that the coil hot spot in the

     magnet was completely safe.

3.   Additional dynamic quench protection would be useful to

     speed up the quenching process.

Table 20 shows the peak operating parameters for the A and B

solenoid magnets. Neither magnet has reached its critical current.

The 804 current reached in the A magnet was reached in its last training

quench. The A magnet should train to a higher current than 804 A.

The B magnet peak current of 920 A was the limit of the power supply

on which the magnet was tested. Future tests of the B magnet should

reach currents above 920 A.

Table 20. The peak operating parameters for the A and B solenoid magnets.

	A Magnet	B Magnet
Design current (A)	700	880
Design matrix current density (Am^{-2})	0.909×10^9	1.120×10^9
Design magnet stored energy (J)	1.931×10^5	3.028×10^3
Estimated critical current at 4.8 K	905	1100
Peak current tested (A)	804	920
Peak matrix current density (Am^{-2})	1.044×10^9	1.171×10^9
Peak magnet stored energy (J)	2.547×10^5	3.347×10^5

VI. SAFETY, ENVIRONMENTAL IMPACT, AND COST

This section discusses the safety, environmental, and cost aspects
of the LBL thin solenoid program. LBL has had a great deal of experience
handling cryogenic fluids such as hydrogen and helium and the procedures
for handling these fluids have long been established. The LBL experiment
itself has little impact on the environment, but the success of the
LBL approach for building superconducting magnets will have substantial
positive impact on the construction and operation of the PEP storage
rings.

The construction of the one-meter diameter prototype magnets
occurred in the main LBL shop. This is an important step toward getting
the construction of superconducting magnets out of the laboratory
and into industry. The one-meter diameter prototypes are large enough
to derive reasonable cost data on the construction of thin superconducting
solenoids which can be scaled to a full-sized experimental magnet.

6.1 Safety Aspects of Thin Solenoids

The safety rules governing the one-meter diameter solenoid experiment
are set by the Lawrence Berkeley Laboratory Safety Committee.[92] Safety
hazards of the experiment take four primary forms: (1) the hazards
associated with the handling of cryogenic fluids; (2) the pressure
hazards due to the sudden boiling of helium in the magnet and liquid
nitrogen in the 80 K shield; (3) pressure hazards due to the evaporation
of air which has accumulated in the vacuum space around the magnet coils;
and (4) hazards due to the stray field around the magnet.

The handling of cryogenic fluids is almost eliminated in the one-meter diameter solenoid experiments. The refrigerator provides the magnet with cold helium. Liquid helium was transferred to the control dewar on some occasions. The cold gas which flashed off during the transfer passed through the refrigerator heat exchanger where most of the sensible refrigeration was recovered, and the helium gas which passed through the refrigerator was vented to either the gas recovery system or the atmosphere. Warm helium, which is nonflammable and non-poisonous, can be vented to the atmosphere in complete safety. This procedure minimizes the hazard of handling liquid helium. The liquid nitrogen fed to the cryostat was controlled by an automatic controller which metered the liquid to the experiment. Failure of this control system would result in spillage of liquid nitrogen onto the ground outside Building 58 or Building 64. The full-scale experiment at Stanford is expected to present less hazard than the one-meter test apparatus.

From an internal pressure standpoint, the LBL thin solenoid is one of the safest cryogenic systems ever built at LBL. The tube around the magnet has a burst pressure in excess of 150 bar (2180 psia). The magnet cooling tube would be entirely safe during a magnet quench even if both ends of the tube were plugged tight. The weakest link in the magnet transfer line piping is a couple of bellows which are rated at 30 bar (450 psi). The control dewar cryostat which is at the return end of the transfer line is rated at nearly 10 bar. There are two relief valves in the magnet cryogenic system: the relief valve located at the top of the magnet was set to a pressure of 1 atu (1 atmosphere differential

pressure), and the relief valve at the control dewar was set at about 0.68 atu (about 10 psig). Another safe feature of the tubular cooling system is the small volume of liquid helium contained therein. It is expected that the inherent safety of the tubular cooling system will be extended to the full-scale PEP detector magnet.

One of the primary safety hazards of the LBL experiment is the vacuum system. The one-meter magnet experiment vacuum can meet the LBL safety specification that requires the vacuum vessel of a cryostat containing nonflammable cryogen to be a 5 atmosphere pressure vessel, which meets the standards for an unfired pressure vessel stated in section 8 of the boiler code.[93] The cryostat has a large relief valve on it. In addition, the normal operating procedure at LBL is to keep the cryostat vacuum vessel on the roughing pump while the magnet is being warmed up. We found that there was considerable frozen air gas buildup inside the vacuum space during the two-week run of the test 7 experiment (July 1976). The buildup of air gases in the vacuum space of the cryostat will be the major safety hazard associated with the full-scale detector magnet.

Stray magnetic field was a major problem during the one-meter thin solenoid tests. The magnets were run as air core solenoids with no iron return paths. Measured stray inductions as high as 100 gauss (0.01 tesla) were measured 1.5 m from the cryostat outer surfaces. The stray induction at the outer surface of the cryostat would have approached 0.1 tesla. Low level magnetic fields at 0.1 tesla and below has no apparent effect on human health, but will damage even a magnetically shielded watch and it will erase the magnetic coating on a BART ticket.

The primary hazard of the stray field around the one-meter magnet experiment is its ability to attract ferromagnetic materials such as screws, bolts, wrenches, screwdrivers, and even larger, more massive objects. Stray fields of magnets at the LBL Bevatron have been responsible for at least two injuries due to the presence of ferromagnetic materials. During the July 1976 test, the power of stray magnetic fields was well demonstrated. An empty gas cylinder, which had a mass of around 70 kg including the dolly it was mounted on, was pulled into the magnet from a distance of about 2 meters. This accident could have caused injury, but fortunately did not. This incident points out the importance of maintaining an iron-free zone around the tests. Stray field will not be a hazard at the PEP detector because there is an iron return path for the magnetic field.

6.2 Environmental Impact of the Experiment and the Full-Scale PEP Detector Magnet

The environmental impact of the one-meter test coil is negligible. The experiment used existing LBL space and facilties. The emissions from the magnet (helium gas) are non-polluting, unless there is a rare endangered species of flea which dies at the slightest trace of helium. (If such a creature exists, there will be environmentalists to find it.) The environmental impact of the full-scale PEP detector magnet should be positive compared to an alternative conventional magnet.

The primary reasons for using superconducting magnets in high energy physics are improved physics and a considerable energy saving. The PEP detector superconducting solenoid will save energy and perform more physics experiments than a conventional magnet occupying

the same space. The electrical energy saved justifies the project

economically. At current electrical energy prices, the energy cost

saved in two years would pay for the superconducting magnet. As a

bonus, the superconducting magnet improves momentum resolution.

The environmental impact of an electrical energy usage reduction

from 3 MW to 0.2 MW is considerable. Less electrical energy needs to

be delivered to the experimental area and conversely, less cooling

is required because all of the energy delivered to a magnet ends up

in the cooling tower. The direct energy delivered to the superconducting

magnet power supply is only about 20 kW (0.02 MW). The remaining energy

consumed by the superconducting magnet goes to the helium refrigerator

compressors. The full-scale detector magnet is expected to be free

of a large stray field or any chemicals which might pollute the atmosphere

or waste water. (The hypothetical flea, of course, is an exception.)

6.3 Economics

The LBL thin superconducting solenoid program is a continuing

research and development program. The construction and testing of

the one-meter diameter solenoids are equivalent to the construction

and testing of a pilot plant. A great deal of the cost associated

with such a project pays the salaries of the permanent support staff

of the research program. Since the one-meter diameter

test solenoids were the first superconducting magnets built by the

LBL main shops, an effort was made to separate the cost of constructing

the magnet from the rest of the experimental program.

Table 21 shows an approximate cost breakdown of the A and B solenoid

magnets. The purchases of materials are the prices paid by LBL, including

Table 21.   A breakdown of the cost of materials and fabrication of the A and B magnets.*

Cost Category	Costs ($)		
	A Magnet	B Magnet	Third Bore Tube
Materials			
Bore Tube	150	150	150
Superconductor	2,970	7,910	--
Cooling tube	60	60	60
Epoxy	110	110	--
Glass-dacron	30	30	--
Copper, copper tube fittings, insulators	320	290	--
Strain gages, quench coils, and thermometry	350	310	50
TOTAL MATERIAL COST	3,990	8,860	260
Labor			
Labor outside LBL	400	430	430
Bore tube fabrication	460	460	460
Parts fabrication	290	390	--
Winding	1,700	1,680	--
Potting	1,350	1,200	--
Assembly and test	2,190	1,570	--
TOTAL LABOR COST	6,390	5,730	890
TOTAL FABRICATION COST	10,380	14,590	1,150
Cost per kilogram	128	185	

* Costs do not include Laboratory overhead or support burden

shipping. The labor costs were calculated in terms of the man-hours worked at a labor charge of $13.91 per hour which includes fringe benefits. Tables 22 and 23 show an approximate cost breakdown of the Laboratory research and development program and which portions of that cost can be more or less directly connected with the engineering, construction, and testing of the A and B solenoid magnets. As one can see from Table 22, a great deal of the program cost is not directly related to the A and B solenoids, but to peripheral functions. For example, considerable effort was expended in testing the performance of the Cti Model 1400 and Model 1200 refrigerators. In addition we built a co-axial transfer line and did experimental and theoretical studies of the quench process.

Furthermore, a Laboratory overhead of 36.5 percent was added to all labor and material costs. The services in the overhead category include the Laboratory director's office and staff, accounting, purchasing, Laboratory administration, and technical information (the division which publishes Laboratory papers).

It is hoped that the information given in Table 21 can be used to help determine the cost of a larger magnet system. So far, our latest solenoid, which is described in the next section, costs less per unit mass than would be predicted by the cost figures given in Table 21. We expect that the figure given in Table 21 will yield a conservative estimate of cost in larger magnets.

Table 23 is a condensed version of the Lawrence Berkeley Laboratory Expense Statement. Shown is a breakdown of materials and labor costs

Table 22. Approximate cost breakdown of the thin coil experimental
magnet program for 16 months (May 1975 through August 1976).

	Cost (k$)
A and B magnet construction (Table 21)	26.2
Cryogenic system*	10.9
Testing**	
November 1976 Test	11.9
March 1976 Test	11.8
July 1976 Test	15.4
Test data reduction[†]	28.8
Direct engineering	13.0
Physics (theory)[††]	14.5
Physics (equipment development)[§]	17.5
Superconductor for two-meter magnet	11.6
Subtotal	161.6
Burden	6.2
Overhead	61.3
TOTAL EXPENSE	229.1

* Cryostat vacuum vessel was acquired from the LBL warehouse.

** Testing includes some of the test preparation.

[†] Includes scanning of the photos as well as hand reduction of the
experimental data.

[††] Quench theory development and theory of the magnetic coupling to
the bore tube.

[§] Includes small coil tests and refrigerator tests.

Table 23. The expenses of the LBL thin superconducting program from May 1975 through August 1976 (source: the LBL accounting office).

Fiscal Year Time Period Account Number	FY75 May,June 1975 4250-04	FY76 July 1975 through June 1976 4100-45	 4202-01	FY76A July, August 1976 4202-01	 16-Month Total
COST CATEGORY					
Supplies					
Stores issues	374	1,438	1,003	3,864	6,679
Blanket order	---	6,695	2,570	3,512	12,777
Purchases	11,188	1,272	11,575	---	24,035
Other	---	140	161	---	301
SUBTOTAL	11,562	9,545	15,309	7,376	43,792
Payroll Expense					
Scientific	---	55,881	604	9,639	66,124
Administrative	---	---	---	---	---
Technical Service	---	---	---	---	---
Construction	---	20	18	---	38
Mechanical Shops	1,376	7,030	5,588	---	13,994
Electrical Engineering	---	1,445	229	---	1,674
Electrical Shops	---	4,475	252	1,195	5,922
Mechanical Engineering	4,051	10,224	2,909	5,382	22,566
Mechanical Technology	183	1,229	4,268	1,761	7,441
SUBTOTAL	5,610	80,304	13,868	17,977	117,759
Support Burden*	673	2,930	1,592	1,053	6,248
Laboratory Overhead**	6,676	33,920	11,249	9,491	61,336
TOTAL EXPENSE	24,521	126,699	42,018	35,897	229,135

*
 Support burden covers the cost of secretarial personnel and the printroom of the Mechanical Department.
**
 The Lawrence Berkeley Laboratory overhead factor was 0.3656.

-211-

by classification. Three different account numbers were used during
the 16-month period. It is important to note that material cost
was almost $44,000. Labor charges were almost $118,000. The cost
of Laboratory overhead and support was around $67,000. The breakdown
is typical of research programs at LBL (particularly programs which
must support a number of permanent laboratory employees).

VII. THE FUTURE COURSE OF THE LAWRENCE BERKELEY LABORATORY THIN COIL
      SUPERCONDUCTING SOLENOID RESEARCH AND DEVELOPMENT PROGRAM

The experimental results discussed in Sections 4 and 5 represent
one step in the development of thin solenoid magnets. The development
program has two primary parts: a tubular cooling system, and a closely
coupled low resistance bore tube used to control magnet quenching.
The series of tests described here show that the cryogenic system
works essentially as planned. There is little technical difficulty
associated with scaling the helium cooling system to a full scale
magnet system. The control of quenching is another matter. The experiments
described here show a substantial improvement of the state of the
art in high current density solenoid magnets; but our experiments
have not proved conclusively that large (ten megajoule stored energy)
magnets will operate safely.

The experiments described in this report are analogous to the
building and testing of a pilot plant. More theoretical and experimental
work is needed before a safe, reliable full-scale detector magnet
can be built. Further scaling laws must be established and new techniques
for improving quench control (in conjunction with the low resistance
bore tube) should be tested. This section is divided into three
parts. They are: 1) improved quench propagation and quench control
methods, 2) further test coils and a test program, and 3) the time
projection chamber magnet proposal (from here on this will be referred
to as the TPC magnet.

7.1. Improved Quench Control Methods

The key to quench control is minimizing the hot spot temperature
in the magnet during a quench. The A and B magnet tests which were
described in Section 5 showed that theoretical hot spot temperatures
in excess of 300 K were developed. Neither magnet showed any damage,
but it is clear that eventually the temperature at the hot spot would
have become excessive. The key to reducing the magnet hot spot temperature
is the reduction of F(T) (see equation 5). F*(T) can be defined in
terms of equation 5:

$$F^*(T) = \int_{T=0}^{T=T_{hot}} \frac{C_m(T)}{\rho_m(T)} \, dt = \frac{r^* + 1}{r^*} \int_{t=0}^{t=\infty} J(t)^2 \, dt \qquad (30)$$

where T is temperature, T_{hot} is the final temperature, C_m is the specific
heat per unit volume of the low resistance normal metal, ρ_m is the
electrical resistivity of the low resistance normal metal, r* is the
ratio of low resistance normal metal to superconductor plus high resistance
normal metal (similar to the copper to superconductor ratio r defined
for equation 5), t is time, and J(t) is the current density as a function
of time in the superconductor matrix. The preceding equation can
be redefined for copper in terms of equation 5 as follows:

$$F*(T) \; = \; \frac{r + 1}{r} \; F(T) \; = \; \frac{r + 1}{r} \int_{t=0}^{\infty} J(t)^2 \, dt \qquad (30a)$$

One can normalize equation in terms of the $J(0)$, the starting value of the matrix current density and $\Xi(t)$, the ratio of $J(t)$ to $J(0)$. This form is as follows:

$$F*(T) \; = \; \frac{r* + 1}{r*} \; J(0)^2 \int_{t=0}^{\infty} \Xi(t)^2 \, dt \qquad (30b)$$

Figure 77 is a plot similar to Figure 5. This plot shows T_{hot} as a function $F*(T)$ for copper-based and aluminum-based conductors. Three curves for each are shown for various starting electrical resistivities at 4 K which correspond to resistivity ratios (the ratio of resistivity at 273 K to resistivity at 4 K) of 10, 100 and 1000. Figure 77 shows that for a given hot spot temperature T_{hot}, $F*(T)$ is smaller if: 1) aluminum is used instead of copper as a superconductor matrix, 2) lower resistivity ratio matrix material is used instead of high resistivity ratio matrix material, and 3) if $r*$ is small.

From the preceding equation, one can see three methods for reducing $F*(T)$ and thus the hot spot temperature. They are: 1) increase $r*$ (the ratio of low resistance metal to superconductor plus high resistivity
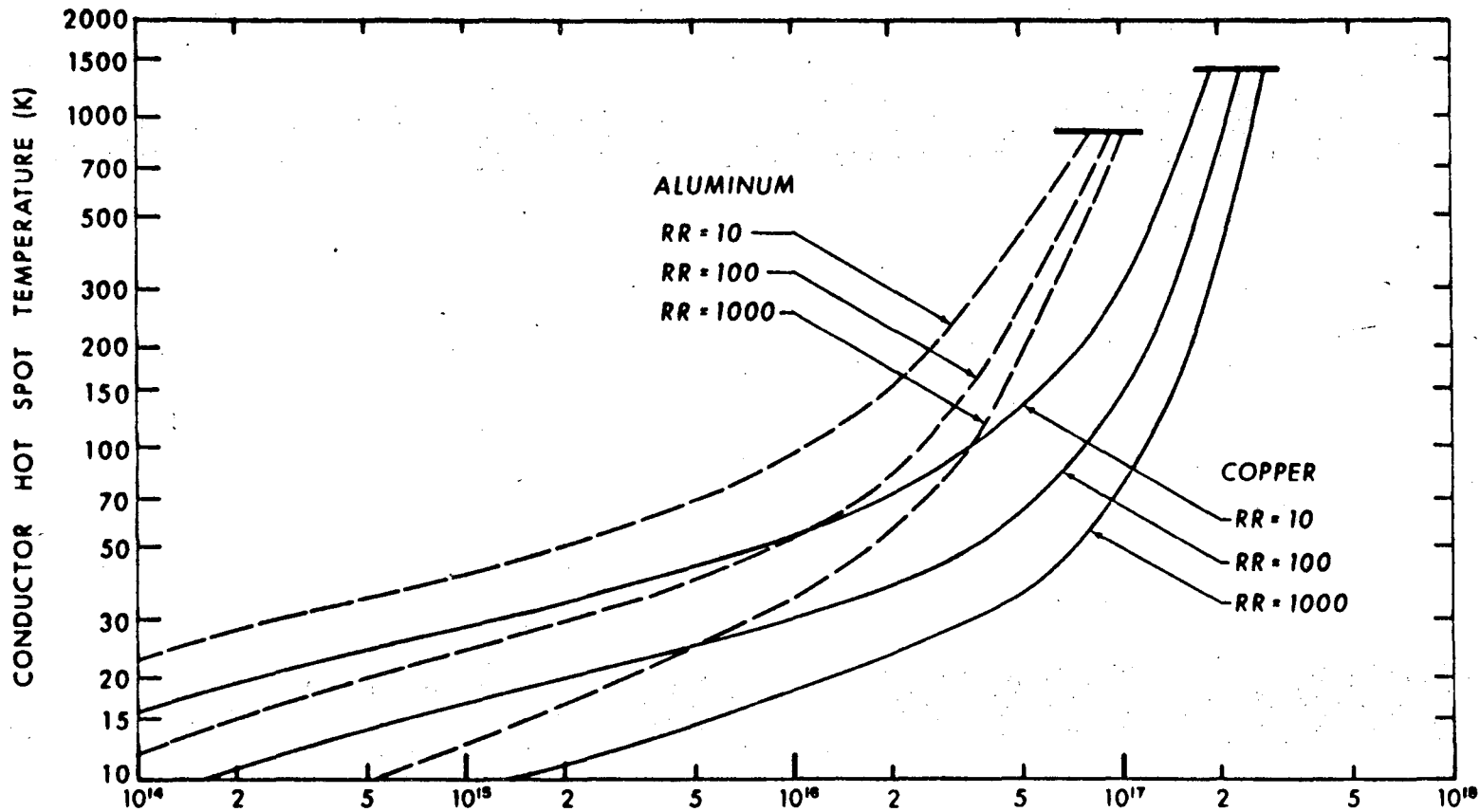
$$F^*(T) = \int_{T=0}^{T_{HOT}} \frac{C(T)}{\rho(T)} \, dT = \frac{r^* + 1}{r^*} \int J^2(t) \, dt \quad (A^2 m^{-4} s)$$

Fig. 77. Peak hot spot temperature vs F* for copper and aluminum which have resistance ratios of 10,100 and 1000. (Resistance ratio is defined as the ratio of 300 K resistance to the 4 K resistance.)

XBL 774-8481

metal); 2) reduce J(0), the starting matrix current density; and 3) reduce $\Xi(t)$ as a function of time. (Note that $\Xi(t)$ is the same thing as $I(t)/I(0)$ which is discussed in section 5.

The least effective method for reducing $F^*(T)$ is increasing r^*. For most practical systems, r^* is between 1 and 2, which means $(r^* + 1)/r^*$ is between 2 and 1.5. Increasing r^* to infinity cannot reduce $F^*(T)$ more than by a factor of two (for a practical system). Often the price paid for reducing $F^*(T)$ by increasing r^* is increased radiation thickness and/or less safety margin on the superconductor critical current. In most cases neither is desirable.

Reducing J(0), which is reducing the current density of the magnet, does not make the spectacular gains one might expect. Reducing J(0) by a factor of two does not reduce $F^*(T)$ by a factor of four. Typically, reduction factors of less than two are more normal. Reducing J(0) has a number of negative implications which are related to the fact that the superconducting coil is made thicker. They are: 1) The coil becomes less closely coupled to the bore tube, which reduces the bore tube effectiveness. 2) The radiation thickness of the coil must increase unless the superconductor stabilizer is changed to a low radiation thickness material. Aluminum could be substituted for the copper stabilizer. However, the $F^*(T)$ for a T of 300 K is considerably lower for aluminum than for copper (by about a factor of three). Thus the gain made by reducing J_o is cancelled by the lower $F^*(T)$ which is inherent in an aluminum system.[94]

The $\Xi(t)$ parameter has the largest effect on $F^*(T)$. It is important that the current be removed from the coil as quickly as possible.

In large high current density magnets, the reduction of $\Xi(t)$ with time t is not quick enough without the use of a low resistance bore tube which shifts the coil current from the magnet coil to the bore tube.

A fast shift of the magnet current from the coil to the bore tube reduces the quench back time. Quench back is an essential ingredient for fail-safe quenching. Two methods for quench back come into play, depending on the rate of current change in the magnet coil:

1. Low rates of coil di/dt cause low rates of magnet flux change in the coil. The current is shifted to the bore tube slowly and as it flows, it heats up. This heat transfer, from the bore tube to the coil, causes the coil to go normal. It takes time to shift current to the bore tube. There is a time constant associated with heating the bore tube and one associated with transferring the heat back to the coil. Further, it requires good thermal contact between the coil and bore tube. This form of quench back, defined as "thermal quench back," prevailed during the tests described in Section 5.

2) High rates of coil di/dt causes high rates of dB/dt in the coil as current shifts into the bore tube. dB/dt depends on whether the coil is inside or outside the bore tube. The magnetic induction in the coil changes; the magnitude and rate of this change influences the ac. loss rate in the superconductor. High rates of dB/dt will quench the superconductor directly. The time for this process is short and it does <u>not</u> require good thermal contact between the

coil and the bore tube. This form of quench back is defined as "magnetic quench back".

The desired form of quench back is "magnetic quench back". The superconductor can be tailored so that "magnetic quench back" is made easier, and the method for doing this becomes apparent when one looks at the equation for ac loss in a superconductor. The superconductor ac loss G for an induction change ΔB takes the following form:[36,57]

$$G = G_o \left[1 + \frac{3\pi}{4\sqrt{\lambda}} \frac{\dot{B}}{\dot{B}_c} - \ldots \right] \tag{31}$$

where

$$G_o = J_c d_f \Delta B \lambda \tag{31a}$$

$$B_c = 32 \; \rho^* \; \frac{J_c d}{\ell_c^2} \; \frac{w}{w + d_f} \tag{31b}$$

$$\lambda = \frac{1}{r + 1} \tag{31c}$$

where J_c is the superconductor critical current density, d_f is the

filament diameter, ΔB is the flux change, $\dot{B} = dB/dt$ the rate of flux
change, ρ^* is average resistivity of the matrix material, d is the
matrix diameter, ℓ_c is the superconductor twist length, r is the
normal metal to superconductor ratio, w is the average distance between
the superconductor filaments, Go is the hysteresis loss per unit volume
per cycle (this loss is a function of ΔB only and is not time dependent),
and G is the total ac loss per unit volume for a given ΔB.

The value of G-Go is often referred to as the superconductor
coupled loss. This form of ac loss is caused by currents which
flow down the superconducting filaments across the matrix and back;
it behaves like an eddy current in that it is frequency dependent
(on a per cycle basis). Coupled currents are greatly restricted by
twisting the multifilament superconductor, as the preceding equations
indicate. One can make a superconductor quench at a high rate of
B simply by not twisting it so much. Some twisting in the superconductor
is necessary for intrinsic stability.

The $\Xi(t)$ parameter, which is reduced by the bore tube, is further
reduced by increasing the resistance of the coil circuit faster.
One may increase the resistance of the coil circuit by the following
ways: 1) one may speed up the quench process and thus make the coil
resistance grow faster, 2) one may put artificially induced quenches
in many places in the coil, or 3) one may put an external resistor
across the coil. All three methods will cause faster current to shift
from the coil to the bore. Quench back will be speeded up and in
many cases quench back will become of the magnetic type.

A speed up of the quench process requires one to speed up the

longitudinal velocity and/or the transverse velocity. Increasing the

longitudinal quench velocity also increases the transverse velocity,

and this is done by increasing coil current density and operating

closer to the critical current limit of the superconductor. In general,

both of these are undesirable things to do. One can, on the other

hand, increase the transverse quench velocity without changing the

longitudinal quench velocity. Transverse quench velocity is typically

a few percent of the longitudinal velocity, so that increasing the

transverse velocity to between 60 to 80 percent of the longitudinal

velocity will have a big effect on the increase rate of the magnet

coil resistance. A method for increasing the effective transverse

quench velocity is given later.

The July 1976 test (test 7) showed that inducing quenches in

two places caused quench back to occur sooner. If a quench is induced

in 20 to 30 places simultaneously the coil resistance should grow

very quickly and with it the time to quench back should decrease markedly.

The use of multiple coils to induce a quench requires a reliable quench

detection system which is capable of detecting quenches within 10

or 20 ms after they occur.

The insertion of a resistor across the leads of the coil drives

coil current into the low resistance bore tube. Much of the coil

current can be reduced in this way, and within a span of 10 to 20 ms.

Large changes of induction within the coil occur in that time. It

should be possible to put a ΔB of 0.5 T into the coil at rates 25-50 Ts^{-1},

which will induce a magnetic quench back (if the coil superconductor

is suitably selected) that is quick, and thus safe. This quench back

will require a reliable quench detection system capable of detecting the quench within 10 to 20 ms. The resistor method is superior to the multiple quench induction method because it is far less complicated electrically and will guarantee magnetic quench back.
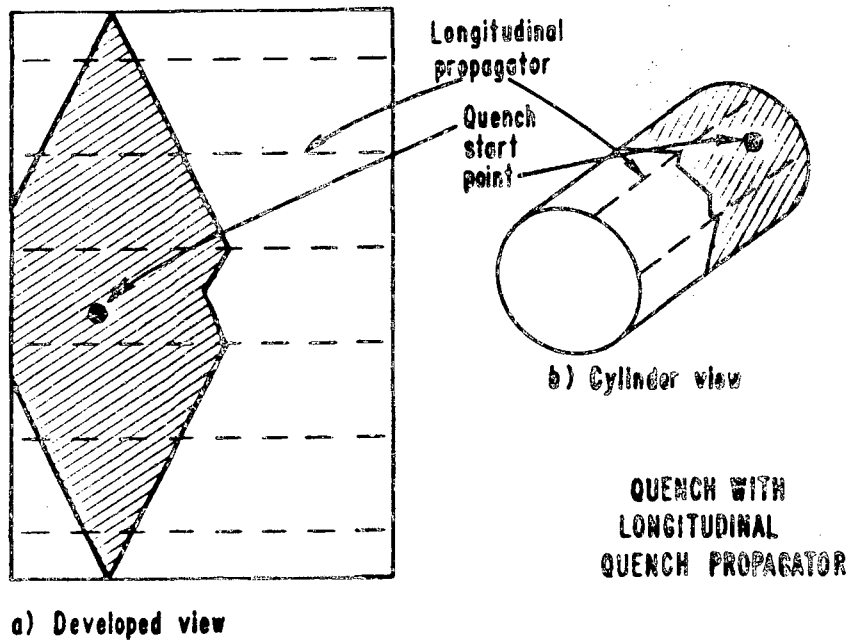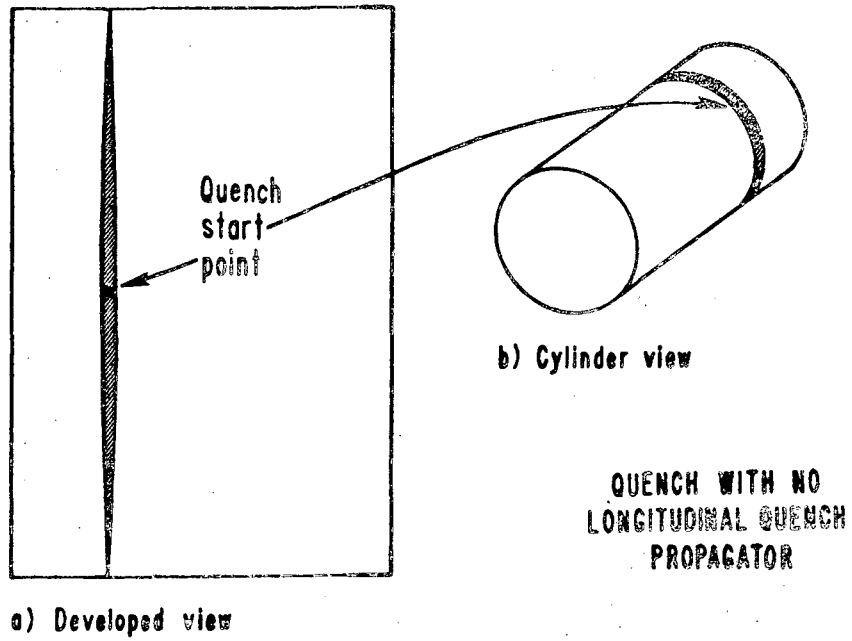
7.2 Proposed Changes for Future Magnets

Future superconducting thin solenoids shall have the following passive and active quench protection features: 1) There shall be a low resistance bore tube which has a resistivity between 3×10^{-10} Ωm and 2×10^{-9} Ωm. 2) There shall be quench propagators to increase the transverse (from turn to turn) quench velocity. From here on these will be referred to as longitudinal quench propagators because they speed up quenching in the longitudinal direction of the magnet (along the axis of the solenoid). 3) The superconductor twist pitch shall be adjusted so that the superconductor will go normal when a ΔB of 0.5 T is applied in 200 ms or less. A twist pitch of 50 mm will be sufficient. 4) A quench protection circuit which switches a resistor across the coil shall be provided. The time constant of the resistor circuit should be at least a factor of three smaller than the time constant for the bore tube circuit.

The first three quench protection features are passive. They are inherent features which are built into the magnet; hence, they are essentially fail-safe. The fourth quench protection feature is an active method. It requires the reliable early detection of a magnet quench. Thus it is not fail-safe. Before proceeding, it is important to point out that the low resistance bore tube is the key to making

the current in the coil drop quickly. Without the bore tube, none of the other quench protection features will work. In general, the low initial resistance bore tubes will carry more of the magnet current. It is clear that a balance between longer magnet charging times and larger current flow in the bore tube during a quench must be struck. (An order of magnitude reduction of the bore tube low temperature resistivity means that charging time of the magnet is increased a factor of three.)

The "longitudinal quench propagators" consist of current carrying bifilar (non inductive) windings which travel in a direction perpendicular to the solenoidal windings. These bifilar windings will carry the full current of the magnet at the same matrix current density as the coil itself. Normal regions which are formed in the solenoidal coil will be propagated along the superconductor. When the superconductor under the longitudinal quench propagator becomes normal, the propagator itself is driven normal by heating. A quench wave now propagated along the quench propagator wire drives other parts of the solenoidal winding normal. Thus, turn to turn quench propagation velocities which are in excess of fifty percent of the quench velocity along the wire should be attainable, and, the normal region within the superconducting coil should grow much faster. Figure 78 illustrates how the quench propagator system increases the normal area of the coil.

Increasing the twist length increases the sensitivity of the wire to quick changes of magnetic flux. Increasing the twist length to 50 mm (in a copper-based superconductor) should make magnetic quench

Quench
start
point

b) Cylinder view

QUENCH WITH NO
LONGITUDINAL QUENCH
PROPAGATOR

a) Developed view

Longitudinal
propagator

Quench
start
point

b) Cylinder view

QUENCH WITH
LONGITUDINAL
QUENCH PROPAGATOR

a) Developed view

XBL 7610-4300 A

Fig. 78. The effect of longitudinal quench
propagators on the growth of the
normal region in thin cylindrical
superconducting magnets.

back easier. The disadvantages here are that the coil becomes more
sensitive to conductor motion, and training becomes more of a problem.
It is proposed that additional support structure be built into the coil
to restrict superconductor motion away from the bore tube in the event
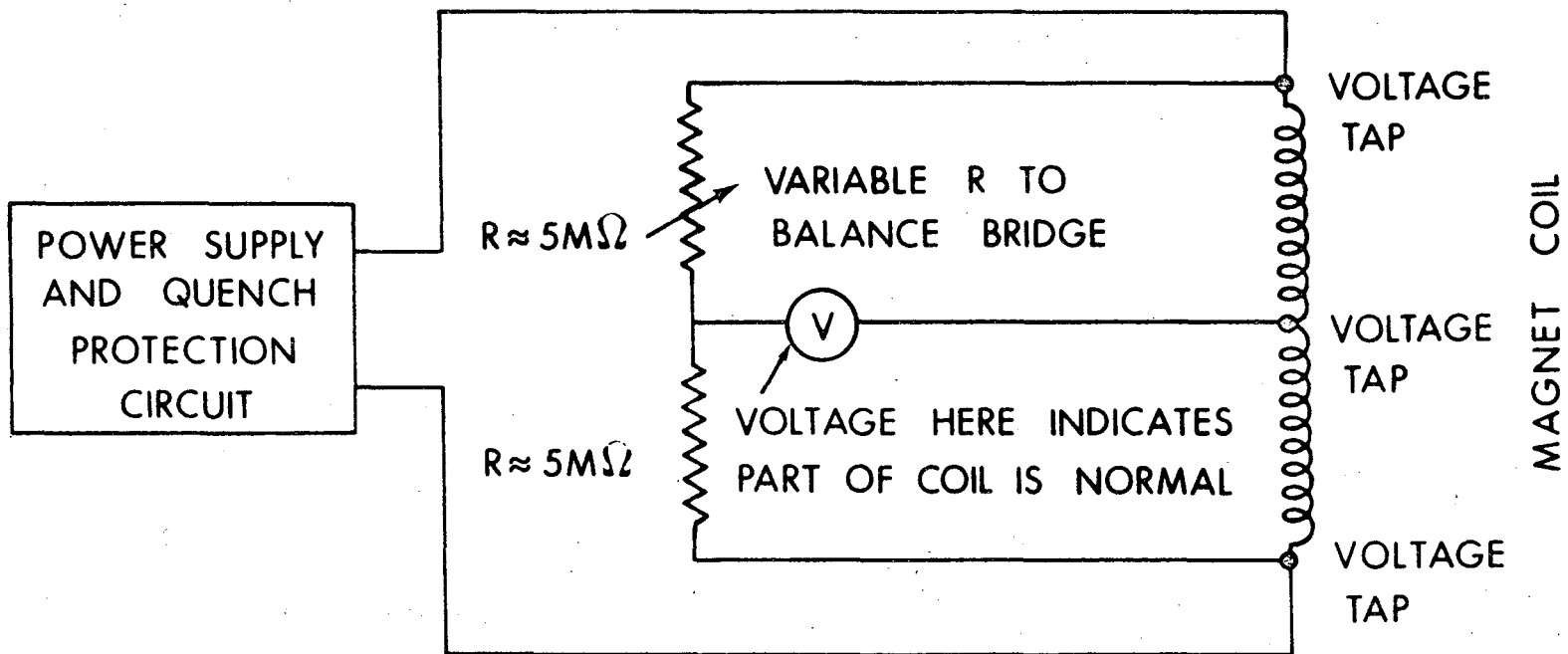of epoxy breakage at the bore tube-coil interface.[95]

The addition of an external resistor quench protection circuit
will insure that minimum hot spot temperatures are achieved during a
quench.[96] The resistor is limited by the voltage to ground that is
allowed for the magnet coil; from practical considerations, this limit
is less than 10 kV. When a constant resistance is put across the magnet
electrical leads, the voltage across the resistor is proportioned to
the magnet coil current. Best results can be obtained if the voltage
put across the coil electrical leads is kept constant; this is possible
with a "varistor" or "thyristor" resistor. A thyristor has a voltage
drop across it which is proportional to current to the one-fifth power.[97]
When the current decreases through such a device its resistance increases
markedly. Thus as current in the magnet coil is shifted to the magnet
bore tube, more resistance is put across the magnet leads, forcing
even more current into the bore tube. The electrical circuit for
the magnet with a varistor quench resistor is shown in Figure 79.

The resistor or "varistor" quench protection system is not fail-
safe. The existence of the quench must be detected before the switch
shown in Figure 79 can be activated. Two methods of quench detection
can be considered: 1) the rate of current change can be measured,
or 2) a bridge circuit across two parts of the coil which are inductively
coupled can be used to detect resistive regions in the coil. Figure 80
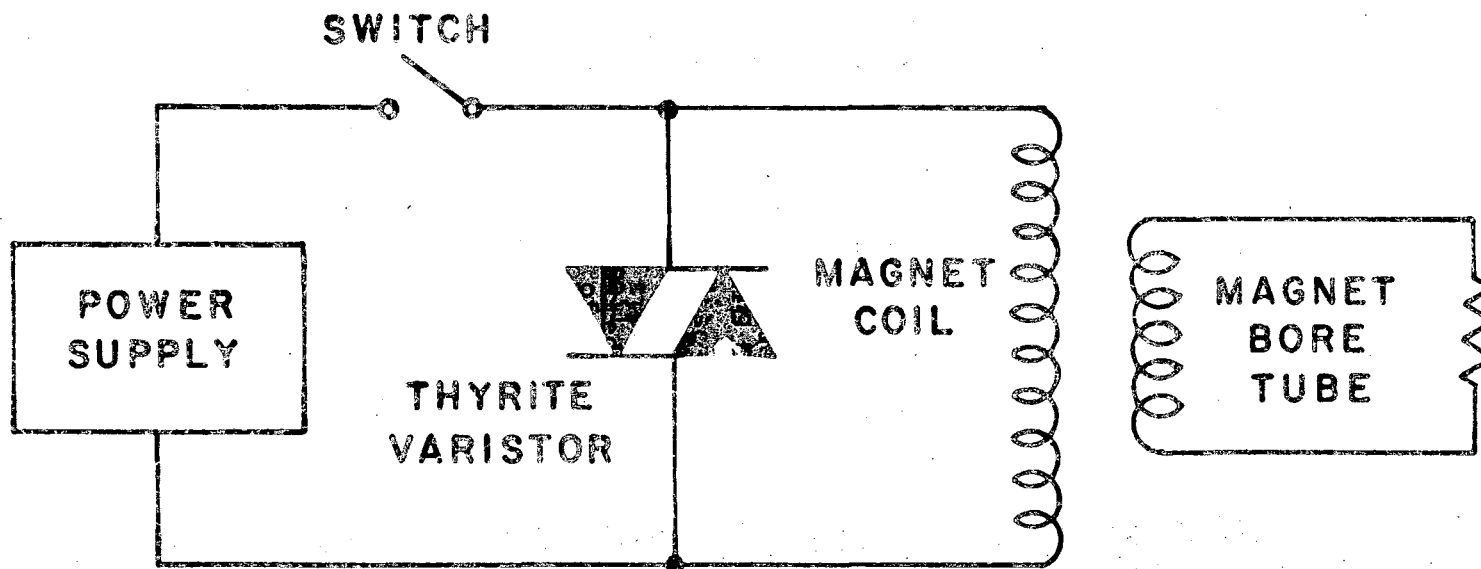
XBL 773-7854

Fig. 79. The solenoid magnet circuit with the conductive bore tube and a thyrite
varistor dump resistor.

POWER SUPPLY
AND QUENCH
PROTECTION
CIRCUIT

$R \approx 5M\Omega$

VARIABLE R TO
BALANCE BRIDGE

$R \approx 5M\Omega$

VOLTAGE HERE INDICATES
PART OF COIL IS NORMAL

VOLTAGE
TAP

VOLTAGE
TAP

VOLTAGE
TAP

MAGNET COIL

XBL 774-8475

Fig. 80. A bridge type quench detection circuit.
(A normal region in one part of the
magnet will unbalance the bridge causing
that normal region to be detected.

shows a simplified electrical diagram of a bridge circuit quench detector.

Once the quench has been detected, the magnet power supply must be switched out of the circuit. Mechanical switches which are used in the electric power industry are reliable but have switching times as long as 50 or 100 ms. Modern solid state switches can have short switching times (say 100 µs) but they are not proven reliable. When either kind of switch is used, a capacitor circuit must be installed to prevent excessive voltage buildup across the switch.

Further tests of the two one-meter diameter magnets and tests on a two-meter diameter prototype magnet will experimentally verify whether the improved quench protection systems proposed here will work. The future LBL test program is outlined in the next subsection.

7.3   The Future Course of the LBL Test Program

The Lawrence Berkeley Laboratory research and development program includes the testing of both small and large superconducting magnets. A number of small test coils have been built to test new copper-based and aluminum-based superconductors. These coils will be used to test the theory of quenching and to debug a new computer-controlled data acquisition system. Two or three large magnet tests will be made before the first high energy physics detector magnet is built. These tests include: 1) a test of the A and B magnets in series such that the magnetic fields go in the same direction, 2) a test of a two-meter diameter solenoid which is 0.7 m long, using 1.5 mm diameter copper-based superconductor, and 3) a test of a one-meter diameter solenoid which is wound with new ALCOA aluminum-based superconductor. The first two tests are to be performed during the spring of 1977. The last test,

if it is to be performed at all, will occur in the summer or autumn

of 1977. All of the large magnet tests will have forced two-phase

helium tubular cooling systems.

The large magnet tests will use a PDP-11 computer to collect

and preprocess test data, which can then be fully processed and plotted

by the CDC-7600 central computer facility at LBL. Thus, fully processed

experimental data should be available overnight.

a) The A plus B Magnet Test

The A and B magnets will be tested one more time for the following

purposes: 1) Further training of the A magnet will be measured.

2) Tests of the B magnet will determine whether the epoxy joint between

the magnet coil and its bore tube is sound. 3) High current tests

(above 920 A) will be performed on coil B. 4) A test of the A and

B magnets together in series with their fields in the same direction

will permit the testing of the thin coil system at stored magnetic

energies as high as 500 kJ. 5) Quench protection using a resistor

and a varistor demonstrates that the coil current can be switched

quickly to the bore tube. 6) It is hoped that the existence of magnetic

quench back can be determined experimentally. 7) A new computer

controlled data acquisition system which uses a PDP-11 computer will

be tested. This system will replace the scanning of the oscilloscope

pictures; this data will be fed directly into the LBL CDC 7600 computer.

b)   The Two-Meter Diameter Solenoid Test

The next step in the LBL test program is the construction and test of a two-meter diameter prototype magnet. This magnet is nearly the diameter required for the proposed detector magnet to be built for the Time Projection Chamber (TPC) experiment at PEP. The magnet coil has a diameter of just over 2.0 meters; its length is 0.7 meters. Its peak stored energy is around 3.0 MJ. The peak current density expected in the coil could be as high as 1.36×10^9 Am^{-2}.

The two-meter diameter magnet, called Magnet C, uses the same general construction techniques as the A and B magnets and consists of five distinct parts: 1) The low resistance bore tube is made from 9.53 mm (3/8 inch) thick 1100-0 aluminum plate. The electrical resistivity characteristics of the plate is expected to be nearly the same as the 1100-0 aluminum plate used in the A and B magnet bore tubes. 2) There will be two layers of 1.6 mm diameter superconductors (the 1.6 mm diameter includes the insulation) with a center tap between them which permits the magnet to be operated as either a single-layer or a double-layer magnet. 3) Just above the two-layer coil will be a longitudinal quench propagator system. Twelve bifilar longitudinal quench propagators will be evenly spaced around the magnet, (one every 30°. 4) Two layers of round, 3.18-mm (1/8-inch) diameter, 6061-T93 wire is wound around the magnet to help support the magnetic forces. This layer will help minimize the effect of a bad epoxy bond between the bore tube and the magnet winding. 5) Fifty-four or fifty-five turns of 12.7-mm (1/2-inch) OD aluminum tube will be wound over the support structure. Figure 81 shows the two-meter diameter test solenoid
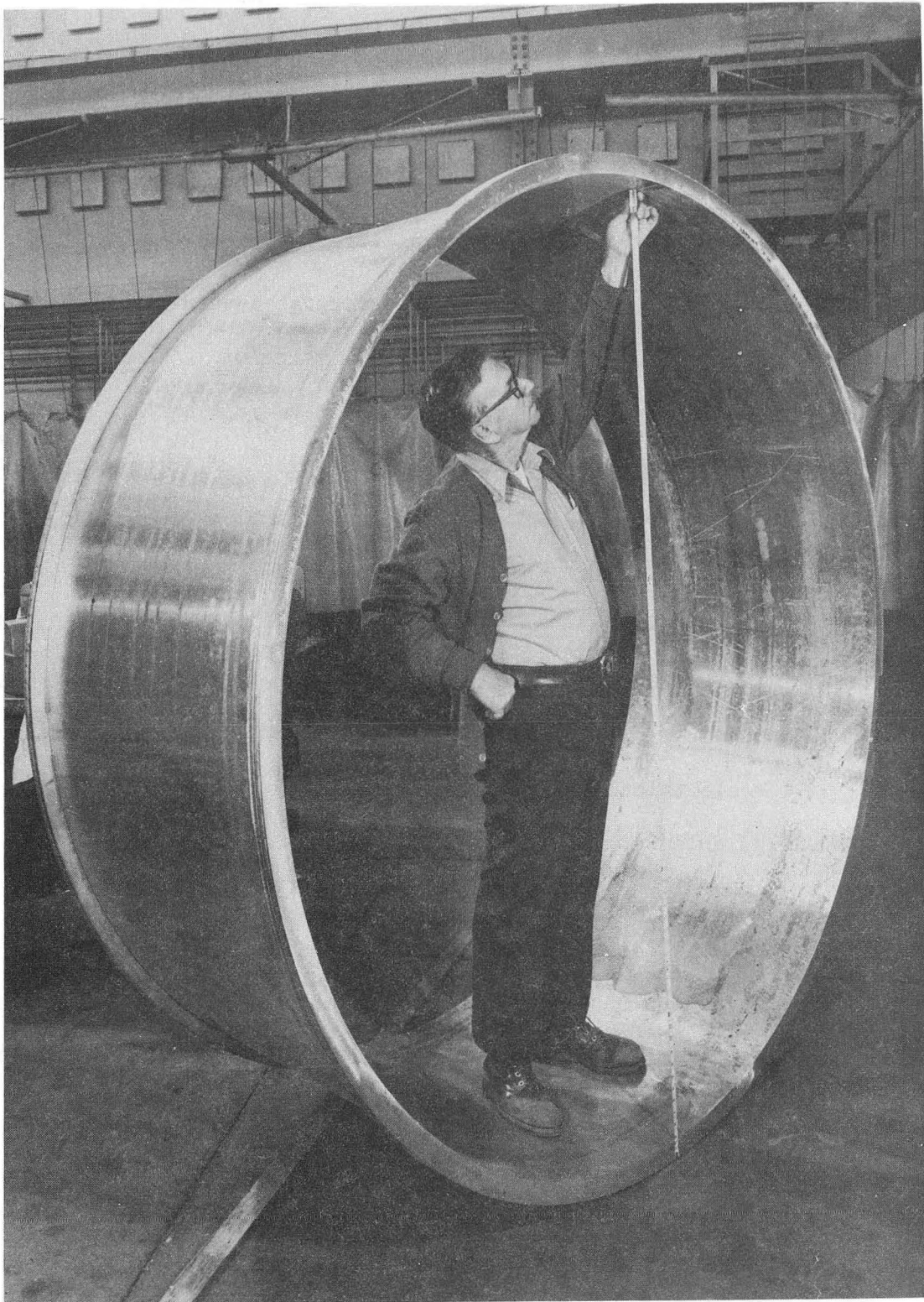
CBB 7612-11056

Fig. 81. The two-meter diameter test solenoid
bore tube.

bore tube; Figure 82 shows a cross section of the two-meter diameter test coil. The radiation thickness of the two-meter test coil will be 0.37 radiation lengths.

The superconductor used in the magnet has a matrix diameter of 1.5 mm. It is insulated with triple formvar insulation which is 0.05-mm thick (the insulated conductor was a diameter of 1.6 mm). The conductor, which was made by Magnetic Corporation of America (MCA), has 2200 filaments imbedded in a low resistivity copper matrix. The copper to superconductor ratio is 1.8 to 1; the filament diameter is about 19 μm; and the super-conductor twist pitch is 20 mm. The conductor was originally ordered for a high current density lumped coil magnet. As a result, it is not ideally suited for a thin coil solenoid. The C magnet superconductor should permit magnetic quench back because of its increased twist pitch.

The electrical characteristics of the two-meter test magnet are shown in Table 24. The design current for the single-layer case is 2000 A; the design current for the double-layer case is 1500 A. In both cases the design current for the magnet lies somewhere between 80 to 85 percent of the superconductor critical current along the load line. Maximum current densities will occur in the single-layer test. (The current density at the superconductor critical current could be as high as 1.36×10^9 AM^{-2}.) Maximum stored energies will occur during the two-layer test (stored energies as high as 3.0 MJ are possible if the magnet goes to its critical current.)

The two-meter diameter test solenoid has four leads on it. There are the two ends of the coil, a center tap between the two coils, and a separate quench propagator lead. The coil can be tested with one
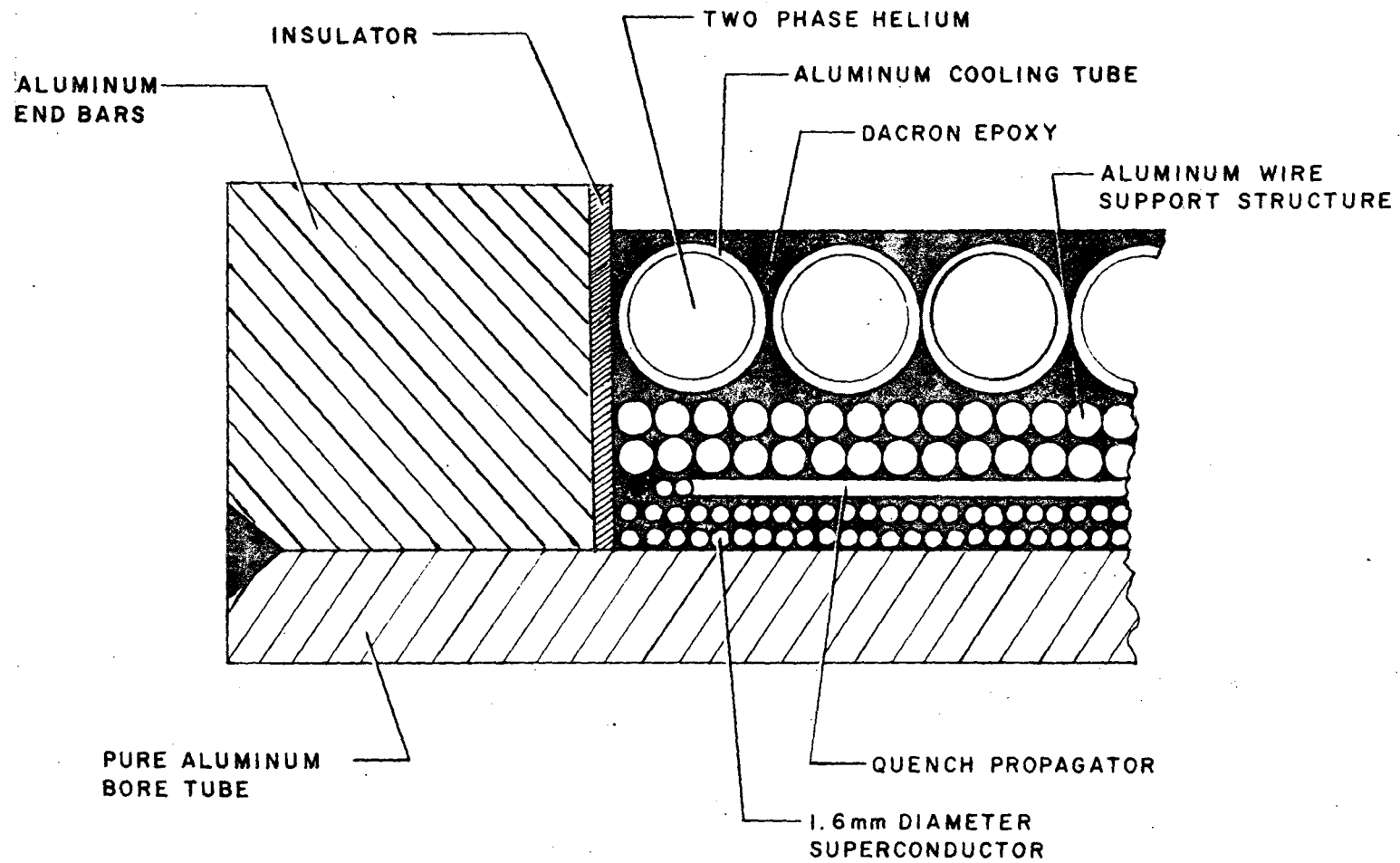
Fig. 82.   A cross section of the two-meter diameter test solenoid coil.

Table 24. The electrical characteristics of the LBL two-meter diameter
test magnet.

	Single layer*	Double layer
Average coil length (m)	0.6968	0.6968
Average coil diameter (m)	2.0062	2.0043
Number of turns	430	860
Magnet coil inductance (H)	0.462	1.847
Bore tube inductance (H)	2.39×10^{-6}	2.39×10^{-6}
Mutual inductance between coil and bore tube (H)	9.87×10^{-4}	1.973×10^{-3}
Design current (A)	2000	1500
Superconductor current density at design current (Am^{-2})	1.131×10^{9}	0.849×10^{9}
Magnet stored energy at design stored current (J)	0.924×10^{6}	2.078×10^{6}
Superconductor critical current(H)	2400	1800
Superconductor current density at the critical current (Am^{-2})	1.358×10^{9}	1.018×10^{9}
Magnet stored energy at critical current (J)	1.331×10^{6}	2.992×10^{6}

* The outer layer which is near the quench propagator.

layer (either the inner or the outer layer) or with two layers, and with or without the quench propagator. The two-meter coil has instrumentation to measure the longitudinal quench velocity directly. By watching the growth of the coil resistance, one can calculate the transverse velocity.

The two-meter test coil bore tube will have eight strain gages on it. In addition, strain gage temperature sensors will be tested. This type of temperature sensor has a very quick response, the calibration from one gage to another is supposed to be more accurate, and it is substantially cheaper than the silicon-diode type sensors. The disadvantage of the strain gage type of sensor is that it cannot be reused once it has been installed on a surface.

The PDP-11 computer data logging system should be fully developed. The data collected by the PDP-11 will be sent to the CDC 7600. Within twenty fours the experimental data should be reduced, correlated and plotted by the 7600 computer. A successful test of the two-meter diameter test coil will dispel the doubts that most critics have on the concept of a large thin superconducting solenoid magnet.

c) Other Possible Solenoid Magnet Tests

Recently Lawrence Berkeley Laboratory bought 100 m of a new type of superconducting material. This material has a matrix made from 5056 aluminum alloy instead of copper; its 54 filaments (called cells by ALCOA[22]) are hollow, and the center of the conductor is filled with ultra pure low resistivity aluminum. All in all, this material is one part niobium-titanium, 1.25 parts 5056 aluminum, and 0.4 parts pure aluminum. For thin coil magnet applications

this material offers a number of potential advantages: 1) the radiation thickness of the superconductor is half that of copper-based materials; 2) the superconductor has a thermal contraction coefficient which matches the bore tube; and 3) the structural properties of the new material are excellent. The separate support structure used in the two-meter diameter coil can be eliminated.

On the other hand, the aluminum-based material has not been used in large coils, so its behavior in a magnet is not understood. The stability of the material, particularly when there is wire motion, has not been established. Another disturbing factor concerning the aluminum material is the fact that the burn temperature occurs at a substantially lower value of the integral of J^2 dt. (See the $F^t(T)$ vs. T curves for aluminum in Figure 77.)

The Lawrence Berkeley Laboratory has wound but has not tested a small oval solenoid using the aluminum-based superconductor. This solenoid has been a testing ground for various soldering techniques, since aluminum is difficult to solder even with special fluxes. 5056 aluminum is especially difficult to solder because it contains about 4 percent magnesium. We were able to tin the aluminum by using pure tin and an ultrasonic soldering bath. Once the material has been tinned, it can be jointed to copper or other materials.

A successful test of the oval solenoid would lead to further large-scale testing of the ALCOA materials. LBL has a third one-meter diameter bore tube which could be used for a large-scale test of the ALCOA superconductor. Such a magnet could have a radiation thickness below

0.19 radiation lengths. The decision to build such a test solenoid has not been made at this time.
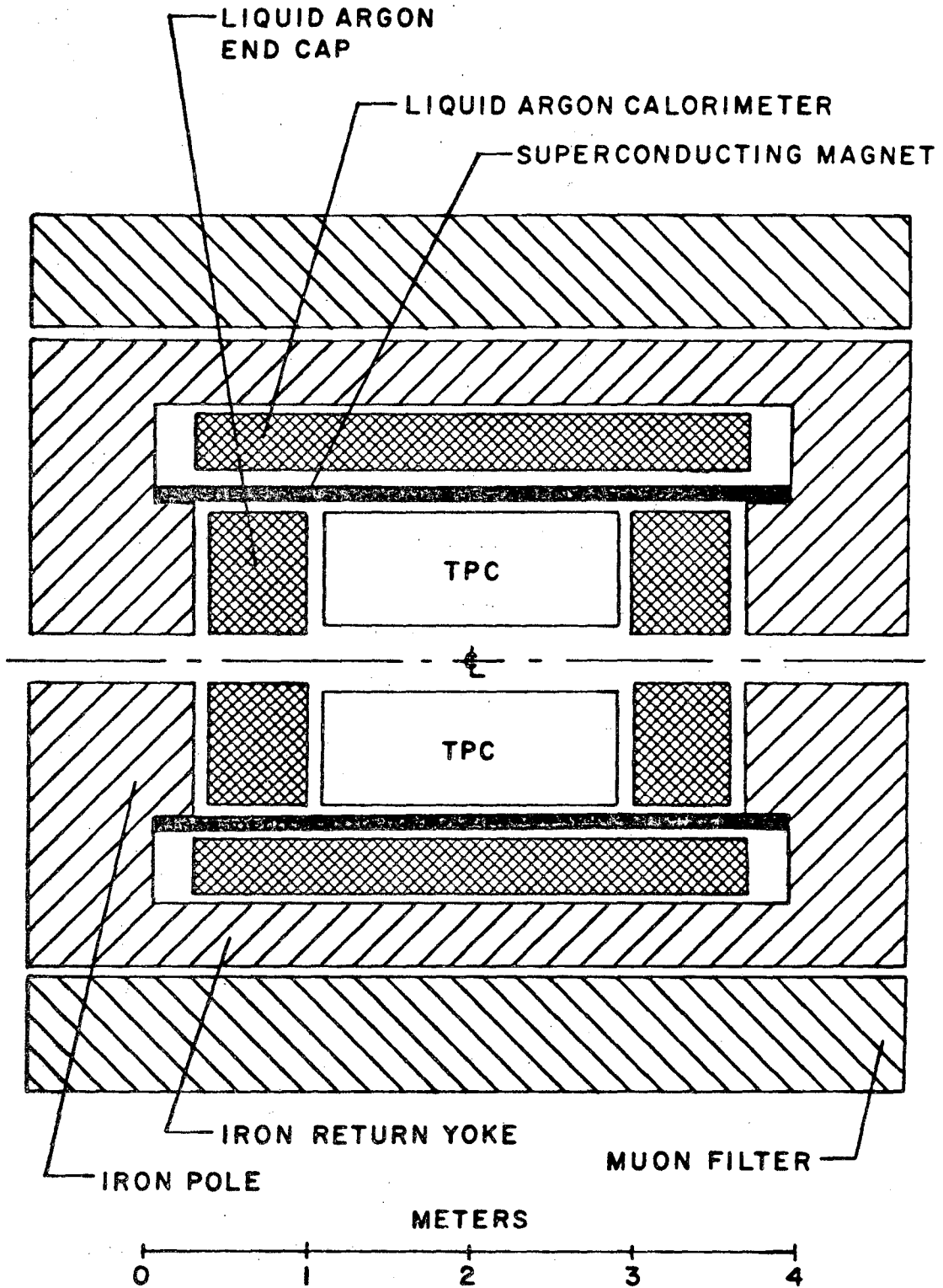
d)   The Time Projection Chamber Proposal

In December of 1976, a number of experiment proposals were submitted to the PEP Experimental Program Committee (EPC), which is charged with approving and funding projects for PEP. The experiments will have to be ready in late 1979 or early 1980. One of the experiments proposed for PEP is the time projection chamber (TPC) experiment.[98] This experiment, which is strongly supported by LBL, consists of four primary parts:

1)   The magnetic detector called the time projection chamber (TPC). This device has very good momentum and spatial resolution of many kinds of particles, given a strong uniform magnetic field.

2)   A thin superconducting solenoid magnet. This magnet must have a thin continuous winding which is under 0.5 radiation lengths thick. The magnet must generate a uniform field which is good to at least one part in 1000 (in the region of the TPC).

3)   The liquid argon calorimeter which consists of alternating layers of liquid argon and lead. This device detects strong neutral particles and gamma radiation.

4)   The muon (mu meson) detector. Muons will pass through many radiation lengths of material without an interaction, but about 0.3 m of iron will get the muon to interact and form particle showers which can be detected by spark chambers.

The thin superconducting solenoid which is being developed at LBL is ideally suited for the TPC experiments.[99,100] The TPC experiment requires a magnet with a clear bore of 2.01 m and a distance between the iron poles of 3.4 m. The central induction of the magnet is 1.5 tesla.
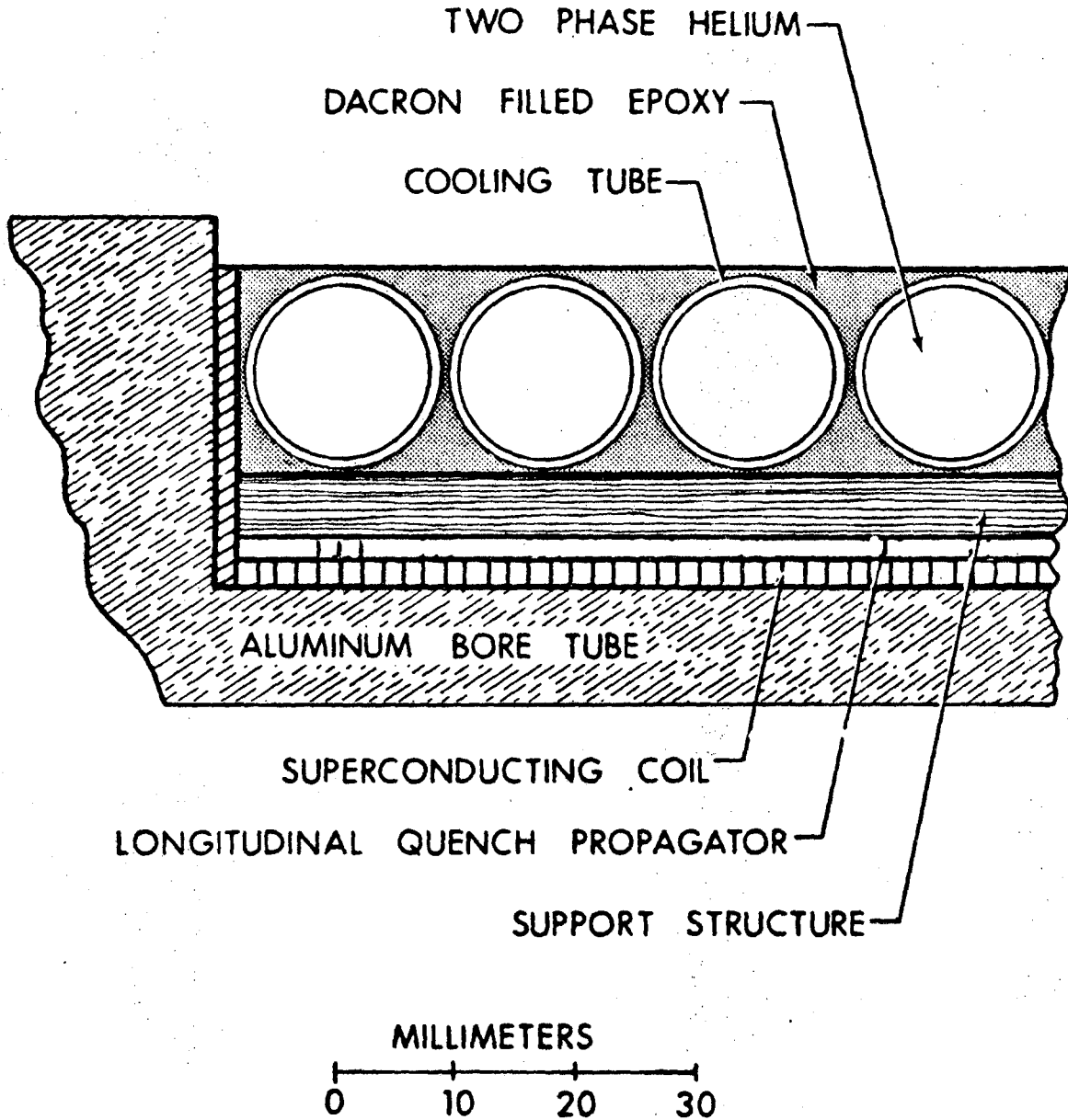
The general layout of the magnet within the TPC experiment is shown in Figure 83. The magnet cryostat has an inside diameter of 2.02 m, an outside diameter of 2.32 m and a length of 3.9 m. The magnet coil package which includes the bore tube, superconductor, support structure and cooling tube has a thickness of 37 mm. The structure of the coil is shown in Figure 84. It is very similar to the ones already tested. Two design alternatives for it are given in the proposal: one uses a copper-based superconductor and has a total radiation thickness of 0.44 radiation lengths while the other uses an aluminum-based conductor and has a projected radiation thickness of 0.29 radiation lenths. The copper-based conductor design is better understood, so it is likely that physicists will accept it more readily.

The design parameters for the two kinds of superconductors are given in Table 25. The specifications given for the copper-based material can be met by all of the niobium-titanium producers in the United States. The price, therefore, will result from competitive bidding. The aluminum-based material is the ALCOA conductor. As ALCOA is currently the only producer of this material, there will be dis-advantages, both in terms of availability and price, associated with the purchase of this material. The magnet design electrical

XBL 773-8037

Fig. 83. A general cross section of the time
projection chamber (TPC) experiment
(the solenoid magnet has a 2-meter
inside diameter and is 3.9 meters long).

TWO PHASE HELIUM

DACRON FILLED EPOXY

COOLING TUBE

ALUMINUM BORE TUBE

SUPERCONDUCTING COIL

LONGITUDINAL QUENCH PROPAGATOR

SUPPORT STRUCTURE

MILLIMETERS

0   10   20   30

XBL 774-8476

Fig. 84. A cross section of the time projection
chamber experiment's superconducting
solenoid coil which uses copper-based
superconductor.

parameters are given in Table 26. They are the same for both types of superconductors.

The magnet cooling system is based on the tubular cooling system described in Section 4. The inside diameter of the cooling tube is 13.9 mm; its length is 1400 m. The cooling circuit is divided into two parallel circuits. The total mass flow through the system is expected to be around 10 gs^{-1}; pressure drop in the circuit during normal operation is expected to be under 0.1 bar. The cold mass of the magnet system is 1510 kg for the copper-based superconductor case and 1150 kg for the aluminum based superconductor case. The expected cool down time from 300 K to 4 K is less than one day, when a 200 W refrigerator is used to cool the magnet.[101]

The cryostat is insulated only by superinsulation except in the end region where liquid nitrogen shields are used. The support system, similar in configuration to bicycle spokes (see Figure 85), will support a force of 2×10^5 N (20 metric tons) longitudinally and 2×10^5 N radially.[102] The magnet cryostat is designed to meet LBL and SLAC safety codes for cryogenic vessels. Although these vessels can be made a number of ways, the way which appears to result in minimum radiation thickness uses a composite honeycomb structure. The honeycomb or hexel structure offers large vessel thickness, which is important to prevent buckling under vacuum load, without large radiation thickness.[103]

The TPC proposal was reviewed during the spring of 1977. It was one of four proposals which use superconducting magnets. Since there will be two experimental areas which can use superconducting
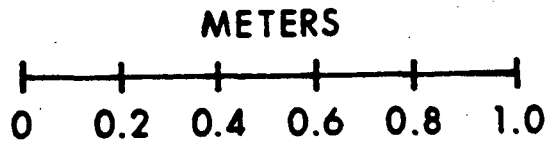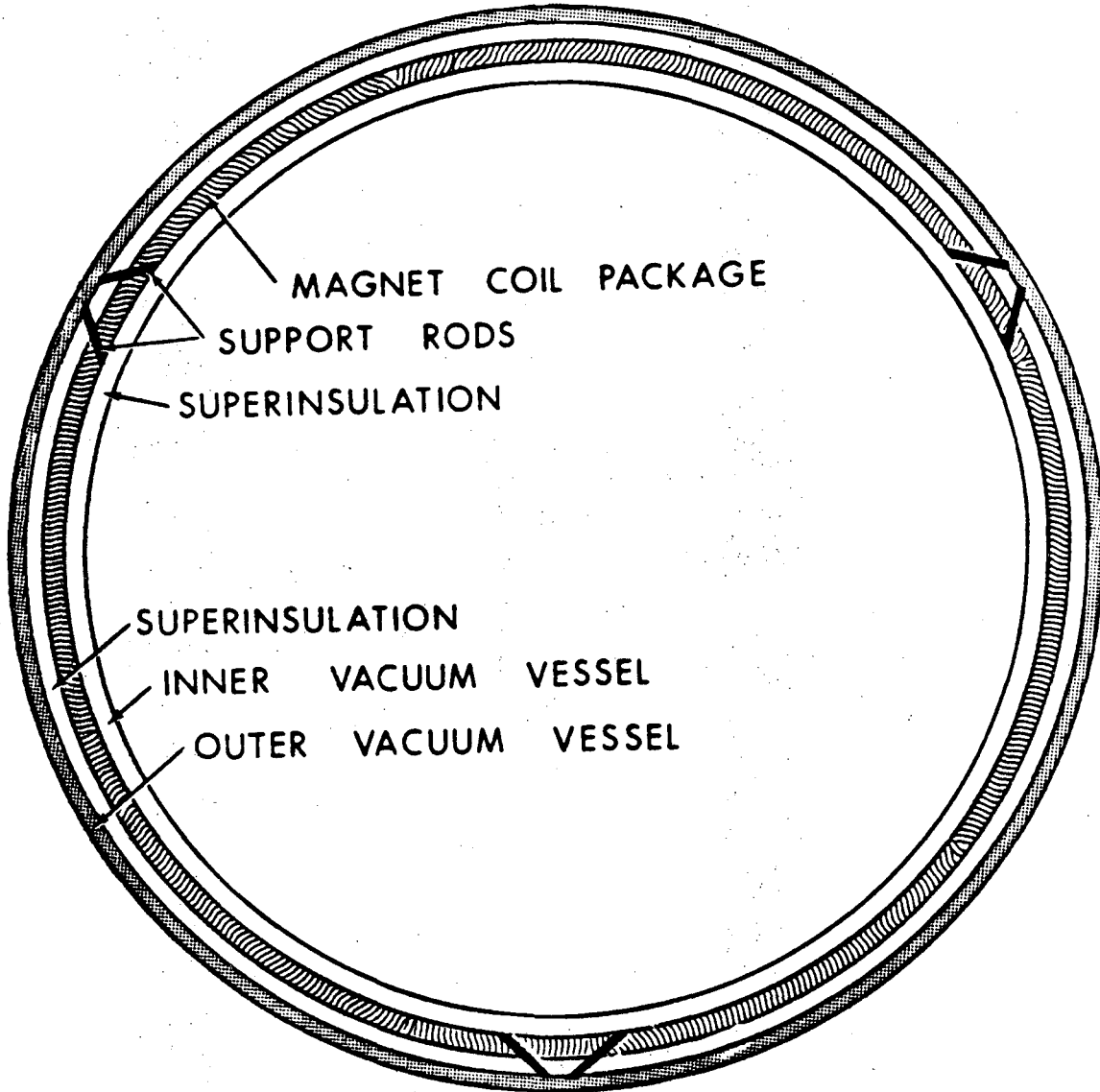
Table 25. Design parameter of the superconductor to be used in the TPC magnet.

Parameter	Copper-Based Superconductor	Aluminum-Based Superconductor*
Matrix dimensions (mm)	1.6x1.5	1.6x1.7
Insulated conductor dimensions (mm)	1.7x1.6	1.7x1.8
Insulation type	formvar	formvar
Normal metal to superconductor ratio	1.5-2.0	1.5-2.5
Number of filaments	>1500	>150
Filament diameter (μm)	<25	<75
Twist pinch (mm)	~50	~120
Critical current at 5.0 K and 1.53 T (A)	>3000	>3000
Design magnet current at 4.8 K and and 1.53 T (A)	2100	2100
Design matrix current density (Am^{-2})	8.75x10^8	7.72x10^8

* Based on the ALCOA conductor.

Table 26. The electrical parameters of the TPC detector superconducting magnet.

Design central induction	1.50 T
Estimated peak induction in the coil	~1.53 T
Ampere turns of conductor	4.10×10^6
Number of layers	1
Number of turns	1950
Design current	2100 A
Design stored energy	10.65 MJ
Coil inductance	4.83 H
Bore tube inductance	0.91 μH
Mutual inductance from the coil to the bore tube	2.07 mH
Coupling coefficient between the coil and the bore tube	>0.99
Charging time	1800 s
Charging voltage	5.64 V

MAGNET COIL PACKAGE

SUPPORT RODS

SUPERINSULATION

SUPERINSULATION

INNER VACUUM VESSEL

OUTER VACUUM VESSEL

METERS

0   0.2   0.4   0.6   0.8   1.0

XBL 774-8479

Fig. 85. An end view of the time projection chamber
solenoid which shows the compression rod,
bicycle-spoke type cryostat support system.

magnets, at least two of the four cryogenic proposals were expected
to be rejected. On April 15, 1977 the TPC proposal was accepted as
an experiment for PEP. It was the only experiment accepted which
uses a large superconducting magnet.

7.4. Other Uses for High Current Density Solenoid Technology

Other high energy physics groups are considering the use of the
LBL thin solenoid technology. Cornell University plans an experiment
for their proposed new storage ring which requires a 2.0 m diameter
thin solenoid and has been working with the LBL group towards that
goal.[104,105]

Other groups outside high energy physics are considering the
use of LBL thin solenoid technique. For example, the two LBL one-
meter diameter test magnets (Magnets A and B) will be used by a group
at Sandia Laboratory in Albuquerque, New Mexico to provide the dc
magnetic field for an experimental pulsed M.H.D. generator.[106] This
pulsed generator is being developed for the laser controlled fusion
program. Other potential users of the LBL technique include people
interested in magnetic separation and in magnetically levitated trains.

The techniques described here have application in many areas where
large dc magnetic fields are required. The integration of the magnet
coil with its cryogenic cooling system has important economic advantages
which should be utilized if the development of superconductivity is
to spread to American industry.

-246-

ACKNOWLEDGEMENTS

REFERENCES

1. J. E. Augustin et al., Discovery of a Narrow Resonance in e^+e^- Annihilation, Physics Review Letters $\underline{33}$(23), 1406 (1974).

2. J. J. Aubert et al., Experimental Observation of a Heavy Particle J, Physics Review Letters $\underline{33}$(23), 1404 (1974).

3. C. Bacci et al., Preliminary Result of Frascati (ADONE) on the Nature of a New 3.1 GeV Particle Produced in e^+e^- Annihilation, Physics Review Letters $\underline{33}$(23), 1408 (1974).

4. "Die Kälte Macht's Möglich PLUTO-Stark und doch Genugasam," DESY Journal, Deutsches Electronen-Synchrotron, Hamburg (April 1976).

5. SPEAR--A Review of the Facility and the SLAC-LBL Experiments: Advent of Charm, SLAC Beam Line $\underline{7}$(11), S-15 (November 1976).

6. SPEAR--A review of the Facility and the SLAC-LBL Experiments: The Detector, SLAC Beam Line $\underline{7}$(11), S-2 (November 1976).

7. PEP Conceptual Design Report, Lawrence Berkeley Laboratory, LBL-4288 (February 1976).

8. G. Voss, The Electron-Positron Storage Ring, PETRA Plans and Status, to be published in IEEE Transactions, NS-24(3).

9. A. Barbaro-Baltieri et al., Report of the General Purpose Detector Group, in 1975 PEP Summer Study Proceedings, pp. 108-115.

10. G. Horlitz, A Thin Wall Superconducting Coil for a Large 4π Detector at PETRA, DESY Technical Note, Hamburg, Germany, DESY-B-1 No. 1/76 (May 1976).

11. Proposal for a 4π Magnetic Detector for PETRA (Cello), a proposal by DESY, IEKP Karlsruhe, MPI Munchen, Orsay, Paris University, and Saday (August 1976).

12. M. A. Green, Superconducting Detector Magnets, Alternatives and Choices, Lawrence Berkeley Laboratory, LBL-4611 (November 1975).

13. F. Lobkowitz et al., General User's Magnet Design for PEP, in 1975 PEP Summer Study Proceedings, pp. 46-75.

14. J. D. Taylor and W. A. Wenzel, The Use of Discrete Coils in Axial Field Spectrometers," in 1975 PEP Summer Study Proceedings, pp. 76-83.

15. M. A. Green, An Engineering Study of 1.6-Meter Inside Diameter Lumped and Thin Solenoid Magnets, Lawrence Berkeley Laboratory, LBL Engineering Note 75045 (May 1977).

16. A Proposal to Study High P Physics with a Large Aperture Hadron Spectrometer of the CERN ISR, British-American-Scandinavian ISR Collaboration CERN/ISRC 75-18, 12 May 1975; also CERN/ISRC 75-21, 15 June 1975.

17. D. Nygren, A Time Projection Chamber 1975, in Proceedings of the 1975 PEP Summer Study, pp. 126-133.

18. M. Alston Garnjost et al., A Proposal to Simultaneously Measure Charged Particles and Gamma Rays Over a Large Solid Angle at SPEAR II, Lawrence Berkeley Laboratory Proposal (Oct. 1974).

19. M. A. Green, The Large Superconducting Solenoid for the MINIMAG Experiment, Advances in Cryogenic Engineering 21, 24 (1975); also Lawrence Berkeley Laboratory, LBL-3677.

20. Particle Properties, April 1974, taken from Review of Particle Properties, Physics Letters 50B(1), 74 (1974).

21. M. A. Green, MINIMAG Experiment, Large Superconducting Solenoid Magnet, the Radiation Thickness of the Magnet and Its Cryostat, Lawrence Berkeley Laboratory, LBL Engineering Note M4835 (March 1975).

22. Douglas Koop, Art Craig, Greg Barthold and Clay Weatstone, (Aluminum Company of America), private communication.

23. Z. J. J. Steckly and Z. L. Zar, Stable Superconducting Coils, IEEE Transactions NS-12 (June 1965).

24. R. Hancox, Physics Letters 16, 208 (1965).

25. P. F. Smith, M. N. Wilson, C. R. Walters, and J. D. Lewin, Intrinsically Stable Conductors, in Proceedings of the 1968 Summer Study on Superconducting Devices and Accelerators (Brookhaven National Laboratory, June 10-July 19, 1968), BNL 50155 (C-55), p. 913.

26. P. F. Chester, Rep. Prof. Physics 20, pt 2, 361 (1967).

27. A. V. Tollestrup (Fermi National Laboratory), private communication on quench protection.

28. P. H. Eberhard and M. A. Green, Quenches in Large Superconducting Magnets, Lawrence Berkeley Laboratory, LBL report, to be published.

29. M. A. Green, PEP Detector Development, Large Test Solenoid, Theoretical Determination of the Test Solenoid Parameters, Lawrence Berkeley Laboratory, LBL Engineering Note M4892A (December 1975).

30. P. T. M. Clee (Rutherford High Energy Laboratory, Chilton Didcot, England), private communication on the role of the conductive bore tube.

31. E. Nordberg (Cornell University), private communication.

32. R. V. Smith, Review of Heat Transfer to Helium I, in <u>Proceedings of the 1968 Summer Study on Superconducting Devices and Accelerators</u> (Brookhaven National Laboratory, June 10-July 19, 1968), BNL 50155.

33. Thermophysical Properties of Helium 4 from 2 to 1500 K with Pressures to 1000 Atmospheres, NBS Technical Note 631 (November 1972).

34. V. Veschey (Swiss Institute for Nuclear Research in Villingen (near Zurich) , Switzerland), private communication.

35. M. MacAshan (Stanford University, Hansen Physics Laboratory), private communication.

36. M. A. Green, Cooling Intrinsically Stable Superconducting Magnets with Supercritical Helium, IEEE Transactions on Nuclear Science <u>NS-18</u>, 669 (June 1971).

37. J. Tanabe, Bevatron Vacuum Pumping System, High Vacuum, Proposed Cryogenic Pumping System (Note #3, Two-Phase Flow), Lawrence Radiation Laboratory, LRL Engineering Note M4296 (May 1970).

38. R. W. Lockhart and R. D. Marinelli, Proposed Correlation of Data for Isothermal Two-Phase, Two-Component Flow in Pipes, Chemical Engineering Process <u>45</u> (1949).

39. M. A. Green, MINIMAG Experiment, Large Superconducting Solenoid Magnet, the Cryogenic System, Lawrence Berkeley Laboratory, LBL Engineering Note M4834 (June 1975).

40. F. Voelker, Resistance in Small Twisted Multicore Superconducting Wire, Particle Accelerators <u>1</u>, 105 (1970).

41. W. S. Gilbert (Lawrence Berkeley Laboratory), W. B. Sampson (Brookhaven National Laboratory) and P. T. M. Clee (Rutherford High Energy Laboratory), private communication.

42. P. H. Eberhard, M. A. Green, and J. D. Taylor, MINIMAG Experiment, Large Superconducting Solenoid Magnet, Oval Solenoid Test, Lawrence Berkeley Laboratory, LBL Engineering Note M4843 (July 1975).

43. M. A. Green, J. D. Taylor, and P. H. Eberhard, PEP Detector Development, Large Superconducting Test Solenoid, Superconductor Test, Lawrence Berkeley Laboratory, LBL Engineering Note M4885 (January 1976).

44. M. A. Green, and J. D. Taylor, MINIMAG Experiment, Large Superconducting Solenoid Magnet, The First Small Experimental Magnet, Lawrence Berkeley Laboratory, LBL Engineering Note M4336 (July 1975).

45. J. W. Evin, F. R. Fickett, and A. F. Clark, Effect of Stress on the Critical Current of NbTi Multifilamentary Composite Wire, Advances in Cryogenic Engineering 22, 449.

46. M. A. Green, and J. D. Taylor, PEP Detector Development Large Superconducting Test Solenoid Construction of the A Coil, Lawrence Berkeley Laboratory, LBL Engineering Note M4886 (Dec. 1975).

47. J. G. Hust (Cryogenics Division, NBS Boulder), private communication on the properties of 1100 aluminum.

48. M. A. Green, MINIMAG Experiment, Large Superconducting Solenoid Magnet, A Description of the Magnet and Its Conductor, Lawrence Berkeley Laboratory, LBL Engineering Note M4833 (May 1975).

49. P. Turowski, J. H. Coupland, and J. Perot, Pulsed Superconducting Dipole Magnets of the GESSS Collaboration, in Proceedings of the IXth International Conference on Accelerators (May 1974).

50. J. O. Turner, Flexibilized Epoxy Formulation, Unfilled, and Its Use in Vacuum Impregnation of Magnet Coils, Lawrence Berkeley Laboratory, LBL Specification M20C (April 1970).

51. Materials for Use in Superconducting Magnet Construction, A Report of the GESSS Collaboration, GESSS-3 (April 1974).

52. D. Evans et al., Epoxy Resins for Superconducting Magnet Encapsulation, Rutherford High Energy Laboratory Report, RHEL/R251 (1972).

53. G. Hartwig, Low Temperature Properties of Potting and Structural Materials of Superconducting Magnets, IEEE Transactions on Magnets, MAG 11(2), 536-539 (March 1975).

54. P. H. Eberhard, A Cautious Method for Testing Superconducting Magnets, Lawrence Berkeley Laboratory, LBL Physics Note 812 (December 1975).

55. P. H. Eberhard, and J. D. Taylor, A Technique to Induce Quenches, Lawrence Berkeley Laboratory, LBL Physics Note 816 (February 1976).

56. P. F. Smith and J. D. Lewin, Pulsed Superconducting Synchrotrons, Nuclear Instruments and Methods 52, 148 (1976).

57. W. S. Gilbert, F. Voelker, R. Acker, and J. Kaugerts, Coupling in Superconducting Cables and Braids, Lawrence Berkeley Laboratory, LBL-571, 1972.

58. K. P. Jungst, Rate Dependent Magnetization of Superconducting Magnet Conductors in Transverse and Longitudinal Fields, in Proceedings of the 5th International Conference on Magnet Technology (Frascati, Italy, April 1975).

59. W. R. Smythe, Static and Dynamic Electricity (McGraw Hill Book Company, New York, 1950).

60. J. M. Swartz and D. L. Swartz, Recent Advances in Resistance, Diode, and Capacitance Thermometers for Use at Cryogenic Temperatures, Advances in Cryogenic Engineering 19, 389.

61. E. Groves, A Constant Current Source for Temperature Sensing Diodes, Lawrence Berkeley Laboratory, LBL Bevatron Note BEV-3205 (June 1976).

62. Lakeshore Cryotronics Catalog, Lakeshore Cryotronics Inc., 9631 Sandrock Road, Eden, New York, 14057.

63. M. A. Green and J. T. Gunn, PEP Detector Development, Large Thin Coil Superconducting Solenoid Test, Strain Gage Selection and Placement, Lawrence Berkeley Laboratory, LBL Engineering Note M4890 (February 1976).

64. J. Simken (Rutherford High Energy Laboratory, Chilton Didcot, England), private communication.

65. Handbook of Chemistry and Physics, Chemical Rubber Publishing Company, 36th Edition (1954).

66. M. A. Green, PEP Detector Development, Large Superconducting Solenoid Magnet, Solenoid Magnetic Field Calculation Using Legendre Functions, Lawrence Berkeley Laboratory, LBL Engineering Note M4891A (October 1975).

67. J. Colonias, Lawrence Berkeley Laboratory, private communication on the use of the TRIM magnetic field calculation program.

68. R. B. Scott, Cryogenic Engineering (D. van Nostrand Co., Inc., New York, 1959).

69. M. A. Green, Dual J-T Value Test at 500 Incorporated, Lawrence Berkeley Laboratory, LBL Engineering Note M4100 (November 1968).

70. M. A. Green, Superconducting Studies, Helium Liquifier, Operating Procedure for the LRL Liquifier, Lawrence Berkeley Laboratory, LBL Engineering Note M4273A (December 1969).

71. M. A. Green, Superconducting Studies, Operating Characteristics of the CTi Model 2100 Liquifier and the Old ADL Liquifier Located in Building 64 Superconducting Laboratory, Lawrence Berkeley Laboratory, LBL Engineering Note M4625 (June 1973).

72. M. A. Green and J. D. Taylor, PEP Detector Development, Large Thin Coil Superconducting Solenoid Test, 25-Foot Transfer Line Construction and Test, Lawrence Berkeley Laboratory, LBL Engineering Note M4888 (March 1976).

73. User's Manual for the CTi Model 1400 Liquifier, Cryogenic Technology Incorporated, Waltham, Mass., USA.

74. W. Chupp (Lawrence Berkeley Laboratory), private communication on the calibration tests of the Building 58 Model 1400 refrigerator taken in May 1976.

75. P. H. Eberhard, G. Gibson and J. D. Taylor, Guidelines for Magnet Test, Lawrence Berkeley Laboratory, LBL Physics Note 818 (February 1976).

76. Z. J. J. Stekly, R. Thome, and B. Strauss, Principles of Stability

in Cooled Superconducting Magnets, in <u>Proceedings of the 1968 Summer Study on Superconducting Devices and Accelerators</u>, (Brookhaven National Laboratory, June 10-July 19, 1968), BNL 50155, p. 748.

77. M. N. Wilson, Normal Region Velocity in Quenching Superconductors, unpublished Rutherford High Energy Laboratory report (1971).

78. P. Turowski (Institut für Experimentelle Kernphysik, Kernforschungszentrum, Karlsruhe, West Germany), private communication.

79. M. A. Green, Foreign Travel Reports, visits to various laboratories and the ICEC-6 conference, Lawrence Berkeley Laboratory, LBL internal report UCID-386 (August 1976).

80. M. A. Green, P. H. Eberhard and J. D. Taylor, Large High Current Density Superconducting Solenoids for Use in High Energy Physics Experiments, in <u>Proceedings of the 6th International Cryogenic Engineering Conference</u> (Grenoble, France, May 11-14, 1976); also Lawrence Berkeley Laboratory, LBL-4824.

81. P. H. Eberhard, M. A. Green, W. B. Michael, J. D. Taylor and W. A. Wenzel, Tests on Large Diameter Superconducting Solenoids Designed for Colliding Beam Accelerators, IEEE Transaction on Magnetics, <u>MAG-13</u>(1), 78 (January 1977).

82. M. A. Green, Large Diameter Thin Superconducting Solenoid Magnets, Cryogenics, p. 17 (January 1977); also Lawrence Berkeley Laboratory, LBL-5515.

83. P. H. Eberhard, M. A. Green, R. G. Smits and V. Vuillemin, Quench Protection for Superconducting Solenoids with a Conducting Bore Tube, Lawrence Berkeley Laboratory, LBL-6444, to be published.

84. M. A. Green and P. H. Eberhard, PEP Detector Development, Large Superconducting Solenoid, the Role of Quench Back in Quench Protection of Thin Solenoids, Lawrence Berkeley Laboratory, LBL Engineering Note M5043 (May 1976).

85. A Compendium of the Properties of Materials at Low Temperature, National Bureau of Standards Cryogenic Laboratory, Boulder, Colorado, WADD Technical Report 60-56 (December 1961).

86. Handbook of Materials for Superconducting Machinery, Metals and Ceramics Information Center, Columbus Laboratories, 505 King Avenue, Columbus, Ohio 43201, MCIC-HB-04 (November 1974).

87. P. Turowski, Transient Phenomena and Quench Propagation in a Pulsed Dipole Magnet, in Proceedings of the 5th International Conference on Magnet Technology (Frascati, Italy, April 1975).

88. K. E. Robins et al., AGS Superconducting Bending Magnets, IEEE Transactions on Magnetics, MAG-13(1), 77-73 (Jan. 1977).

89. W. B. Fowler et al., The Technology of Producing Reliable Superconducting Dipoles at Fermilab, pp. 279-282 (Janury 1977).

90. J. H. Coupland and D. E. Baynham, Measurements on Pulsed Superconducting Dipole Magnets, in Proceedings of the 4th International Conference on Magnet Technology (Brookhaven National Laboratory, 1972).

91. T. Elioff et al., ESCAR-First Superconducting Synchrotron, Storage Ring, IEEE Transactions on Magnets MAG-11(2), 447-450 (March 1975).

92. H. P. Hernandez et al., Rules and Procedures for the Design of Hazardous Research Equipment at Lawrence Berkeley Laboratory, (part of the overall rules and procedures for the design of hazardous equipment), LBL Engineering Note M3954B (Dec. 1967).

93. ASME Boiler and Pressure Vessel Code, Section VIII on Pressure Vessels, 1974 Edition with Winter 1976 Addenda.

94. M. A. Green, PEP Detector Development, Large Superconducting Solenoid, Copper Stabilized vs Aluminum Stabilized Superconductors, Lawrence Berkeley Laboratory, LBL Engineering Note M5044 (May 1976).

95. M. A. Green, PEP Detector Development, Large Thin Superconducting Solenoid Magnet, Magnetic Force Constraining Numbers, Lawrence Berkeley Laboratory, LBL Engineering Note M5010 (December 1976).

96. P. H. Eberhard, and V. Vuillemin, Voltage Induced in the Coil of a Superconducting Solenoid by the Currents in Its Conducting Bore Tube, Lawrence Berkeley Laboratory, LBL Physics Note 829 (December 1976).

97. R. Smits (Lawrence Berkeley Laboratory), private communication on SCR switching of magnet current into a varistor.

98. A Proposal for a PEP Facility Based on the Time Projection Chamber, PEP-4 (December 1976).

99. P. H. Eberhard and M. A. Green, Intrinsic Stability vs Cryostability for the TPC Magnet, Lawrence Berkeley Laboratory, LBL Physics Note 832 (February 1977).

100. P. H. Eberhard and M. A. Green. Comparison of PEP-3 and PEP-4 Refrigeration Requirements, Lawrence Berkeley Laboratory, LBL Physics Note 834 (March 1977).

101. M. A. Green, Large PEP Detector, Large Thin Superconducting Solenoid Magnet, Cool Down of the TPC Thin Solenoid, Lawrence Berkeley Laboratory, LBL Engineering Note M5034 (March 1977).

102. M. A. Green, Large PEP Detector, Large Thin Superconducting Solenoid Magnet, Cryostat Support System for the Large Solenoid Magnet, Lawrence Berkeley Laboratory, LBL Engineering Note M5010 (December 1976).

103. M. A. Green, PEP Detector Magnet, Large Thin Solenoid Magnet Cryostat, the Design of Minimum Radiation Length Vacuum Vessels, Lawrence Berkeley Laboratory, LBL Engineering Note M5009 (December 1976).

104. D. Andrews, Superconducting Solenoid Design Study I, Cornell University Internal Report (December 1977).

105. D. Andrews, Superconducting Coil Design Study II, Cornell University Internal Report (March 1977).

106. M. Cowan et al., Pulsed Energy Conversion with a dc Super-conducting Magnet, Cryogenics pp. 699-704 (December 1976).